Module name: Coastal inlets and tidal basins

Module code: CT 5303

Date: 08 – 2006

TU Delft
Faculty CiTG

Prof. dr. ir. M.J.F. Stive (editor and co-author)
Prof. dr. ir. H.J. de Vriend (co-author)
Dr. J. Dronkers (co-author)
Dr. ir. A. van Dongeren (co-author)
Dr. ir. Z.B. Wang (co-author)

“In Greek mythology Ocean, the personification of the waters flowing along the coasts of the Earth, was a powerful and good man. Daily he gave birth and shelter to the sun and the moon and all the gods of the sea called him “father”. His wife was Tethys, personifying the fertility of the sea. She gave him 3000 children, all the waves of the ocean.”

These lecture notes intend to highlight the importance of some particular entities of the coastal zone, viz. coastal inlets, estuaries and tidal basins, which may only be on “the periphery of the periphery” of the ocean, but which – due to their fertile conditions – play an important role in both the global functioning of the ocean and in the – hopefully sustainable – human exploitation of the earth’s space.

On behalf of the Section of Hydraulic Engineering published by:
VSSD
Leeghwaterstraat 42, 2628 CA Delft, The Netherlands
tel. +31 15 278 2124, telefax +31 15 278 7585, e-mail: hlf@vssd.nl
internet: http://www.vssd.nl/hlf

Foreword

These lecture notes serve to support and supplement the course on “COASTAL INLETS AND TIDAL BASINS”. This is a relative recent (per the academic course year 1998-1999) fifth-year course for MSc graduate students following the Hydraulics Engineering direction of the Faculty of Civil Engineering and Geosciences of Delft University of Technology. This course focuses on the interrelation between physical flow- and transport-phenomena and the morphodynamics of coastal inlet, estuarine and tidal basin systems. The objective is to provide both insights into the phenomenological, theoretical and applied aspects for civil engineering MSc students. It builds upon the MSc courses treating flow, wave and transport dynamics, and is complimentary to the course on “COASTAL MORPHOLOGY”. Chapter 4 (until mid 2006 in Dutch) is derived from the MSc graduate lecture notes on “PHYSICS OF COASTAL SYSTEMS” given until 2004 at the Faculty of Physics and Astronomy of the University of Utrecht by Job Dronkers, assisted by Marcel Stive. A translation and revision of Chapter 4 was made in August 2006; the largest change besides the language concerns the shortening of Section 4.9 on mixing processes. Except for this Foreword the remainder of the lecture notes is unmodified.

The course responsibility rests with Marcel Stive and Huib De Vriend. These lecture notes were composed from contributions made by Marcel Stive (editor and co-author), Huib de Vriend (co-author), Zheng Bin Wang (co-author), Job Dronkers (co-author), Ap van Dongeren (co-author), and the first version (February 1999) was realised with the valuable assistance of Birgit Cloin (WL | Delft Hydraulics and Delft University of Technology), Edwin Elias (Delft University of Technology) and Anneke Hibma (Delft University of Technology).

Although there exist several valuable course monographs and books on the topic of coastal inlets, tidal basins and estuaries we feel that there are no complete standard teaching books for the purposes that we have in mind, as yet. It is our expectation that the present notes may develop towards that end. The present form and format of these notes is not final and far from perfect, both in language and contents. We feel that this is a matter of evolution, strongly steered by the experience of both teaching and examination.

Delft, August 2006

Contents

1 Introduction

1.1 Problem definition

Tidal inlets and their associated basins (lagoons) are a common feature of lowland coasts all around the world. A significant part of the world's coastlines is formed by barrier island coasts, and most other tidal coasts are interrupted by estuaries and lagoon inlets. These tidal systems play a crucial role in the sediment budget of the coastal zone and thus influence the long-term coastal evolution.

From a morphological point of view, tidal inlets form highly dynamical systems, which are interlinked with the adjacent coast and the tidal basin or backbarrier area to which they give access. Often, the natural morphodynamic behaviour interferes with unnatural constraints (e.g. coastal defence works) and with the effects of human utilisation (e.g. sand mining).

Estuaries and tidal lagoons attract a variety of human activities, such as navigation, recreation, fishing and aquaculture, economical activity in the border zone, sand mining, land reclamation and in some cases hydrocarbon mining. On the other hand, many estuaries and lagoons form the basis of highly valuable and sometimes unique ecosystems. They function as nursery grounds for many species and as resting and feeding grounds for many others. Hence human activities which affect the properties of such a system, or put the environmental functions otherwise at risk, may have important environmental implications. For the proper management of these systems, it is therefore most important to be able to predict the impacts of such activities.

At a larger scale, a deficit of sediment in the backbarrier area, due to sea level rise, for instance, can have major effects on the sediment budget of the coastal zone. The outer deltas of the inlets seem to act as sediment buffers, but the ultimate source of the sediment which goes to the backbarrier area is the coast. Since long-term coastal zone management should include sediment management, the capability to predict the large-scale exchange of sediment is of great importance to ICZM (Integrated Coastal Zone Management). The inlets and their outer deltas play a key role in this exchange.

These lectures intend to develop an insight into the physical functioning of coastal inlets and tidal basins, such that possible engineering interventions are executed from a

sustainable, holistic and integrated management perspective. The emphasis will be on inlet and basin systems which are subject to a mixed tidal and wave forcing, with negligible fresh water run-off, typical examples being the Wadden Sea and the Zeeland inlets and basins. Foreign examples are typically barrier-inlet coasts, such as found abundantly along the east-coast of the USA. This implies that fresh and salt water dynamics are not of strong relevance, and that the morphodynamics of these systems are largely determined by the interaction between the coarser sediment (fine to medium sands) and the tide and wave induced water motions.

1.2 Predictability and scales

Tidal inlet and basin morphology is the result of a stochastically forced, non-linear interaction between the water and sediment motion and the bed topography. Understanding and predicting their functioning is one of the major scientific challenges of coastal physics. It implies dealing with a wide range of space and time scales, with complex multi-scale interactions of the constituent processes, and with strong, partly stochastic variations of the forcing. Besides complexity, the possibility of limited predictability has to be taken into account, because these systems seem to satisfy all conditions for inherently unpredictable behaviour (cf. De Vriend, 1998). This would imply that large-scale behaviour cannot be derived in a deterministic way from small-scale processes.
At the moment, the hypothesis of the existence of inherent predictability limits in tidal inlets, other than those associated with turbulence and individual grain motion, has neither been verified, nor falsified. Practical limits, associated with computer time, for instance, have been encountered. One example is the simulation of a two-day storm event around Thyborøn Inlet, Denmark, which took about one day of computer time (Brøker et al., 1996).
Moreover, recent experience with a number of 2-D and 3-D morphological simulations of inlet systems in The Netherlands has shown, that we are not yet in full control of these models. Including new small-scale mechanisms, such as curvature-induced secondary flow, sometimes improves the results, sometimes it does the opposite, but we are unable to explain why. Apparently, the physical understanding which has to underpin the modelling is still insufficient.

In summary, we must conclude that our capability to predict the morphological behaviour of tidal inlets and tidal basins is still unsatisfactory for practical use. This is for instance true for coastal inlet systems, with its complex, multi-scale dynamical interaction of waves, currents and bed topography. Since the deltas play a key role in the large-scale behaviour of barrier island coasts, as a sediment buffer and as a link between the islands, the lack of sufficient knowledge on how they work is a major obstacle to a better capability to predict the behaviour of inlets and interrupted coasts.
In order to tackle the problem of limited predictability we introduce the concept of dealing with our interest on a *cascade of scales*:

the *micro-scale* level, i.e. the level inherent to the underlying processes[1] and the smallest-scale morphological phenomena (ripple and dune formation); the principal forcings are the diurnal tide and the weather,
the *meso-scale* level, i.e. the level of the principal morphological features, such as channels and shoals (hundreds of metres in space, years in time); the principal forcings are seasonal and interannual variations in the tide and the weather conditions, and human activities such as sand mining; a special category of phenomena at this level is the response to extreme events,
the *macro-scale* level, i.e. the level at which these features interact (e.g. the outer delta in space, decades in time); the principal forcings are the longer-term cycles in the tide, decadal-scale variations in the wave climate, consistently repeated human interference activities, etc.,
the *mega-scale* level, i.e. the level at which the principal elements of the entire system (barrier islands, outer deltas, inlets, lagoon) interact, so generally many kilometres in space and centuries in time; the principal forcings are mean sea level rise, climatic change, long-term tidal variation, subsidence, etc.
The highly dynamic nature of the non-linear, stochastically forced systems we are dealing with makes it not very likely that one model will be able to cover all these scale levels at one time. At various points, one must expect to run into intrinsic or practical limits of predictability (cf. De Vriend, 1998; also see Figure 1.1). In other words: brute-force computing is probably not a viable approach to predicting the macro- and mega-scale behaviour of these systems.

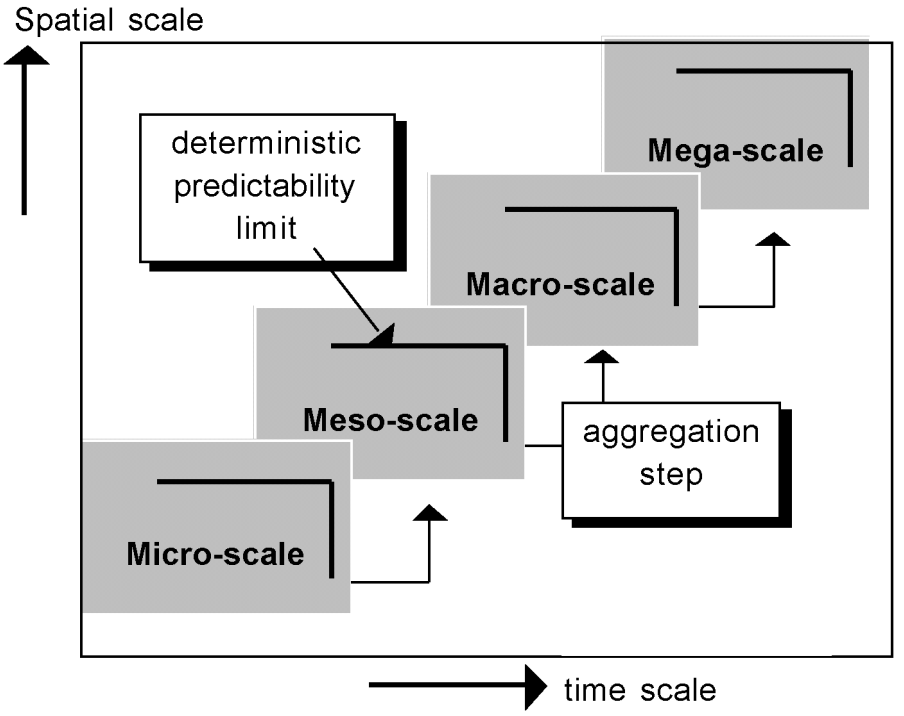

Figure 1.1 Scale cascade (De Vriend, 1998).

[1] The term *processes* is used here for the water and sediment motion at its own appropriate scale level (e.g. for wind waves: wave length in space, wave period in time)

In general, predictability limits can be overcome by aggregation. Based on what is known of the system's behaviour at scales below and above this limit, another model is formulated at the higher scale level, without attempting to describe every detail of what happens at the lower scale level. Hence, we should aim at a cascade of models at different levels of aggregation.
According to the present insights, the transitions in the above scale cascade approximately correspond with the points where predictability limits are to be expected. Hence this cascade should be reflected in the cascade of models. This leads to the system diagram shown in Figure 1.2.

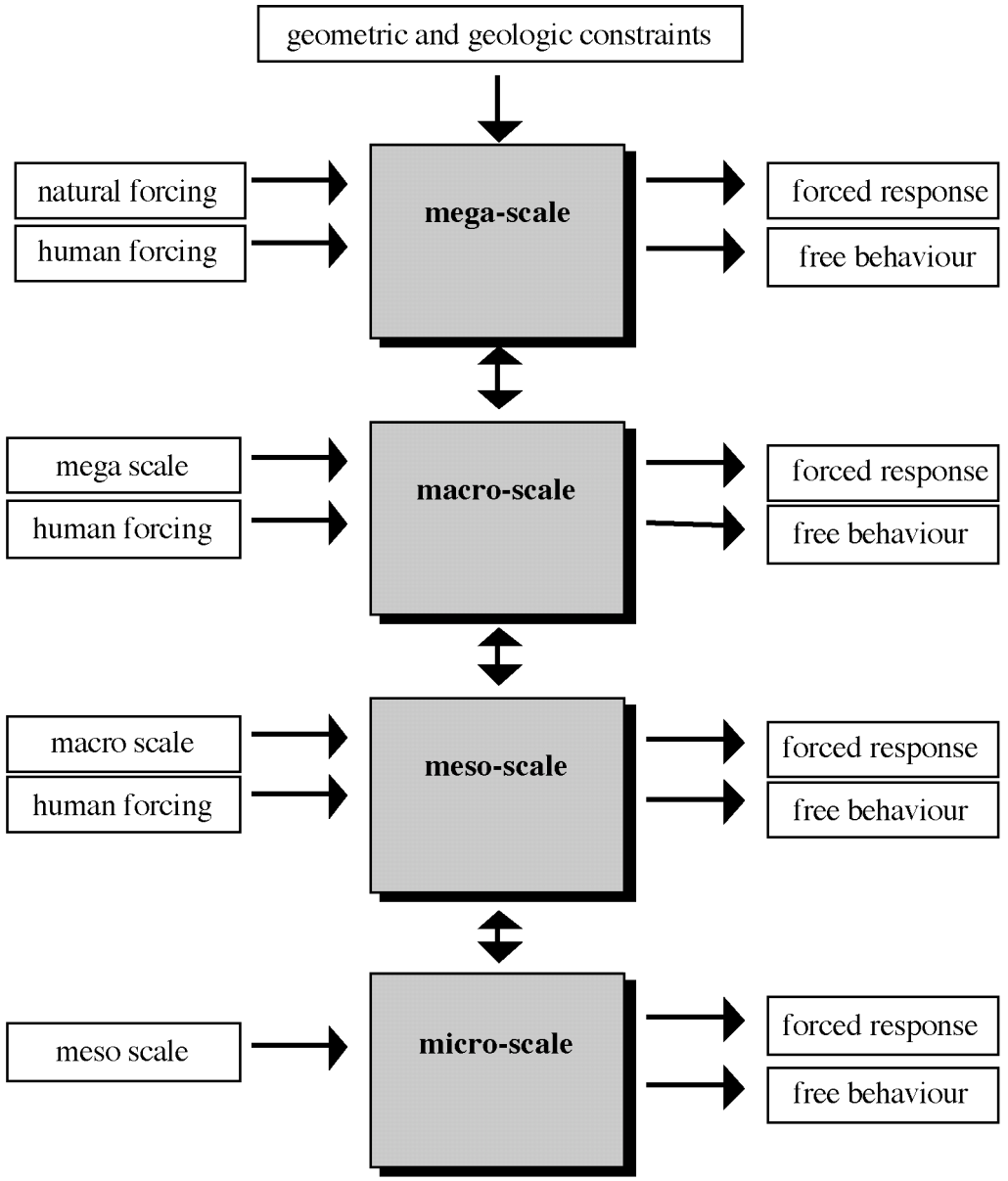

Figure 1.2 System diagram.

The scales typically addressed in these lectures are the meso- and macro-scale. On the macro-scale one typically reverts to more aggregated modelling approaches, while the process-based modelling is typically relevant on the meso-scale. It is noted that in these

lectures the use of the term coastal system is sometimes applied to the natural system and sometimes to the model system, i.e. the representation of the natural system in measurable characteristics or in mathematical variables. It is however important to make a distinction between the natural and the model system.
In the context of coastal inlets and tidal basins one may think of the following processes on each of these scales:

- micro-scale: bottom ripple and dune structures due to flow and waves;
- meso-scale: ebb- and flood chutes; channel-flat exchange;
- macro-scale: ebb-tidal delta functioning;
- mega-scale: morphologic interaction between coastal inlet, tidal basin and adjacent coast.

1.3 Mathematical-physical modelling

As explained in Section 1.2, the physical laws that are described by a mathematical-physical model represent a limited class of processes, the characteristic scales of which are limited, temporally and spatially. In a certain sense, a mathematical-physical model is a filtered description of the natural system: only for a restricted window of spatial and temporal scales a description of the system's dynamics is represented. For smaller space and time scales certain parameterizations are introduced; in the matter balance equations these are for instance the diffusion and dispersion terms. For time and space scales external to the boundaries of the model or system forcing terms or boundary conditions are adopted.
Some models only describe the response of the coastal system due to a small external forcing, such that the system is only slightly out of its equilibrium state. These are linear models; the response does not exhibit any other frequencies than that of the forcing. The spatial structures are coupled to the geometrical scales which are adopted in the model. The model doesn't display "internal" dynamics; as soon as the forcing is released the system will return to its original equilibrium state.
When describing watermotion and transport processes in coastal ocean systems one commonly applies (geo)morphostatic models. In these models the bottom is assumed to be fixed from the consideration that significant changes in the bottom morphology occur on much larger time-scales than the time-scales involved with the adaptation of the flow and matter transport patterns. When the model includes non-linear processes scale-interactions may occur, not due to the boundary forcing, such as longshore flow instabilities (meandering longshore flow). The morphostatic assumption causes the model to return to its original state as soon as the forcing is released; evolution of the coastal system on larger scales is not described.
In (geo)morphodynamic models the bottom morphology is dynamically coupled into the system. Also due to a periodic and symmetric oscillating forcing residual transports may occur due to non-linear interactions, such that the bottom undergoes a non-periodic change. In this case bottom structures may develop on a wide range of time and space scales. Yet it must be realised that processes on the smaller time and space scales are not

described dynamically correct by the model. In case of discrete numerical models the timestep and the gridsize determine the lower scale boundary on which processes can be described. In a morphodynamic model the system will generally not return to its original state when the boundary forcing is turned off.

The physical laws described by mathematical models are generally balance equations, that are derived from conservation laws for the balance variable; for instance conservation of mass, momentum, vorticity, energy or energy flux, suspended matter or sediment. In the 3-dimensional space these balance equations take the form:

$$\partial f / \partial t = -\nabla.\Phi - \nabla.\Psi + P \tag{1.1}$$

The various terms have the following meanings:

- left-hand term: temporal change of the balance variable *f* in a unit volume element, averaged over the time and space scales of small scale processes;
- first right-hand term: spatial gradient in the transport of *f* (difference between influx and outflux of *f*); often Φ is given by $\Phi = u.f$;
- third right-hand term: production or destruction of *f*;
- second right-hand term: transport due to fluctuations in the flowfield caused by small scale processes.

Often Ψ is given by:

$$\psi = <\overline{u' f'}> \text{ (= diffusion or dispersion)} \tag{1.2}$$

In case of sufficient small scale processes state in time and space the following is approximately valid:

$$\psi \approx -N_1(u) f_x - N_2(u) f_y - N_3 f_z \tag{1.3}$$

The nonlinearity is especially due to the transport term $\Phi = u.f$.
We may make a distinction in cases where *f = f (u)*, e.g.

- momentum balance *f = u, v, w*;
- bottom or sand transport $f \propto |u|^{b-1} u$, in which he coefficient b ranges from 3 to 4;

and cases in which *u = u (f)*, e.g.

- density driven flow (*f* = density);
- bottom form.

Balance equations may also be derived in two-dimensional space (either after depth- or width averaging) or in one-dimensional space (after cross-sectional averaging). In the latter case the balance equation takes the form:

$$(A\overline{\overline{f}})_t + (A.\overline{\overline{u}}.\overline{\overline{f}})_x = A\overline{\overline{P}} - \psi_x \tag{1.4}$$

in which Ψ is the dispersive transport:

$$\Psi = \overline{\overline{A(u-\overline{u}).(f-\overline{f})}} \tag{1.5}$$

In some cases this may be approximated by a gradient-type transport, with dispersion coefficient D:

$$\Psi \approx -AD\overline{\overline{f_x}} \tag{1.6}$$

See for example the sections on "Physics of tidal inlets and of basins".

When the balance variable *f* is depending on a periodically varying function, it is attractive to attempt a formal averaging over the periodic motion. This is e.g. the case as when *f* represents the sand transport due to an orbital wave motion or due to a tidal motion. Let us consider the general case of the periodic temporal dependence of *f* on *u (t)* as suggested above, while *u (t)* consists of a small residual component and of a first and second harmonic component:

$$f(t) \propto |u(t)|^2 u(t), \text{in which } u(t) = < u > + u_1 \cos(\omega t) + u_2 \cos(2\omega t + \varphi_2) \tag{1.7}$$

In the case of

- orbital wave motion:
  - the residual component <*u*> may be due wave drift or undertow;
  - the first order component is the primary wave frequency, viz. the first order Stokes component
  - the second harmonic or second order Stokes component;
- tidal motion:
  - the residual component <*u*> may be due a river run-off, an internal ebb-flood channel circulation and/or a HW-LW induced channel-flat flow difference;
  - the first order component is the primary tidal wave frequency, viz. diurnal M_2 tide;
  - the second harmonic or the M_4 tide.

Note that when the second order component is involved in the case of water waves one speaks of asymmetric waves, while in the case of tidal waves one speaks of “overtides”. Let us now first perform a formal time-averaging of *f (t)* under the assumption that the residual component is small compared to the oscillating component, which yields the following result:

$$< f(t) > \propto < u(t)|u(t)|^2 > \cong < \tilde{u}|\tilde{u}|^2 > + 3\overline{u} < |\tilde{u}|^2 \tag{1.8}$$

This result indicates that the sediment transport is determined by two components, one due to the oscillating motion, which is zero in case the oscillating component is purely due to a first harmonic motion, and another one due to the transport by the residual component of the periodic stirring of the sediment, yielding the assumption that the concentration is often assumed to be proportional to *b*–1. The latter case is usually the case when there exists little or no asymmetry in the periodic motion. The oscillatory

motion stirrs up the sediment and the residual motion advects the sediment (cf. the Bijker transport formula).

Let us now consider the transport due to the oscillating motion in case the oscillating component is due to both a first and a second harmonic, including a possible phase shift between these components. In that case we may derive:

$$< \tilde{u} \mid \tilde{u} \mid^2 > \cong 3/4 u_1^2 u_2 \cos\varphi_2 \qquad (1.9)$$

Note that in this result we may conclude that in case the phase shift is zero an asymmetry in the periodic motion may induce an important contribution, since both $<u>$ and u_2 may be of the same order, viz. some 10% of the primary harmonic amplitude. Also note that the phase shift φ_2 is fairly important, viz. if it approaches $\pi/2$ the asymmetry contribution goes to zero and no contribution due to asymmetry is exerted.

In the chapters to follow, the dynamical model descriptions are often derived from the balance equations. The variables defined from the balance equations and associated boundary conditions are mathematical objects. These should be separated from the physical reality. We may only demand a limited agreement with physical reality, concerning those processes which are represented correctly on those time and space scales which are represented by the balance equations.

2 The coastal ocean in global perspective

2.1 The importance of the coastal ocean

Along the edges of the continents there exists an intensive interaction between land and sea. At this interface a large variety of coastal ocean systems has developed. These coastal ocean systems may be characterized as relative shallow areas (i.e. depths less than approximately 100 m) bordered by or partly enclosed by land, influenced by the sea and connected to the oceans, and in which ocean disturbances propagate. Relatively shallow may be defined as those depths at which the bottom is disturbed by the water motions, such that the bottom affects the water motion and whereby the bottom itself is changed. So, there exists an interaction between bottom morphology and water motion, where there develops a mutual balance. The transitional zone between the ocean and the continents or the ocean's peripheri has a characteristic form (see Figures 2.1 and 2.2), along which the dominant water motions change. This zone is named the continental shelf, while the peripheri of the continental shelf is referred to as the shoreface. This shoreface may be defined as – on its landward side – to include the partially enclosed basins, such as tidal rivers, estuaries, tidal basins (lagoons), and coastal inlets, of which the latter two are central in these lectures.

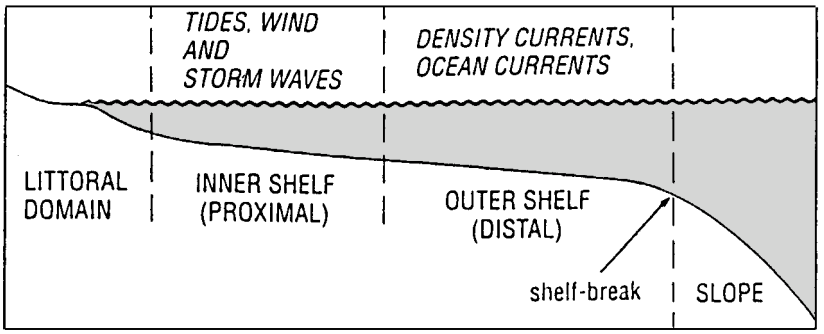

Figure 2.1: The shelf and dominant processes

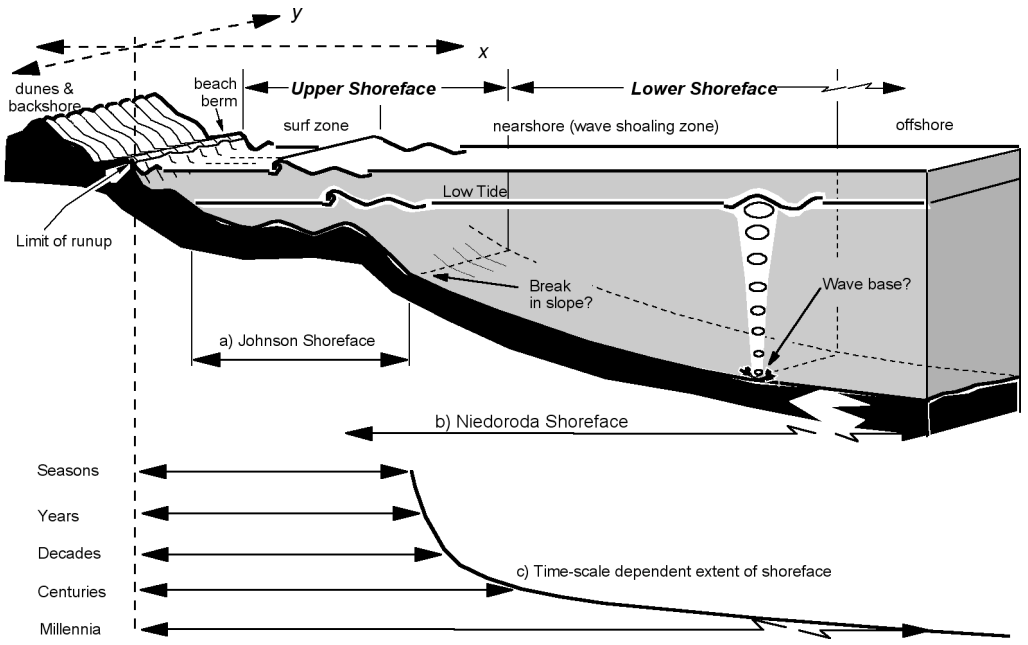

Figure 2.2: The shoreface (after Cowell et al, 1998)

Coastal ocean systems have developed due to the deposition of erosional products and organically produced particles towards the land ocean interface. These erosional products are primarily transferred by rivers, but also transfer by wind and local erosion, and local production may play a role. These products determine the coastal ocean bottom sediment, that is moved by the local water motions. These water motions are driven by several forces, primarily tides and wind. Tidal energy is confined to some small frequency bands, while the influence of wind and atmospheric variations is manifest over a wider frequency spectrum, varying from windwaves to storm surges (see Figure 2.3).

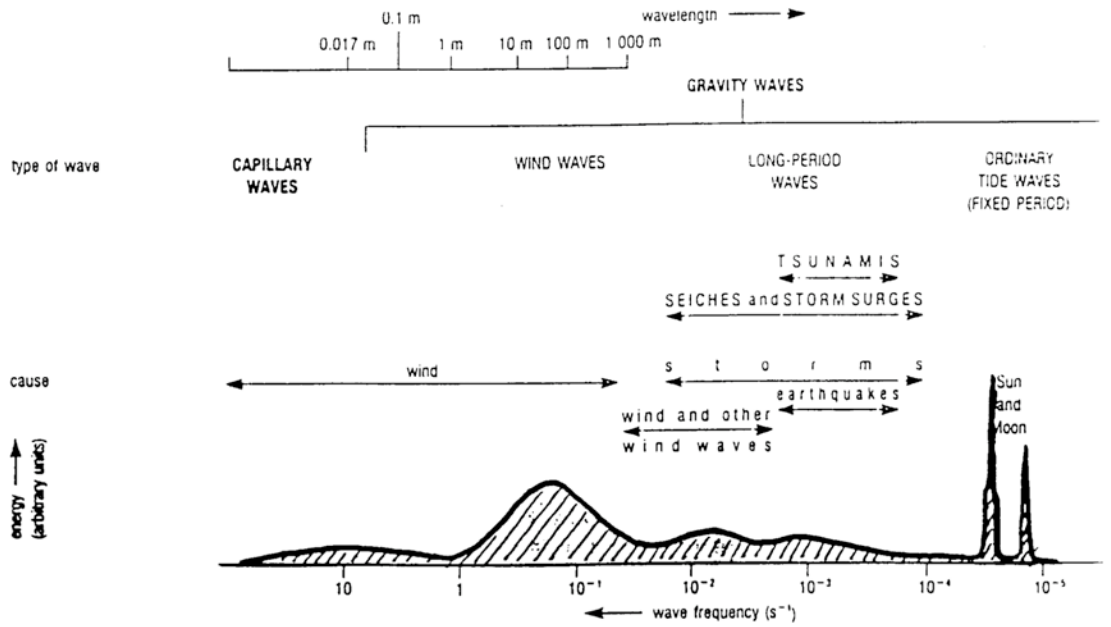

Figure 2.3: Energy spectrum in the coastal sea.

Table 2.1: Characteristics and importance of the coastal zone

THE COASTAL OCEAN'S PASSPORT
COASTAL OCEAN DATA
• occupies 18 % of the globe's surface • accounts for 25 % of the global primary production is the area where around 60% of the human population lives • is the area where between 60% and 70% of the world's cities with populations of over 1.6 million people are located • supplies approximately 90% of world fish catch
THE COASTAL OCEAN ACCOUNTS FOR
• 8% of the ocean surface • < 0.5% of the ocean volume • between 18% and 33% of global ocean production • 80% of the global organic matter burial • 90% of the global sedimentary mineralisation • 75% to 90% of the global sink of suspended river load and its associated elements/pollutants • in excess of 50% of pesent day global carbonate deposition

The importance of the coastal ocean systems both in physical, biological and human terms is highlighted in Table 2.1. This data explains why globally coastal areas are the areas with the largest growth in population and what is the importance of the coastal ocean for the ocean itself. In its turn, the importance of the oceans both for the global climate and its resources is indicated in Table 2.2. Clearly, pressures on the coastal ocean are of global impact. It is expected that these pressures increase in future due to:

- trends in tourism, population migration and transport, modifying physically large coastal areas, and threathening habitats and landscape,
- changes in land use and ineffective catchment management, causing coastal and marine pollution, in particular by diffuse pollution sources,
- overexploitation of resources, related to a lack of consistent institutional and legal frameworks, causing depletion of fish stocks and destruction of the coastal zone,
- climate change and sea level rise, causing coastal erosion and threathening safety of life and investments.

Table 2.2: Characteristics and importance of the ocean

THE OCEAN'S PASSPORT	
Sex:	male
Colour:	varying from greys and browns to deep-blue
Mean depth:	3,750 m
Largest depth:	11,034 m Marianen abyss, Phillippines
Water volume:	13,988,983 * 1000 km^3 (98 % of all water on earth)
Surface extent:	360,000,000 km^2 (70.8 % of the earth's surface)
Mean temperature:	varying from 30 degrees Celsius on the surface to 2 degrees celsius at the deepest location
Salt content:	34 to 37 grams per liter
Species:	1.7 milion known, between 5 and 100 million estimated, representing about 80 % of the earth's biodiversity
Married to:	the atmosphere
Children:	the world climate and the ocean circulation
Profession:	climate regulator, resource provider, fish producer, transport facilitator, garbage processor, therapist and inspirator
Coastal length:	504,000 km (a little more than 12 times the equator's circumvention)

In conclusion, it is obvious that knowledge of the physical dynamics of coastal inlets and tidal basins as important elements of the coastal ocean systems is a necessary prerequisite to allow for an efficient and sustainable development of these systems. This knowledge however needs to be translated into quantitative predictive abilities, for which these lectures intend to provide the skills.

2.2 Coastal classifications

(Source: P.D. Komar; Beach Processes and sedimentation.)

A variety of coastal features have been considered and generally referred to as erosional or accretional. It is worthwhile to further categorize coastal morphology in order to bring about a better understanding of the factors that are significant in controlling the morphology. This has led to the development of coastal-classification schemes. Coastal morphology reflects the complex imprint of the tectonic setting, modified by the combined actions of more local agents and processes. The resulting classifications have included purely descriptive schemes, as well as systems that relate to physical processes

important to the morphology.
The classification scheme developed by Inman and Nordstrom (1971) is modern in its outlook in that it is based on the concepts of global plate tectonics discovered in the 1960s. Inman and Nordstrom recognized that the gross aspects of the topography of a coast are related to its position on the moving tectonic plates. For example, this can explain the observed contrast in the west versus the east coasts of the United States, shorelines dominated, respectively, by erosion (i.e., sea cliffs, rocky headlands, etc.) and deposition (barrier islands). Along the northwest coast of the United States, portions of the tectonic plate in the ocean basin are moving eastward and colliding with the continental plate of North America. This collision has resulted in earthquakes, coastal uplift, and the formation of mountains immediately inland from the coast. In contrast, the east and Gulf coasts of the United States lie within the interior of the North American plate, and therefore experience little tectonic activity and are either stable or subside rather than being uplifted. Furthermore, larger quantities of sediments are delivered by rivers to the east and Gulf coasts due to the overall asymmetry of North America, with the largest mountains and divides located closer to the west coast.
Inman and Nordstrom (1971) have classified coasts into three categories according to their positions within the moving tectonic plates:

1. Collision coasts (convergent margins)
   - Continental collision coast: the margin of a thick continental plate colliding with a thin oceanic plate (e.g., west coasts of North and South America)
   - Island arc collision coasts: along island arcs where thin oceanic plates collide (e.g., the Aleutian island arc)
2. Trailing-edge coasts (divergent margins)
   - Neo-trailing-edge coasts: new trailing-edge coasts formed near beginning spreading centers and rifts (e.g., the Red Sea and Gulf of California)
   - Amero-trailing-edge coasts: the trailing edge of a continent having a collision coast on its opposite side (e.g., east coasts of the Americas)
   - Afro-trailing-edge coasts: the coast on the opposite side of the continent is also trailing (e.g., the east and west coasts of Africa)
3. Marginal sea coasts: coasts fronting on marginal seas and protected from the open ocean by island arcs (e.g., Korea)

Figure 2.4 shows the worldwide distribution of coastal and shelf types as determined by Inman and Nordstrom. They distinguish between Afro-trailing-edge coasts and Amero-trailingedge coasts due to differences in the resulting sediment supplies. As was pointed out previously, the east and Gulf coasts of the United States receive large quantities of sediments since many of the rivers originate in mountainous regions and have very large drainage basins.

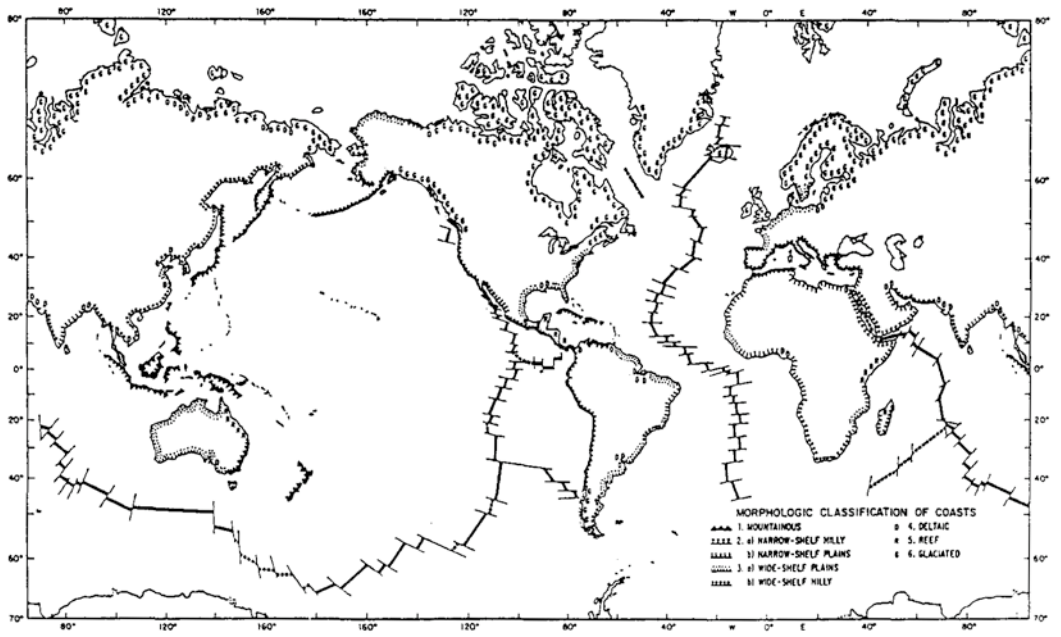

Figure 2.4: A tectonic-based classification of coasts.

This contrasts with Africa, which lacks significant mountains due to the absence of plate collisions, and accordingly smaller quantities of sediment are delivered to the coastal zone.

As noted by Inman and Nordstrom, the categories within their classification correspond at least grossly to the physical nature of the coast.The collision coasts are all relatively straight and mountainous and generally are characterized by sea cliffs, raised terraces, and narrow continental shelves. The trailing-edge types of coasts are more variable. The 'Amero" types have low-lying depositional coastal forms such as barrier islands and the widest continental shelves. The neo-trailing-edge coasts only recently have come into being, as spreading between two newly formed plates has split the continental crust apart. The coast is typically steep with beaches backed by sea cliffs, so in many respects these new-trailing-edge coasts are similar to collision coasts. The marginal-sea coasts have the greatest diversity of form. The land may be low lying or hilly, and the form of the coast can be dominated by local processes such as the formation of river deltas.

Inman and Nordstrom refer to the above-mentioned tectonic classification as the control on first-order features, the gross morphology of the coast. They further recognize the importance of second-order features superimposed on the first-order tectonic control. They have in mind the formation of river deltas, the development of barrier islands, the erosion of sea cliffs, special processes such as glaciation that produces fjords, and organic action that forms coral reefs and mangrove coastlines. This level of smaller-scale coastal features and processes has been the primary focus of most classifications. For example, Figure 2-5 is derived from the classification of Shepard (1976), which relates the groupings of such features to the level of coastal stability.

Such classifications can be useful in helping one to focus on the tectonic controls, geologic history, and the many processes that have shaped a specific area of shore or have given rise to a certain coastal landform. For example, Glaeser (1978) has examined the

global distribution of barrier islands in terms of the classification of Inman and Nordstrom (1971), leading to a better understanding of the physical setting required for the formation of that coastal landform.

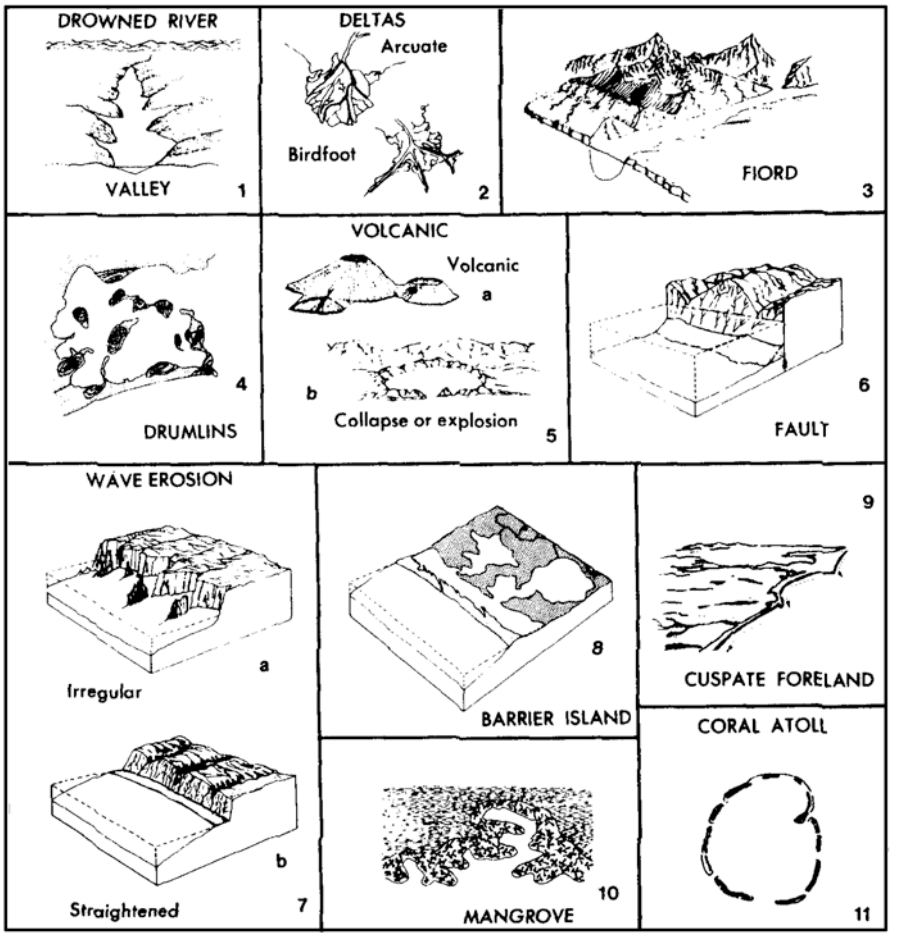

Figure 2.5: A coastal classification based on tne second-order level of features and processes, the tectonic settling being the first-order control.

2.3 Geological sea-level changes

The Quaternary, a period of the Cenozoic, the youngest geological area, is characterized by the occurrence of an alternatory interglacial and glacial climate at the higher latitudes of the northern hemisphere. These glacial-interglacial cycles occurred approximately every 100.000 year during the last one million years. The forcing factor is likely to be changes in the earth's radiation budget due to orbital parameter effects.
An important phenomenon of the Quaternary are changes in sea-level. During the cold periods -the glacials- enormous icecaps were developed, resulting in an important lowering of the oceanlevel (more than 100 m) and large parts of the Continental Shelf became dry land or coastal swamp. In Southeast Asia large parts of the Sunda Shelf became dry land or coastal swamp, accordingly fauna and flora could migrate from continental Asia to the present islands of the archipel (Indonesia and Malaysia). The melting down of the icecaps during the warmer periods – the interglacials – resulted in

the restoration of ocean level. These changes in sea-level are called "eustatic".

There are local and regional factors that influence the eustatic sea-level changes, such as upward and downward tectonic movements and compaction of sediments. Since these factors are difficult to separate from each other we use the terminology relative sea-level changes, thus indicating the combined result of eustatic, tectonic and compaction factors.

2.3.1 Old Concept

Until 1971 relative sea-level changes were thought to be caused by eustatic and tectonic movement. Thus, in so-named "stable areas", where no tectonic processes occurred, the observed sea-level changes were assumed to be due to eustatic effects only. The eustatic sea-level changes in the stable areas during the last 6,000 years, as reported by several authors, were rather divergent. There exist three groups of results:

- the oscillating sea-level (e.g. Fairbridge)
- the standing sea-level (e.g Fisk)
- the continuous rising sea-level (e.g. Shepard)

2.3.2 New Concept

The controversial findings of the above mentioned three groups could not be explained until a new concept of sea-level changes came into being due to a new geophysical concept. The definition of eustasy in the sense of worldwide simultaneous changes in sea-level is not correct.

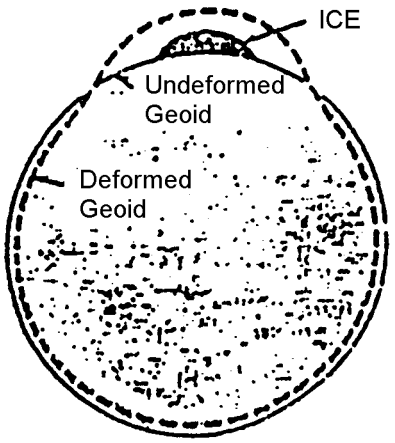

Figure 2.6: Sketch illustrating the sea-level movement, connected equipotential surface is a completely to gravity change. The deformed geoid is the sea-level position. The undeformed geoid is the spherical surface, the sea-level position after ice melting.

The sea-level is an equipotential surface of the earth’s gravity field (Figure 2.6). Sea-level can be measured only over the oceans but can also be defined at the land area, as the corresponding equipotential surface is a completely closed surface. Unlike ice, water can flow rapidly to create an equilibrium ocean surface on a gravitational equipotential surface, the geoid. The redistribution of water causes differential loading of the ocean basins and additional deformation of the ocean floor. This feed back process continues

until equilibrium is attained.

The above factors controlling sea-level are interrelated because both the ice sheets and the water load deform the earth's surface and perturb the geoid. Geophysicists have made a model of the deformation of the geoid and the earth's surface in the last 6000 years as a result of viscoelastic isostatic responses to water and ice loads (Clark et al, 1978). This model results in six zones (Figure 2.7) with typical relative sea-level change curves.

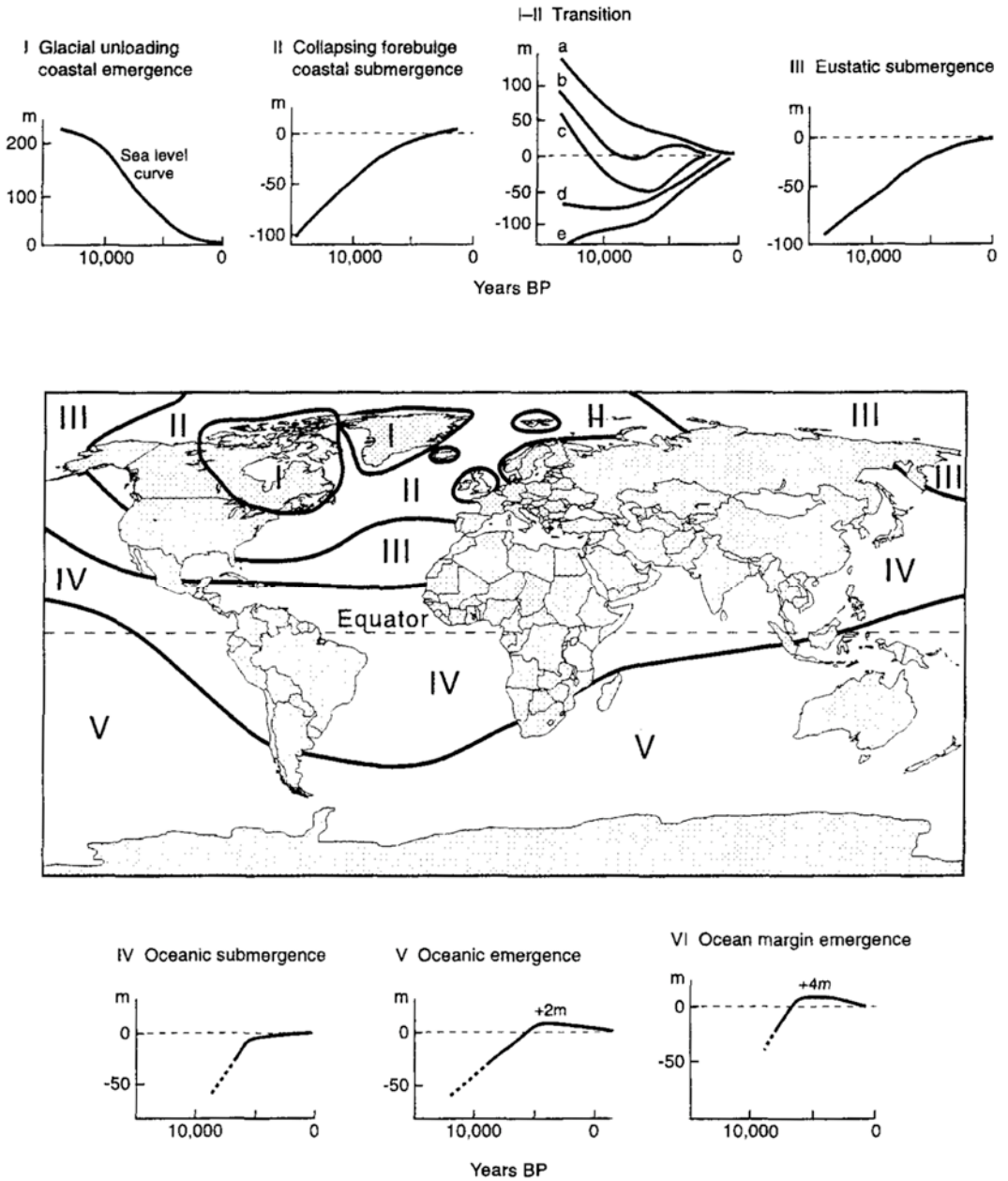

Figure 2.7: Global distribution of six sea-level zones resulting from retreat of northern hemispheric ice sheets (Clark et al 1978)

However, also the local tectonic environment of individual coastal areas and islands must be understoood. Figure 2.8 shows causes and effects, affecting both land and sea levels and resulting in relative sea-level changes. for instance, there are areas with important

tectonic movements like the earthquake zones in the western and southwestern pacific and in the mediterranean. In these areas shorelines can be uplifted, submerged and or tilted by these earth movements. Most deltas are situated in slowly subsiding sedimentary basins (tectonic subsidence between 2 and 10 cm per century).

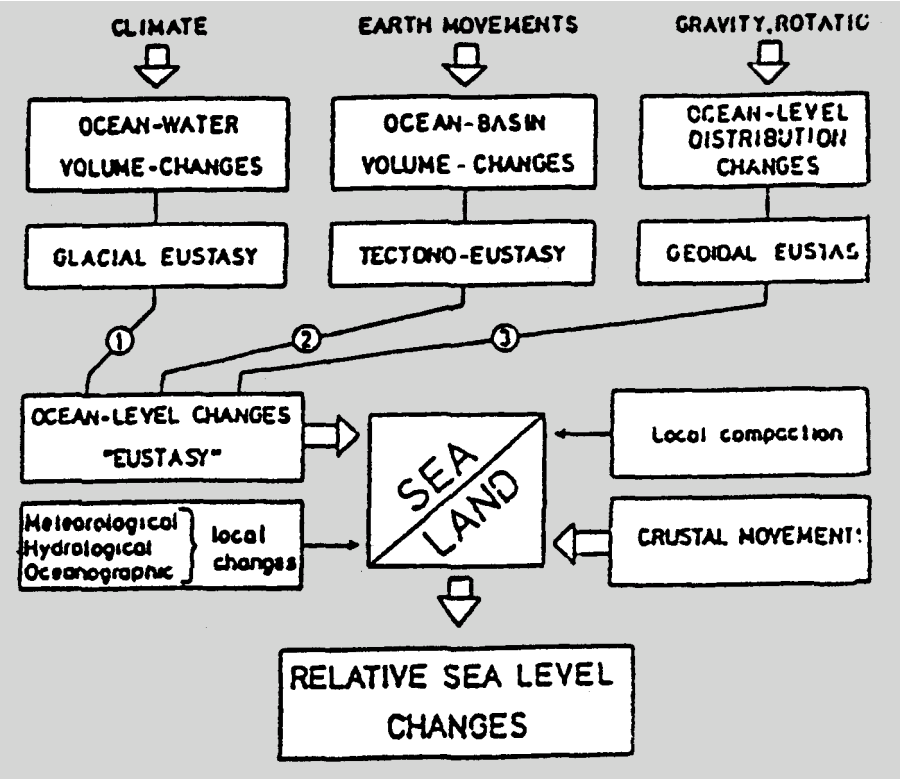

Figure 2.8: Processes controlling the factors which give rise to the three different types of eustacy. Together with crustal movements these largely determine the relative sea-level changes.

In conclusion, during the last 6,000 years, when the landicecaps had already nearly vanished, sealevel changes are due to the above mentioned local and regional factors. Accordingly, the curves of relative sea-level rise versus time show large local and regional variations.

Finally, in stable areas sea-level changes are as indicated in Figure 2.9.

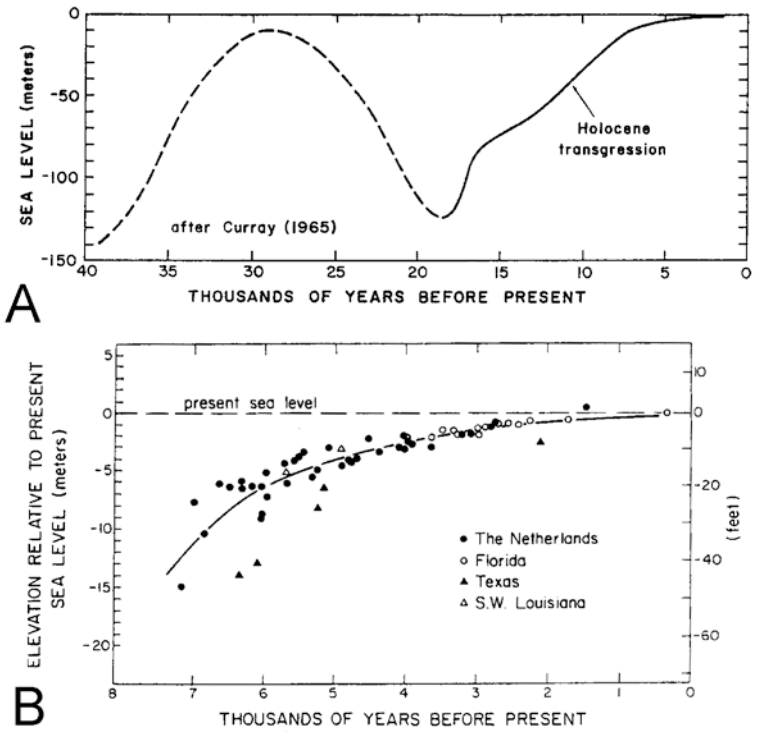

Figure 2.9: Indication sea-level changes in stable areas

2.4 Role of sea-level rise in Holocene coastal evolution

Bird's (1985) worldwide inventory indicates that approximately 70% of the world's sandy coastlines have shown retreat over the past few decades; less than 10% have shown net progradation, while the remaining 20% to 25% have remained approximately stable. While shore retreat on a geological time scale is undoubtedly connected with eustatic sea-level rise, it is more or less generally assumed that even the relatively small rate of sea-level rise of the last century is driving this worldwide tendency of shore retreat (cf. Vellinga and Leatherman, 1989). It must be borne in mind though that there generally exists a complicated interaction of agents affecting shore retreat (as illustrated in Figure 2.10). For instance, both the sea-level rise relative to the land and its effects are rather site-specific. Besides the eustatic sea-level rise local contributions can for instance be due to glacial rebound, subsidence, compaction, and changes in ocean circulation. Additional (and often dominating) causes of erosion can be due to longshore or cross-shore losses, which in their turn can be due to a variety of causes such as the physical geometry (e.g. headlands, submarine canyons), hydraulic boundary conditions (e.g. related to waves, tides, wind) or human interference (e.g. harbours, erosion mitigating structures). At a very high level of aggregation these latter losses can be summarized to be represented by the terminology "sediment availability". The following three literature references illustrate and confirm this description.

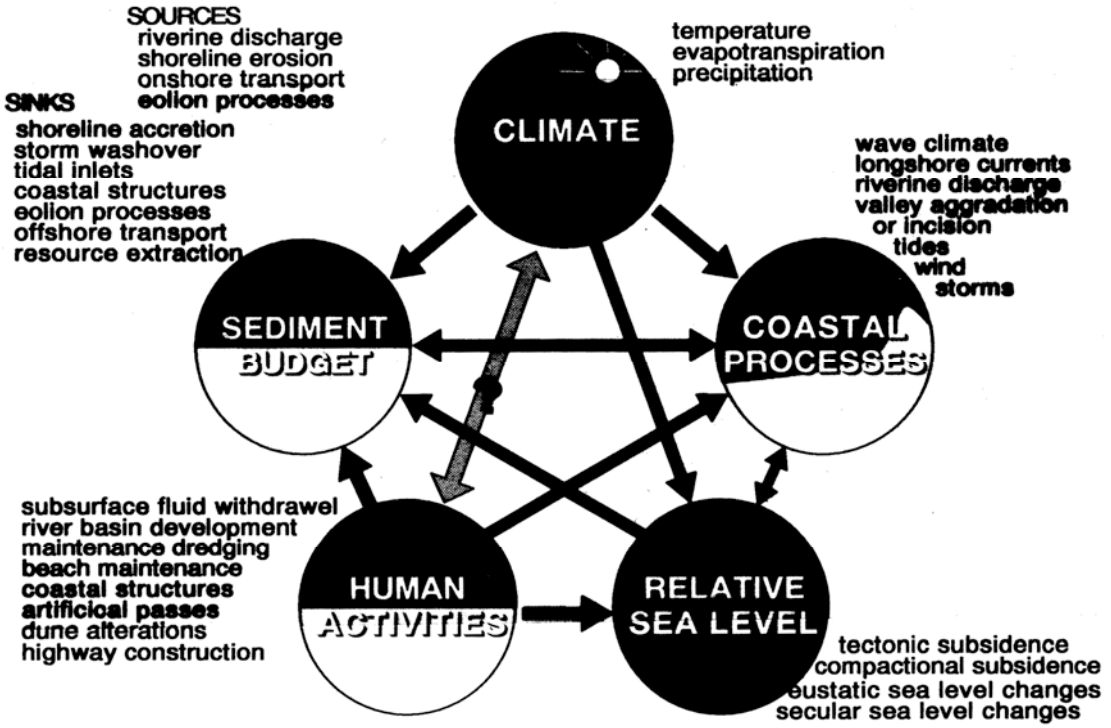

Figure 2.10: Interaction of agents affecting shore retreat and erosion (after Morton, 1977)

With respect to the behaviour of barriers, Curray (1964) summarized the effects of both relative sea-level changes and sediment availability on the displacement of the coastline in a qualitative way as follows. In the case of absence of a net source or a net sink for sediment regression occurs in the case of a falling sea-level or emergence and transgression occurs in the case of a rising sea-level or subsidence. With a net source of sediment the transition between regression and transgression shifts towards low levels of rising relative sea-level, and alternatively with a net sink of sediment towards low levels of falling relative sea-level.

Also, Swift (1976) adopts this basic "model" and adds to it by giving valuable specifications of the shifts mentioned above. He relates the presence of either a sink or a source for the upper shoreface to either longshore or cross-shore processes. In the longshore process sediment discharge by rivers is one of the more important factors, while for the cross-shore process the relative importance of storm and fair weather conditions is described.

For a larger variety of sedimentary environments the reasonably well-documented Holocene coastal evolution of the Netherlands (cf. Beets et al., 1990) gives the following qualitative picture of the role of sea-level rise (Van der Valk, 1990):

Table 2.3 Effects of sea-level rise on sedimentary environments in the western Netherlands (adapted from Van der Valk, 1990)

	rate of sea-level rise	
area	fast	slow
river	vertical architecture	horizontal architecture
peat-bog	drowning	spreading
tidal basin/estuary	drowning	surface stabilization
barrier	retreat	depending on sediment availability: nil : transgressive med : static high: regressive

Thus, the influence of relative sea-level rise is generally acknowledged, but the more precise quantification is a matter of discussion. In this context it is noteworthy that there is a large amount of literature devoted to the description and subsequent discussion of concepts to quantify the effect. One of the most wellknown concepts is that of Bruun (1954, 1962), which basically states that the shore profile is vertically invariant in space and time relative to mean sea level. If no sediment sinks and sources are introduced this determines the profile shift in a simple way. Valuable extensions of the concept and discussions on the validity of the concept have been made by Dean (see Dean, 1990, for a review). Here, it will be argued and discussed in more detail furtheron that the Bruun-concept is not a valid approach in general. In this context it is also important to note that time is required for equilibrium to be established. Often this point is not considered by coastal scientists. Hands (1983) noted that (a) the Bruun rule requires a lag if it is to predict shoreline behaviour and (b) the depth of the active profile increases as one considers longer timescales. Both of these conclusions are of relevance when considering shore nourishment in relation to sea-level rise.

Another important point that should be stressed here is that the timescale on which present sea-level rise influences coastal evolution in general and coastal erosion in particular, is relatively large. This is not generally true for coastal response in cases of larger rates of sea-level rise, since rapid sea-level rise induces rapid coastal response in general. Present coastal evolution on smaller time and space scales is dominated by other causes.

2.4.1 REFERENCES

Beets, D.J., Valk, B. van de, and Stive, M.J.F. (1991)
Holocene evolution of the coast of Holland
Marine Geology, 103, 423-443

Bird, E.C.F. (1985)
Coastline Changes - A Global Review
Chichester, Wiley Interscience, 219 p.

Bruun, P. (1954)
Coast erosion and the development of beach profiles
Techn. Mem. No. 44, Beach Erosion Board, U.S. Army Corps of Engineers

Bruun, P. (1962)
Sea-level rise as a cause of shore erosion
J. Waterways and Harbors Division, ASCE, Vol. 88, No. WW1, pp. 117-130
Curray, J.R. (1964)
Transgressions and regressions
in: R.L. Miller ed., Papers in Marine Geology, MacMillan, New York
Dean, R.G. (1990)
Beach response to sea level change
In: Le Méhauté, B. and Hanes, D.M., eds., The Sea, Vol 9, Wiley, New York
Hands, E.B. (1983)
Erosion of the Great Lakes due to changes in the waterlevel
In Komar, P.D., ed., Handbook of Coastal Processes and Erosion, CRC Press, Boca Raton, FL, p. 167-189
Morton, R.A. (1977)
Historical Shoreline Changes and Their Causes, Texas Gulf Coast
Trans. Gulf Coast Assoc. Geol. Soc, 27, 352-364
Swift, D.J.P. (1976)
Coastal Sedimentation
In: Marine Sediment Transport and Environmental Management
Stanley, D.J. and Swift, D.J.P., eds., Wiley, New York, p. 255-310
Van der Valk, L. (1990)
Holocene sea-level change and its geological consequences
Proc. 6th Congress Int. Ass. Eng. Geol., Amsterdam
Vellinga, P. and Leatherman, S.P. (1989)
Sea-level rise, consequences and policies
Climatic Change, 15: 175-189

2.5 Greenhouse effect, climate change and future sea-level changes

(Main Source: Commonwealth Secretariat, 1989, updated with IPCC FAR, 1990)

2.5.1 The Greenhouse effect

It has long been realised that the atmosphere acts in a similar way to the glass walls and roof of a greenhouse in trapping heat from the sun: the effect was described by John Tyndall in 1861. The possibility that increasing concentrations of carbon dioxide due to the burning of fossil fuel could lead to global warming was raised by Arrhenius in 1896, and he calculated that a doubling of carbon dioxide could raise average temperatures by 5º Celcius (note the correlation between carbon dioxide and global temperature, Figure 2.11). Another scientist, G.S. Callendar, attributed an apparent rise in surface temperatures from the 1880s to the 1930s to industrial pollution by carbon dioxide. Interest in the subject waned when the earlier temperature rise was not sustained. But it has returned with unprecedented strength now that evidence has accumulated of the rise

in atmospheric concentrations of carbon dioxide and other greenhouse gases and because there are now clear indications of an actual rise in global mean temperature. There is no scientific doubt that the atmospheric concentrations of a number of "greenhouse gases" capable of global warming have increased. Such gases are transparent to short-wave radiation, but retain long-wave radiation that would, in their absence, pass from the Earth into space, thus warming the Earth's surface and lower atmosphere. These gases (excluding water vapour, also a greenhouse gas) are (data from Bolin et al, 1986, and Warrick et al, 1988):

a) carbon dioxide (CO_2), whose atmospheric concentration has increased from an estimated 275 parts per million by volume (ppmv) in "pre-industrial" times (mid-eighteenth centruy) to 315 ppmv in 1958, and to about 350 ppmv in 1988;
b) methane (CH_4) which has increased annualy by about 15 parts per billion by volume (ppbv) (equivalent to a growth rate of 1.0 percent averaged over the ten years between 1975 and 1985), and has now reached over double the pre-industrial concentration of 700 ppbv;
c) nitrous oxide (N_2O) which has been increasing at about 0.25 per cent per year to reach about 310 ppbv by 1988, as against 280 ppbv in preindustrial times;
d) chlorofluorcarbons (CFC's), which increased rapidly (5 to 7 per cent per annum) throughout the 1970's.

In addition, tropospheric ozone, which is being produced near the earth's surface in industrialised areas as a result of chemical reactions involving hydrocarbons (largely from motor vehicle emissions) and nitrogen oxides, is also a greenhouse gas, but its contribution to the greenhouse effect is hard to estimate due in aprt to its high spatial and temporal variability.

The increasing concentration of greenhouse gases is the result of human activities related to energy use, agriculture and industrial expansion, especially the first. Some 65 to 90 per cent of the increase of carbon emissions in the atmosphere today is believed to come from the burning of "fossil fuels" (coal, oil, gas). The remainder presumably comes from the biosphere, and especially from the clearance of tropical forests.

It is generally accepted within the scientific community that the continuing increase in greenhouse gas concentrations will result in substantial global warming (see Figure 2.12 for an illustration of the principle system). There is, however, uncertainty over the magnitude and timing of the warming, the regional patterns of climate change, the seasonal differences, the effects on climate variablity and extreme events and the extent of changes in the global sea-level.

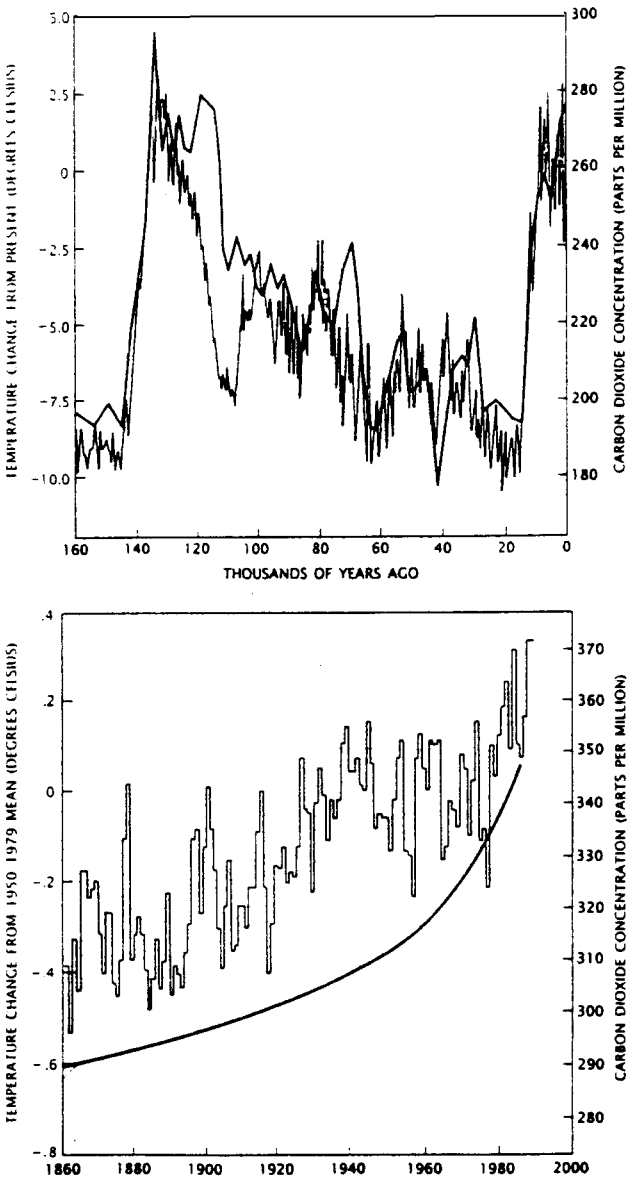

CARBON DIOXIDE AND TEMPERATURE are very closely correlated over the past 160,000 years (*top*) and, to a lesser extent, over the past 100 years (*bottom*). The long-term record, based on evidence from Antarctica, shows how the local temperature (*color*) and atmospheric carbon dioxide rose nearly in step as an ice age ended about 130,000 years ago, fell almost in synchrony at the onset of a new glacial period and rose again as the ice retreated about 10,000 years ago. The recent temperature record shows a slight global warming (*color*), as traced by workers at the Climatic Research Unit of the University of East Anglia. Whether the accompanying buildup of carbon dioxide in the atmosphere caused the half-degree warming is hotly debated.

Figure 2.11: From: S.H. Schneider, Scientific America, September 1989

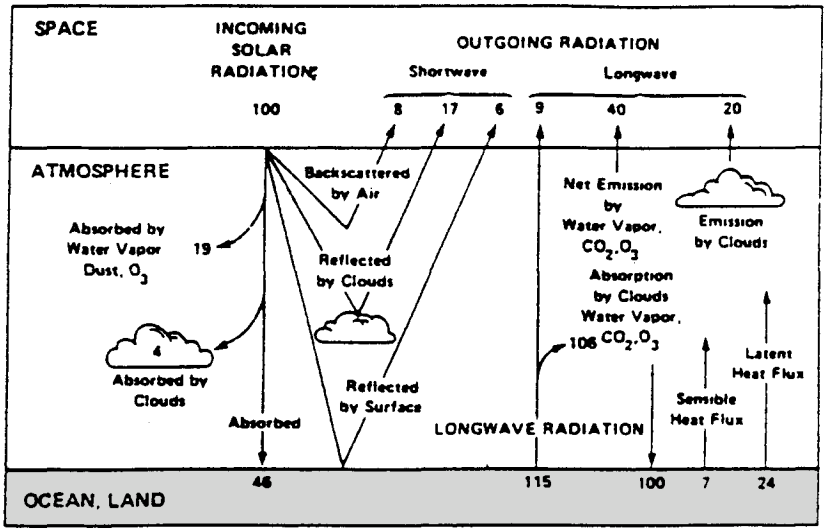

Figure 2.12: Earth's heat balance

Predictions of climate change depend on the validity of climate models and the accuracy with which trends in the greenhouse gas emissions and atmospheric concentrations are simulated. Many of those used sofar have grossly simplified the complex atmospheric system and, especially, have been unable to deal adequately with the crucial processes at the interface between atmosphere and ocean (e.g. Clark, 1982). Because of the resolution of global climate models, cloud processes are not adequately represented. Despite the uncertainties, however, the best models available today are consistent with one another in indicating a warming of global mean tempreature.

It is also important to model accurately the global carbon cycle. This is necessary in order to predict future CO2 concentrations, as well as to suggest ways of effectively preventing further increases. About half the carbon dioxide emitted today is taken up by the oceans, which provide the main "sink" for CO2, for example in the shape of limestone sediments. Carbon cycle modellers have difficulty, however, in balancing their carbon budgets, and some components of the carbon cycle are not well understood. For example, it is not clear how plant growth might be stimulated by higher CO2-concentrations and increase the global sink for CO2.

2.5.2 Climate change

Given the best estimates of the increase of greenhouse gas concentrations due to anthropogenic emissions it is most likely that during the next century these emissions could increase global mean temperature by 0.2ºC to 0.5ºC per decade if no additional steps are taken to reduce them (Business As Usual scenario, 1990 First Assessment Report by IPCC).

It is difficult to predict how climate will change within specific regions of the world (the 1990 FAR by IPCC gives some best regional estimates). The climate models are still unable to simulate reliably the regional details of climate. But there are reasons to expect that some parts of the world will experience climate chanegs significantly greater than the global average. The greatest warming is likely to occur in winter at high latitude (60-90º), especially in the northern hemisphere, and the least warming in the tropical latitudes

in summer. Climate models agree that global average precipitation should increase, with higher precipitation tending to occur in high latitudes in winter (see Table 2.4).

Table 2.4: Regional scenarios for climate change (Commonwealth, 1989)

Region	Temperature change (as a multiple of global average increase)		Precipation change
	Summer	Winter	
High latitudes (60-90 deg)	0.5 x to 0.7x	2.0x to 2.4x	Enhanced in winter
Mid latitudes (30-60 deg)	0.8x to 1.0x	1.2x to 1.4x	Possible reduced in summer
Low latitudes (0-30 deg)	0.9x to 0.7x	0.9x to 0.7x	Enhanced in places with heavy rainfall today

It is also likely that changes in climate will change the frequency of extreme events such as severe tropical storms, floods, droughts or extremes of heat. Some changes in climatic extremes could be relatively large. In the changed frequencies of short-term, climatic extremes the social impacts of long-term climate change are most likely to be manifested.

2.5.3 Sea level changes

There is a general consensus that global warming will be accompanied by a rise in global mean sea level. The best estimate for the policy scenario "Business As Usual" is that this will lie in between about 8 and 29 cm by 2030, and between 31 and 110 cm by 2100, with 66 cm as the best estimate of the average rise by 2100 (Figure 2.13). The main factors changing the ocean water volume are likely to be the melting of mountain glaciers and the expansion of the warming seas (see Table 2.4). Because of the slow process of heat transfer from atmosphere to ocean, and of the very long response times of polar ice, even if global warming stopped abruptly in 2030, global sea-level would continue to rise for many decades, and possibly hundreds or even many hundreds of years (Warrick et al, 1988).

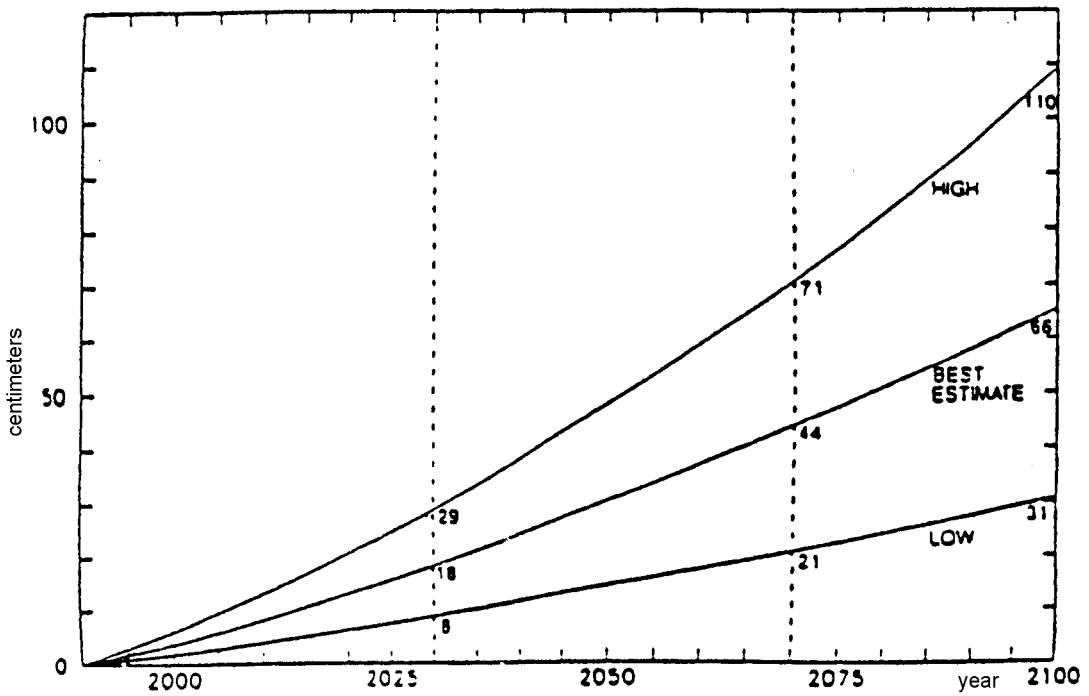

Figure 2.13: Global sea-level rize for Policy Scenario Business-as-Usual

Table 2.4: Factor contributing to sea-level rice in (cm) 1985-2030

	Thermal expansion	Mountain glaciers	Greenland	Antartica	Total
High	14.9 6.8	10.3	3.7	0.0	28.9
Best Estimate	10.1	7.0	1.8	0.6	18.3
Low	6.8	2.3	0.5	-0.8	8.7

3 Phenomenology of coastal inlets and tidal basins

3.1 Delineation of the coastal system type

In nature a large variety of coastal systems exists. As described in Section 2.2 a first-order classification (related to space scales of 1000's of km's) is based on global plate tectonics. The second-order features (related to space scales of 100's of km's) are numerous. One way to distinguish second-order features consists of looking at the hydraulic boundary forcings to the coastal system. Figure 3.1 indicates which coasts are subject to either ocean storms and swells (*storm-dominated*), to ocean currents (*ocean-dominated*), to locally generated wind waves (*wave-dominated*), or to tides (*tide-dominated*). Note that this classification does not take into account the influence of rivers (sediment supply, shorenormal circulation), of sediment type (silt, sand, shingle, rock), or of individual plate tectonics (out of equilibrium morphology).
The diversity is the result of the simultaneous occurrence of all coastal system determining factors in a nearly infinite number of combinations. That is why there exists no truly unique classification system of coastal ocean systems; and that is why one encounters a large variety of classification systems in literature. A classification which comes close to the one that is central in our lectures and that is relevant to the typical Netherlands situation (being an example of a marginal sea system; other ones being the Mexican gulf and the Chinese coast) and to trailing edge coasts (such as the USA east coast) is one that distinguishes river-dominated, tide-dominated and wave-dominated coastal systems (see Figure 3.2 for example sketches). In the hydraulic engineering education we focus on:

- tide-dominated systems (tidal bays and tidal lagoons);
- tide- and river-dominated systems (tidal rivers and estuaries);

- wave-dominated systems (uninterrupted coastal stretches);
- tide- and wave-dominated systems (coastal seas, coastal inlets, shorefaces).

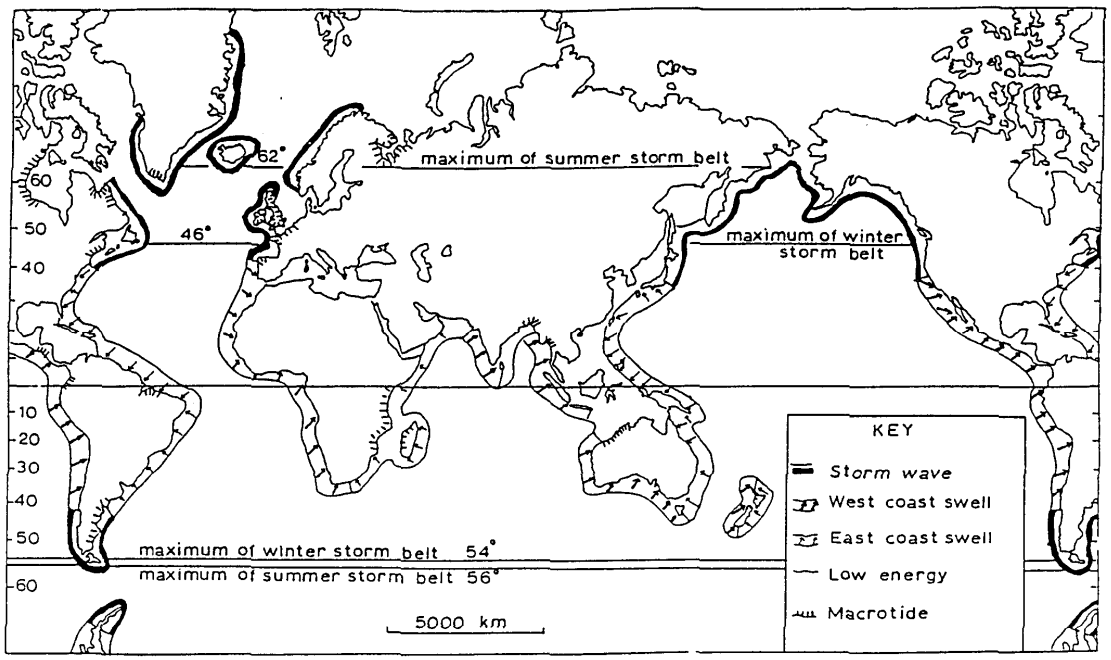

Figure 3.1: World distribution of wave types

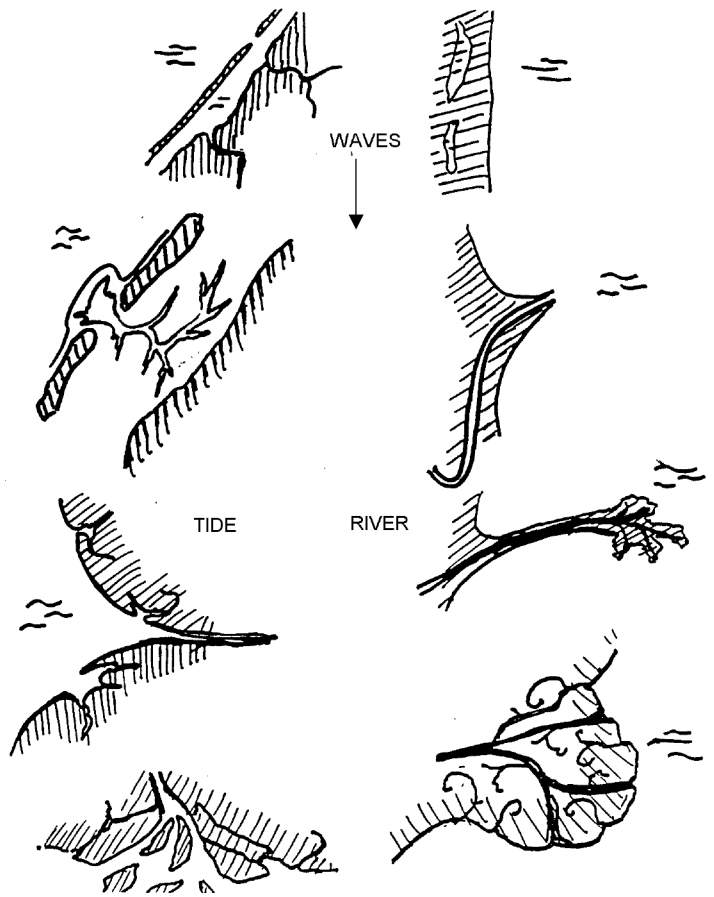

Figure 3.2: Example sketches different coastal systems

In these lectures we make a further restriction by focusing on relatively stable coastal inlets and tidal basins, where we define the latter to consist of tidal lagoons with approximately equal influx and outflux of water (e.g. Wadden Sea basins) and of estuaries with negligible influence of river run-off (western section of the Westerschelde, Oosterschelde, Haringvliet). The reason being we wish to refrain from giving due attention the fresh-salt water mixing problem, a topic which would require a rather extensive treatment. Before describing tidal basin characteristics in Section 3.3 and the coastal inlet characteristics in Section 3.4, we quote a more general description of "Tidal environments" given by Carter (1988).

3.2 Tidal environments: bays, lagoons and estuaries

(source: R.W.G. Carter; Coastal Environments, 1988)
Tidal conditions dominate where wave energy is relatively low. This may occur due to restricted fetch or where offshore conditions trap or deflect incident wave energy. Such environments include tidal bays, lagoons and estuaries. While there are affinities and overlaps between all three, each possesses a certain distinctiveness (see table 3.1), particularly relating to the mode of wave energy dissipation or exclusion and the presence of fresh and salt water, causing marine influences to be tempered by terrestrial ones.

Table 3.1: Distinctive attributes of tidal environments

Environment	Distinctive attributes
Tidal bays	
Baie de St. Michel	High levels of wave energy dissipation;
Normandy / Brittany	sediment fines onshore;
West coast of South Korea	little freshwaer run-off
Tidal lagoons	Waves exluded by barriers;
Wadden Sea,	Tidal flows via passes;
Netherlands/Germany/Denmark	infilling wetlands;
Laguna Madre, Texas	little freshwater run-off
Estuaries	Waves exluded by barriers or sand
Bay of Fundy, Nova Scotia	shoals;
Bristol Channel	high freshwater run-off

3.2.1 Lagoons

Tidal lagoons are water bodies entrapped behind coastal barriers. They have a surface or sub-surface connection with the sea allowing water levels to be modulated by the tide, although considerable distortion and attenuation of the tidal wave may occur within the confines of the lagoon. There are many types of tidal lagoons from almost semi-enclosed bays, like the Wadden Sea, to near-estuaries with significant freshwater throughputs. Despite the variety, the lagoon must not be viewed as a link between bays and estuaries. Almost 12% of the world's coastline is made up of barriers, many of them enclosing lagoons. There are many studies investigating barrier-lagoon systems, and it is

clear that no one process prevails in their information and maintenance, rather a set of co-dominate and sub-ordinate processes. It is divided into three parts: barriers, lagoons and tidal passes, but you should bear in mind that such a tripartite is somewhat false, as all three are highly intertwined.

There are three basic categories of lagoons, based on the water volume and the mode of water exchange between the sea and the lagoon (see table 3.2). In most cases the tidal fluxes in and out of the lagoon are balanced over a tidal period. Water flows into the lagoon with the flood and out during the ebb. Propagation of the tidal wave is affected by the geometry and nature of the barrier as well as the traces of the previous incursion. The volume of exchanged water is known as the tidal prism. This may be estimated crudely by measuring the lagoon area up to the tidal limit and multiplying by the tidal range. In some cases the seawater input exceeds due to evaporation. These lagoons are called sabkhas and are common on low-latitude arid coasts.

Table 3.2: Types of lagoons

Hydraulic balance	Barrier form
Inflow = outflow	Pass - back barrier
(tidal)	Seepage - throughflow lagoon
(wave set-up)	Reef - atoll
Inflow > outflow	Sabkha
Inflow < outflow	Pass - estuary
	Seepage - liman

Figure 3.3 (Carter (19)) gives an overview of the Wadden Sea. Many of the Wadden Sea passes have distinct catchment areas separated by a low watershed or wantide zone, conducive to fine-grain deposition. Large tidal eddies are common along the back barrier flanks, sometimes superimposed on a unidirectional stream creating a spiralling current.

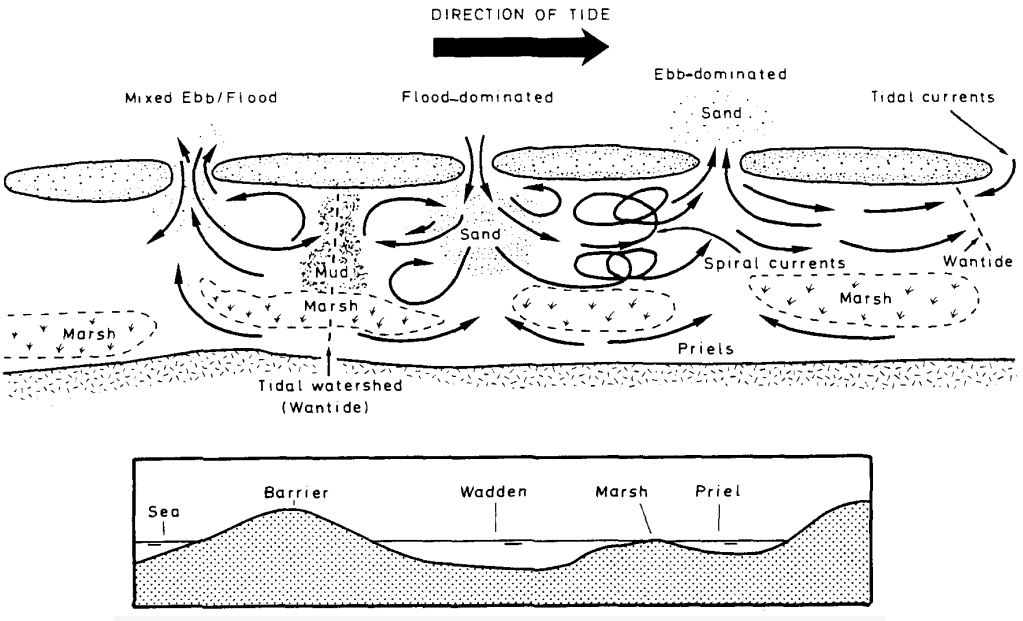

Figure 3.3: The Wadden Sea tidal dynamics model, displaying the types of tidal passes and the wantide zones. The movement of tide is from left to right.

3.2.2 Estuaries

Discharge of terrestrial runoff and its associated transport products to the sea results in a mingling of processes and a mixing of mass. Mingling may take place within a discrete basin or estuary, often semi-enclosed by a seaward barrier. An estuary is a somewhat 'hybrid' environment incorporating terrestrial and marine, lake and ocean dynamics. Estuaries are semi-enclosed water bodies, connected to the sea, within which seawater is measurably diluted by freshwater. Interaction of two chemically and physically-different water masses gives rise to complex sedimentological and biological process and patterns. Estuaries, unlike river mouths, tend to be tide-dominated.
Almost without exception estuaries are basins of non-marine origin that have been invaded by the sea. Many estuaries are the result of marine flooding due to the global rise in the post-glacial sea-level. Some of them are further constricted by the development of spits, shoals or barriers across their mouths. Processes of basin formation include tectonic subsidence, fluvial erosion and glacial action.
The most fundamental characteristic of an estuary is the interaction between salt- and fresh water. This leads to a common classification by salinity structure relating to the degree of separation or mixing of the two water masses. Three different mixing regimes are identified: stratified, partially mixed and mixed or homogeneous.
In stratified estuaries the fresh- and saltwater masses remain distinct. As the less dense fresh water meets the salt water, so it overrides it. The landward-facing gradient of the salt wedge is proportional to the hydraulic force of the freshwater internal waves, which may break causing entrainment of saltwater particles within the seaward-flowing fresh water. Eventually this process mixes the two water masses. To maintain continuity, salt water moves upstream, creating opposing currents at the wedge front. Near the bottom this counteraction favours deposition.
Tidal waves propagating into estuaries may be either progressive or standing waves, or a mixture of the two. In long narrow estuaries a multi-nodal standing wave and tide may develop.

3.3 Tidal basins

Tide-dominated coasts, with relatively stable inlets and basins, are characterised by a large number of inlets having ebb- and flood-tidal deltas, giving access to tidal basins. These were created by breakthroughs and flooding of coastal plains as sea level rose or by abandonce of river branches forming deltas. Bottom subsidence of the coastal plains due to human interferences (peat-harvesting, empoldering, water, oil and gas extraction) is sometimes an additional cause for the creation of tidal basins.
The characteristic morphology of tidal basins is that of a meandering, braided and/or branched channelsystem, ebb- and flood chutes, intertidal sand and mud flats, and marshes. Along barrier island coasts the basins are often rectangular or near square, and the channel structure is often more branched than braided. The branching structure is found to show fractal characteristics. Not seldomly, rivers discharge in tidal basins. When this concerns larger rivers the tidal basin is often funnel shaped, and the channel

structure is more braided than branched.
If in the latter case the river discharge is large, there exists a transitional region in the basin between salt and fresh water. As described in section 3.2, these basins are called estuaries. In the case of small and medium discharges the salt-fresh water transition region is located near the river mouth, which is then called the estuary. In the more seaward region the tidal water motion dominates and the water is mainly saline. In the more landward region the river flow dominates and the water is mainly fresh. The pressure gradient associated with the density difference between the saline (of sea origin mainly) water and the upstream fresh river water drives a vertical flow circulation, the so-called estuarine circulation. Along the bottom the flow is net (i.e tidally averaged) landward, while it is seaward along the surface. This phenomenon contributes to the formation of the turbidity maximum, which is the concentration of fine sediments at the end of the salt water wedge.
In short tidal basins the tidal wave is reflected and it has a standing character. When these basins are long enough the tidal wave resonates. When they are even longer the tidal wave is dampened by friction and the reflected wave is weak, so that the tidal wave has a propagating character. However, the tidal propagation is of such nonlinear nature, that we may not really speak of a wave-like motion. In most tidal basins the tidal discharges are largest in the inlet gorge, while decreasing in landward direction. This is associated with a decrease of the discharging cross-sectional area, which leads to the typical funnel-shaped river mouth. Tidal-asymmetry and estuarine circulation also play a role in this shaping.
Caused by the large tidal discharges in the inlet gorge there is a strong sediment exchange between the basin and the adjacent coast. In the divergent ebb-tidal discharging flow, the flow velocities decrease and sediment is deposited, thus creating the ebb-tidal or outer delta which displays a variety of dynamic phenomena (see section 3.4).
Also inside the tidal basin there exists a morphologic activity, primarily driven by the interaction between bottom morphology and tidal motion. This interaction is the cause of a complex three-dimensional structure of residual circulations, which are both cause and result of the morphologic structures of the basins. In a meandering channel residual circulations are the cause of a spiralling flow structure. Sedimentation, erosion and sand- and marshflats are connected with these flow-structures.
Within the basin the tide is deformed by bottom friction and other non-linear effects associated with the basin geometry. This tidal distortion causes both an asymmetry between high- and low-water flow change. These asymmetries greatly impact on the net movement of sediment, both sand and silt. Also, the turbidity maximum is determined by the tidal asymmetry. In tidal basins with an extremely strong tide (amplitudes of the order of 10 m) the tidal wave is deformed so strongly that a tidal bore may develop. The tidal flood wave is than of such strength that a “wall of water” enters the basin. Examples of such basins are the Amazone, the Tsientang and the Severn.
Examples of tidally dominated coastal systems of the estuarine type are the Schelde, the Thames, the Elbe (all three in the winter season), the Seine, the Yangtse, the Mekong, the Ganges-Brahmaputra, the Fly River, Chesapeake Bay and the Rio de la Plata.

Examples of tidal basins without strong river influence are the Irish Sea, the Channel, the (Eastern) Wadden Sea, the Oosterschelde, the Gulf of St.Lawrence, Colorado River, San Francisco Bay (the latter two both in summer).

3.4 The ebb tidal delta or outer delta

(sources: Steyn & Sha / vd Berg)

3.4.1 Introduction

A typical ebb tidal delta includes a main ebb channel, channel margin linear bars, a terminal lobe, swash platforms and bars, and marginal flood channels (Figure 3.4). It is noted that the flood channels as these occur, for instance, at the inlets at the SW of the Netherlands are not marginal at all, but quite distinct.

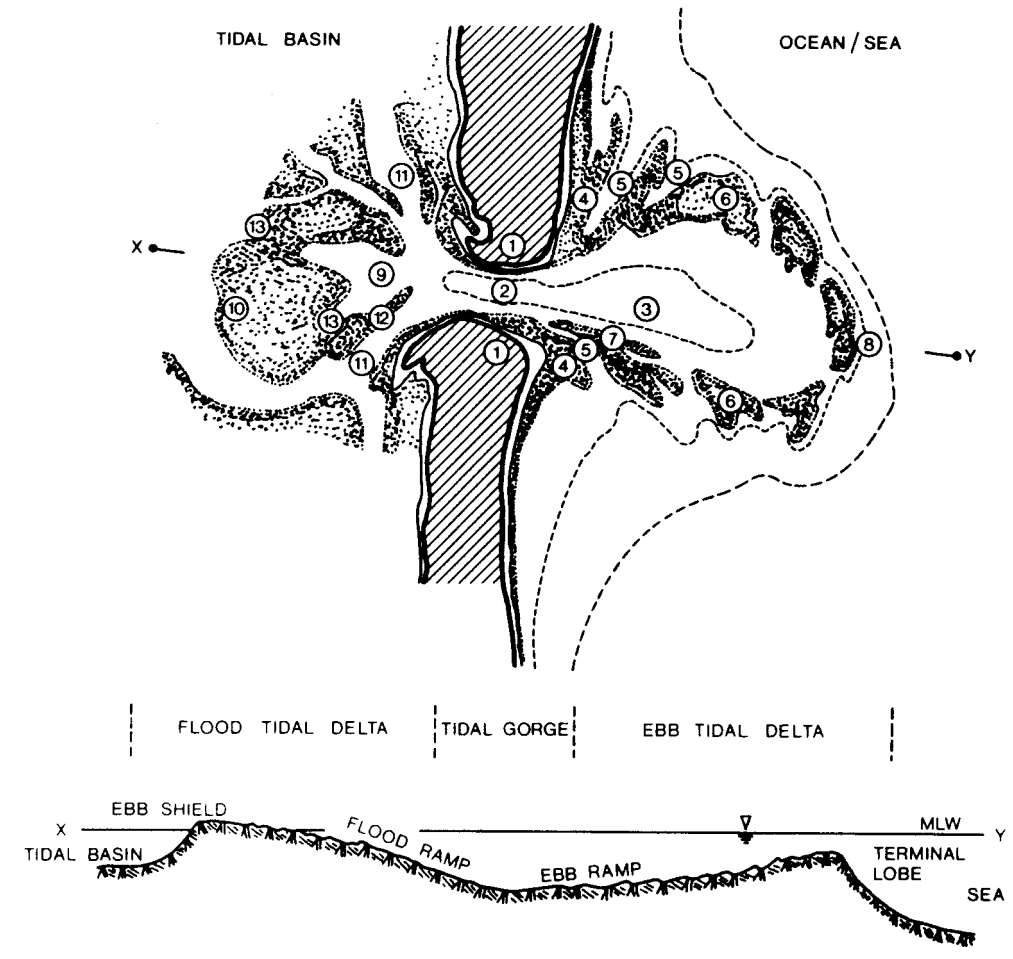

1) coastal barrier or spit headland;
2) the tidal gorge;
3) the main ebb channel and ebb ramp;
4) swash platforms;
5) marginal flood channels;
6) marginal shoals;
7) ebb tidal levee;
8) ebb delta terminal lobe;
9) the flood ramp;
10) the ebb shield;
11) main ebb dominated inner channels;
12) ebb spit;
13) spill over channels.

Figure 3.4: Morphological units of tidal inlets

The channel margin linear bars flank the ebb tidal channel and are deposits built up by the interaction between flood- and ebb tidal currents with wave-generated currents. In the Dutch inlets these distinct bars are not recognisable; in stead, there are wide flats. The terminal lobe is a rather steep seaward-sloping body of sand, which forms the outer end of the ebb tidal delta. The main ebb channel is flanked by swash platforms, which are broad sheets of sand. On these swash platforms, isolated swash bars can be recognised, built up by swash action of waves. Marginal flood channels usually occur between the barrier islands coast and the swash platforms. The boundaries of the ebb tidal delta can be found via the no-inlet bathymetry: where the differences in bottom height is nil between the actual and no-inlet bathymetry.
The occurrence of ebb- and flood dominated tidal channels is of prime importance to the morphology of the ebb tidal delta. Postma (1967) explains this phenomenon by the time-velocity asymmetry of tidal currents: the maximum ebb- and flood currents do not occur at mid tide. Often the maximum ebb currents occur near low water. The flood currents therefore, choose the way of least resistance, i.e. around the margin of the delta. The overall morphology of the ebb tidal delta depends on the interaction of tidal currents and waves. Generally speaking, the ebb tidal delta morphology is determined by the (dynamic) balance between a net offshore directed sediment flux induced by the inlet currents (ebb dominance) and a net onshore directed sediment flux induced by offshore waves. Although, these principles can not solely explain the ebb tidal delta morphology, it gives a basic explanation for the apparent mechanism that "holds the ebb tidal delta together".

3.4.2 Sediment

The great importance of the ebb tidal delta can be indicated by the volume of sand that is accumulated in this delta. This volume will be larger in case of low onshore directed wave energy and large tidal forces. Under these circumstances the ebb tidal delta can extend far seawards without a distinct terminal lobe. Quite often the volume of sand deposited in an ebb tidal delta is much larger then the total volume of the adjacent barrier beaches. Although the governing physical processes are not yet fully understood, sediment exchange takes place between the adjacent barrier beaches and the ebb tidal delta. The volume of sand stored in the ebb tidal delta is related to the tidal prism of the backbarrier system and the wave climate, see Figure 3.5 Even small changes herein (by nature or human interference’s) may result in changes of the volumetric contents of the ebb tidal delta. For example, suppose the tidal prism of an inlet is enlarged after flooding of part of the hinterland. According to the empirical relationships (Figure 3.5), this will result in an enlargement of the volumetric contents of the ebb tidal delta.

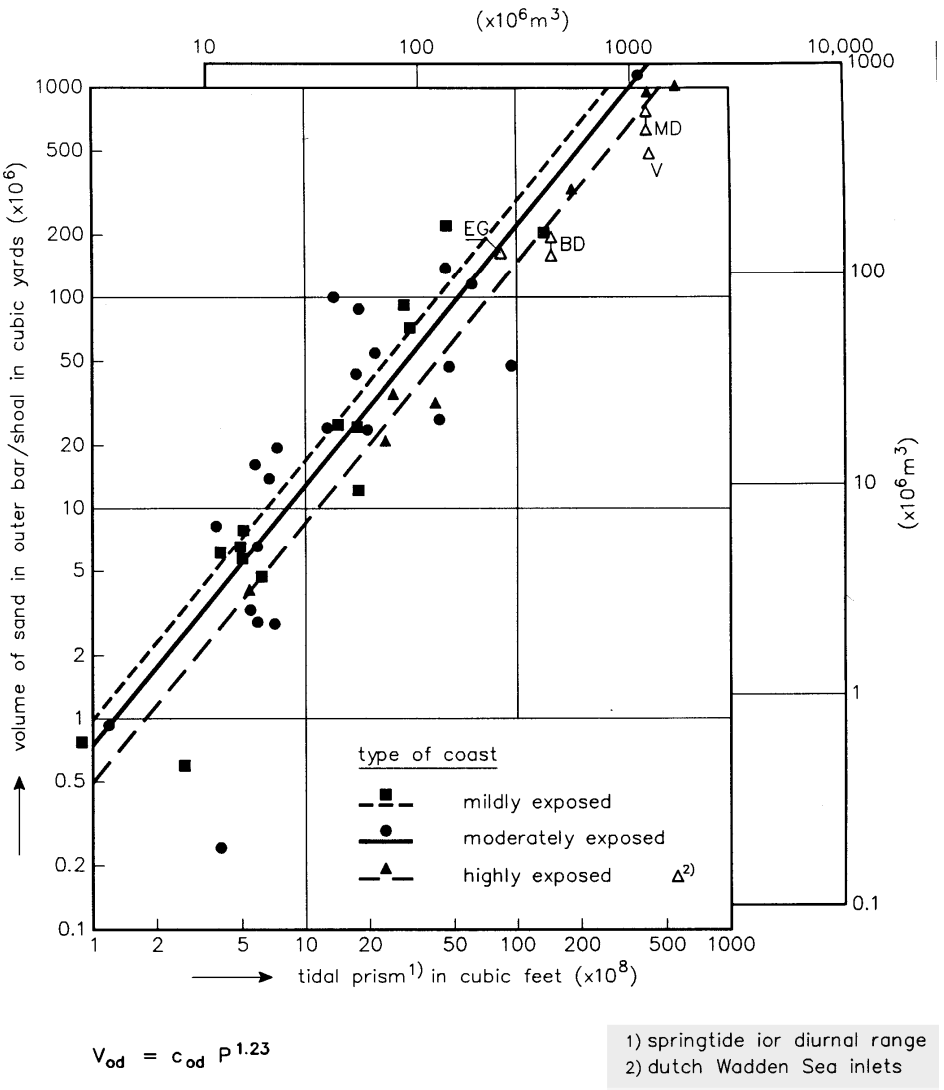

Figure 3.5: Emperical relationship between tidal prism and the volume of sand in the outer delta

The sediment required for this enlargement may originate from the adjacent barrier coast, the backbarrier system or from offshore. Most probably it will be a combination of these three sources, the distribution of which is very hard to determine without thorough knowledge of the underlying physics. Probably, erosion of tidal gullies will contribute relatively most to the ‘sand demand’ of the (ebb) tidal delta, because of the relatively small morphological time scales of such adjustments. Due to increased flow velocities the tidal channels will (immediately) start to erode. The eroded material will mainly be deposited at the ebb tidal delta where the flow decelerates. On the other hand, the contributions of the adjacent barrier coasts are much more vulnerable as small changes in the sediment balance may cause severe coastline retreats.

3.4.3 Hydrodynamic classification

The tidal range outside an inlet depends primarily on the ocean tides and their interaction with the continental shelf. The wave conditions are generated seaward (and thus independently) of the inlet. Since both parameters are independent of the inlet system

configuration they are very suitable to be used for classification.
An inverse relation between tidal range and the length of a barrier island seems present: large tidal ranges apparently result in shorter barrier islands. Hayes e.a. (1979) used the following classification:

- microtidal, tidal range < 1.0 m
- low mesotidal, tidal range 1.0 - 2.0 m
- high mesotidal, tidal range 2.0 - 3.5 m
- low macrotidal, tidal range 3.5 - 5.5 m
- high macrotidal, tidal range > 5.5 m

Wave action is generally considered to act as a bulldozer on the tidal inlet morphology (Hageman, 1969); it moves sediment onshore and limits the area over which the ebb tidal delta can spread out. The wave climate is generally characterised by the mean significant wave height H_s on a yearly average basis:

- low wave energy, $H_s < 0.6$ m
- medium wave energy, $0.6 \text{ m} < H_s < 1.5$ m
- high wave energy, $H_s > 1.5$ m

The actual classification of tidal inlets is based on a combination of the tidal range and wave energy classification as described above, because the relative effect of waves and tides is really important. Hayes distinguishes the following five classes of tidal inlets with respect to tidal/wave dominance:

1. wave dominated inlets
2. mixed energy - wave dominant
3. mixed energy - tide dominant
4. tide dominated - low
5. tide dominated - high

This hydrodynamical classification is shown in Figure 3.6. Each class develops its own specific morphologic features, viz.:

Ad 1 Wave dominant inlets have long continuous barriers, with only few tidal inlets and a lot of washovers.

Ad 2 Mixed energy inlets (wave dominant) have a larger number of inlets and a smaller number of washovers. The size of the ebb-tidal delta will become somewhat larger.

Ad 3 Mixed energy coasts (tide dominant) have abundant tidal inlets, larger ebb tidal deltas and usually drumstick barriers.

Ad 4 Tide dominated inlets (low dominance) occasionally show wave built bars. Transitional forms can be recognized.

Ad 5 Tide dominated (high dominance) are characterised by predominant tidal

current ridges, extensive salt marshes and tidal flats. Inlets of this type often have large ebb tidal deltas and very deep inlet gorges.

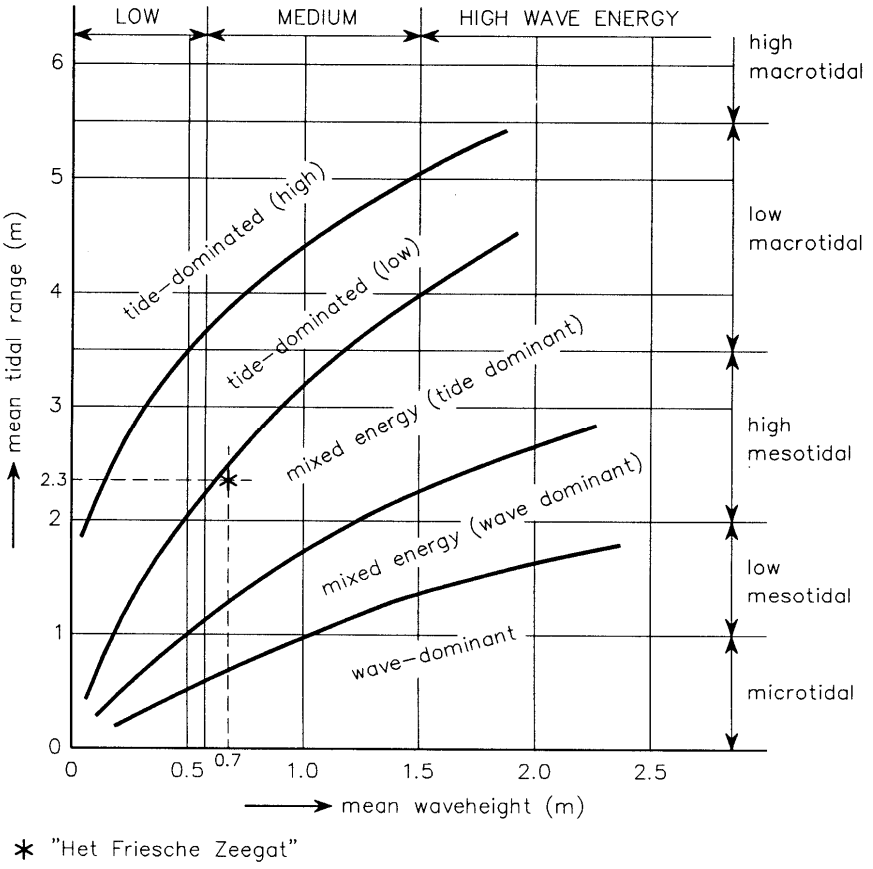

Figure 3.6: Hydrodynamical classification of tidal inlets.

For classification of tidal inlets not only the above relative dominance of waves or tides is important, but also the surface area of the inlet basin.

3.4.4 Geometry

The geometry of ebb tidal deltas largely depends on offshore wave climate and characteristics of the tidal regime. This is described by van den Berg and Sha (1993), using the tidal inlets in the south-western part of the Netherlands and those at the western Wadden Sea as study material.

The tidal wave propagates along the North Sea coast in north-east direction, while the amplitude of the tidal wave rapidly diminishes from about 4 m near Vlissingen to 1.7 m at Hoek van Holland. A minimum value of less than 1.4m is reached south of Den Helder. The tidal range then gradually increases north-eastward along the West and East Frisian Islands coast to about 3 m.

Along the West and East Frisian Islands the longshore tidal currents reach their maximum at about mid-tide water level. A rather contrasting situation is found along the SW-part of the Netherlands. Here, the relatively large difference in tidal range results in significant longshore water surface gradients at low and high water levels. For this reason and because of the hysteresis effects the curve of the horizontal tide lags about

three hours behind the curve of the vertical tide, resulting in a coincidence of maximum longshore directed flood- and ebb-tidal currents with the high and low water levels respectively.
In Figure 3.7 possible inlet flow patterns over the tidal cycle are shown for these two basic cases. It is noted that a flat bottom topography and a tidal wave propagation from left to right is assumed.

Case 1: no phase differences are present (Wadden Sea inlets). Two basic flow patterns (marked as A and B) can be recognised. The flow concentrates on the left side of the inlet.

Case 2: the phase difference equals a quarter of the tidal period (SW-part of the Netherlands). Now, eight different flow patterns (marked as A to H) can be recognised.

The effect of waves on this concept is shown schematically in the lower drawing of Figure 3.7. Four situations are considered here: A and B correspond with the Wadden Sea inlets, i.e. no phase differences, and C and D correspond with the SW-coast, i.e. with a phase difference of a quarter of the tidal cycle. The direction of the energy flux is from the right (so opposing to the direction of the tidal wave propagation) for situation A and C, and from the left (so in line with the tidal wave propagation) for situations B and D. The table in figure.3.7 gives classification of several Dutch inlets according to this scheme. This classification has been compared by van den Berg (1987) with the appearance of these inlets in 1850, well before human interventions in the systems. The agreement is good. It shows that:

- the inlets in the south western part of the Netherlands were typically type C inlets (with a slight southward located ebb channel due to wave flux coming from the north), and that
- the Wadden Sea inlets were typically type B inlets (with more distinct westward located main ebb channel due to the zero-phase lag of the tidal currents at open sea and in the inlet gorge; the predominant wave energy flux reduces this effect).

It should be noted however, that the difference in morphology between type B and C is not very large. The only noticeable difference is the orientation of the main ebb-channel, which is subject to periodic changes as well.

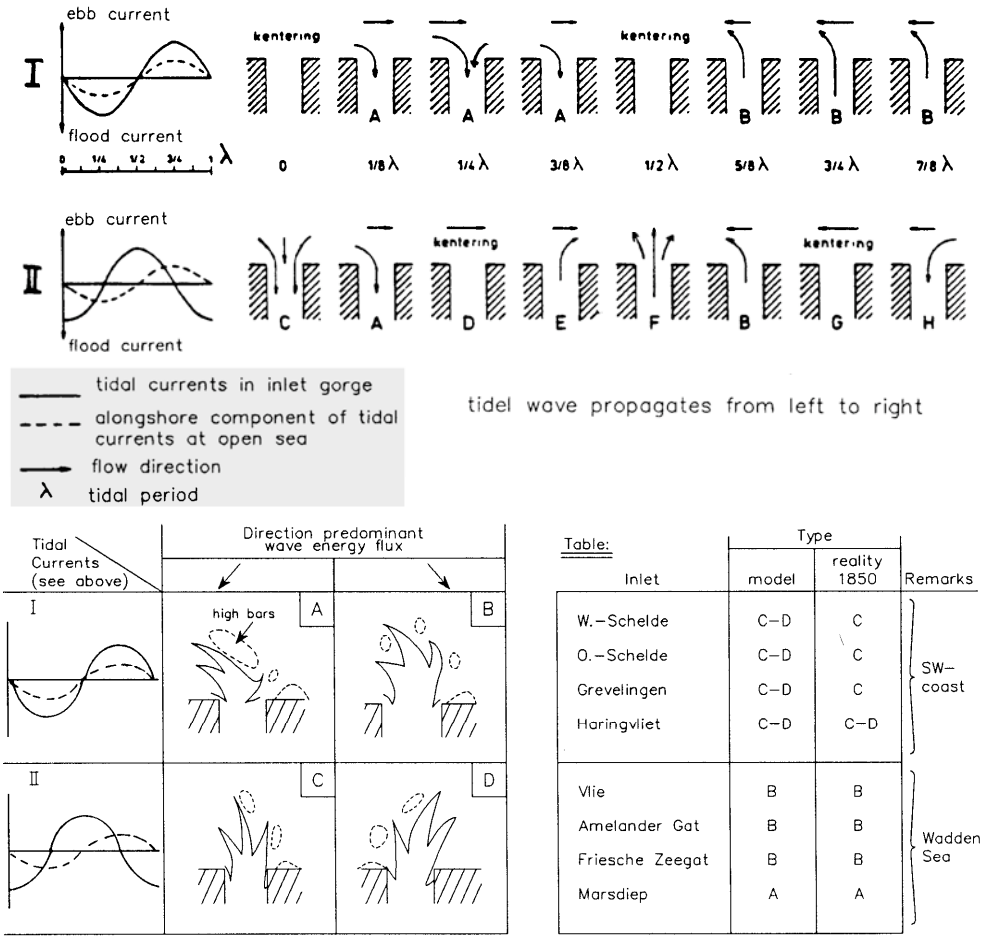

Figure 3.7: Effect of interaction of tidal currents on inlet morphology

3.4.5 Processes at the outer delta

The main processes acting in the outer delta are the waves and the tides. The morphology of the outer delta depends on the interaction of these tidal currents and waves and is determined by the balance between the offshore transport, caused by the ebb tidal currents, and the wave action. The sediment circulation at the outer delta can be thought of as an intermittent process, according to de Vriend and Bakker (19..), in which the sediment is transported, deposited and picked up, depending on the prevailing conditions. For transport near the gorge the representative conditions are moderate waves and a tide slightly above the mean (Steijn and Hartsuiker 1992) whereas the transport along the delta margin requires higher representative waves. If the inlet is in equilibrium then a balance exists, the sediment fluxes due to tidal and wave effects form a closed circulation system.

By-passing of tidal inlets

If the waves approach the coast at an angle, there will be a longshore drift along the coast. The outer delta forms a barrier for the longshore transport of sediment which may enter the inlet via the flood channel or may be transported from the updrift island to the downdrift island either around or over the delta. This result in the long term sediment

transport paths that are not closed but spiral or zigzag along the delta as indicated in Figure 3.8.

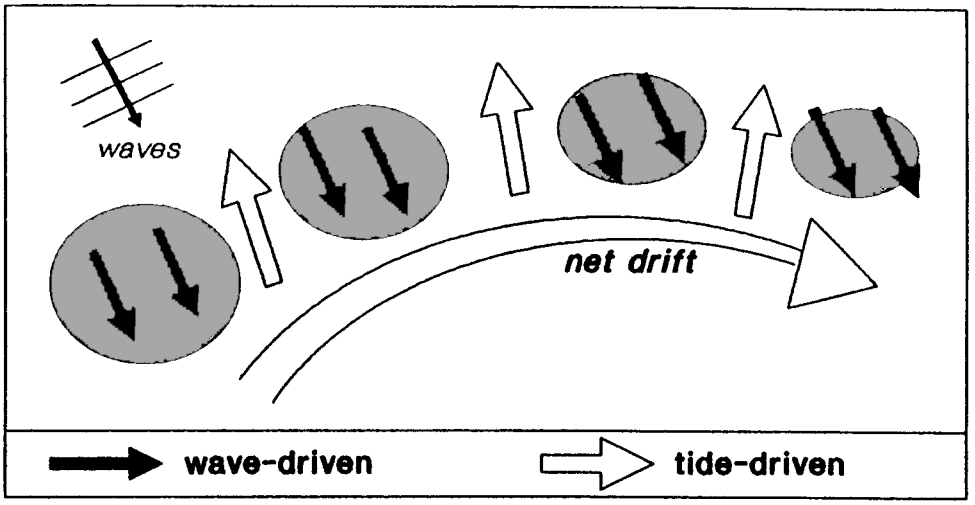

Figure 3.8: Residual drift via the shoals on the terminal lobe of the outer delta

Sediment by-passing is defined as the process which allows material, after a short interruption caused by an inlet, pass, channel, jetty, or other type of littoral barrier, to become part again of the normal littoral drift zone a short distance downdrift from the littoral barrier. Bruun & Gerritsen (1959) describe the two main principles of by-passing by natural action:

1. by-passing via offshore bars, and
2. by-passing by tidal flow action.

1. Bar-by-passing

The upper sketch of Figure 3.9 shows an inlet with a submerged bar. Littoral drift "simply" continues over the submerged bar to the down-drift barrier island. The integrated longshore drift capacity is kept at the same level. If the littoral drift (and its distribution cross-shore) is known for profile AA, i.e. the normal beach, it is possible to estimate the required dimensions (depth and width) of the submerged bar. In the lower sketch of Figure 3.9, this principle is shown. By increasing amounts of littoral drift the depth of the bar will decrease and its width will increase. The depth over the bar is usually limited to the breaker depth for storm waves.
This type of by-passing can only occur in situations with considerable wave action. Bar by-passing is rather hazardous for navigation, as any (dredged) channel will be subject to sand deposition. For navigation purposes these type of tidal inlets are often "improved" by jetties. However, mostly these improvements only are temporarily effective and require maintenance dredging after some time.

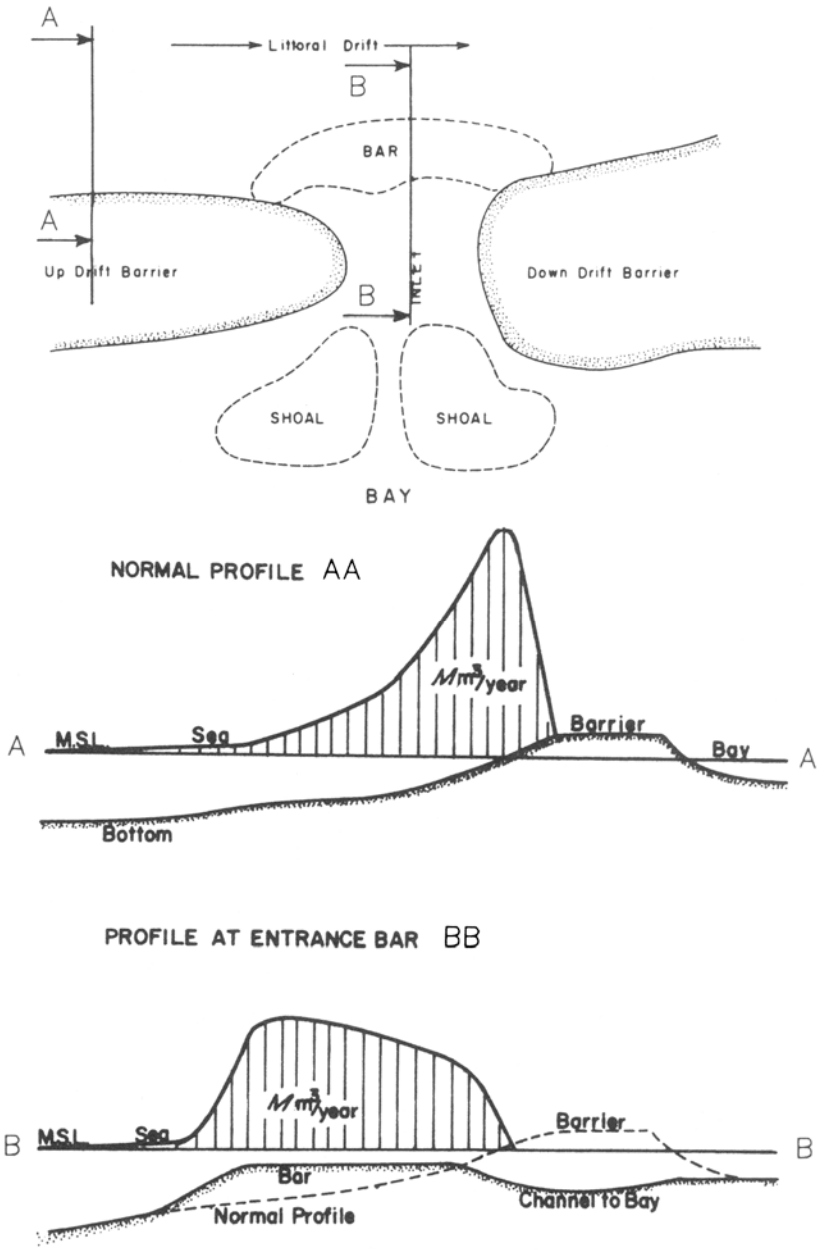

Figure 3.9 : By-passing principle on a submerged bar

2. Tidal flow by-passing

When tidal flow plays an important part in the by-passing of material, sand transfer can take place in two different ways, viz.:

- migration of channels and bars. Tidal channels can migrate over the inlet throat. Figure 3.10 shows two phases of an inlet/channel system. A new channel has developed and another has disappeared. Generally, tidal channels migrate in downdrift direction.

  One of the reasons for this may be that littoral material is deposited on the updrift banks of the channels forcing the shift down-drift. Another process forcing curved channels to migrate is the meandering capacity, as also occurs in rivers. The bars in between the channels may follow this migration and occasionally join the

downdrift barrier coast.

- transport by tidal flow in the channels. The vectors in Figure 3.10 indicate the resultant direction of sediment transport in the flood- and ebb channels.

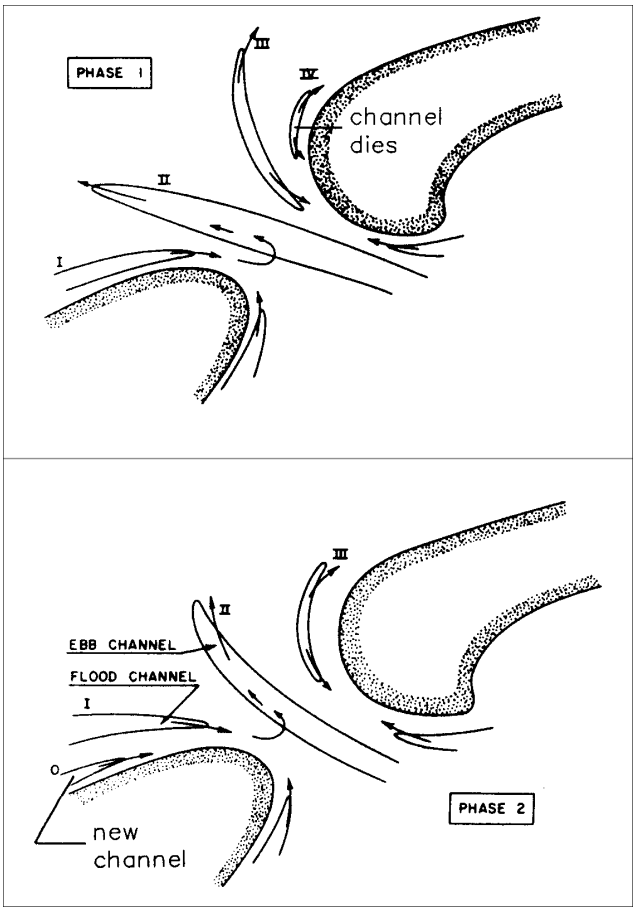

Figure 3.10: Migration of tidal inlet channels. Vectors indicatw resultant direction of snad transport in flood and abb channels.

Bruun & Gerritsen (1959) propose a parameter r to indicate the type of bypassing:

$$r = \frac{M_{\text{mean}}}{Q_{\text{max}}} \tag{3.1}$$

in which:
M_{mean} is the mean value for the longshore sediment transport rate to the inlet
Q_{max} is the maximum discharge through the inlet during spring tide.

In case $r < 10 – 20$, predominantly tidal flow by-passing will occur. In case $r >$ 200 – 300, predominantly bar by-passing will occur. For intermediate values of r an intermediate type of by-passing will occur. Later Bruun and Gerritsen (1960) and Bruun (1978) converted the expression for r to:

$$r = \frac{P}{M_{\text{max}}} \tag{2.2}$$

in which:
P is the tidal prism (cubic meters per tidal cycle)
M_{tot} the total littoral drift (cubic meters per year).

The stability of the inlet (in terms of by-pass capacity) expressed in this latter expression for is as follows:

$r < 20$:	inlets become unstable non-permanent overflow channels
$20 < r < 50$:	the inlets are typical bar-by-passers
$50 < r < 150$:	the entrance bars are still pronounced (combination of bar-by-passing and flow-by-passing);
$r > 150$	the inlets are predominant tidal flow by-passers (little bar and good flushing).

Equation (2.2) is a commonly used and accepted criterion. Bruun (1991) mentions that he obtains more and more examples that fit in the description. Backgrounds of the expression are given in Bruun, e.a. (1974).

Table 3.3: Stability figures of some tidal inlets.

Inlet	Tidal Prism P [m^3/half cycle] *10^6	Total Littotal Drift M_{tot} [m^3/y] *10^6	r	Stability	Comments
Inlet of Texel, Holland	1.000	~ 1	~	good	↕ Wadden Sea Inlets going from West to East
Eyerlandse Gat, Holland	200	~ 1	1.000	good	
Inlet of the Vlie, Holland	900	~ 1	~ 200	good	
Borndiep, Holland	500	~ 1	~ 900	good	
Friesche zeegat, Holland	300	< 1 (est.)	~ 500	good	
Nordeneyer Seegat,	160	< 1 (est.)	~ 400	good	
Germany	42	< 1 (est.)	~ 250	poor/fair	
Wichter Ee, Germany	110	< 1 (est.)	~ 60	fair	
Otzumer Balje, Germany	14	0.1	~150	fair	
John's Pass, Florida	20	0.1	140	good	
Longboat Pass, Florida	60	1	200	poor/fair	
Aveiro, Portugal	10	0.01	60	fair	
Big Pass, Florida	20	0.3	100	poor/fair	
Masonboro Inlet, Florida	3	0.1	70	poor	
Saratosa Pass, Florida	700	0.6	30	good	
Penang Harbour, Malaysia	10	0.6	~	poor	
Krishnapatam, India	100	0.8	1.000	fair	jettied inlet
Thybor∅n, Denmark	40	0.1	17	good	weir jetty
East Pass, Florida	60	1	120	poor/fair	
Oregon Inlet, N.-Car	47	1.6	400	poor	
Tan My, Vietnam			60		
			30		

In Table 3.3 some values for r are given (from: Bruun, 1978). The tidal inlets along the West-Frisian Barrier islands all show a large value for r, which indicates that tidal flow by-passing is dominant. In general, increased values of r produce greater seaward

displacement of inlet bars (Oertel, 1988). The first eight inlets in Table 3.3 are Wadden Sea inlets. The given values for r show that r is decreasing in eastward direction. This seems to correspond with the occurrence of sand ridges at the more easterly located inlets.

Following the early work of Bruun and Gerritsen (1959), FitzGerald (1988) proposed three explanatory models for inlet sediment by-passing along mixed energy coasts (Figure 3.11).

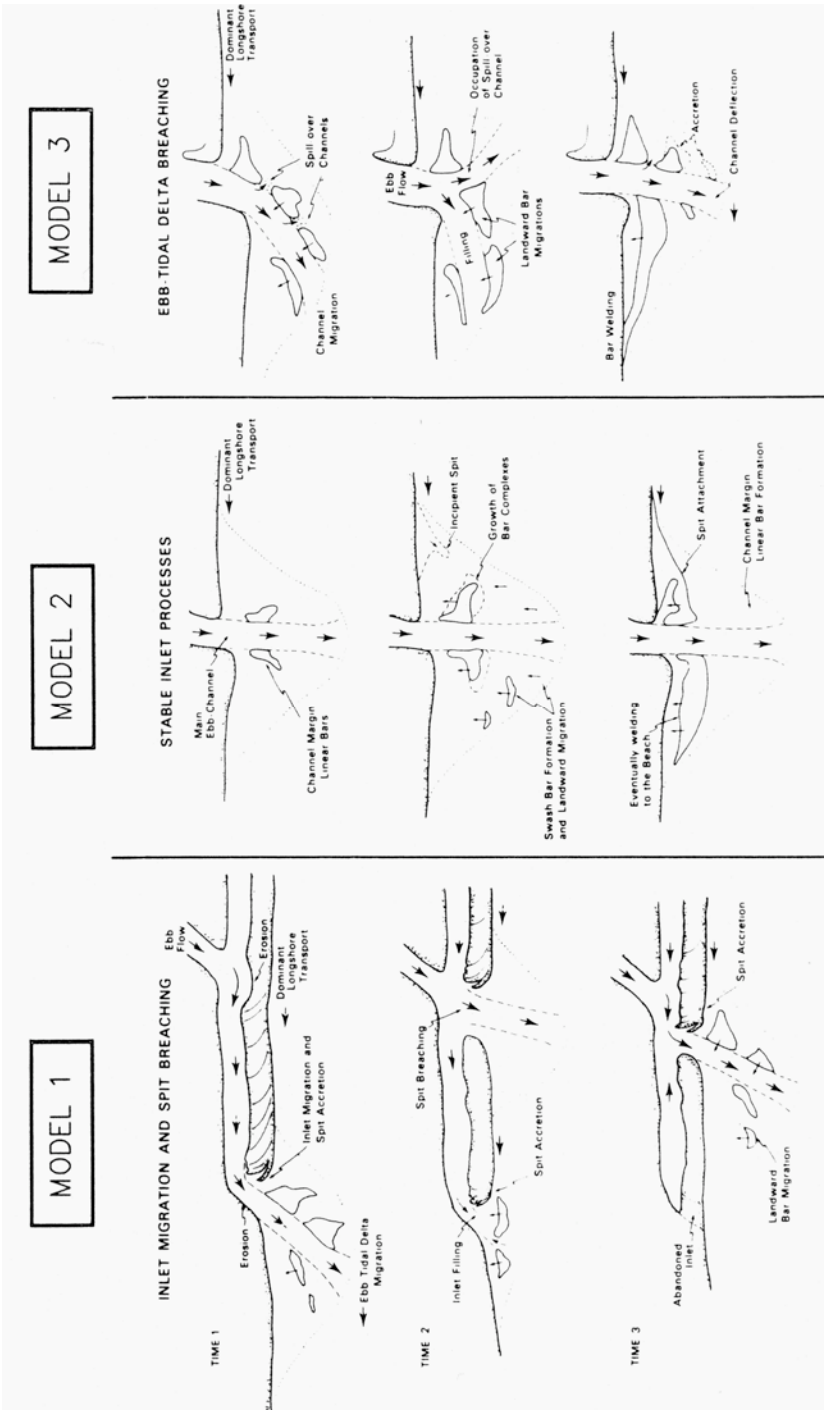

Figure 3.11: Models of inlet sediment by-passing

Model 1: Inlet migration and spit breaching

Littoral material transported to a tidal inlet can cause constriction of the inlet throat. The decrease in cross-sectional area will result in greater scouring capacities, which will cause erosion of the downdrift barrier beaches. The rate of migration is dependent on sediment supply, wave energy, tidal currents and the composition of the channel bank. The inlet channel in this way is elongated, which results in a lower discharge efficiency. When after a storm a short-cut has been created, this new channel will take over from the old one. The new location of such an inlet is rather difficult to predict, but it is quite often located just in front of the ebb channel. Once the old inlet has attached to the downdrift coast, a large quantity of sand has by-passed the inlet. Most inlets migrate downdrift, however, some examples exist of updrift migration.

Model 2: Stable inlet processes

Stable inlets have a stable throat position and a non-migrating main ebb channel. Sand by-passing at these inlets occur through the formation of bars which migrate and attach to the downdrift coast. These large bars have been formed by the stacking and coalescing of wave built accumulations of sand (swash bars) on the ebb tidal delta platform. Due to flood dominance at these parts of the ebb tidal delta in combination with breaking and shoaling waves, the swash bars move onshore. New bars will constantly develop due to a more or less continuous sand delivery by the ebb tidal channel. Thus, sediment by-passing in this model depends on sand deliveries through the channel system.

The rate of migration of the swash bars decreases when they reach the coast. FitzGerald (1988) explains this as the swash bars gain a greater intertidal exposure when they migrate up the shoreface. Thus, wave swash operates over an increasingly shorter period of the tidal cycle. The deceleration of the migration of swash bars results in the stacking and coalescing of individual bars to large bar complexes. These bars can be 1 - 2 km long and 100 - 250 m wide. The size of the bar complexes and the time required for the bars to migrate onshore decreases as the size of the inlet decreases.

Model 3: Ebb-tidal delta breaching

Tidal inlets that by-pass sediments by ebb-tidal delta breaching have a stable inlet throat position, but a variable position of the main ebb tidal channel. The main ebb channel will be pushed towards the downdrift coast by the predominant littoral drift. In a similar way as described for model 1, the flow efficiency of this elongated channel decreases and hydraulic gradients over the bars steadily increase. The inlet will divert its flow to a more seaward direction via so-called spillover lobe channels. Consequently, the discharge through the old ebb channel decreases. The result is that a large portion of the ebb tidal delta sand bodies is by-passed.

FitzGerald (1988) mentions that in real tidal inlets all three by-pass processes can occur simultaneously or may dominate alternately. The movement of sand along the terminal lobe by wave action is almost always present at mixed-energy coasts.

An interesting feature of bar complexes that approach a downdrift coast is the formation of tombolos on this coast. An example of this is shown for the north-eastern end of

Kiawah Island, South Carolina (FitzGerald, 1988). Basically, the bar complex acts as a sort of offshore breakwater, reducing the littoral drift capacity between the bar and the coast (sheltering effect).

3.4.6 Human interference

Removal of sand from the outer delta

The sand in the outer delta may be used as a sand source for, say, beach nourishment or it may be necessary to dredge navigation channels through the outer delta. In both of these cases the sand is removed from the inlet system and the inlet will have been disturbed from the "equilibrium state". Since the tidal prism and the protrusion ratio of the delta remain constant, the supply of sand into the inlet via the flood channels does not change.
The delta will retreat rapidly, while the barrier islands show no erosion in the first few years. This trend reverses however, as the outer delta will demand sand in order to return to its equilibrium state. Assuming that the inlet is a "closed system" then the demanded sand will be supplied by the barrier island coastlines.
The erosion of the barrier islands will begin on the foreshore, the beach profile steepens and gradually the erosion of the beach will become evident. Since the erosion of the barrier islands occurs tens of years after the dredging, the cause of the erosion may not be linked to the dredging operation.
In order to minimise this additional erosion it may be wise to consider the option of dredging sand from the inner delta instead of from the outer delta. The final result, after 100 years, is the same as for the previous case but that the delta retreats more slowly and to a lesser extent. This will reduce the additional erosion on the downdrift island.
If the amount of sand removed from the inlet system per year is less than or equal to the total volume of sand transported into the inlet per year via the flood channels, then the effects of dredging the inner and outer delta will be the same.

Effects of the construction of a groin on the updrift island

The construction of a groin on the updrift island will trap sediment that previously entered the inlet via the updrift flood channels. Not only can one expect lee-side erosion but the outer delta and the downdrift island will also erode.
The outer delta act as a buffer for the other elements of the inlet system. When sand is removed from one portion of the inlet the outer delta will respond by sharing sand with the other elements but this supply is only a "short term loan" which will be repaid by the adjacent coastlines in the longer term.
So erosion of the outer delta can be expected to occur rapidly, while on the downdrift island this will take place after tens of years.
In the case of a longer groin, more sand will be trapped behind the groin and it will also take more time before by-passing begins and consequently the erosion of the outer delta and the downdrift island will be more severe.

3.5 Empirical relations for tidal inlets and tidal basins

Morphodynamics of tidal inlets can be defined as the dynamic behaviour of all morphological units of an inlet, such as ebb tidal delta, tidal channels, flood tidal delta and barrier islands. This behaviour is a very complex one, dependent of a lot of factors. The stability of the morphological units can be described with empirical relations. The geometric properties are related to hydraulic boundary conditions.
O'Brien derived a relationship for inlets along the Pacific coast, the cross-sectional area in the throat, A_c, is related to the tidal prism, P, at spring tide. From data of a tidal channel in the Wadden Sea it appeared that also along a channel the flow area was related to the tidal volume passing the local cross section. Later on it is was found that for various tidal channels in the Wadden Sea and in the estuaries in the Dutch Delta in the South this relationship was valid.
This relationship is presented by:

$$A_{MSL} = c_A P \tag{3.2}$$

in which:
A_{MSL} = flow area below MSL
c_A = empirical coefficient
P = tidal prism
A relationship for channel volume of a tidal basin or estuary and the tidal prism is presented by:

$$V_C = c_C P^{\frac{3}{2}} \tag{3.3}$$

in which:
V_C = channel volume below MSL
c_C = empirical coefficient

For example, the empirical coefficient c_C is $65 \cdot 10^{-6}$ for the Wadden Sea and $73 - 80 \cdot 10^{-6}$ for the Eastern Scheldt and the Grevelingen, see Figure 3.12.
Another important relationship is the one for the sand volume stored in the outer deltas in front of the tidal inlet. This relationship is derived for outer deltas in the USA and reads:

$$V_0 = c_0 P^{1.23} \tag{3.4}$$

in which:
V_O = sand volume stored in the outer delta
c_O = empirical coefficient
Finally the relationship between the relative tidal flat area an the total basin area is given. The cross sectional area of the channels is proportional to the tidal prism and the length of the channels is proportional to the square root of the basin area:

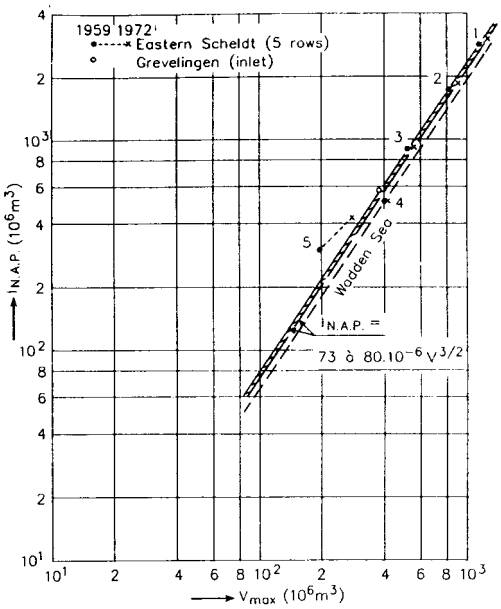

Figure 3.12: Channel volume - mean tidal volume relation Eastern Scheldt and Grevelingen

$$A_c \therefore P$$
$$L_c \therefore \sqrt{A_b} \therefore \sqrt{P} \rightarrow V_c = c_c P^{\frac{3}{2}} \tag{3.5}$$

The flats area is equal to the total basin area minus the channels area:

$$A_f = A_b - A_c \approx A_b - \alpha \frac{P\sqrt{A_b}}{D_c} \approx A_b - \beta \frac{H_m}{D_c} A_b^{\frac{3}{2}} \tag{3.6}$$

in which

P = tidal prism [m^3]
L_c = length of channels [m]
V_c = volume of chanels [m^3]
A_c = channel cross section [m^2]
A_f = the flats ‘area 1.e. the area above MSL [m^2]
A_b = the gross basin area (flats and channels) [m^2]
A_{ch} = the horizontal area covered by all channels [m^2]
α, β = constants of proportionality [m^{-1}]
D_{ch} = characteristic channel depth [m]
H_m = mean tidal range [m]

Renger and Partenscky found for the German Bight:

$$A_f = A_b - 0.025 A_b^{\frac{3}{2}} \tag{3.7}$$

Such a relationship was also found for the estuaries in the south of the Netherlands, however, this one differs from the one in the Wadden Sea, see Figure 3.13. An explanation for the trend of the relation could be the increasing activity of local wind waves in larger basins.

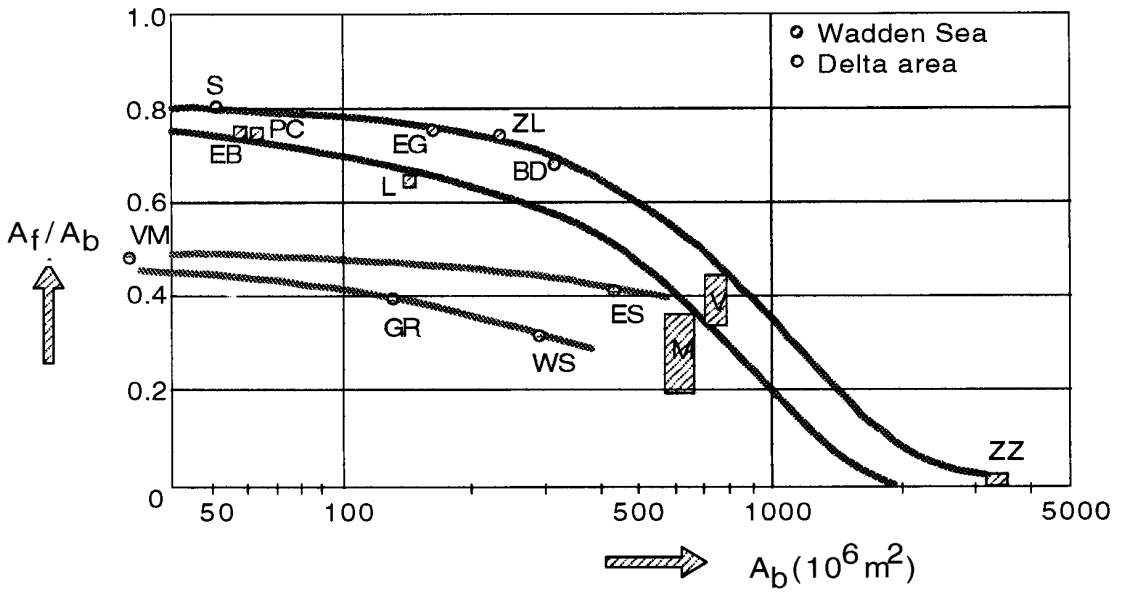

Figure 3.13.: Morphologic relationships

3.5.1 Application of relationships

The relationships are very helpful to determine the response of the inlet to changes in the dynamic equilibrium.
The relations of the relative tidal flat area and the height of the tidal flats may be helpful in the interpretation in what way the development will occur in combination with knowledge on general sediment transport theories and hydraulics. Two examples will be given.

1. Closure of a part of the tidal basin

The closure of a part of the tidal basin will result in a reduction of the channel volume, V_c, and the tidal prism, V. The inlet will adapt itself to the new situation, see Figure 3.14. The two lines represent the relationship of the channel volume and the tidal prism and the relationship of the sand volume of the outer delta and the tidal prism.
Assume an equilibrium situation with tidal prism V and corresponding channel volume V_{msl} and sand volume of the outer delta V_{od}. At a certain time, a part of the tidal basin is closed, which results in a reduction of the channel volume and a reduction of the tidal prism ΔV. A new equilibrium will arise at the equilibrium lines for tidal prism $V - \Delta V$. This means that the channel volume is a m^3 too big and the sand volume of the tidal basin is b m^3 too big.
The sand of the outer delta is available for the adaptation of the channels. The rest, in case $a - b > 0$ has to be supplied from outside.

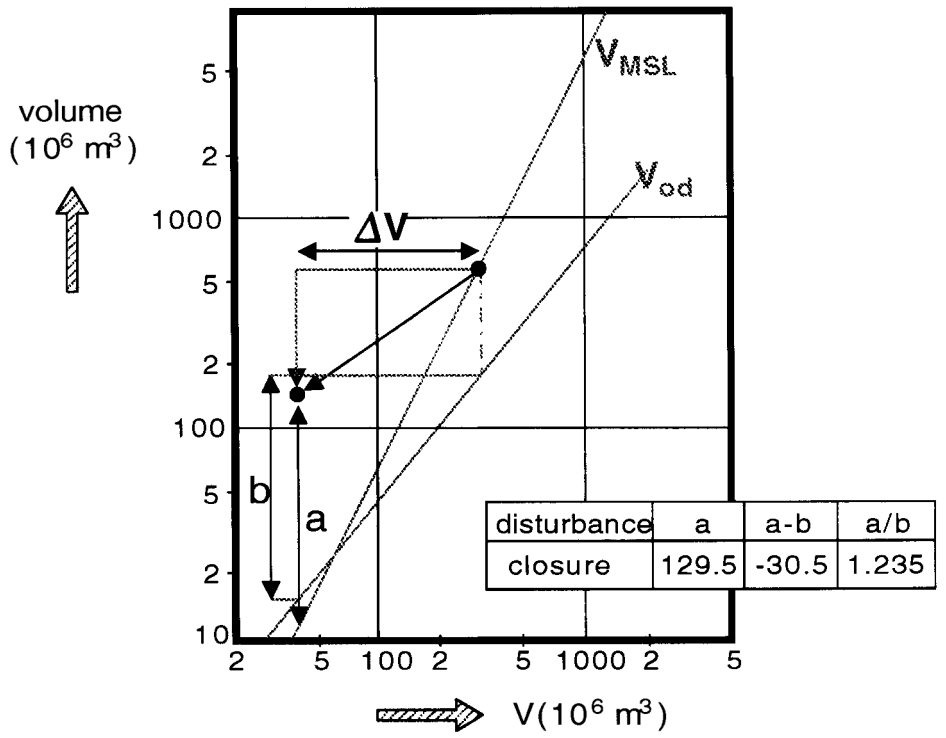

Figure 3.14: Morphologic relationships

2. Accretion of new land

Natural accretion along the borders of the basin, due to the deposition of silt is a very slow process. This process causes a gradual reduction of the tidal prism, see Figure 3.15. Due to this reduction the channel volume is a m^3 too large and the sand volume of the ebb tidal delta is *b* m^3 too big. This results in a sand demand from outside.

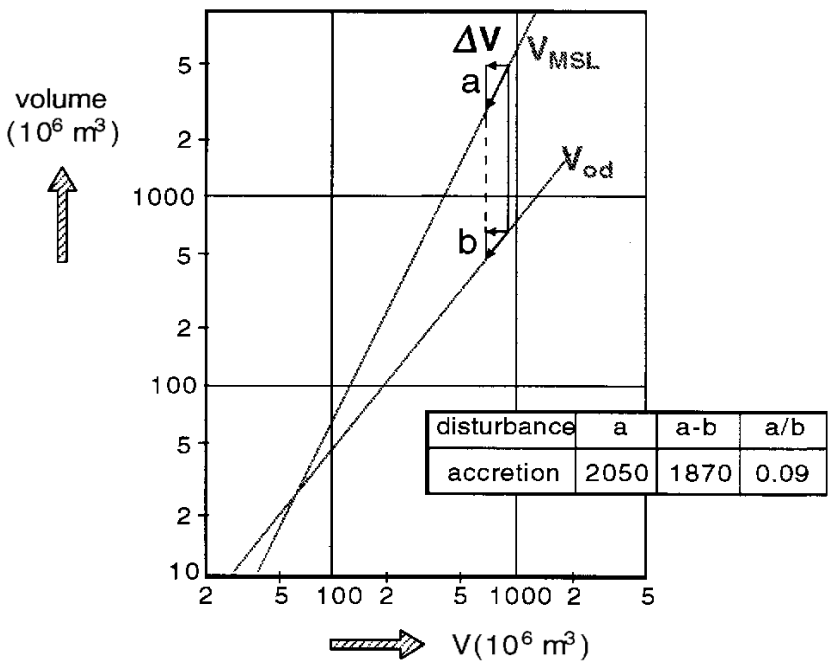

Figure 3.15: Morphologic relations

With respect to the effects of increased sea level rise the answers are more difficult to assess. From storage curves of the different basins it follows that, without adaptation of the level of the tidal flats, the tidal volume will increase and the area of intertidal zones will decrease. The latter effect will be most serious in the Wadden Sea, especially in the western part where the levels of the tidal flats are low. If this scenario is realistic, the channels in the basin will widen and sand will be transported partly to the outer delta, which will extend, and partly will become available for accretion of the North Sea Coast adjacent to the tidal inlet.
However, an increase of sea level rise also will effect the level of the tidal flats. In a relative sense the disturbance of the characteristic water depth at the flats will be much greater than in the channels. Hence, the sediment transports in the channel will be far less effected than those on the flats. Consequently, it seems realistic to assume that the response of Nature will be the strongest on the tidal flats. If it is assumed that the levels of the tidal flats can follow the extra sea level rise, this implies that the tidal volume of the basin remains unchanged, whereas the volume of the channels increases. Thus, this scenario results in a demand of sand from outside.
The above mentioned relationships only give an indication of the new equilibrium between morphology and hydrodynamic conditions in case of changes. They don't give any information how the adaptation will take place and what time this will take.
In general, adaptation processes show a logarithmic character, see Figure 3.16.
The expression that shows the adaptation history is given by:

$$\frac{X}{X_0} = e^{-\frac{t}{\tau}} \tag{3.9}$$

in which:
t = time since disturbance of existing equilibrium
X = quantity representing difference from new equilibrium
X_0 = initial difference from new equilibrium
τ = characteristic time for adaptation

$$\tau = \frac{X_0}{\Delta X_0}$$

in which:
ΔX_0 = initial rate of adaptation.

This approach is not valid in case of change in sea level rise as this is a process of continuous growing disturbance of the existing equilibrium. In this case it is not realistic to assume that this will result in an immediate response of the sea bed in a tidal basin.

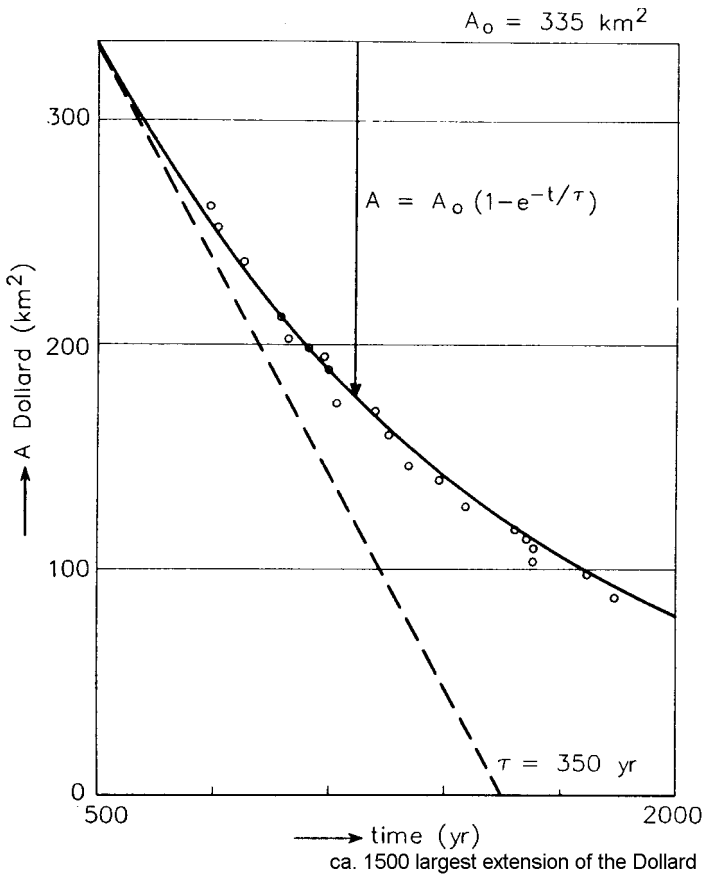

Figure 3.16: Accretion of the Dollard

4 Physics of tidal basins

4.1 Characteristics of tidal basins

Worldwide coastal plains are the regions with the largest population growth. Especially around coastal inlets and tidal basins a strong interaction exists between natural and socio-economic dynamics. Due to reclamations, dewatering and other modes of development the vulnerability of coastal plains increases. Knowledge of the physical and ecological processes in these regions is therefore essential to facilitate an efficient and sustainable development. It is imperative that this knowledge is translated into predictive models. In these course notes the most important building elements hereto are developed. The emphasis in this chapter is more on physical insight than on predictive numerical methods. Physical insight is especially crucial in order to make predictions about changes, which are expected to occur on the scale of the tidal basin itself. This does not only concern changes in water motion, but rather changes in the physical structure of the basin, i.e. the morphology. Relevant practical questions are amongst others:

- What is the response of a tidal basin to sea-level rise (does the basin follow the rise by sedimentation)?
- What are the consequences of dredging for navigation or sand extraction (does sedimentation increase, does salinity intrusion increase)?
- What is the effect of a dike or beach barrier breach (does a new tidal basin form)?
- What are the impacts of a reclamation (does the inlet close, does sedimentation or erosion occur, does the water exchange time change)?

Tidal basins were nearly always created by flooding of coastal plains. These occur at low-lying coasts with a strong tidal energy and with little sediment discharge from rivers. Examples are: Chesapeake Bay, San Francisco Bay, Waddenzee, Baie d'Arcachon.

Sometimes tidal basins co-occur with river deltas, such as in the case of the Ooster- and Westerschelde, but often this is not the case, such as in the case of the Waddensea.
In tidal basins the water motion is controlled munch more by the tides than by the river discharge. Also, sedimentation is primarily controlled by import from the adjacent coastal region. The coarser sediment (sand) is primarily settling in the seaside regions, while the finer sediment (silt) settles in the more protected landward regions.
The length of tidal basins is generally much shorter than the tidal wave length. The tidal range in the basins is of similar magnitude as on the open sea. In longer basins resonance can occur when the basin length is approximately a quarter of the tidal wave length; the tidal amplitude will than increase. Due to frictional losses the tide will be damped, which in the mouth results in tidal wave that partly has a propagating character (especially for long basins) and partly a standing character (especially for short basins).
The seaborne tides fill and empty the basin via channels that cut through (large) intertidal flats. These flats serve to accommodate the tidal prisms: at low water the flats fall dry partly, while at high water only the most landward, higher and vegetated parts remain dry, the so named supra-tidal flats (in Dutch: *kwelders* or *schorren*). The channels meander, especially in the sandy parts of the basin. The maximal ebb and flood flows do not follow the same pathways, especially due to changes in centrifugal forces, but also due to earth rotation (Coriolis). This causes the existence of ebb and flood channels, channel sills and channel bifurcations. During a tidal period water masses are determined by circulations induced by the flat channel systems, which are of importance for the exchange of the basin water with sea water. Also, the temporary entrapment of water masses in so-called dead zones (flats, schorren, channel branches) contributes to the mixing. Vertical salt-fresh gradients hardly occur in tidal basins due to the dominance of the tidal over the river flow and due to the strong horizontal exchange processes of the water masses.
The topographical characteristics of tidal basins or the hypsometry (e.g. the ratio of flat and channel surfaces) determine the tidal propagation. This can either strengthen or weaken the magnitude of the maximum flood flow compared the maximum ebb flow. This is determining a net import or a net export of sediment and hence it is determining the morphological development of the basin in time. Due to this feedback mechanism the basin in essence determines its evolution, although external conditions such as sediment availability and storm surges also play a role. Many tidal basins are deposition areas for fine sediments. This is due to their protective character, but the import of fines is especially determined by the tidal asymmetry. In this respect it is especially the slack water durations before flood and ebb that are important: these determine to a large extent how much sediment at the initiation of flood and ebb can be transported. Besides, wave stirring and storm surges can cause a strong erosion and export of sediment.
Some tidal basins are unstable and sedimentate or silt up in a relatively short period, such as the Zwin that gave navigational access to the town of Bruges. In other basins there is a dynamic equilibrium between import and export of sediment. This is for instance the case for the Eastern Waddensea that has the same topography for nearly a thousand years. The location of flats and channels fluctuates over timescales of tens to hundreds of years.

4.2 Contens of the course

The physics of tidal basins is treated in four parts.
In part 1 insight is provided into the complex geometric structure of tidal basins, which is formed by meandering and branching channels. These incise flat areas, which are partly composed of sandy sediments and partly of silty sediments, with vegetation on the higher landward regions. An explanation is given how a flat-channel pattern develops and how a continuously fluctuating, dynamic equilibrium is maintained. The flow structure in curved channels is treated and it is explained how this leads to the formation of ebb and flood chutes. Also it is shown how this leads to large-scale tide-averaged horizontal circulations that are related to the basin topography.
In part 2 the propagation of the tide in the basin is described. An analytical description is only possible for simplified geometries. The one-dimensional tidal wave propagation equation is derived for the case of a uniform channel-flat geometry along the channel direction. The emphasis is on the deformation of the tidal wave propagating and reflecting in the basin, with a dominant role for bottom friction. Due to the tidal deformation an asymmetry evolves between the ebb and flood flows. This asymmetry is responsible for a net tide-induced transport of sediment in the basin.
Part 3 treats the process of sedimentation in basins. Insight is given into the factors, which determine import or export of sediment. These factors may differ for coarse and fine bottom sediments, especially due to the differences in response time of sedimentation and erosion to fluctuations in the flow velocity. In an intermezzo some important properties of sediment particles, ranging from silt to sand, are treated concisely. Whether import or export occurs is also determined by the basin topography; several typical topographies are treated. It will be shown how tidal asymmetry causes a residual transport for the cases of coarse and fine sediment. The one-dimensional tide propagation equation relates tidal asymmetry to the geometrical characteristics of the basin. Hence, a relation is derived between the geometry of the basin on the one hand and the resulting (residual) sediment transport on the other hand. This relation allows drawing conclusions on the morphological stability of tidal basins.
Finally, part 4 treats the flushing of tidal basins. Insight is given into the processes that play a role in mixing and flushing. The phenomenon dispersion is introduced with the aid of a "tidal random walk" model of water masses. This tidal random model is applied to estimate the magnitude of the tide-averaged mixing. On the one hand this concerns dispersion by a combination of tidal transport and topographically induced circulations. On the other hand this concerns dispersion related to momentum exchange between water masses transported with the tide and water masses retained in areas adjacent to the main flow channels.

4.2.1 Knowledge base

Linear wave propagation theory, basic equations fluid mechanics, sediment properties.

Table 4.1: Charateristics of tidal basins

Origin of tidal basins	Flooded coastal plain, settled lowlands function as "vloedkuil" (depression of the tidal amplitude)
Tidal wave	On the landward side primarily standing wave, on the sea ward side primarily propagating wave; resonance suppressed by damping of the reflected wave
Tidal propagation	Follows the main channel, one-dimensional character
Tidal asymmetry	Deformation of tide due to non-linear bottom friction and due to interaction with basin geometry
Morphology	Meandering and/or branching channel system, sills (in Dutch: drempels), flats, marshes (in Dutch: slikken, schorren/kwelders)
Tide induced flow	Spiraling flow pattern in channel meanders, residual circulations in ebb-flood cells stimulate flat formation and sill formation
River influence	Subordinate to tide influence, virtually no vertical salinity structure, density driven circulation has a 3-dimensional structure, is of negligible importance for salt intrusion
Morphodynamics	On larger scale due to nonlinear interaction between tidal propagation and morphology, on local scale by nonlinear ineraction between secundary flow structure and channel-flat geometry. Leads to cyclic variations in ebb-flood channel patterns
Sedimentation	Deposition of sand on the more seaward part, deposition of silt on the more landward part (at the end of the transport path); in dead channel branches, on higher, vegetated or protected flats, neaar tidal diveides (in Dutch: wantijen)
Mixing and flushing	By topographically induced shear in the tidal vflow field, by secundary circulations in ebb-flood cells and channel meanders, by exchange with dead zones, by chaotic transportpaths

The Western Scheldt is a charateristic tidal basin; see Figure 4.1.

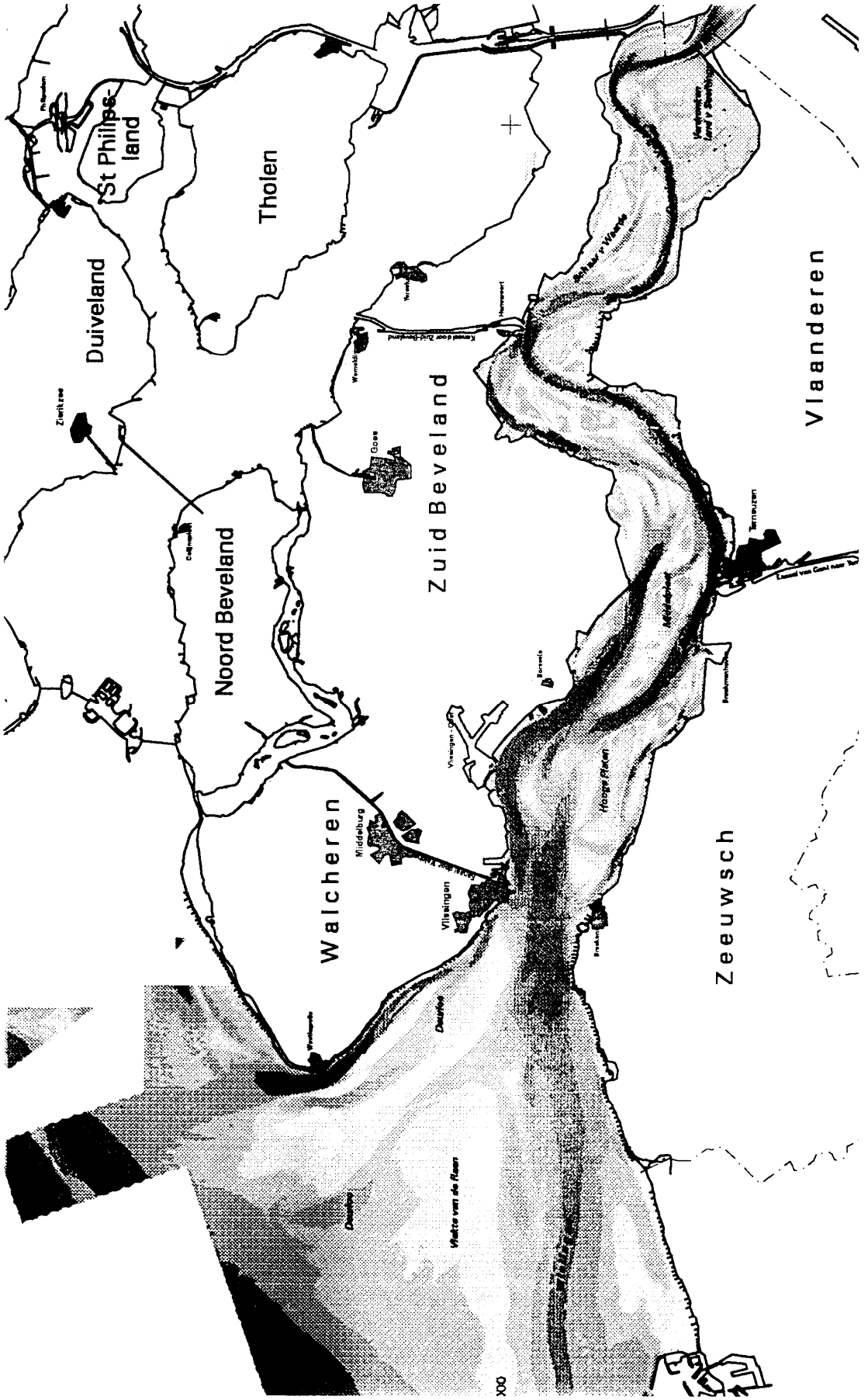

Figure 4.1: Flat-channel systems in the Westerschelde

4.3 The complex geometry of tidal basins

4.3.1 Bendflow and flat formation

A very good description of the morphodynamics of tidal basins is found in Van Veen (1950; originally published in Dutch under the title "Eb- en vloedschaarsystemen in de Nederlandse getijdewateren"; translated and annotated by V.d. Spek, Stive and Zitman 2001; republished in JCR in 2005 by Van Veen et al.). The characteristic topography, with meandering and branching channels, ebb and flood dominated channels and flats, is primarily due to the horizontal and transversal circulatory flows induced by the channel bends. These circulatory flows play een active role in the morphological evolution of channel meanders and of ebb and flood chutes. Figure 4.2 gives a schematic representation of a channel bend; both in cross-section and in plan view.

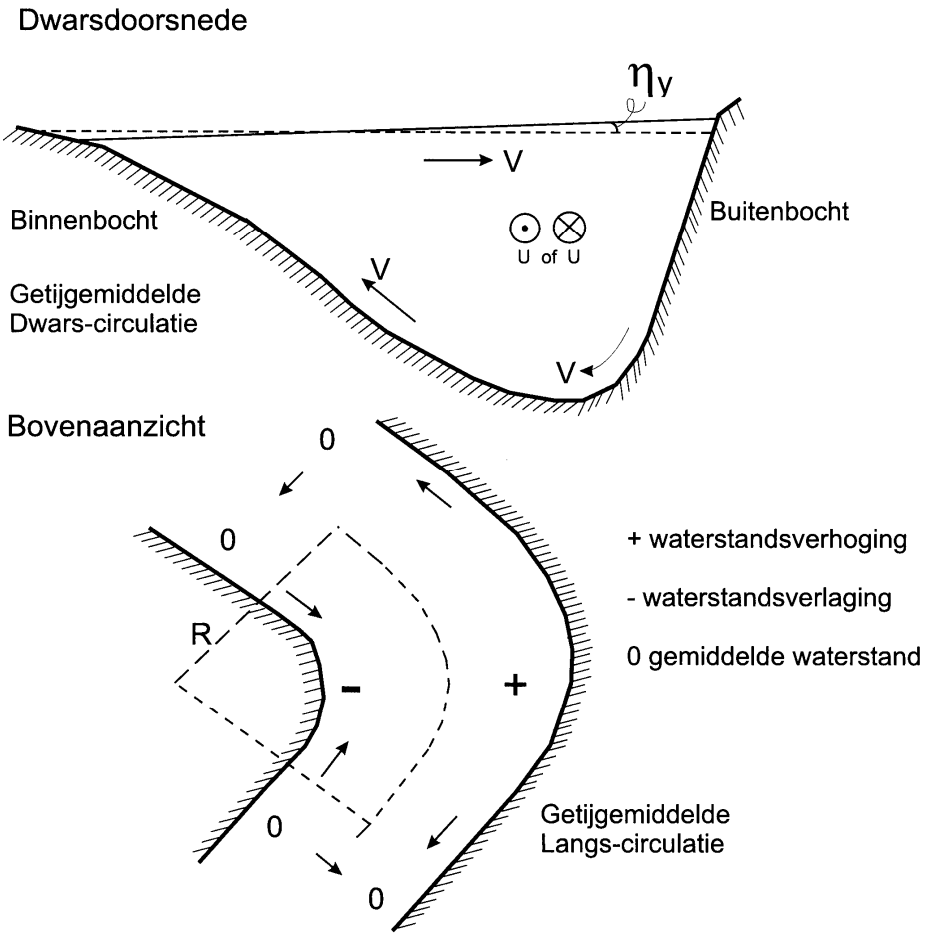

Figure 4.2: Residual circulations in a channel bend

A simple description of transversal circulation in a channel bend is obtained when the assumption is adopted that the flow (both ebb and flood) has adapted to the channel bend under the influence of bottom friction and mean surface slope (pressure gradient) and that both the channel and flow structure are angle independent in a cylindrical coordinate system. The transversal (perpendicular to the mean flow) force balance then

reads:

$$\underbrace{-\frac{u^2}{R}}_{\text{centrifugal force}} + \underbrace{f\,u}_{\text{Coriolis}} + \underbrace{\frac{1}{\rho}\,p_y}_{\text{pressure gradient}} - \underbrace{(N\,v_z)_z}_{\text{turbulent viscosity}} = 0\,. \qquad (4.1)$$

where

R radius of the channel bend (assumed to be much larger than the channel width),
u the local velocity along the channel axis and $x = R\,\theta$ the lateral coordinate,
z the vertical coordinate (bottom: $z = -h$, surface $z = \eta$),
v the transversal velocity,
y the transversal coordinate,
N the eddy viscosity.

The transversal pressure gradient is due to the water level slope, counteracting the centrifugal and Coriolis forces. The equation describes the evolution of a transversal circulation $v(y,z)$ due to the vertical shear in the lateral channel flow $u(y,z)$. Both the centrifugal and the Coriolis force are of importance, the bend radius R determines their relative importance. The Coriolis contribution changes sign at ebb and flood (hence neutral in a tide-averaged sense); the centrifugal force exerts its influence at ebb and flood in the same direction. Density differences can potentially play an important role in the force balance; these influence the vertical structure of the lateral flowvelocity (density current), the magnitude and vertical structure of the eddy-viscosity N and the magnitude and vertical structure of the transversal pressure p_y. When the vertical stratification is strong a transversal slope of the boundary plane may compensate the shear in the centrifugal force; hence no strong transversal circulation is generated. In the absence of stratification the transversal circulation is strengthened due to damping of the eddy-viscosity.

Under the following assumptions:

- Stratification is neglected (i.e. $p_y = g\rho\eta_y$),
- Water level variations are neglected (i.e. $\eta << h$),
- N is assumed constant,
- The shear in the lateral flow velocity is constant (i.e. $u(z) = u(0)\,(1 + \frac{z}{h})$),
- At the surface and at the bottom we respectively take the slip- en no-slip boundary conditions (i.e. $v(z = -h) = 0$, $v_z(z = 0) = 0$),

we may twice integrate the force balance over depth to derive the following expression for the transversal circulation:

$$v(z) = \frac{h^2 u(0)}{24N}\left[-\frac{u(0)}{5R}\left(10z^{*4} + 40z^{*3} + 33z^{*2} - 3\right) + \frac{f}{2}\left(8z^{*3} + 9z^{*2} - 1\right)\right], \quad z^* = \frac{z}{h}\,. \qquad (4.2)$$

Near the bottom this circulation is towards the inner bend generating a transport of

sediment transport from the outer bend, which erodes, towards the inner bend, which sedimentates. This transversal circulation gives the tidal flow a spiralling character. The Coriolis-acceleration strengthens the transversal circulation when from the perspective of the main flow the channel bend attaches a right bank (i.e. at ebb and flood this implies opposite bends, and this holds for the Northern hemisphere). Due to earth rotation the flood flow will be more concentrated along the right bank, viewed from the flood flow, while the ebb flow will be more concentrated on the right bank, viewed from the ebb flow (Kelvin wave type tidal propagation).
The transversal water level slope is as follows:

$$\eta_y = \frac{9}{20}\frac{u(0)^2}{gR} - \frac{5}{8}\frac{fu(0)}{g}. \qquad (4.3)$$

4.3.2 Ebb and flood chutes and horizontal circulations

The mean surface water level in the outer bend is slightly elevated compared to that in the inner bend. Hence, this slope in water level also creates a slope in longitudinal direction. Along the bank of the outer bend the water level increases longitudinally towards the centre of the bend and vice versa along the bank of the inner bend. These longitudinal slopes induce a horizontal circulation, which is directed away from the bend along the outer bend bank and towards the bend along the inner bend bank. This horizontal circulation is also referred to as "headland eddy". This eddy is generally superposed on a strong tidal current; the instantaneous situation is that of a tidal current that is inclined to go off (overshoot) the bend pathway (or take a wider bend; in Dutch: “uit de bocht schieten”), both at ebb and at flood.
The horizontal circulation has a similar effect on the transport of sediment as the transversal circulation: a net sediment transport occurs from the outer bend towards the inner bend. Both circulations cause further curving and deepening of the outer bend and a shallowing of the inner bend. Hence, this phenomenon has a positive feedback mechanism. Straight channels are inherently unstable; a small eccentricity in the channel alignment will be inclined to grow. Due to the same mechanism a wide channel that follows an S-curved alignment will be inclined to split up in an ebb-dominated and a flood-dominated channel.
By the flows taking a wider bend (due to inertia) ebb and flood chutes occur at the ending of the bends in the flat areas located in the inner bends of the adjacent channel bends. Due to the fact that the mean water level during flood (especially near the ending of the flood) is higher than during ebb, the flood channels are generally better developed than the ebb channels. At flood the water flows more generally over the flats, while the ebb primarily follows the main channel. Figure 4.3 sketches the characteristic structure of ebb and flood channels in a meandering channel system, with an indication of the depth-mean residual flow pattern.

The flats are especially fed with sand through the ebb and flood chutes. This feeding process causes the existence of sills between the ebb and flood chutes. When a sill

breaches the channel bend is cut-off. A new, straighter channel is formed, while the old main channel sedimentates. However, in the course of time the new channel will start to increase its curvature. Hence, the morphology of tidal basins is not static but dynamic; cycles of increasing channel curvature and channel cut-off are an important part of this internal dynamics.

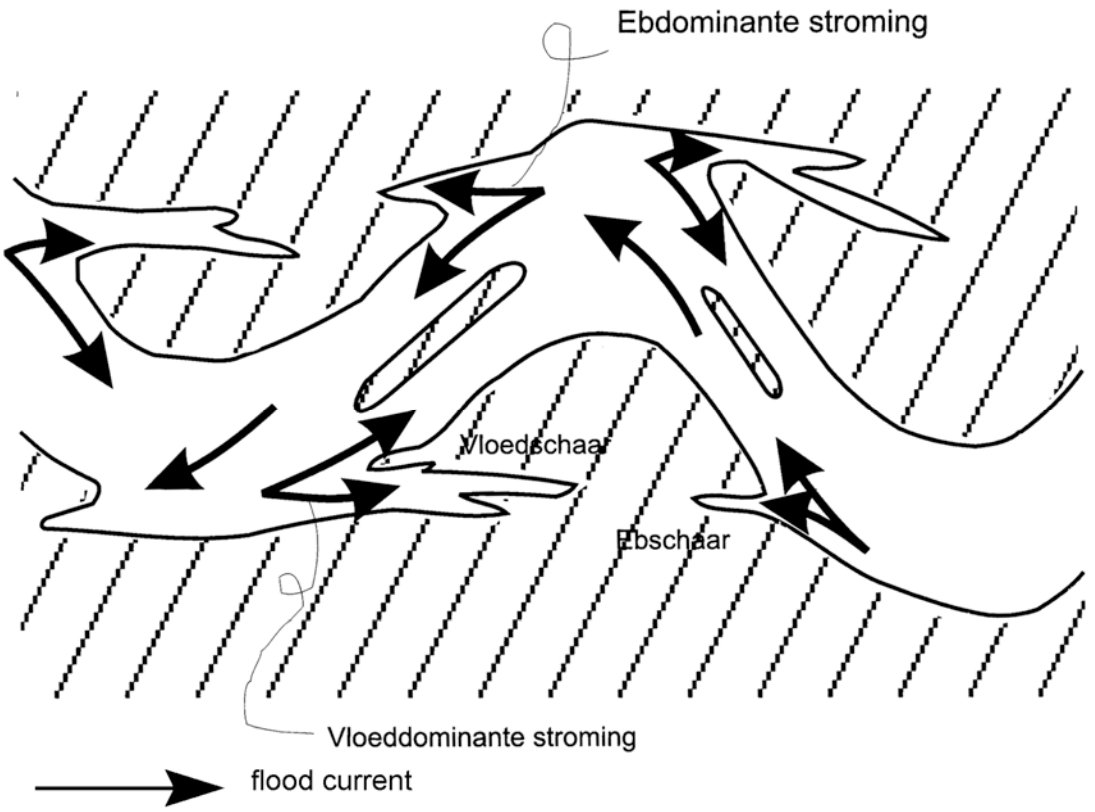

Figure 4.3: Meandering tidal channel with ebb and flood chutes

4.4 Propagation and reflection of the tidal wave

4.4.1 The one-dimensional tidal propagation equations

In tidal basins we generally find a main channel, which transports the majority ebb and flood discharge. It is along this main channel that the tidal wave primarily is propagated. If we choose to align the x-axis with the channel-axis, we may approximate the tidal propagation with a set of one-dimensional equations. These are the balance equations for mass and momentum in x-direction.

To derive these equations we schematise the cross-section of the basin $A(x,t)$ into two parts. One part represents the flow carrying part of the cross-section, discharging all the flow, and the storage part, which only stores water without discharging, see Figure 4.4.

The flow-carrying cross-section has a surface $A_S(x,t)$, which is the product of a flow-carrying width $b_S(x,t)$ and a representative instantaneous depth $H(x,t)$. The representative instantaneous depth is the sum of the representative flow-carrying water depth $h(x,t)$ relative to a horizontal mean water level and the tidal level $\eta(x,t)$. The mean

flow velocity in the flow-carrying cross-section is indicated as $u_S(x,t)$. In equation form:

Flow-carrying cross-section $A_S = b_S H = b_S(h+\eta)$,

Discharge $Q = A\bar{\bar{u}} = A_S u_S$.

The double overlining of the velocity *u* indicates averaging over the total cross-section. The one-dimensional balance equations are derived for an infinitesimal short section in the basin. The mass balance (continuity equation) yields:

$$\underset{\substack{\text{volume change}\\ \text{duc to in- and outgoing transport}}}{(A_s u_s)_x} + \underset{\substack{\text{volume change}\\ \text{duc to water level change}}}{b_K \eta_t} = 0 \qquad (4.4)$$

The mass balance equations can be rewritten as

$$\frac{1}{b_K}(b_S H u_S)_x + \eta_t = 0 \qquad (4.5)$$

The momentum balance reads

$$\underset{\substack{\text{momentum}\\ \text{change}}}{(A_S u_S)_t} + \underset{\substack{\text{in- and outgoing momentum}\\ \text{transport in along and cross}\\ \text{direction}}}{(A_S u_S{}^2)_x + (b_K - b_S)\eta_t u_S} + \underset{\substack{\text{pressure}\\ \text{gradient}}}{g A_S \eta_x} + \underset{\substack{\text{bottom}\\ \text{friction}}}{\frac{b_S}{\rho}\tau_b} = 0 \qquad (4.6)$$

This equation can be simplified to yield the well-known shallow water tidal propagation expression:

$$u_t + u u_x + g\eta_x + c_D \frac{|u|u}{H} = 0 \qquad (4.7)$$

Here and in the following we drop the subscript *S* for *u*.
Also for the tidal energy a balance equation may be derived. The tidal energy per unit length is given by

$$E = < b_K \tfrac{1}{2} g\rho\eta^2 + A_S \tfrac{1}{2}\rho u^2 > \qquad (4.8)$$

where < > represents averaging over the tidal period. We assume a cyclic tide, hence $E_t = 0$.
The energy balance yields:

$$\underset{\substack{\text{in- and outgoing energy transport}\\ \text{in along and cross direction}}}{\frac{\partial}{\partial x} < A_s u (\tfrac{1}{2}\rho u^2 + \rho g\eta) >} + \underset{\substack{\text{energy dissipation}\\ \text{duc to bottom friction}}}{< (b_K - b_S)\,\eta_t \tfrac{1}{2}\rho u^2 >} = - < b_S \tau_b u > \qquad (4.9)$$

This equation can not be expressed in the common form of a energy balance equation due to the fact that tidal energy is not only transferred by advective transport but also by

pressure.
For a symmetrical (sinusoidal) tidal wave it applies that:

$$< A_S u \tfrac{1}{2}\rho u^2 + \rho g \eta) > \approx < (b_K - b_S)\,\eta_t \tfrac{1}{2}\rho u^2 > 0 \qquad (4.10)$$

If we further assume that the tide propagates as a propagating wave and if river discharge is neglected, then the left hand side of the energy balance apporoximately equals:

$$< A_S\, \rho g u \eta) > \approx b_S c E\,, \quad E = \tfrac{1}{2} g \rho a^2 \qquad (4.11)$$

which indicates that in a symmetrical, propagating tidal wave the tidal energy is propagated with the wave phase velocity

$$c = \sqrt{gh} \qquad (4.12)$$

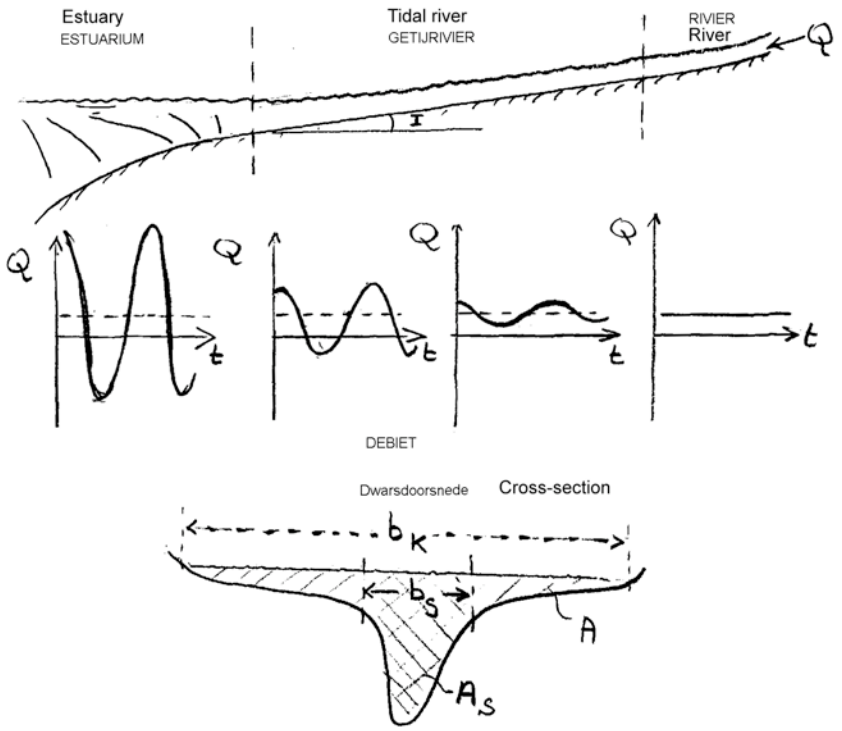

Figure 4.4: Charatrecistics of a tidal river

4.4.2 Scale analysis

In order to implement simplifications in the tidal propagation equations we conduct a scale analysis, which shows under what conditions which terms are of similar order-of-magnitude and which terms may be neglected.
We introduce the following scaling:

$$\bar{\bar{u}} = \{u\}u^*, \quad \eta = \{\eta\}\eta^*, \quad H = \{H\}H^*, \quad t = \{t\}t^*$$

All variables with an asterisk are of order 1. The terms in parentheses indicate the order-of-magnitude of the non-scaled variables; these values are constant.
We assume that the geometry of the tidal river is approximately uniform. Hence, two

length-scales remain: the tidal wave length $L = \frac{2\pi}{\omega}\sqrt{gh}$, and the length-scale of the tidal intrusion. We adopt *{x}* for this latter length-scale, since this is the scale that dominates the variation of the tidal parameters.

Furthermore $\{\eta\} = a, \quad \{t\} = 1/\omega, \quad \{H\} = h$.

From substition in the continuity equation we find $U \approx \frac{b_K}{b_S}\frac{a}{h}\omega\{x\}$.

Introduce $P = \frac{b_K}{b_S}(2\pi\{x\}/L)^2$, and the momentum balance becomes:

$$Pu^*_{t^*} + P\frac{b_K}{b_S}\frac{a}{h}u^*u^*_{x^*} + \eta^*_{x^*} + P\frac{b_K}{b_S}\frac{a}{h}\frac{\{x\}}{h}c_D\frac{|u^*|u^*}{H^*} = 0 \qquad (4.13)$$

For characteristic orders-of-magnitude $a/h = O[10^{-1}]$, $b_K/b_S = O[1]$, $h \approx O[10\text{m}]$ the second term on the left-hand side can be neglected.
If friction may also be neglected then it follows that $P \approx 1$ and $\{x\} \approx L/2\pi$.
For strong friction the friction term (fourth) must be of the same order-of-magnitude as the pressure gradient term (third), hence:

$$P\frac{b_K}{b_S}\frac{a}{h}\frac{\{x\}}{h}c_D \approx 1 \ , \quad \{x\} \approx \left(\frac{2\pi}{T\sqrt{g}}\frac{\sqrt{h}}{\frac{a}{h}c_D}\right)^{1/3} \approx 0.8\frac{L}{2\pi} \qquad (4.14)$$

(assuming *a/h* ≈ 0.1, c_D = 0.003).

For strong friction {*x*} is smaller than for weak friction; friction decreases the tidal intrusion significantly.
When c_D is large, *h* small and, *a/h* large, the flow is friction dominated. The first two terms in the momentum balance equations may then be neglected to a first approximation. In many tidal basins this is the case.
In most tidal basins the geometry may not be considered uniform over the tidal intrusion length. This implies that in the scaling analysis also a geometrical length scale must be introduced. If this geometrical length scale is much smaller than the tidal intrusion length, other terms in the mass balance start to play an important role, so that the above analysis does not hold.

Propagating tidal wave under friction-dominated flow

As discussed abvove, for a friction-dominated flow and a uniform geometry we can simplify the tidal equations to:

$$g\,\eta_x + c_D\frac{|u|u}{H} = 0 \ , \quad b_S\,H\,u_x + b_K\,\eta_t = 0 \qquad (4.15)$$

By elimination of η from these equations we find:

$$u_t = \Xi\, u_{xx}\,, \quad \Xi = \frac{g b_S H^2}{2 b_K C_D |u|} \quad = \text{a diffusion coefficient} \tag{4.16}$$

This is a diffusion equation. To a first approximation the tide does not propagate as a wave, but diffuses in the basin. However, around slack water (in Dutch: stroomkentering, het stil vallen van de stroming bij de overgang van vloed naar eb en vice versa) the flow will not be described correctly by the tidal diffusion equation; during the slack waters friction is not dominant, the tide then propagates approximately as a wave. Especially due to the dependence on the flow magnitude the tidal diffusion coefficient varies strongly over the tidal period. The tidal diffusion equation is therefore nonlinear, and cannot be solved with elementary methods. This nonlinear character implies that the basin deforms the tidal wave during diffusion and it loses its sinusoidal character. This implies that the symmetry between ebb and flood is broken. The behaviour of the model wave described by the diffusion equation approximates the real wave only during the periods in which the flow strength is sufficiently large and the friction term dominates over the acceleration terms. We assume that this is the case during the major part of the tide, so that the model wave gives a satisfactory description of the real tidal wave.

In the following we search for an approximate solution for the nonlinear tidal diffusion equation. This solution will indicate that the maximum flood flow occurs just before HW (one eighth of a tidal period); similarly this is true for the moments of maximum ebb and LW. Around maximum flood and ebb flow the variation of the velocity is small. Around HW and LW the variation of the water level is small. This implies that both between maximum flood and HW and between maximum ebb and LW an interval exists in which H and u hardly vary. During these periods we assume H and u_T constant, respectively $H \approx H^{\pm} = h + \eta^{\pm}$, $u_T \approx u_T{}^{\pm}$ are constants.
The tidal diffusion coefficient may in these cases be considered approximately constant. We assume that the flow during both intervals is friction-dominated.

We now consider a tidal basin that is of such length that the tidal wave at the end of the basin is nearly damped out. This was for instance the case in the former Zuiderzee, where de tidal wave entering through the Marsdiep and the Vlie was large damped out at Amsterdam and the Veluwe banks. Also in tidal rivers we find slowly damping propagating tidal waves, e.g. the Lek and the Waal in the Netherlands and the St. Lawrence river in Canada. In these tidal rivers the reflected tidal wave is negligibly small, so that the tide has the character of an inland diffusing wave. In the periods that H and u vary marginally the wave can be parameterised by (in complex notation; only the real part is of relevance):

$$u \propto e^{i\kappa x + i\omega t} \tag{4.17}$$

Through substitution in the tidal equations we find for the HW-interval (resp. the LW-interval) to good approximation:

$$\eta = a\, e^{-kx + i(kx - \omega(t - \frac{T}{8}))}, \quad u = -u_R + \frac{1}{\sqrt{2}} \frac{a}{h} c\, e^{-kx + i(kx - \omega t)} \tag{4.18}$$

The above expressions are valid only for respectively the HW and LW periods; the wave number *k* and the propagation speed *c* for these periods are:

$$k^{\pm} = \sqrt{\frac{c_D b_K^{\pm} \omega |-u_R + u_T{}^{\pm}}{g b_S^2 H^{\pm 2}}}, \quad c^{\pm} = \frac{\omega}{k^{\pm}}$$
$$H^{\pm} = h + \eta^{\pm}, \ \eta^{\pm} \approx \pm a(1 - e^{-1}), \ u_T{}^{\pm} \approx \pm \tfrac{1}{2}(1 - e^{-1}) \frac{a\omega}{h k^{\pm}} \tag{4.19}$$

The last expressions are obtained by assuming that the tidal amplitude over the trajectory of tidal intrusion is approximately damped exponentially.
The flow velocity has two components: u_R, the flow velocity due to the river discharge alone, and u_T, the flow velocity due to the tide. In tidal basins the former is generally small compared to the latter. In the following we generally assume $u \approx u_T$.
In tidal rivers, where the river flow velocity and the tidal flow velocity are of similar order, this assumption does not hold. In tidal rivers the wave number (equivalent to the inverse of the damping length) is significantly smaller for the HW-period than for the LW-period: $k^+ \prec k^-$. This is especially due to the much larger flow velocity at maximum ebb than at maximum flood. This causes the damping during ebb around LW to be stronger than during flood around HW. Also the propagation speed $c^+ = \omega / k^+$ of the HW is significantly higher than the propagation speed $c^- = \omega / k^-$ of the LW. This difference in propagation speed causes a deformation of the tidal wave: the period of water level increase is shorter than the period of water level decrease (so-named tidal asymmetry). This implies that in upriver flow direction the flood velocities relatively increase, while in down river direction these relatively decrease (the flood and ebb dischargers are approximately the same); see Figures 4.5 and 4.6.

In long tidal basins where the river discharge is negligible compared to the tidal discharge in general also tidal asymmetry will develop, but this is due to other factors. On the one hand this concerns the ratio between storage and flow width, which can be quite different at HW and LW. This is also relevant for shorter tidal basins, where the tidal wave has more a standing wave character. In the following we will treat this in more detail. On the other hand in long basins the phase difference between water level and flow velocity is of relevance to the tidal asymmetry. In a propagating wave this phase difference is smaller than $\pi/2$, so that the water level averaged over flood is higher than that averaged over ebb. Since during ebb the discharge is similar to the discharge during flood, the ebb velocities must on average be larger because of the smaller flow cross-section. This would implicate that for long tidal basins the sediment transport at ebb is always larger than at flood. In the following we will find that other geometrical effects can counteract this ebb dominance. Nevertheless the ebb dominant behaviour of a damped tidal wave is an important driver for the formation of a tidal basin in coastal lowlands after a barrier breach.

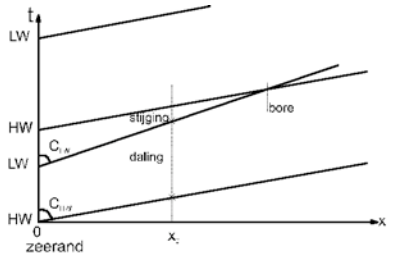

Vervorming getij bij snellere voortplanting HW tov LW;
periode van getijstijging wordt korter en van getijdaling langer.

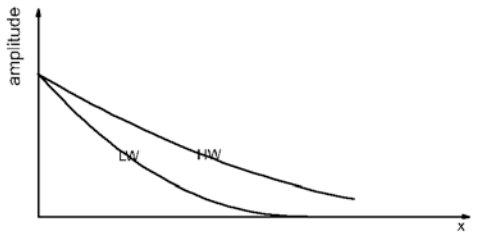

Bij snellere voortplanting HW tov LW wordt het HW
minder snel gedempt dan het LW.

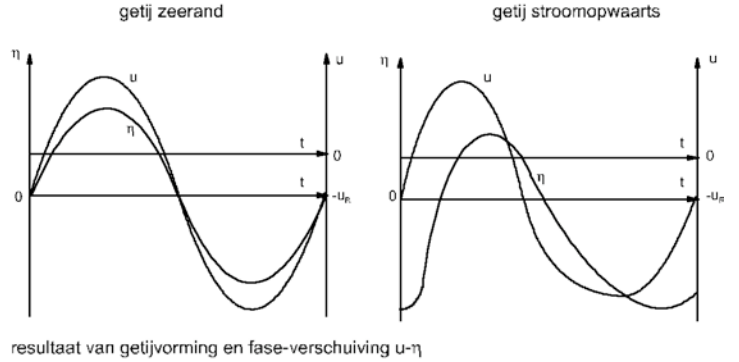

resultaat van getijvorming en fase-verschuiving u-η

Figure 4.5: Deformation of a tidal wave in a tidal river

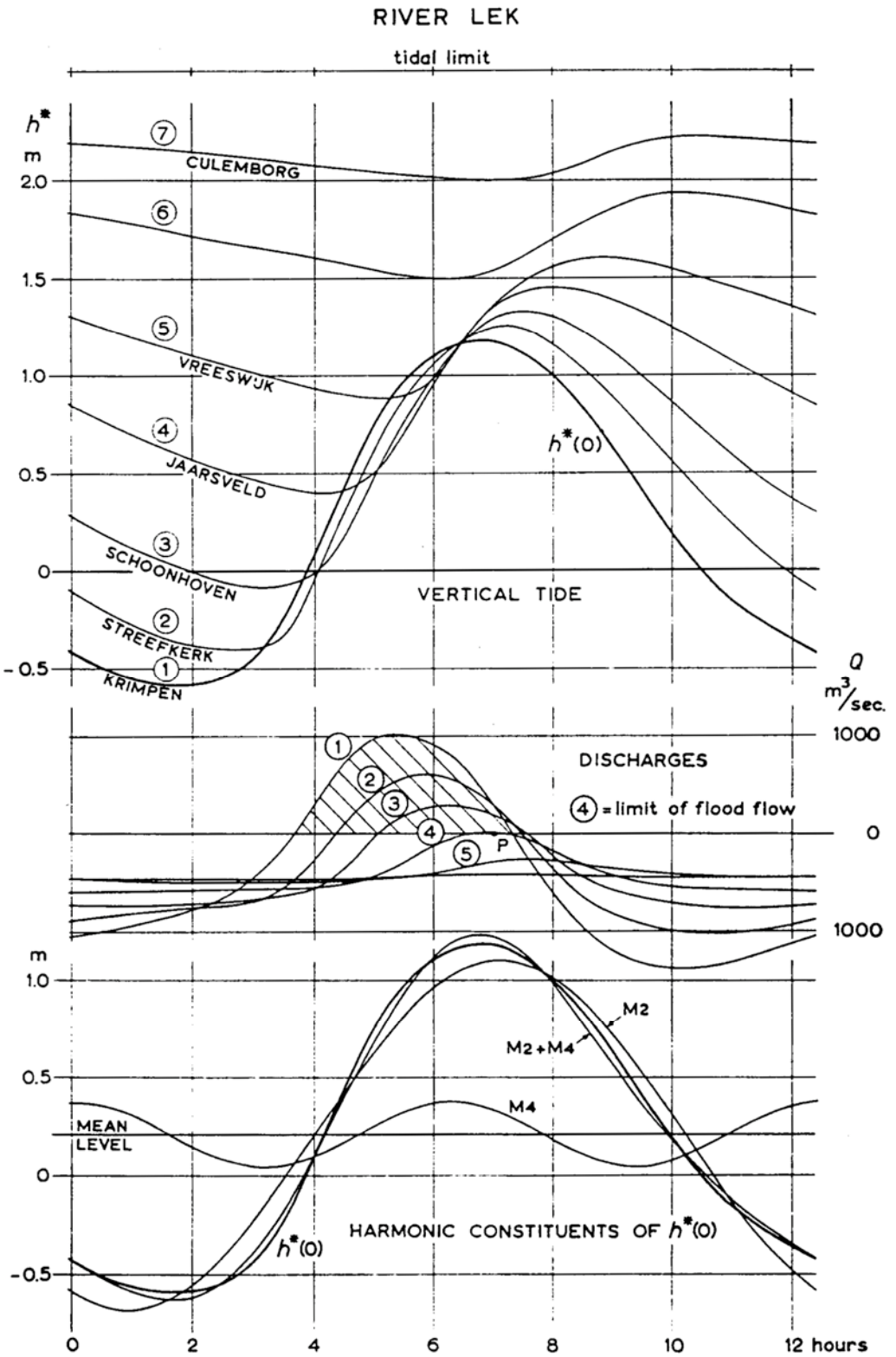

Figure 4.6: Tidal deformation the river Lek

4.4.3 Standing tidal wave, resonance

If the tidal wave is not strongly damped in he basin, reflection will occur at the landward end of the basin. We still consider a uniform tidal basin in which the tidal wave primarily

follows the main channel, so that the tidal propagation can be approximated by a one-dimensional description. The flow is schematised with an approximately uniform profile in the flow-carrying cross-section and no net flow in x-direction outside this profile. The one-dimensional flow equations can then be written as:

Mass balance $$h_K u_x + \eta_t = 0 \tag{4.20}$$

Momentum balance $$u_t + g\eta_x + c_D \frac{|u|u}{H} = 0 \tag{4.21}$$

The momentum transport term uu_x is neglected here, but the acceleration term is maintained. Here u is not the cross-section averaged flow velocity but the ratio of discharge and flow-carrying cross-section:

$$u = Q / A_S \tag{4.22}$$

Furthermore h_K is an equivalent depth that accounts for the difference between flow-carrying and storage width:

$$h_K = A_S / b_K = Hb_S / b_K \tag{4.23}$$

When the tide is very small ($a/h \ll 1$) h_K can be assumed constant.
First we consider the (mostly unrealistic) case of negligible friction, $c_D = 0$. In this case the non-deformed tidal wave is reflected at the basin end $x = l$; the result is a standing tidal wave:

$$\eta(x,t) = \frac{1}{2} a_l [\cos(k(x-l) - \omega t) + \cos(k(x-l) + \omega t)] = a \frac{\cos(k(x-l))}{\cos kl} \cos \omega t \tag{4.24a}$$

$$u(x,t) = \frac{1}{2} \frac{a\,c}{h_K \cos kl} [\cos(k(x-l) - \omega t) - \cos(k(x-l) + \omega t)] = u_0 \frac{\sin(k(x-l))}{\sin kl} \sin \omega t \tag{4.24b}$$

where $a_l = \dfrac{a}{\cos kl}$, $U = u(0,0) = \dfrac{a\,c}{h_K} \tan kl$.

The velocity at the landward end $x = l$ is zero. The tidal amplitude at the landward end is larger than that at the seaward end. Water level and flow velocity are 90^0 out of phase; the mean water level at ebb and at flood are therefore the same. This further implies that no influx or outflux of tidal energy $E = \frac{1}{2}\rho u^2 + \rho g \eta$ occurs, since $< uE >= 0$.
If the basin length equals a quarter of the tidal wave length, resonance will occur:

$$l = \frac{1}{4} L = \frac{1}{4} T \sqrt{g h_K} = \frac{\pi}{2k} \Rightarrow \cos kl = 0 \Rightarrow U, a_l \to \infty \tag{4.25}$$

In that case bottom friction can certainly not be neglected.

4.4.4 Damped reflected tidal wave

In most tidal basins the tidal wave can be described as the superposition of an incoming and a reflected damped wave. We derive this for a small tide (*a/h << 1*) and for a linearised friction term:

$$c_D \frac{|u|u}{H} \rightarrow r\frac{u}{h}, \quad r \approx \frac{8}{3\pi} c_D |u| \tag{4.26}$$

The latter expression (the linearised friction coefficient) is assumed constant.
Substitution in the tidal equations yields the following solution:

$$\eta = \frac{1}{2} a_l [\, e^{-\mu(x-l)} \cos(k(x-l) - \omega t) + e^{\mu(x-l)} \cos(k(x-l) + \omega t)\,] \tag{4.27}$$

$$u = \tfrac{1}{2} \frac{a_l}{h_K} \frac{\omega}{\sqrt{k^2+\mu^2}} [\, e^{\mu(l-x)} \cos(k(l-x) + \omega t + \phi) - e^{\mu(x-l)} \cos(k(x-l) + \omega t + \phi)\,] \tag{4.28}$$

where $a_l = \dfrac{a}{\sqrt{\cos^2 kl \cosh^2 \mu l + \sin^2 kl \sinh^2 \mu l}}$, (4.29)

and

$$k = \frac{\omega}{\sqrt{2gh_K}} [1 + \sqrt{1+\beta^2}\,]^{\frac{1}{2}}, \quad \mu = \frac{\omega}{\sqrt{2gh_K}} [-1 + \sqrt{1+\beta^2}\,]^{\frac{1}{2}}, \quad \cos\phi = \frac{k}{\sqrt{k^2+\mu^2}}$$

with $\beta = \dfrac{r}{h\omega}$ (4.30)

In case the friction term dominates over the acceleration term (which is mostly the case) we have $\beta > 1$. Sometimes even $\beta \gg 1$, so that

$$k \approx \mu \approx \sqrt{\frac{r\omega}{2ghh_K}} \tag{4.31}$$

In the latter case *u* is approximately 45° out of phase with η. This corresponds with the picture of a tidal wave that propagates by diffusion.
Also when

$$kl = \frac{\pi}{2} \tag{4.32}$$

a_l and *U* remain finite.
The fact that energy is dissipated in the basin is reflected in de net influx of tidal energy:

$$< uE > > 0 \tag{4.33}$$

4.4.5 Radiation damping

Besides due to bottom friction also energy loss is occurring due to radiation in the basin mouth. The basin functions as a momentum source for the open sea:

$$u = -u_0 \sin \omega t \tag{4.34}$$

This momentum radiation causes a correction to the tide at the basin entrance:

$$\eta \rightarrow \eta + \eta_r , \quad \eta_r = a_r \cos \omega t \tag{4.35}$$

From the propagation equation of the momentum source to the open sea we find:

$$a_r = F_r \frac{h u_0}{c} \tag{4.36}$$

Here u_0 is the flow velocity in the mouth induced by the basin resonance,

$$u_0 = -\frac{a + a_r}{h} c \tan kl , \tag{4.37}$$

and F_r is a factor given by

$$F_r = -\frac{2}{\pi}\frac{1}{k}\frac{h}{h_z}\frac{d}{dr} H_0^{(2)}\left(\frac{wr}{\sqrt{gh_z}}\right)_{r=\frac{1}{2}b}, \qquad H_0^{(2)} = \text{Hankelfunctie} , \tag{4.38}$$

The Hankelfunction $H_0^{(2)}\left(\frac{wr}{\sqrt{gh_z}}\right)$ describes the radial propagation of a tidal wave that radiates towards an infinitely large sea of uniform depth h_z. This wave absorbs tidal energy from the basin:

$$< uE >|_{r=\frac{1}{2}b} < 0 \tag{4.39}.$$

From the above equations it follows that

$$a_r = -a \frac{F_r \tan kl}{1 + F_r \tan kl} . \tag{4.40}$$

Hence the resonance in the basin remains bounded

$$\left|\frac{a_l}{a + a_r}\right| = \frac{1}{|\cos kl + F_r \sin kl|} < \infty . \tag{4.41}$$

4.5 Tidal deformation; ebb and flood asymmetry

In most tidal basins the tidal curves for water level and flow velocity (or discharge) strongly differ from a sinusoidal curve. This is illustrated in Figure 4.7 for a number of tidal basins in the Netherlands. The underlying processes are discussed in this section,

where we will find out that the causes for the deformation are partly due to the morphological characteristics of the basins themselves.

4.5.1 Impact of bottom friction

Bottom friction is especially of importance for long tidal basins (i.e. a length of some tens of kilometres at least) with maximum tidal velocities at least 1 m/s. The bottom friction introduces ebb-flood asymmetry in case the tidal amplitude cannot be neglected relative to the basin depth, i.e. if the depths H and $H_K = Hb_S / b_K$ vary over the tide and hence cannot be assumed constant. In that case the tidal equations are no longer linear, and also no longer simply solvable.
However, in order to gain some insight in the tidal deformation and tidal asymmetry we adopt a similar assumption as was done before for the propagating tidal wave. In the period between high water (HW) and high water slack (HWK) we consider H and H_K as constants with values H^+ en H_K^+. Other variables that are considered constant in this period are also indicated with the superscript +. Also during the period between low water (LW) and low water slack (LWK) we consider H and H_K as constants, with values H^- and H_K^-. Other variables that are considered constant in this period are also indicated with the superscript - .
We adopt the earlier derived expressions for u and η (damped reflected tidal wave):

$$\eta = \frac{1}{2} a_l [\, e^{-\mu(x-l)} \cos(k(x-l) - \omega t) + e^{\mu(x-l)} \cos(k(x-l) + \omega t) \,] \qquad (4.42)$$

and

$$u = \tfrac{1}{2} \frac{a_l}{H_K} \frac{\omega}{\sqrt{k^2+\mu^2}} [\, e^{\mu(l-x)} \cos(k(l-x) + \omega t + \phi) - e^{\mu(x-l)} \cos(k(x-l) + \omega t + \phi) \,] \qquad (4.43)$$

These expressions remain valid for the indicated periods, but with a different value for the wave number, the propagation speed and the phase (resp. $k^{\pm}, c^{\pm}, \phi^{\pm}$).
In these expressions the time-axis is chosen such that $t = 0$ coincides with HW at the basin end $x=l$ and that $t = T/2$ coincides with LW at the basin end. Relative to these instants the instants of slack water, resp. HWK en LWK, can be obtained by solving the equation $u(x,t) = 0$:

$$e^{\mu(l-x)} \cos(k(l-x) + \omega t + \phi) = e^{\mu(x-l)} \cos(k(x-l) + \omega t + \phi) \,] \,,$$

or

$$\cos(\omega t + \phi) \cos(k(x-l)[e^{-\mu(x-l)} - e^{\mu(x-l)}] = -\sin(\omega t + \phi) \sin(k(l-x)[e^{-\mu(x-l)} + e^{\mu(x-l)}] \qquad (4.44)$$

In the relatvely short basins that we consider here, the following always holds:

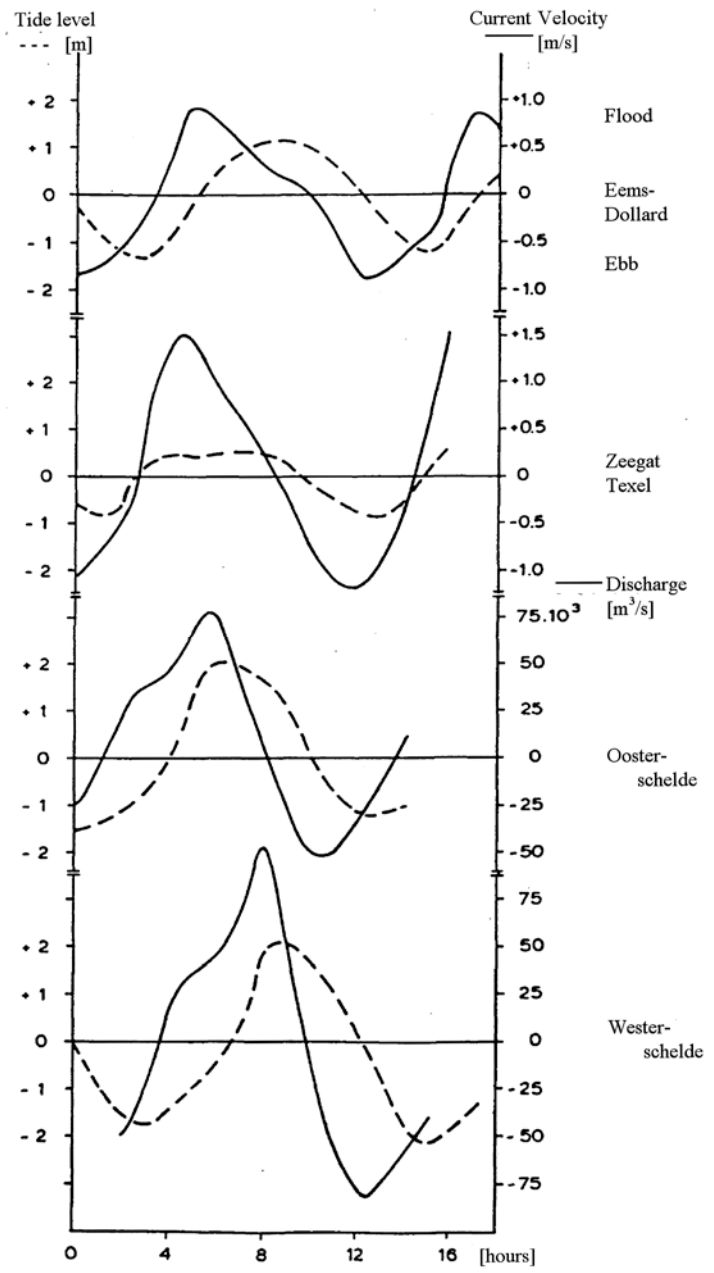

Figure 4.7: Tidal curves for water level, flow velocity and discharge

$(\mu l)^2 >> 1, (kl)^2 >> 1$. In that case we may approximate:

$$\tan(\omega t + \phi) = \frac{\tanh(\mu(x-l))}{\tan(k(x-l))} \approx \frac{\mu}{k} \tag{4.45}$$

This implies that slack water takes place virtually at the same moment all over the basin. Since at the basin end ($x \to l$) high/low water and high/low water slack coincide, we find:

$$t_{HWK}(x) - t_{HWK}(l) \approx t_{HWK}(x) - t_{HW}(l) \approx 0 \tag{4.46}$$

$$t_{LWK}(x) - t_{LWK}(l) \approx t_{LWK}(x) - t_{LW}(l) \approx 0 \tag{4.47}$$

By solving the equation $\eta_t = 0$ we can determine the high and low water instants in the basin at different locations relative to each other. This follows the same procedure as for $u = 0$. The result is

$$\tan(\omega t) = -\tan(k(x-l))\tanh(\mu(x-l)) \approx -k\mu(x-l)^2 \approx \omega t \tag{4.48}$$

implying that:

$$t_{HW}(x) - t_{HW}(l) \approx t_{HW}(x) - t_{HWK}(l) \approx \frac{k^+\mu^+}{\omega}[l^2 - (x-l)^2] \tag{4.49}$$

$$t_{LW}(x) - t_{LW}(l) \approx t_{LW}(x) - t_{LWK}(l) \approx \frac{k^-\mu^-}{\omega}[l^2 - (x-l)^2] \tag{4.50}$$

Now let us assume that the tide at the seaward entrance ($x = 0$) is symmetrical, i.e.

$$t_{HW}(0) - t_{LW}(0) = \tfrac{1}{2}T \tag{4.51}$$

This implies that the difference in duration of ebb and flood approximately is given by

$$\Delta t_{\text{flood}} - \Delta t_{\text{eb}} \approx \frac{2\pi}{\omega} l^2 [k^+\mu^+ - k^-\mu^-] \tag{4.52}$$

By substitution of the expressions for k and μ we arrive at

$$\Delta t_{\text{flood}} - \Delta t_{\text{eb}} \approx \pi \frac{rl^2}{g}\left[\frac{1}{H^+H_K^+} - \frac{1}{H^-H_K^-}\right] \tag{4.53}$$

or in other words:

$$\Delta t_{\text{flood}} - \Delta t_{\text{eb}} \propto -H^+ H_K^+ + H^- H_K^- \tag{4.54}$$

A difference between flood and ebb duration implies (because of the equality of flood and ebb discharge) that the average flow velocity at flood differs from that at ebb, and consequently that the average sediment transport a flood differs from that at ebb.
In many tidal basins the storage width at HW is often much larger that that at LW, especially when large intertidal flats are present. In that case we have

$$(b_K / b_S)^+ >> (b_K / b_S)^- \tag{4.55}$$

Moreover if the channels are deep ($a/h << 1$), it follows that $H^+ \approx H^-$, so that

$$(HH_K)^+ << (HH_K)^- \tag{4.56}$$

This implies that the flood period is larger than the ebb period. As a consequence the maximum ebb flow velocity is larger than that of flood. For tidal basins with little storage providing intertidal flat areas and shallow channels we find the opposite:

$$(b_K / b_S)^+ \approx (b_K / b_S)^- , H^+ > H^- , (HH_K)^+ > (HH_K)^- \tag{4.57}$$

This implies that the maximum flood velocity is larger than the maximum ebb velocity. In summary, in tidal basins tidal asymmetry and resulting sediment transport occur that are related to the morphology of the basin. We will discuss and evaluate these findings in what follows.

4.5.2 Short tidal basins; impact of basin geometry

Also in shorter tidal basins the tidal asymmetry is influenced by the basin geometry. However, in this case we deal with a different type of asymmetry, viz. a difference between the flow velocity variation around HW and LW slack. As we will discuss later this asymmetry is of large importance for the net transport of fine sediment in the basin. In the case of a short basin (length much smaller than a quarter of the tidal resonance length, with the amplitudes of the incoming and reflected tidal wave of the same order) the tidal phase difference between seaward and landward end is negligible. In that case we may integrate the continuity equation over the length of the basin:

$$u(x,t) = \frac{\eta_t(t)}{A_s(x,t)} \int_x^l b_K(x,t)dx \approx (l-x)\frac{\eta_t(t)}{H_K(t)} \tag{4.58}$$

For the last approximation in the above equation the cross-section is assumed constant. In a short basin η and u are out-of-phase; at HWK (high water slack) and at LWK we have:

$$\eta_t \approx 0 \tag{4.59}$$

Hence, we find for the flow velocity variation around HWK relative to that around LWK:

$$\frac{|u_t|_{HWK}}{|u_t|_{LWK}} \approx \frac{H_K^-}{H_K^+}\frac{|\eta_{tt}|_{HWK}}{|\eta_{tt}|_{LWK}}. \tag{4.60}$$

Suppose the tide at sea is symmetrical around HW relative to LW, than the last factor is approximately equal to 1. The above equation then tells us that in a basin with vast storage offering tidal flats and deep channels ($H_K{}^+ < H_K{}^-$) a vast variation of the flow velocity occurs around HWK relative to LWK: the HW-slack duration is shorter than that of LW-slack duration.
In a basin with shallow channels and little storage offering flats ($H_K{}^+ > H_K{}^-$) a relative slow variation around HWK relative to LWK occurs: the HW-slack duration is longer than of LW-slack duration. In the former case stronger sedimentation will take place at LWK than at HWK, in the latter case it will be vice versa.

4.5.3 Impact of the tide at sea

The asymmetry of the velocity variation in a tidal basin will strongly depend on the water level variation of the tide at sea. This holds especially for short basins, and to a lesser degree also for longer basins. A faster water level rise than fall at sea causes higher flood flow velocities than ebb flow velocities in the basin and vice versa.

A long duration of HW at sea causes a long slack water duration and a short duration of HW at sea a short slack water duration. The same holds for LW. Deformation of the tidal wave along the coast has an impact on the ebb-flood asymmetry in the adjacent tidal basins and hence on the net inward or seaward sediment transport and the morphological evolution.
Figure 4.8 illustrates the tidal variation for the Dutch coast and the adjacent tidal basins; this shows how the sea-borne tidal asymmetry is transferred into the basins.

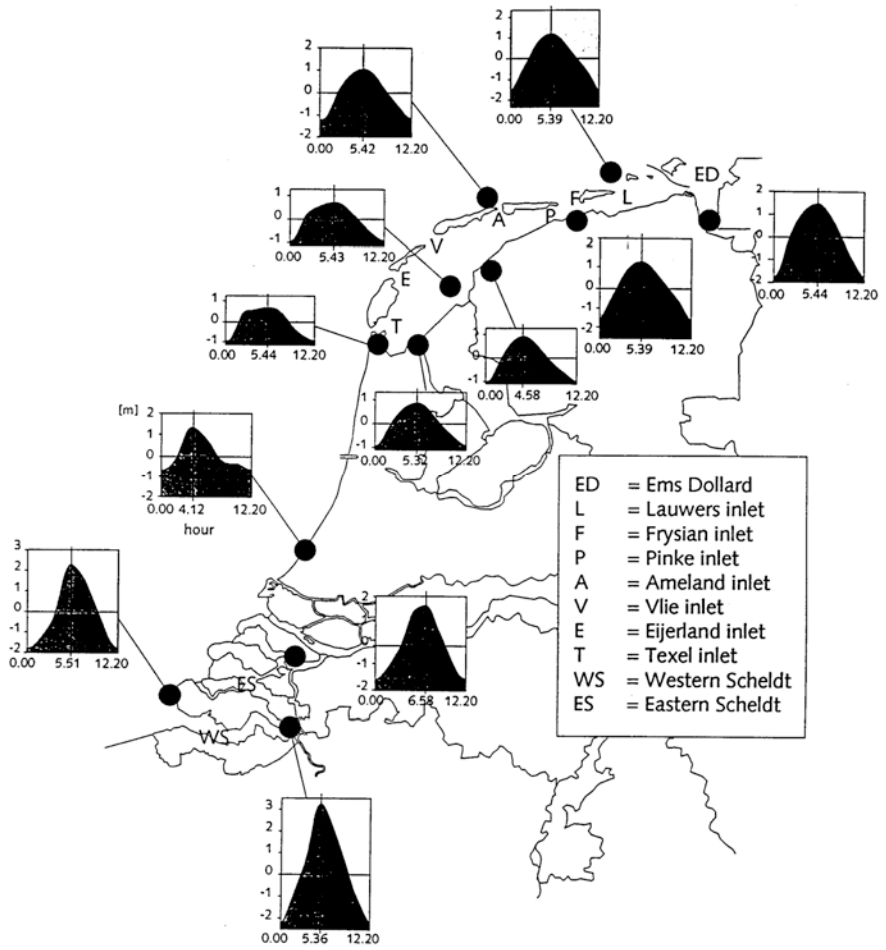

Figure 4.8: Tidal variation of the water levels along he Dutch coast and in the adjacent basins

4.6 Intermezzo: sediment properties

Bottom material in coastal regions consists of a variety of sediment types. An important characteristic distinction for Sediments is the diameter. The diameter can vary strongly from silt (diameter ca. 10^{-6} m) to sand (diameter ca. 10^{-4} m) and gravel (diameter ca. 10^{-3} m). The density or specific weight (in Dutch: soortelijk gewicht (s.g.)) of the sediment particles is on average 2,5 to 3 times the density of water; however, heavy minerals with much higher density can also be found.
Due to their higher density sediment particles will settle in water in the absence of turbulence or vortices. For small particles the mean fall velocity in water can be derived from Stokes' law:

$$w = \frac{g}{18\upsilon} d^2 \frac{\Delta\rho}{\rho} \tag{4.61}$$

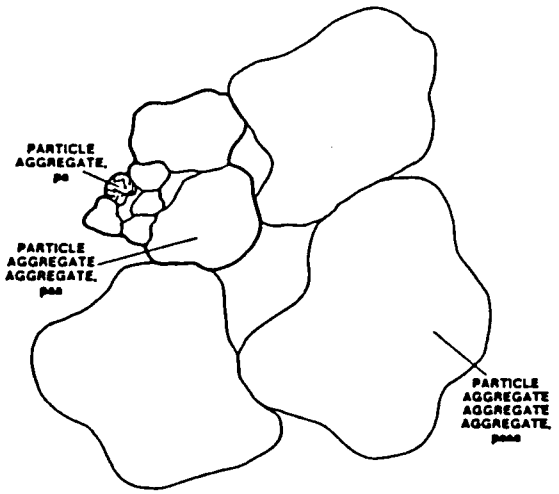

Figure 4.9: Flocculation of sediment particles

This derivation is only valid for Reynolds numbers smaller than 1, i.e. for very small particles. However, such particles are inclined to flocculate (in Dutch: klonteren), so that particle aggregates are formed with a much larger diameter (figure 4.9). Flocs have therefore a much larger fall velocity than that of the individual particles, even though the floc density is less than that of the composing particles.

Several factors play a role in the flocculation process:

- The particle concentration: The floc growth and the size of the flocs increase with increasing particle contact. Measurements show that the fall velocity of flocs formed in high concentrations is larger than that in lower concentrations (approximately linear or quadratic increase with concentration). In very high concentrations (e.g. close to the bottom) particles hinder one another during settling, resulting in a decrease of fall velocity with increasing concentration. This process is referred to as "hindered settling".
- The turbulence intensity: Turbulence increases the frequency of particle contacts and hence promotes flocculation growth. In very intense turbulence and associated shear stresses (e.g. at the bottom) big flocs will break up, so that the fall velocity decreases and particles are resuspended.
- The salinity: Clay particles have surface charges enabling particles to stick together. Presence of Cl^- ions promotes this attraction process.
- Presence of organic materials, bacteria and other organisms. Particles in aggregates are often interconnected by large molecules (sugars, proteins; in Dutch: suikers, eiwitten) and fine threads that are excreted in the water by organisms.

Particle aggregates are strongly variable in composition. The diameter can be 1000 times larger as that of the composing particles. Such large flocs are however very fragile. For

the fall velocity not only the diameter is of importance, but also the density (water content) and the drag (hydrodynamic form). In practice fall velocities of particle aggregates can only be determined empirically (figures 4.10 and 4.11).

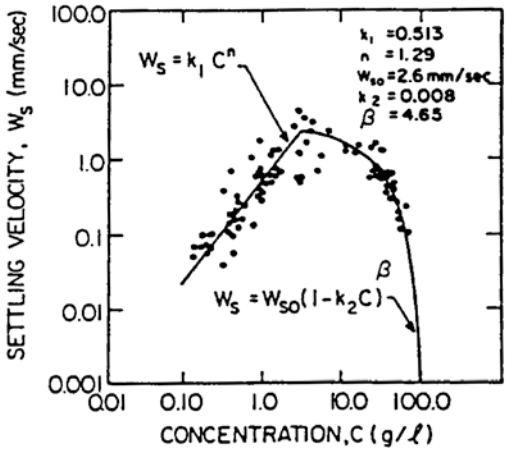

Figure 4.10: Fall velocity of sediment particles as a function of the concentration (fine cohesive sediment)

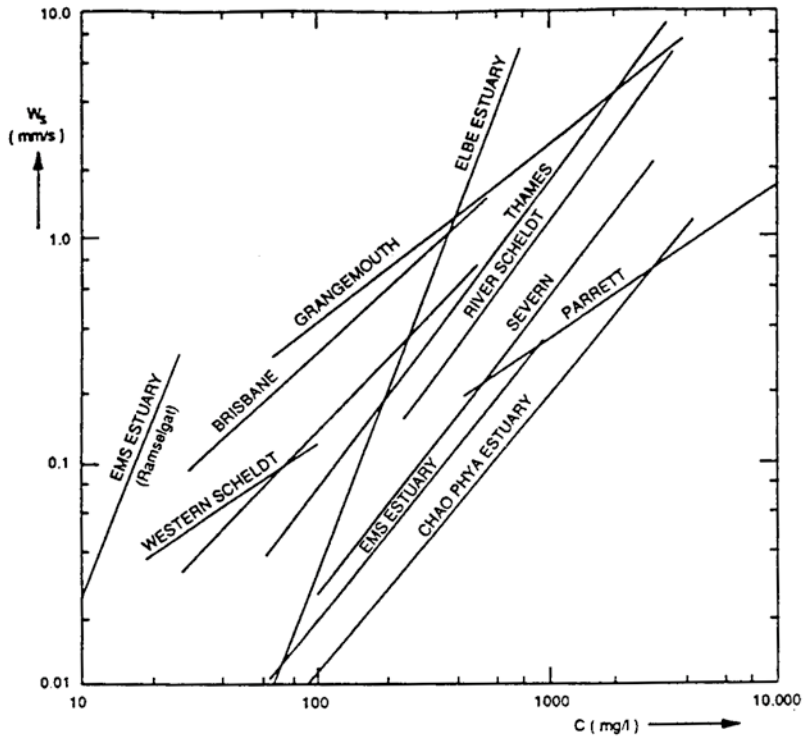

Figure 4.11: Variability of fall velocities of fine sediments in different coastal systems

Due to the settling of sediment particles a suspension close to the bottom may occur with a significantly higher density than that of the suspension layer above (on the condition that sufficient turbulent mixing in the bottom layer occurs). If turbulent mixing between the two layers is sufficiently suppressed by the density difference, a clear separation plane is formed (lutocline). Increasing fall velocities due to flocculation in the upper layer and decreasing fall velocities due to hindered settling) in the lower layer

contribute to the formation of the dense bottom layer.

The rate of resuspension of settled sediments by the flow is also depending on a large number of factors. This concerns, amongst others, the degree of consolidation or packing of the sediment, that increases with the age of the sedimentation during which sediment compacts and drains (in Dutch: ontwateren) under its own weight. In a loosely packed, water saturated bottom water stresses cause separation of particles facilitating resuspension and transport by flow. A bottom in which the pores between the larger particles are filled with smaller particles is less erodible. The bottom is than closed from the water column, so that pressure fluctuations are absorbed by the smaller particles and hardly transferred to the water pressure in the bottom. Also cohesive properties play a role. Organisms that excrete sticky substances determine these; on the bottom for instance diatoms (in Dutch: algenmatten) can be formed. Furthermore there are various organisms that rework sediments (this is named “bioturbation”). Also bacteria may cause chemical processes in the bottom (e.g. gas formation). The net impact of biota on the erodibility of bottoms can both be positive and negative.

The shear stress caused by the flow along the bottom is primarily responsible for erosion of sediment particles. Especially important are the turbulent water motions ("bursts" and "sweeps"). These resuspend the particles. Below a critical shear stress, which depends on the cohesion, the density and the particle size, no sediment is eroded. Figure 4.12 gives an impression of the minimal or critical flow velocity that is required to cause erosion for different types and sizes of sediment. This figure however, does not show that also wave action has a large impact on erodibility; in the presence of waves erosion occurs at much lower flow mean velocities. This has a lot to do with the wave-induced fluctuations in the water pressure in the bottom.
When the flow velocity is larger than the critical flow velocity, bottom material is resuspended and transported. Partly the transport occurs along de bottom (in rolling and jumping mode), and partly the transport takes place in the water column where turbulence keeps the particles in suspension. The ratio between bottom and suspension transport depends on the flow velocity and the sediment diameter (see Figure 4.13). The bottom transport is strongly related to the small-scale structures on the bottom. Depending on the type of sediment, the sediment diameter and the near bottom flow velocity different bottom structures are formed, see Table 4. 1. These structures have a large impact on the bottom roughness that is experienced by the flow. Empirically it follows that under stationary flow the shear stress between water and bottom can well be described by the expression:

$$\tau_b \approx \rho c_D \,|\mathbf{u}|\,\mathbf{u} \tag{4.62}$$

The value of the friction coefficient c_D ("bottom roughness") is generally between 0.002 and 0.004, depending on sediment diameter and smaller scale bottom structures. A physical description of the interaction between flow properties, bottom roughness, bottom transport and the formation bottom structures is very complex and largely

unknown. In practice empirical relations are used that are experimentally derived for common flow situations and sediment conditions.

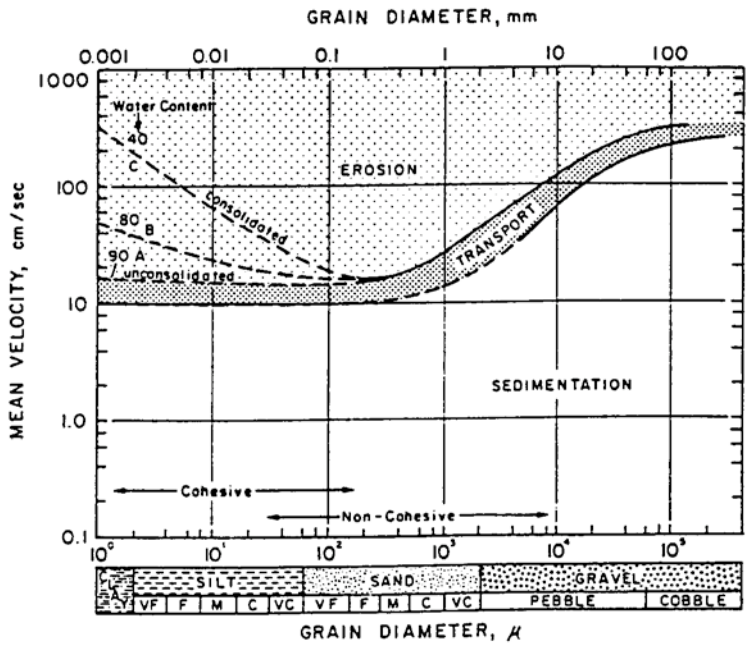

Erosion, transport, and deposition regimes for mean current velocities versus grain size. Solid lines represent critical velocities required for erosion, transport, and deposition of bed sediment while dashed lines represent extrapolated trends. Lines A-C and critical velocities for various stages of consolidation represented by decreasing water content. Adapted from Hjulstrom (1939), Postma (1967), and McDowell and O'Connor (1977).

Figure 4.12: Critical flow velocity as a function of sediment type and size

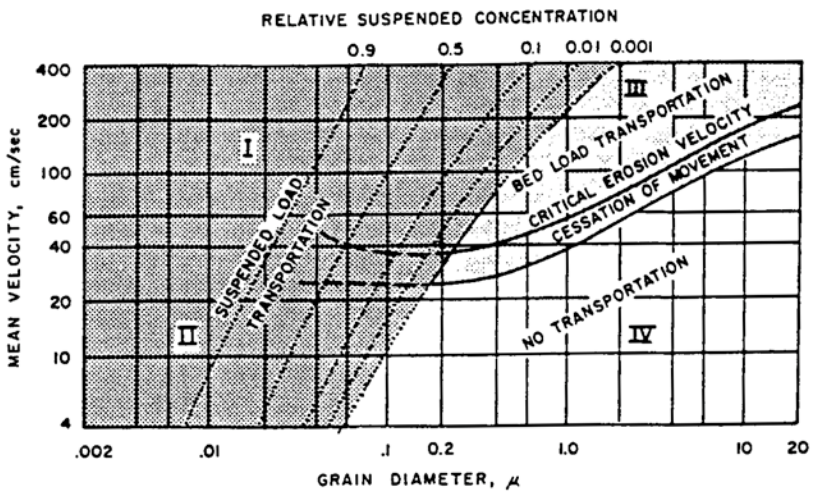

Relationship between flow velocity, grain size, and state of movement for uniform sediment of 2.65 density. The curves representing the relative concentration of suspended sediment indicate the ratio between the concentration at one-half the water depth and a reference level near the bed. Dotted lines represent diffuse boundaries. Velocity is measured at 100 cm above the bed; after Reineck and Singh (1980) and Sundborg (1967).

Figure 4.13: Sediment transport type (bottom transport or suspended transport) as a function of flow velocity and sediment diameter

Table 4.1 Characteristics of lower flow regime bedforms (modified after Harms et al., 1975)

	Ripples	Megaripples	Low-energy sand waves	High-energy sand waves
Spacing	<60 cm	60 cm–10 m	> 6 m	> 10 m
Height/spacing ratio	variable	relatively large	relatively small	very small
Geometry	highly variable	sinuous to highly three-dimensional, prominent scour pits in troughs	straight to sinuous, uniform scour in troughs	straight to sinuous
Characteristic flow velocity	low (> 25–30 cm/sec < 40–50 cm/sec)	high (> 70–80 cm/sec, < 100–150 cm/sec)	moderate (> 30–40 cm/sec, < 70–80 cm/sec)	high (> 70–80 cm/sec, may be 150 cm/se
Velocity asymmetry	negligible to substantial	negligible to substantial	usually substantial	small to substantial

The magnitude of bottom transport can be approximated by the empirical expression (valid for small bottom slopes):

$$S \approx \rho_{sed} \beta \, |\mathbf{u}^{b-1}| \, \mathbf{u}, \;\; b = 3-5, \;\; \beta = 10^{-7} - 10^{-4} \;\; [m^{2-b} s^{b-1}] \qquad (4.63)$$

In this course we mostly propose $b = 3$.
For suspension transport of normal to coarse, non-cohesive bottom material (sand) often a similar expression is used. For suspension transport of fine (cohesive) sediment other formulations need to be adopted, that take account of the time lags involved with settling and resuspension. This is treated in the next section.

4.7 Transport of fine sediment

The net amount of sediment per unit width, M, that is transported in one tidal period through the plane x_0 is given by:

$$M(x_0) = \int_0^T h(x_0,t) u(x_0,t) c(x_0,t) dt \qquad (4.64)$$

where c = depth-averaged concentration of fine sediment in suspension
u = depth-averaged flow velocity
This expression is only valid if the flow velocity can be assumed approximately uniform over the cross-section. In the case of density driven circulation that is certainly not the case and it is then necessary to include under the integral vertical and lateral variations in flow velocity and sediment concentration.
In a moving cordinate frame $(\frac{D}{Dt} = \frac{\partial}{\partial t} + u\frac{\partial}{\partial x})$ we have:

$$\frac{Dc}{Dt} = \frac{1}{h}[\,Er - Se\,] \qquad (4.65)$$

change in sediment load = erosion minus sedimentation

For fine, cohesive sediment the following semi-empirical relations have been derived:

Sedimentation $$Se = W_s c\,(1 - \frac{\tau}{\tau_{Se}})\,\theta(\tau_{Se} - \tau) \qquad (4.66)$$

Erosion $$Er = \mu_{Er}\,(\frac{\tau}{\tau_{Er}} - 1)\,\theta(\tau - \tau_{Er}) \qquad (4.67)$$

Where θ is the step-function, $\theta(x) = 0$ for $x < 0$, and $\theta(x) = 1$ for $x \geq 0$. The coefficients W_{Se} [m/s] and μ_{Er} [kg/m^{2}s] and the critical shear stresses τ_{Se} and τ_{Er} are depending on the type and concentration of the sediment, the bottom condition (i.e. the degree of consolidation) and other factors (i.e. chemical and biological).
In our case we are not so much interested in the most accurate description of the sedimentation-erosion process, but rather in the time-scales of erosion and sedimentation. This is a characteristic that causes an essential difference in the tidal dynamics of fine sediment (silt) compared to coarser sediment (sand). For sand this time-scale is an order-of-magnitude smaller than the tidal period, where as for fine sediment the time-scales are of similar order. For fine sediment we denote this time-scale as T_{sed}. If we assume that under the condition of a constant flow velocity after some time an equilibrium concentration c_{eq} is reached, than T_{sed} is the time-scale for which the suspended concentration approaches the equilibrium concentration. In formula form:

$$\frac{Dc}{Dt} = \frac{1}{T_{\text{sed}}}(c_{eq} - c)\,. \qquad (4.68)$$

The equilibrium concentration c_{eq} can be determined experimentally; it appears that often

$$c_{eq} \approx \beta\,|u|^{b-1} \qquad (4.69)$$

in which $b \approx 3$ (depending on the type of sediment).
In principle a distinction must be made between the relaxation time-scales T_{sed} for erosion and for sedimentation, resp. T_{Er} and T_{Se} . The latter is amongst others dependent on the water depth, viz. $T_{Se} \approx h / w_s$.
This implies that the amount of sedimentation at HW can strongly differ from that at LW. This is particularly the case when the wet surface of the basin is much larger at HW than at LW, implying that $H_K^+ \prec\prec H_K^-$. The impact of this larger sedimentation at HW than at LW can be strengthened by the effect of a longer slack water period at HW than at LW (or vice versa be weakened in case the slack water period at HW is shorter than at LW).

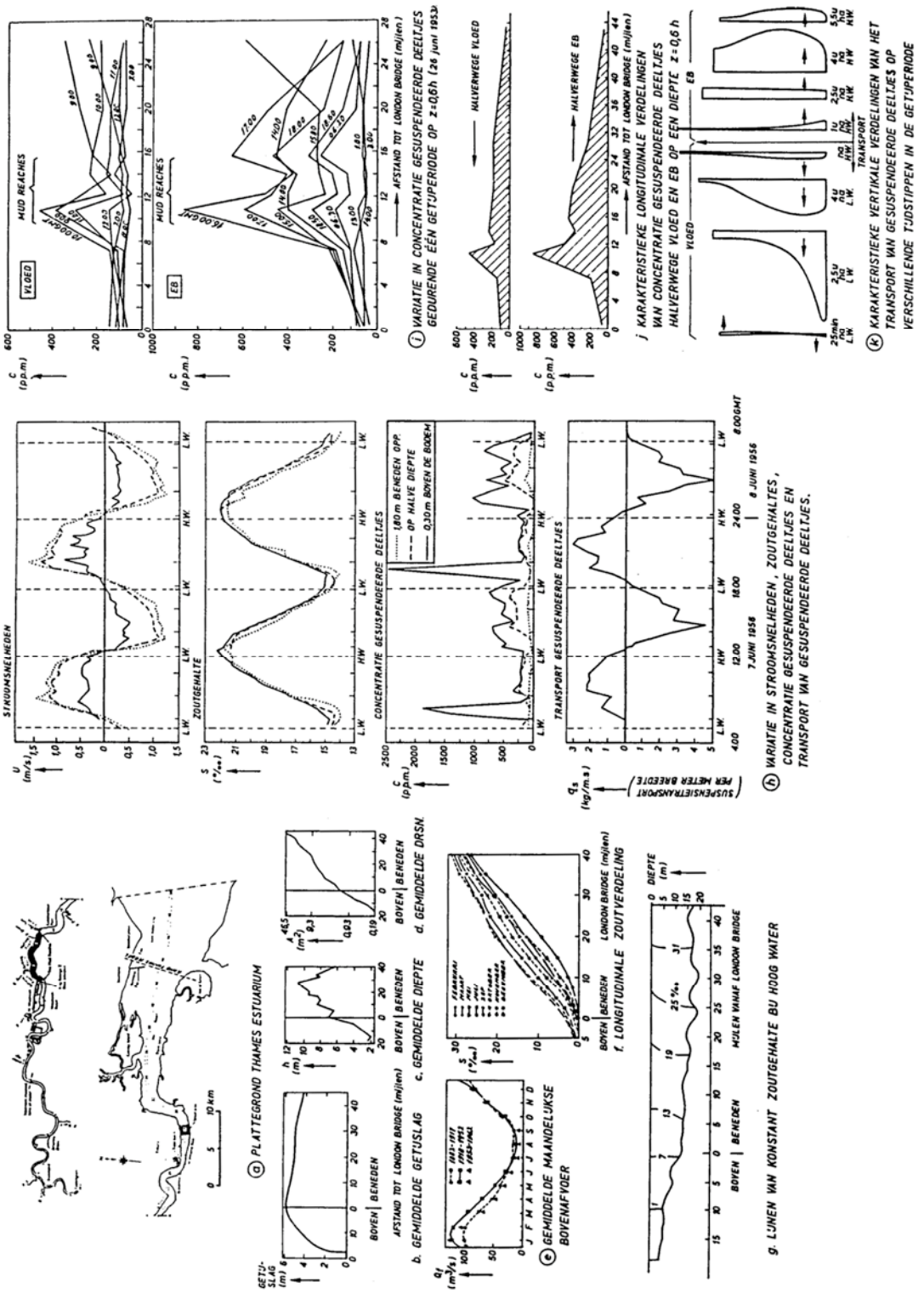

Figure 4.14: Sediment transport due to tidal asymmetry (middle figure)

The relaxation equation for the suspended concentration shows that an asymmetry in the slack water periods around HW and LW can cause a resulting transport of fine sediment. Let us assume that the slack water duration at HW is much longer than that around LW. Earlier we found that this is a characteristic property of a tidal basin with shallow channels and limited tidal storage flats. In that case a strong sedimentation

occurs around HWK; in the initial ebb phase only little material is in suspension and the concentration only slowly increases. Only later in the ebb period more fine sediment is suspended that is transported. Around LWK part of this sediment settles, but not so much because of the short slack water duration. When the flood current increases in strength immediately a relatively large amount of suspended material is transported. Subsequently, the suspended concentration increases even further. Averaged over flood the concentration of suspended sediment is therefore larger than that during ebb. Over the whole tidal period we therefore observe a net landward-directed transport. An example of the reverse, a short HWK and a net seaward-directed transport of fines, can be observed in Figure 4.14 for the Thames estuary.

In case $T_{Er} = T_{Se} = T_{sed}$ = constant the erosion-sedimentation equation can be integrated to yield:

$$c(t) = c(t_0) + \frac{e^{-\frac{t}{T_{sed}}}}{T_{sed}} \int_{t_0}^{t} e^{\frac{t'}{T_{sed}}} \left(c_{eq}(t') - c(t_0) \right) dt' \tag{4.70}$$

We are dealing here with the suspended concentration in a moving coordinate system along with the tide. For the derivation of the tidal-integrated transport this result cannot be used straightforwardly since in the transport-integral the fixed cross-section x_0 is considered. In stead of a transport-integral over a fixed cross-section we therefore consider transport through a plane that moves with the average tidal velocity $u(x,t)$. The position of the plane is denoted by $X(t)$, yielding:

$$\frac{dX}{dt} = u(X,t) \tag{4.71}$$

If the tidal motion is assumed cyclic and if we neglect river discharge, than $X(t= 0) = X(t=T) = x_0$. After a full tidal cycle the moving plane than returns to its original position. The amount of material transported through the moving plane averaged over a tidal period is therefore identical to the net transport though the fixed plane:

$$M(x_0,t) = \int_0^T h(x_0,t)u(x_0,t)c(x_0,t)dt = \int_0^T h(X(t),t)u(X(t),t)c(X(t),t)dt \tag{4.72}$$

The last integral can be rewritten by reasoning that through the moving plane only material is transported that originates from the bottom. Hence material that is eroded in front of the moving plane does not pass the plane and must be subtracted; in contrast, material that sedimentates in front of the plane will pass the plane and must be added to the transport. If we assume that no sedimentation or erosion occurs over the trajectory of the plane during a full tidal cycle, we may write the transport integral as:

$$M(x_0,t) = \int_0^T dt \int_{x_0}^{X(t)} (Se - Er)\, dx \tag{4.73}$$

This expression shows that sedimentation at HWK plays a role in the landward part of the basin (between x_0 and $X(HWK)$) and at LWK in the seaward part (between $X(LWK)$ and x_0 . For erosion the same holds. Particularly for fine sediment it holds that if in the landward part of the basin at HWK a stronger sedimentation and weaker erosion occurs than in the seaward part at LWK, a resulting landward sediment transport occurs. Hence for fine sediment the asymmetry in slack water duration in the HWK and LWK locations is of importance.

The above can be expresses in the following expressions, in which also the effect of the wet surface area (hence average basin depth) on the magnitude of the sedimentation is accounted for. Net flood transport occurs if:

$$|\frac{du}{dt}(LWK, X_{LWK})| > |\frac{du}{dt}(HWK, X_{HWK})|, \quad h(LWK, X_{LWK}) > h(HWK, X_{HWK}) \tag{4.74}$$

and net ebb transport occurs if:

$$|\frac{du}{dt}(LWK, X_{LWK})| < |\frac{du}{dt}(HWK, X_{HWK})|, \quad h(LWK, X_{LWK}) < h(HWK, X_{HWK}) \tag{4.75}$$

(HWK = slack HW preceding the ebb, LWK = slack LW preceding the flood).

A large storage offering flat area has two opposing effects on the net transport of fine sediment: on the one hand a large storage prism causes a short slack duration in the flow channel at HWK; on the other hand in this short period a strong settling can occur due to the small water depth. The latter effect often dominates.
For coarser sediment (sand) slack water duration does not play a role of importance because of the short sedimentation time-scale. In this case it is the difference between near-bed and suspended concentrations during ebb or flood that is important. Generally speaking we may state that we have net flood trasnport for u_{max}(flood) > u_{max}(ebb) , and net ebb transport in the reverse case.

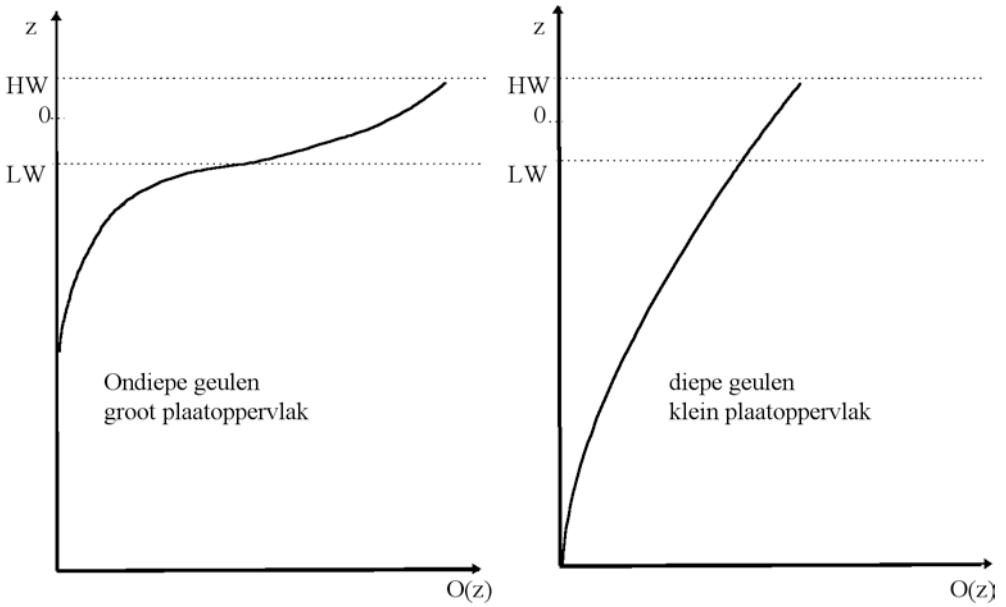

O(Z)= bekkenoppervlak [m^2] als functie van de afstand tot het wateroppervlak z

Figure 4.15: Different basin types (these curves are also referred to as hypsometric curves)

4.8 Overview of the relation sediment transport and morphology

From the above sections we may derive qualitative relations between net sediment transport and the morphological characteristics of tidal basins. Table 4.2 gives an overview, in which also the role of external conditions (tides, waves) is indicated. Conditions for net transport of fine sediment (silt):

Table 4.2: Conditions for net transport of sediment

NET FLOOD-TRANSPORT	NET EBB TRANSPORT	TIDAL ASYMMETRY
Small storage flat area	Large storage flat area	u_{max} flood/ebb slack duration HW/LW
Large storage flat area	Small storage flat area	sedimentation HW/LW (this effect often dominates over the above effect)
Strong landward depth decrease	Landward deep channels	sedimentation HW/LW
Shallow channels	Deep channels	u_{max} flood/ebb slack duration HW/LW
Landward decreasing flow	Strong landward flow	slack duration HW/LW
Long HW-period at sea	Short HW-period at sea	slack duration HW/LW
Protected location, few waves	Open, many waves	sedimentation HW/LW
Conditions for net transport of sand:		
NET FLOOD-TRANSPORT	NET EBB TRANSPORT	TIDAL ASYMMETRY
Small storage flat area	Large storage flat area	u_{max} flood/ebb
Long shallow channels	Long deep channels	u_{max} flood/ebb
Fast tidal rise at sea	Fast tidal fall at sea	u_{max} flood/ebb
Landward decreasing flow	Strong landward flow	Gradient in sediment transport

4.9 Large-scale morphodynamics

4.9.1 Morphological equilibrium

We speak of morphological equilibrium in case ebb and flood sediment transports are equal. This is also dependent on external conditions, but if we assume these to be neutral different basin geometries may fulfil the condition for equilibrium:

- Shallow channels and large intertidal (storage) flat area (e.g. Wadden Sea)
- Deep channels and small intertidal (storage) flat area (e.g. Oosterschelde)
- Intermediate geometries

In the equilibrium condition the geometrical characteristics of the basin are such that the durations of ebb and flood are approximately equal. In case the tidal asymmetry at sea is not strong this implies that:

$$\left(HH_K\right)^+ \approx \left(HH_K\right)^- \tag{4.76}$$

Since in many tidal basins the flow carrying width at HW (+) is not strongly different from that at LW (-) the above condition for tidal symmetry may be approximated by

$$\frac{H^+}{H^-} = \alpha \sqrt{\frac{b_K^+}{b_K^-}} \tag{4.77}$$

For α larger than 1 the basin is importing (the basin is too shallow), for α smaller than 1 exporting. In practice α will be a little larger than 1 to compensate for sea level rise (requiring import) and Stokes' drift (which increases the ebb flow strength).

4.9.2 Morphological stability

Given tidal boundary conditions we have derived that the tidally averaged sediemnt transport <S> can be described as a function of the basin geometry

$$< S >= f(b_S, h_S, b_P, h_P) \tag{4.78}$$

and to good approximation:

$$< S > \propto \Delta_E - \Delta_F \propto \left(HH_K\right)^+ - \left(HH_K\right)^- \tag{4.79}$$

Where b_S, h_S, b_P, h_P respectively is the flow carrying width (channel width), the flow carrying depth (channel depth), the flat width ($b_P = b_K^+ - b_S^+$) and the flat depth. We assume that the basin is sufficiently uniform longitudinally to characterize the basin topography by these characteristic measures in a single cross-section A. Further we will shorten our notation to

$$< S >=< S(A) > \tag{4.80}$$

For morphological equilibrium it holds that:

$$< S(A^{eq}) >= 0 \tag{4.81}$$

If we disturb this equilibrium slightly, such that $A = A^{eq} + A'$, where $A' << A^{eq}$, we may derive:

$$< S(A) > \approx < S(A^{eq}) > + A' \frac{\partial < S >}{\partial A}|_{eq} = A' \frac{\partial < S >}{\partial A}|_{eq} \tag{4.82}$$

The latter term is a short notation for

$$A' \frac{\partial < S >}{\partial A} = b'_S \frac{\partial < S >}{\partial b_S} + h'_S \frac{\partial < S >}{\partial h_S} + b'_P \frac{\partial < S >}{\partial b_P} + h'_S \frac{\partial < S >}{\partial h_P} \tag{4.83}$$

the dashes indicate a smal perturbation relative to the equilibrium values.
The sediment balance equation reads:

$$\frac{\partial A}{dt} = \frac{\partial < S >}{\partial x} \tag{4.84}$$

Integration from x to the basin end l yields:

$$\frac{\partial A'}{\partial t} \approx - \frac{1}{l - x} < S(A) > \approx - \frac{A'}{l - x} \frac{\partial < S >}{\partial A}|_{eq} \tag{4.85}$$

where $\frac{\partial A'}{\partial t} = b_S \frac{\partial h'_S}{\partial t} + h_S \frac{\partial b'_S}{\partial t} + b_P \frac{\partial h'_P}{\partial t} + h_P \frac{\partial b'_P}{\partial t}$ (4.86)

If the morphological characteristics are independent mutually than the above equation indicates a stable morphological equilibrium requires that all derivatives are positive:

$$\frac{\partial < S >}{\partial b_S}|_{eq}, \frac{\partial < S >}{\partial h_S}|_{eq}. \frac{\partial < S >}{\partial b_P}|_{eq}. \frac{\partial < S >}{\partial h_P}|_{eq} > 0 \tag{4.87}$$

If one of the derivatives is negative a disturbance will initially grow exponentially.
In a basin with a large intertidal area and deep channels net sediment transport is in seaward direction; morphological equilibrium requires shallow channels. A positive disturbance (increase) of the equilibrium depth h_S of the channel will thus lead to net sediment export causing further deepening; this is a case of unstable morphological equilibrium.
The latter result also follows from our earlier derivation that for long, friction-dominated basins the tidally averaged sediment transport <S> increases or decreases proportionally to the increase or decrease of the difference in ebb and flood duration:

$$\delta < S > \propto \delta[H^+ H_K^+ - H^- H_K^-] \propto -[H^{+^2} \frac{b_S^+}{b_K^+} - H^{-^2} \frac{b_S^-}{b_K^-}] \tag{4.88}$$

If the channel depth increases, especially H^- increases, hence

$$\frac{\partial < S >}{\partial h_S} < 0 \tag{4.89}$$

A positive disturbance of the channel width b_S is equivalent to a relative increase of the

intertidal area at LW, b_K^- , so in this case

$$\frac{\partial < S >}{\partial b_S} > 0 \tag{4.90}$$

In this case a net sediment import occurs annihilating the initial disturbance (stable equilibrium).
The fact that tidal basins exist implies that they display a large degree of morphological stability. This stability requires that channel width, channel depth flat width and flat depth are dynamically coupled. Especially the transversal transports in tidal basins are responsible for this dynamic coupling. This internal dynamic coupling can restore the morphological stability of the basin after for instance the channel depth is disturbed in positive or negative sense. Figure 4.16 indicates that for Dutch tidal basins the ration between the average channel depths and flat surface area is such that net ebb and flood transports are approximately equal.

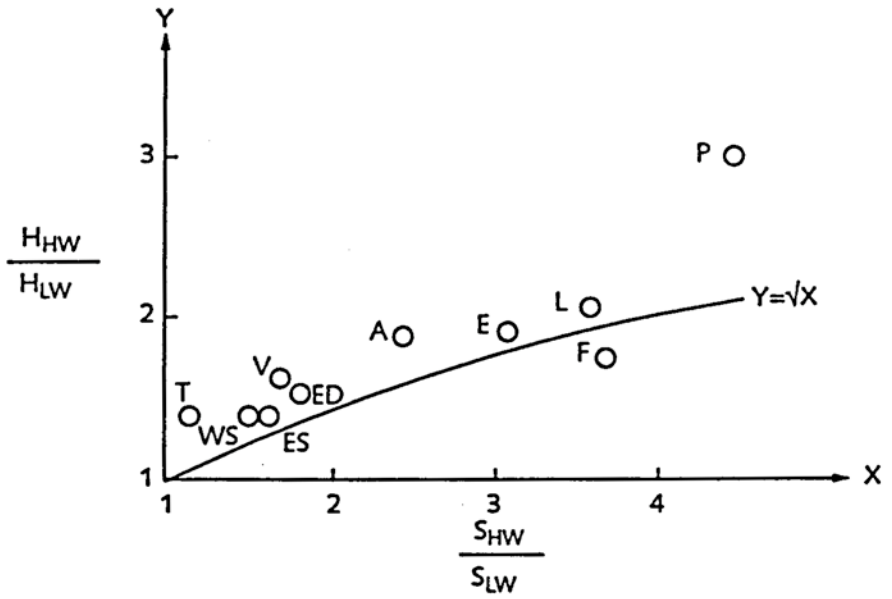

Figure 4.16: Relation between basin averged channel depth and flat area for Dutch tidal basins (for legend see fig. 4.3)

4.9.3 Local morphological equilibrium

The above stability analysis relates to disturbances on basin scale. Often disturbances of depth and width have a more local character. Such disturbances can be annihilated by ebb or flood transports without the occurrence of a net tidally averaged sediment transport. Where flow velocities decrease often a sill is formed, where a local narrowing causes a flow velocity increase erosion occurs.
This implies that we need another equilibrium condition, viz. that gradients in ebb or flood transports cannot be strong. We will investigate this in the following. We start by posing that for a certain cross-section the basin is in equilibrium:

$$A(x) = A^{eq}(x) \ , \quad < S(x) >_{\text{vloed}} = - < S(x) >_{\text{eb}} \equiv S(A^{eq}) \tag{4.91}$$

We now impose a local disturbance

$$A = A^{eq} + A' \tag{4.92}$$

with a lengthscale *l'*.
We assume that this length scale is much smaller than the length scale l_m along which sediment transport reaches equilibrium (l_m is the trajectory along which the flow exchanges a surplus or shortage in suspension concentration with the bottom).
We consider flow in flood direction. A bottom disturbance between *x* and *x+l'* than increases or decreases according to:

$$\frac{\partial A'}{\partial t} \approx \frac{1}{l'}[S(x+l') - S(x)] \approx \frac{A'}{l_m}\frac{\partial S}{\partial A}\Big|_{eq}. \tag{4.93}$$

where we have used $S(x+l') \approx S(x) + \frac{l'}{l_m}(S(A) - S(A_{eq}))$.

For sand transport, in case of an approximately sinusoidal tide, we have:

$$S \propto \tau_{\max}{}^{\frac{3}{2}} \tag{4.94}$$

where $\tau_{\max}$ is the maximum bottom shear stress.
For a small disturbance we than have the stability condition:

$$\frac{1}{A'}\frac{\partial A'}{\partial t} \propto \frac{1}{l_m}\frac{\partial S}{\partial A}\Big|_{eq} \propto \frac{\partial \tau_{\max}}{\partial A}\Big|_{eq} < 0 \tag{4.95}$$

At first sight it seems that this condition is automatically fulfilled: the flow velocity increases if the cross-section is decreased. Yet, this is not always the case, for instance if more parallel channels run in the basin. Also, in the next section on inlets, it will be shown that also in case of a single channel instability can occur.
Annihilation of a local disturbance implies that sediment from nearby areas needs to be stored or eroded. Effectively the disturbance propagates. However, if flood and ebb flow velocities are of the same order no propagation occurs, but only diffusion. It is in this sense that a disturbance in a morphologically stable channel is cancelled.
In the above we have assumed that no secondary circulation currents have been caused by the disturbances. This assumption is not automatically justified: in tidal basins we encounter a multitude of topographically induced circulation flows. However, we have assumed that these circulation patterns are not fundamentally disturbed by the perturbations. In reality this can be the case; due to positive feedback between topography and residual circulations various bottom structures appear, such as bottom ripples, sand waves and channel meanders.

4.9.4 Stability of the inlet channel

From observations it is known that the equilibrium bottom shear stress $\tau_{max}(eq)$ that the tide exerts on the bottom of an inlet channel corresponds with a maximum flow velocity u_{max} of approximately 1 m/s. When the tidal flow velocity in the inlet channel is

insufficiently strong the channel will be closed by wave induced sand transport. When the tidal shear stress is larger than the equilibrium shear stress the channel will deepen until the equilibrium shear stress magnitude is reached. Normally, the sand is transported seaward and deposited in the ebb-tidal delta (in Dutch: buitendelta). Just outside the inlet gorge the ebb flow dominates over the flood flow, even though the discharges are equal. This is due to the fact that the ebb flow is more concentrated in the main channel and leaves the gorge as a jet flow, while the flood radially attracts water from a large area towards the inlet gorge.

Two situations can occur for which the shear stress is initially smaller than the equilibrium value:

1. the channel cross-section is larger than the equilibrium cross-section; in this case sedimentation takes place until the equilibrium cross-section is reached;
2. the channel cross-section is smaller than the equilibrium cross-section; in this case also sedimentation takes place, but now until the channel is completely closed.

We will demonstrate this in the following.
We start by deriving the equilibrium cross-section by assuming that the basin is emptied and filled by a gorge (channel) in which the water level gradient is related to the friction:

$$b\,h\,u(t) = O\,\eta_t(\text{basin})\,, \tag{4.96}$$

$$g\,h\,(\eta(\text{sea}) - \eta(\text{basin})) \approx \frac{8}{3\pi}\,c_D\,l\,u_{\max}\,u(t)\,. \tag{4.97}$$

Suppose $\eta(\text{sea}) = a\sin\omega t$, we may solve the above equations to yield a relation between the maximum flow velocity u_{max} and the cross-section A:

$$\tau \propto {u_{\max}}^2 = \frac{1}{2}\left(\frac{3\pi g}{8c_D\omega}\frac{A^2}{blO}\right)^2\left[-1+\sqrt{1+\left(\frac{3\pi c_D\omega^2}{4g}\frac{ablO^2}{A^3}\right)^2}\right] \tag{4.98}$$

where O is the basin surface and l the length of the gorge channel.
If the following condition is fulfilled:

$$\left(\frac{4g\omega}{3\pi c_D}\frac{Oa^2}{bl}\right)^{\frac{1}{3}} > u_{eq} \approx 1 \text{ m/s} \tag{4.99}$$

then two equilibrium cross-sections exist ${A_1}^{eq}$ and ${A_2}^{eq}$, where

$${A_1}^{eq} > A_c \quad , \quad {A_2}^{eq} < A_c \quad \text{and} \quad A_c = \frac{1}{\sqrt{2}}\left(\frac{3\pi c_D\omega^2}{4g}ablO^2\right)^{\frac{1}{3}}. \tag{4.100}$$

Suppose that the channel cross-section A corresponds to one of the equilibrium cross-sections and subsequently experiences a small disturbance A'. A positive disturbance

will grow if the shear stress increases due to the disturbance, a negative disturbance will grow in the reverse case.

$$\text{For } A = A_2^{eq} \text{ we have } \frac{d\tau}{dA} < 0 \qquad (4.101),$$

the inlet channel is stable.

$$\text{For } A = A_1^{eq} \text{ we have } \frac{dt}{dA} > 0 \qquad (4.102)$$

the channel is unstable; if $A' < 0$ the channel will close, for $A' > 0$ the channel will erode twowards the stable cross-section A_2^{eq}.

If the inflow is not strongly influenced by bottom friction in the gorge channel, the maximum tidal flow velocity u_{max} is proportional to the ratio of tidal prism and cross-section. From the empirical relation $u_{max} = O$ (1 m/s) it then follows that for many tidal basins this ratio has an approximate fixed characteristic value. Figure 4.17 indicates that this relation is reasonably valid for Dutch tidal basin. Since strong longitudinal variation of flood and ebb transport is not allowed (as discussed in the foregoing section) this implies that also further landward in the basin $u_{max} = O$ (1 m/s).

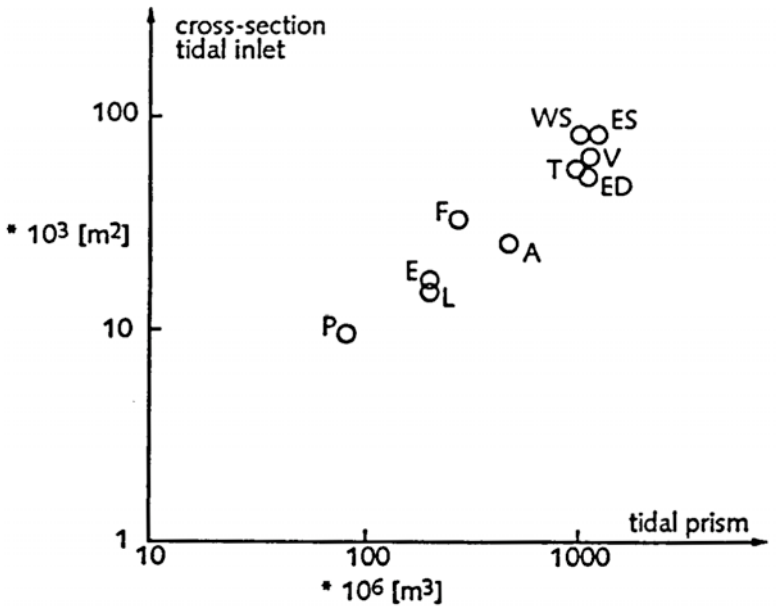

Figure 4..17: Relation between tidal inlet channel cross-section and tidal prism for Dutch tidal basins

4.10 Mixing processes

Due to flat/channel and ebb/flood chute systems tidal basins often display a complex topography. That complexity is mirrored in the flow structures, which is especially valid for the horizontally, depth-averaged flow field. During a tidal period fluid packages follow an irregular, random pathway, which is impacted by horizontal and transversal

circulations and by temporary stays in sheltered areas, such as flats and creeks. Fluid packages will therefore seldom return to the same location after a tidal period, even though the tide is cyclic and even when there is no river discharge. Also adjacent fluid packages can take very different pathways over a tidal cycle, and be separated strongly. These processes are synonymous to mixing, which manifests itself in a short flushing time of the basin with seawater or in a fast solution of discharged substances.
An exact description of mixing requires the accurate detection of all motions of fluid packages in the basin. In practice that is not well feasible, even large computer models find this difficult. In order to determine the global characteristics of mixing such a detailed analysis is not really necessary. Instead we may statistically describe the mean net displacement of fluid packages over a tidal period. The mixing processes are often described through a stochastic representation of dispersive transport. In this course we refrain from presenting this. We restrict ourselves to an overview of the different mixing processes (Table 4.3) and to two figures giving examples of spatial distribution of diffusion coefficients and lifespan times of water packages.

Table 4.3: Mixing processes

Mechanisms for mixing and flushing	Description of net displacement of water packages	When of interest
River discharge	Flushing by river discharge, preventing salt water intrusion; diffusion is of secondary interest	Tidal rivers
Turbulence	Mixing by vortices on various temporal and spatial scales, with a 3D-structure or with a vertical rotation axis. Order of magnitude of the diffusion coefficient $D \sim h\sqrt{\tau/\rho} \sim O$ [1 m^2/s]	In all tidal systems on small spatial and temporal scales; especially in combination with shear in the flow field
Residual circulations on basin scale	Residual circulations through the basin transport water parcels. A diffusion approach is often not applicable.	Large-scale wind driven circulation in coastal seas; salt wedge estuaries with strong entrainment
Residual shear diffusion: residual circulations combined with turbulent diffusion	Diffusive effect of turbulent vortices strengthened by the distribution of water packages over different residual cells. Order of magnitude of the diffusion coefficient $D \sim O$ [100 m^2/s]	Tidal basins with complex topographies
Tidal shear diffusion: shear in the tidal flow field combined with turbulent diffusion	The diffusive effect of turbulent diffusion is enforced by distribution of water parcels over gradients in the tidal flow field, so that differential advection over the tide occurs. Order of magnitude of the diffusion coefficient $D \sim O$[100 m^2/s]	Tidal basins with complex topographies and strong tidal flow
Deterministic mixing	Water parcels follow different flow trajectories during different tidal phases, e.g. flow trajectories in channels, over flats and towards	Tidal basins with complex topographies, i.e. strong branching channels

	storage areas, etc. Order of magnitude of the diffusion coefficient $D \sim O[100\ m^2/s]$	
Chaotic transport pathways	Water parcels follow each tidal period different flow trajectories and thereby experience quasi-stochastic net displacements. Order of magnitude of the diffusion coefficient $D \sim O$ [100 m^2/s]	Tidal basins with a large tidal excursion relative to the topographical structures

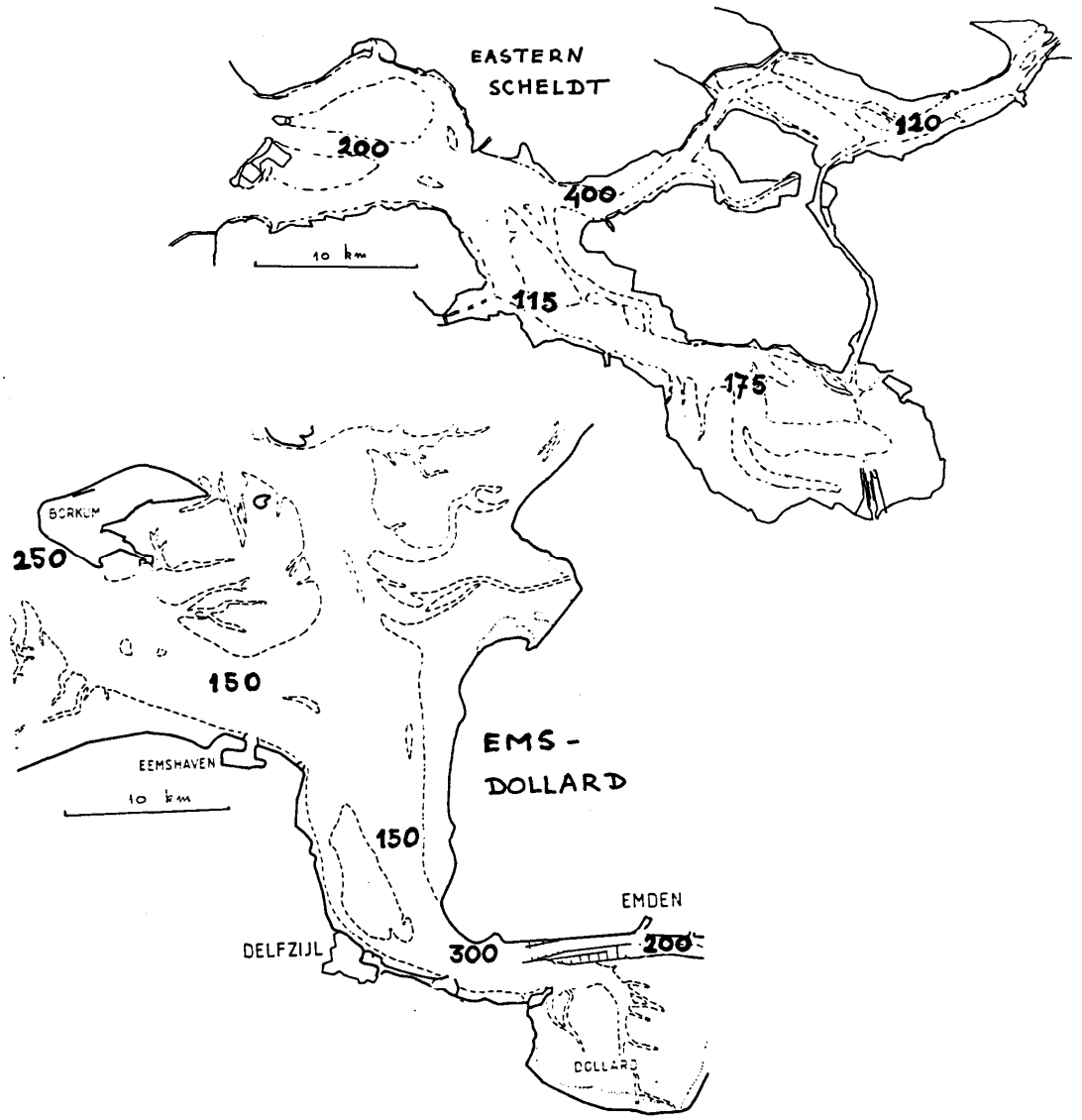

Figure 4.18: Magnitude of longitudinal dispersion coefficient [m^2/s] in Eastern Scheldt and Eems-Dollard

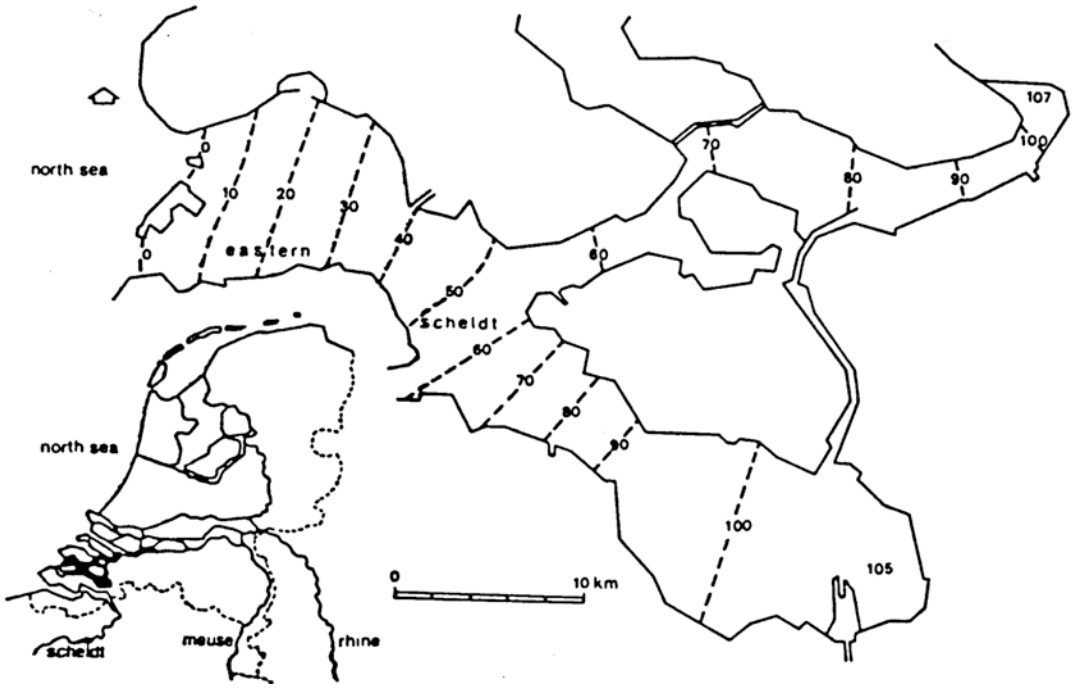

Figure 4.19: Isolines of lifespan time (in tidal cycles) in Oosterschelde (before strom surge barrier)

4.11 Literature

Dronkers JJ 1964. Tidal Computations in Rivers and Coastal Waters. North Holland, Amsterdam.

Dronkers J 1986. Tidal Asymmetry and Estuarine Morphology. Neth. Journal of Sea Research 20:117-131.

Dronkers J & Zimmerman JTF 1982. Some Principles of Mixing in Coastal Lagoons. Oceanologica Acta SP:107-117.

Fischer HB, List EJ, Koh RCY, Imberger J & Brooks NH 1979. Mixing in Inland and Coastal Waters. Academic Press, New York.

Groen P 1967. On the Residual Transport of Suspended Matter by an Alternating Current. Neth. Journal of Sea Research 3:564-574.

Lamb H 1932. Hydrodynamics. Cambridge University Press: par.185,187.

LeBlond P 1987. On Tidal Propagation in Shallow Rivers. Journal of Geophysical Research 83: 4717-4721.

Parker BB (ed) 1991. Progress in Tidal Hydrodynamics. John Wiley, New York.

Van Veen J 1950. Eb- en vloedschaar systemen in de Nederlandse getijdewateren. Tijdschrift Kon. Ned. Aardrijkskundig Genootschap 67: 303-325.

Zimmerman JTF 1986. The Tidal Whirlpool: A Review of Horizontal Dispersion by Tidal and Residual Currents. Neth. Journal of Sea Research 20:133-154.

5 Physics of tidal inlets

5.1 Introduction

The foregoing parts of this course have focused on the tidal basin, i.e. the estuary or the back-barrier lagoon, where the tide is the principal hydrodynamical agent. In this chapter, we will focus on the inlet proper, the outer delta and the adjacent coast. In preparation of the chapters on how to model these areas, we will concentrate on the physical processes which play a role there.

5.2 Morphology

The morphology of tidal inlets has been discussed extensively in the previous chapters. We have also seen that there is no generally valid ‘prototype-inlet’: the morphology depends to a large extent on local conditions, such as the tidal amplitude, the longshore drift, the sediment properties, etc.Yet, in order to have a reference frame for the description of the physical processes, we will briefly focus on a specific inlet, viz. the Wichter Ee, one of the the meso-tidal inlets of the East-Frisain Wadden Sea (see Figure 5.1). The littoral drift along this part of the North-Sea coast is from west to east, as can be seen from the sand abundance at the eastern tip of Northerney and the lack of sand at the western tip of Baltrum. Apparently, the sand is bypassed via a number of shoals which migrate on the outer delta and get welded with the coast of Baltrum somewhere east of the tip, where sand abundance is found, again. This pattern is typical of most of the Wadden Sea inlets.

Depending on the spatial scale of interest, we can distinguish a variety of morphological elements in such an inlet.

At the micro-scale, there are all sorts of small-scale bedforms, which are hardly visible in Figure 5.1. Figure 5.2 shows an example of such a bedform pattern. This particular case concerns wind-induced ripples, but current-induced ripples exhibit the same behaviour.

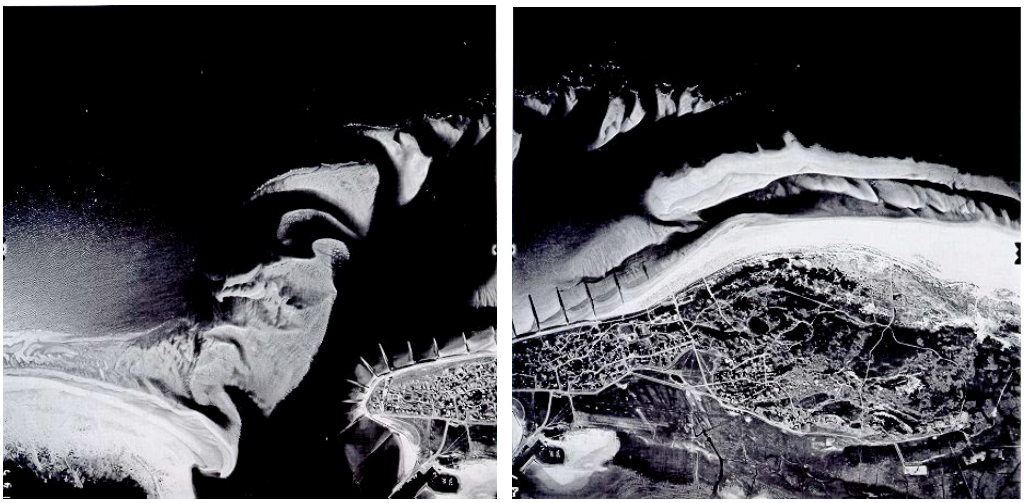

Figure 5.1. Aerial photograph of the morphology of the tidal inlet Wichter Ee, between the islands Norderney (left) and Baltrum (right) [from: Ehlers, 1988]

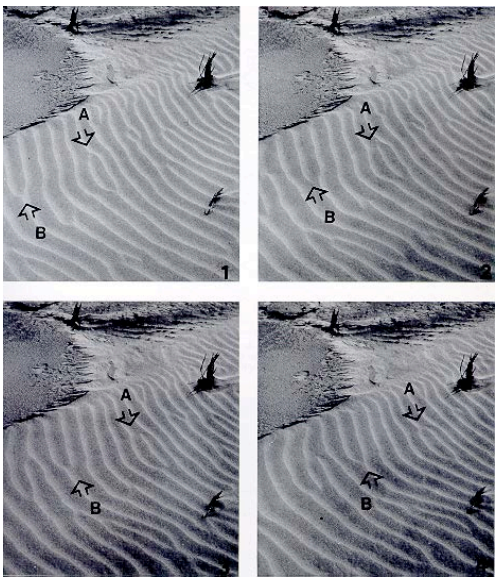

Fig.ure 5.2. Evolution of a wind-induced ripple pattern. The pictures have been taken at 5 minute intervals [from: Ehlers, 1988]

At the next higher scale level, Figure 5.1 shows a variety of morphological features. Quite obious is the system of shoals on the outer delta. They tend to migrate from the updrift to the downdrift island and probably form the principal sediment bypass mechanism across the inlet.

The shoals are separated by distinct channels, which all branch off from the main channel. In this particular case, the latter is strongly deflected eastward, but other inlets show that the main channel can just as well have a different direction. Also, the main channel tends to migrate and change direction through time.

The main channel and its branches are probably all ebb-dominant. If this is true, the principle of conservation of water mass requires that other parts of the area are flood-dominant. Often there are more or less distinct flood-channels, e.g. around the tip of the updrift island. In the case of the Wichter Ee, at least at the time that the photos of Figure

5.1 were taken, these flood channels were not so well-developed.
Another striking meso-scale phenomenon, which does not appear from Figure 5.1, is the formation of the so-called *sawtooth-bars*, systems of long-crested and slowly migrating waves in the seabed, with a wave length of typically 100 m, and a crest orientation under a large angle with the coastline (Figure 5.3).

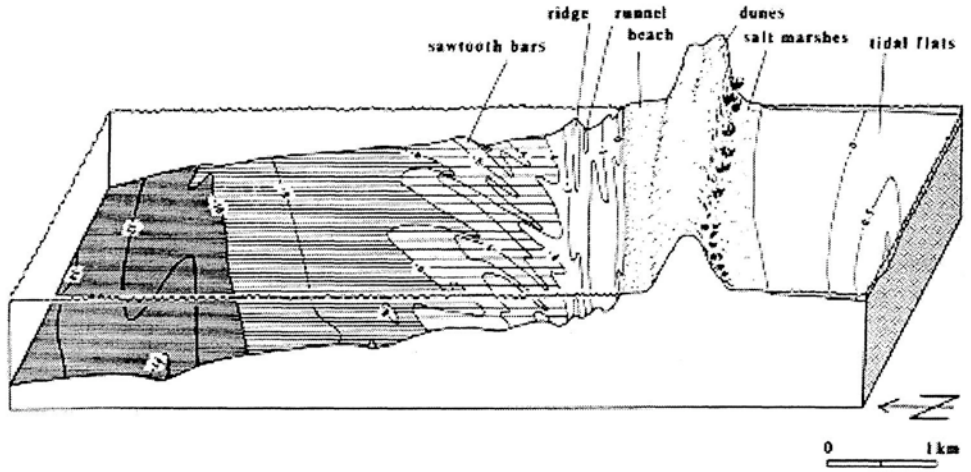

Figure 5.3. Sawtooth bars, beach and barrier forms in the vicinity of a tidal inlet [from Ehlers, 1988)

At a still higher scale level, the *macro-scale*, tidal inlets have a basin, sometimes with a distinct inner delta, a gorge, a more or less pronounced outer delta, two adjacent coasts and the adjacent shoreface and seabed. The basin consists of a system of channels, shoals and marshes, as has been discussed before. The gorge is usually dominated by the main channel, but some are split by a shoal or a small island (cf. the Frisian Inlet, between the isles of Ameland and Schiermonnikoog in the West-Frisian Wadden Sea). The outer delta involves of a bypassing shoal system, an ebb-dominated main channel and a number of flood channels. Together they form a sediment circulation system, as schematically indicated in Figure 5.4.

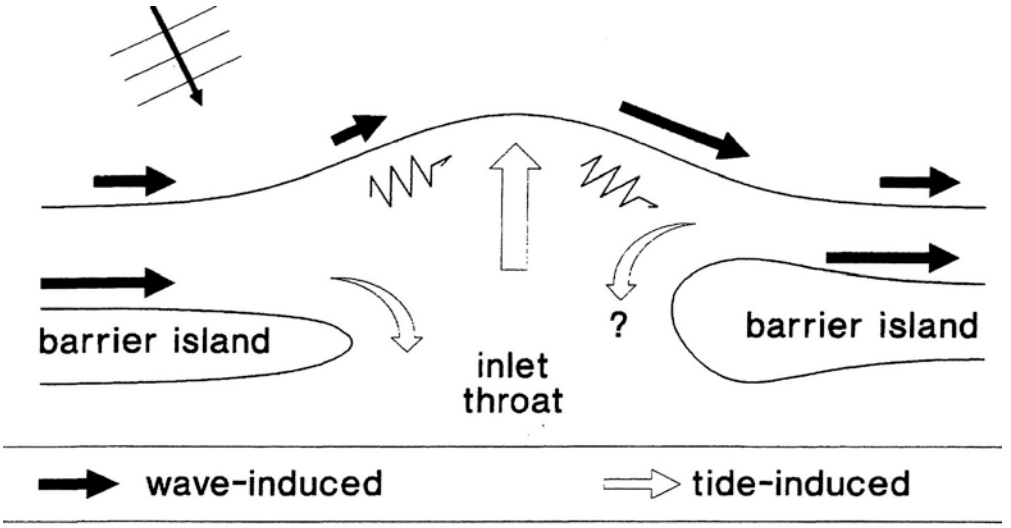

Figure 5.4. Schematic diagram of the outer delta residual sediment transport

At the highest scale level which within our sight, the *mega-scale*, considers a barrier-island system as a whole. An individual inlet is one element in this system, a barrier island is another. At this scale, one usually considers phenomena such as barrier island retreat, inlet formation and closure, etc. In this part of the course, we will not focus too much on this scale-level, simply because we don't know how the small-scale processes we will discuss here influence the coastal behaviour this scale.

5.3 Waves

We can safely state that the morphology of the outer delta is highly complicated and variable. This means that waves and currents encounter a very complex bed topography, with length scales which are not much larger than the wavelength of wind waves or swell, for instance. Via refraction, diffraction and reflection, this can lead to complex wave patterns. Figure 5.5 gives an example for the relatively simple case of refraction on a sawtooth bar system.

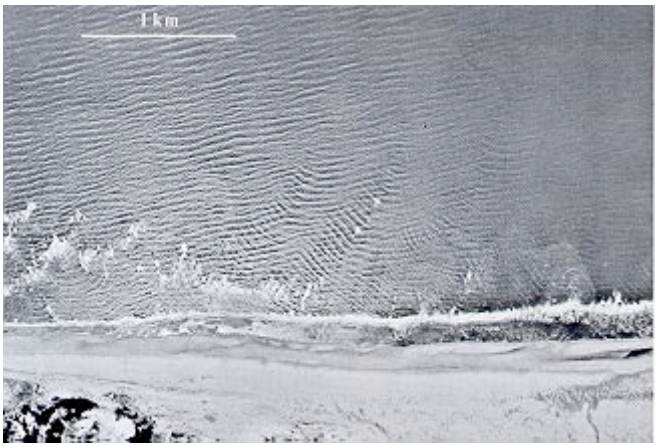

Figure 5.5. Refracting and breaking swell waves on a sawtooth bar system [from Ehlers, 1988]

An obvious consequence of this is a strong spatial variability of the wave field. Hence it hardly makes sense to take point measurements of the wave field in a tidal inlet: wave measurements have to be synoptic, it is the overall pattern that matters, much more than the local wave parameters. The same goes for models: they may be able to give correct predictions of the overall wave pattern, but by no means the local wave properties at every point in the area.

As to the large-scale pattern of waves, there are a few points of consideration, such as the penetration of wave energy into the gorge and the sheltering from wave exposure in various parts of the system.

In the case of normally incident waves, the entire delta edge and the gorge are exposed to wave energy. Due to refraction, the side lobes of the delta with be less exposed than the front part, and due to breaking on the outer delta shoals, the gorge will also be less exposed (Figure 5.6).

In the case of obliquely incident waves, one side lobe will be exposed, and the other will be sheltered. By implication, the wave climate one the side lobes will be different from

that offshore or at the front edge of the delta. The western lobe in Figure 5.7, for instance, will be fully exposed to westerly waves, less exposed (due to refraction) to northerly waves and sheltered from easterly waves. As a consequence, wave-driven longshore currents in the vicintity of this western lobe are predominantly eastbound. Similarly, the currents near the eastern lobe are predominantly westbound.

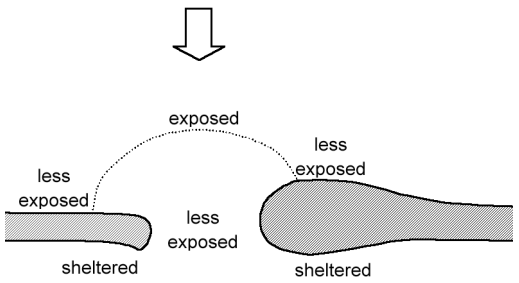

Figure 5.6. Exposure to normally incident waves

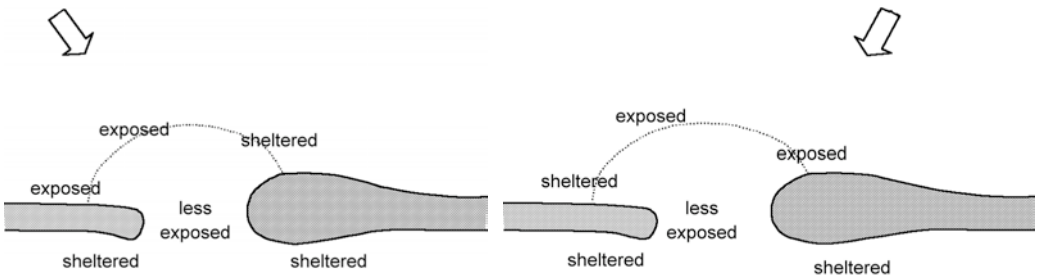

Figure 5.7. Sheltering and exposure to obliquely incident waves.

Another aspect which deserves attention is the wave penetration into the inlet. Clearly, the barrier islands provide considerable shelter to the basin, but wave energy can penetrate through the gorge. The latter, however, is sheltered to a certain extent from the open sea by the outer delta. Hence the wave energy which reaches the back of the gorge is much less than offshore. Subsequently, this energy usually radiates into the basin, whence the energy density and the wave height rapidly decay. Hence the wave energy which penetrates from the open sea into the basin is usually rather small and it is restricted to the area right behind the gorge. Wave energy further into the basin must is generally due to waves generated inside the basin, if the prevailing wind meets a sufficiently long fetch. A drastically different situation may arise if ‘channeling’ of the wave energy occurs (Figure 5.8). This phenomenon is associated with trapping of the waves in the channel if the wave direction is almost parallel to the banks. In such a case, areas which are at first sight sheltered from sea waves can be exposed to reatively high wave energy and thus to much more erosion than expected.

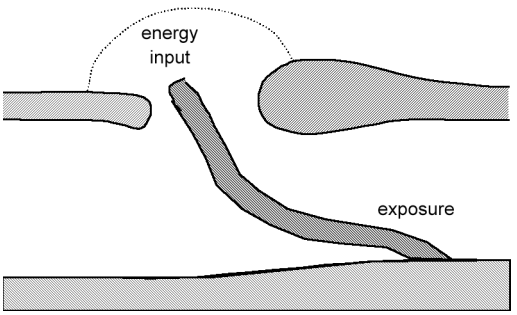

Figure 5.8. Exposure of a sheltered area due to wave channeling

The complexity of the bed topography and the mixture of sea/swell waves coming from offshore and locally generated waves of a much shorter period inside the basin make wave modelling for tidal inlets particularly difficult. A model for long-crested monochromatic waves (i.e. wave fields with one direction, one period and one height in each point of the model domain) will not work here. Instead, one would need a spectral wave model which allows for irregular, short-crested waves of various periods and which includes wave generation. Such fully spectral wave models exist since some time for deep-water wave prediction, but this concept has been translated only recently to shallower water.

5.4 Currents

5.4.1 General

The currents in the vicinity of a tidal inlet are partly tidal, partly wave-driven, and partly wind-driven. The tidal currents are primarily concentrated in the main channels, the wave-driven currents in areas where waves are breaking. Wind-driven currents occur mainly during storm events and are therefore rather episodic, but nonetheless important (though often forgotten!).

5.4.2 Tidal residual circulation

An important physical mechanism to bear in mind when interpreting the tidal currents is inertia. The tidal flow in the gorge has so much momentum, that it cannot spread out fast enough when leaving the gorge: it forms a ‘tidal jet’. The length scale of such an inertial jet is a few hundred times the water depth, so a few kilometres. On the other hand, the water flowing into the gorge has to accelerate and is therefore inertia-dominated, i.e. close to potential flow. This means that the highest velocities coincide with the shortest path through the gorge, i.e. just around the tips of the islands (Figure 5.9).
The tidal residual current pattern in this highly schematized situation boils down to a quadruplet of gyres, two at either side of the inlet (Figure 5.10).
In reality, the residual current picture is much more complicated than this. There is usually a distinct ebb-dominated current over the outer delta, and often there are flood channels near the tips of the islands. In the Wadden Sea, well-developed flood deltas are hardly found (the entire basin acts as a flood delta), and the corresponding flood-

residual current is difficult to distinguish. Many inlets on the east coast of the USA, however, do exhibit such a feature and have a well-developed residual circulation inside the inlet.

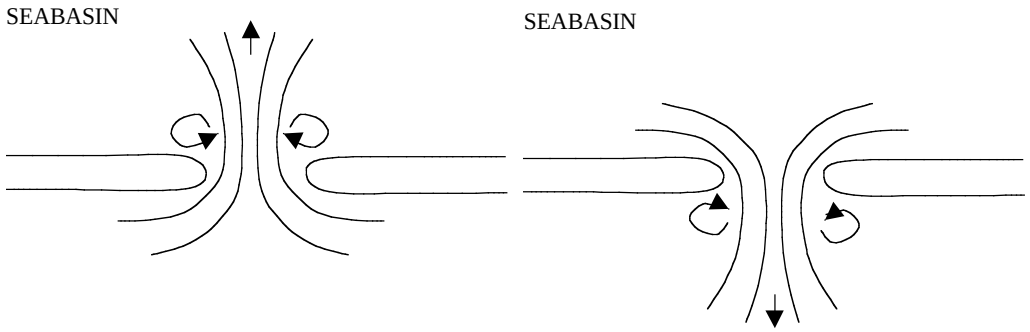

Figure 5.9. In- and outgoing tidal jet

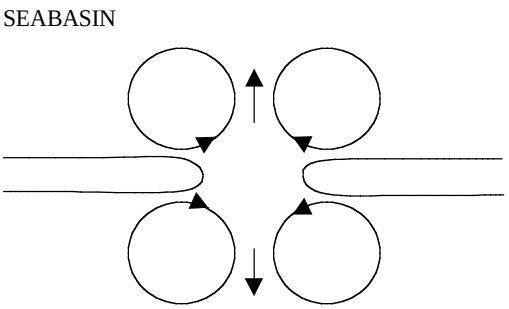

Figure 5.10. Schematized tidal residual currents around an inlet

Since the tidal current is coupled to the variation of the water level, there is another type of residual current, associated with the phase coupling between the horizontal and the vertical tide. This can be shown by the following example. Suppose u is the tidal current velocity in a 1-D channel, h the mean water depth and ζ the water surface elevation above mean sea level, and let u and ζ be given by

$$u = U\sin(\omega t - kx - \varphi) \quad \text{and} \quad \zeta = Z\sin(\omega t - kx)$$

then the tidal residual flux of water is given by

$$q_{res} = U(h+Z)\frac{1}{T}\int_0^T \sin(\omega t - kx - \varphi)\sin(\omega t - kx)\,dt = \frac{1}{2}U(h+Z)\cos\varphi$$

So, if the horizontal tide (u) and the vertical tide (ζ) are 90° out of phase ($\varphi = \pi/2$), like they are in deep water, there is no residual flux. But if they are more or less in phase ($\varphi \approx 0$), there can be a considerable residual current. This becomes even more apparent for shoals bordering a tidal channel which are flooding and drying during the tide. There the largest part of the flooded stage coincides with the flood tide, so there must be a flood-dominant residual current.By implication, the residual current in the channel must be ebb-dominant.

In summary, there is a variety of mechanisms which lead to tidal residual currents, and hence to residual sediment transports and moprphological changes. In shallow areas such as a tidal inlet, we have to give up thinking of the tide as a small-amplitude wave.

5.4.3 Tidal asymmetry

Tidal asymmetry has been treated in the previous chapters as one of the mechanisms to import or export sediment to or from a tidal basin. It generally does not give rise to residual currents, but in wide channels it may, as a consequence of the coriolis effect (due to the earth's rotation). On the northern hemisphere, this effect gives every moving particle a tendency to bend to the right. If a water flow is laterally bounded, e.g. by a channel bank, this tendency is translated into a transverse water surface slope, which exerts an additional force on the particles, such that these keep moving straight on. Thus the tide at the right side of a tidal channel (when looking in the direction of tidal wave propagation) tends to be slightly higher than at the left side. If the tide is flood-dominant, it means that the inward residual current at the right side is somewhat stronger than at the left side. If, moreover, the tidal wave is reflected, the reflected wave will have induce a slightly stronger outgoing current at the other side of the channel. Thus the overall residual current pattern in wide channels can be as shown if Figure 5.11.

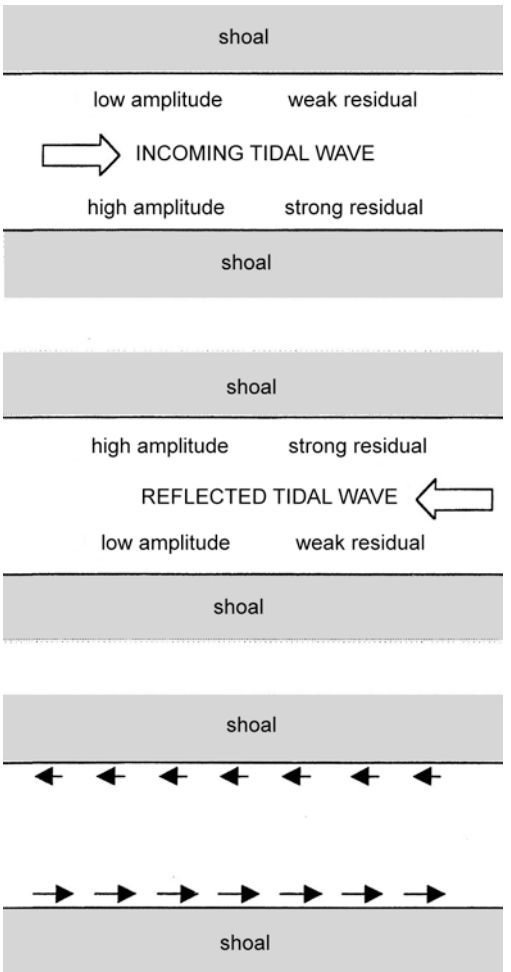

Figure 5.11. Tidal residual current due to a combination of tidal asymmetry and the coriolis effect

5.4.4 Secondary flows

So far, we have considered the depth-averaged tidal current field. When considering this to be representative of the entire flow pattern, one makes the implicit assumption of vertical similarity of the velocity profiel, i.e. the velocity profile in every point in the horizontal has the same shape (e.g. logarithmic). In reality, however, the velocity field is more complex than this. Like in rivers, the curvature of the tidal current, as well as the coriolis effect, give rise to secondary flow components:

$$v_{\mathrm{curv}} = \frac{h\bar{u}_{\mathrm{tot}}}{R_c} f_{\mathrm{curv}}\left(\frac{z-z_b}{h}\right) \quad \text{and} \quad v_{\mathrm{cor}} = -f_c\, h \frac{\bar{u}_{\mathrm{tot}}}{\left|\bar{u}_{\mathrm{tot}}\right|} f_{cor}\left(\frac{z-z_b}{h}\right) \qquad (5.1)$$

in which v is the transverse velocity component (perpendicular to the depth-averaged flow, positive to the left), h is the water depth, R_c is the radius of curvature of the depth-averaged tidal flow (positive when turning to the right), f_c is the coriolis factor ($1.2\ 10^{-4}$ at our latitude), z is the vertical co-ordinate, z_b is the bed level, and f_{curv} and f_{cor} are the vertical distribution functions of these secondary flow components.

These secondary flows, though rather weak compared to the maximum tidal current, can have a significant residual effect, on the current, but also on the sediment transport and the bed topography. This goes especially for the curvature-induced secondary flow, which does not change sign as the tide turns: in the upper part of the water column it is always directed towards the centre of curvature of the flow, in the lower part always away from it. Thus the curvature-induced secondary flow contributes to the maintenance of shoals, for instance (see Figure 5.12).

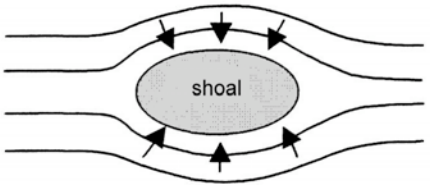

Figure 5.12 Curvature-induced secondary flow: always directed towards the shoal

A striking example of the role of curvature-induced secondary flow on an outer delta is the case of the groyne which was built to protect the north part of the coast of Texel, one of the barrier islands of the Dutch Wadden Sea. The idea was to let this groyne interrupt the longshore drift into the inlet called Eijerlandse Gat. Studies with 2-D depth-averaged models revealed, that this would lead to the 'textbook-'pattern of updrift accretion and downdrift erosion, so to strong erosion north of the groyne. It was foreseen that the groyne would have to be connected by a hard structure to the existing revetment which protects the tip of the island.

Once the groyne had been built, however, accretion occurred at either side of it, to the effect that it is now largely buried in sand (so the project turns out to be extremely successful!). This must be attributed to a large extent to the curvature-induced secondary flow in the gully around the tip of the groyne, which consistently brings sediment towards the groyne (see Figure 5.13). New computations with a model which includes

this secondary flow effect have reproduced the observed morphological evolution (further see Steijn et al., 1998).

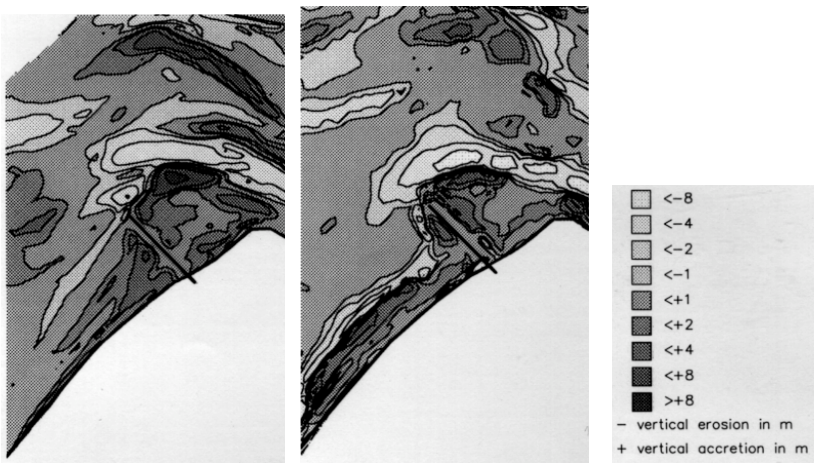

Figure 5.13. Observed (left) and computed (right) sedimentation and erosion around the groyne at the north point of Texel during the first two years after construction [from Steijn et al., 1998]

5.4.5 Wave-induced currents

As stated before, an outer delta is nowhere near a straight prismatic coast. This means that the traditional way of thinking about wave-driven currents (longshore and cross-shore) is hardly applicable here. In order to build up a more 3-D view on wave-driven currents, we consider the depth-averaged shallow-water equations

$$\frac{\partial \bar{u}}{\partial t}+\bar{u}\frac{\partial \bar{u}}{\partial x}+\bar{v}\frac{\partial \bar{u}}{\partial y}=-g\frac{\partial z_s}{\partial x}-\frac{\tau_{bx}}{\rho h}-\frac{1}{\rho h}\left[\frac{\partial S_{xx}}{\partial x}+\frac{\partial S_{xy}}{\partial y}\right]+HDT \tag{5.2}$$

$$\frac{\partial \bar{v}}{\partial t}+\bar{u}\frac{\partial \bar{v}}{\partial x}+\bar{v}\frac{\partial \bar{v}}{\partial y}=-g\frac{\partial z_s}{\partial y}-\frac{\tau_{by}}{\rho h}-\frac{1}{\rho h}\left[\frac{\partial S_{xy}}{\partial x}+\frac{\partial S_{yy}}{\partial y}\right]+HDT \tag{5.3}$$

$$\frac{\partial h}{\partial t}+\bar{u}\frac{\partial h}{\partial x}+\bar{v}\frac{\partial h}{\partial y}+h\frac{\partial \bar{u}}{\partial x}+h\frac{\partial \bar{v}}{\partial y}=0 \tag{5.4}$$

in which x and y are cartesian co-ordinates in the horizontal plane, u and v are the horizontal velocity components in the x- and y-direction, respectively, the overbars denote depth-averaging, h is the water depth, g is the acceleration due to gravity, z_s is the water surface level, τ_{bx} and τ_{by} are the components of the bed shear stress, S_{xx}, S_{xy} and S_{yy} are the radiation stress components and *HDT* stands for the horizontal diffusion terms. The dependent variables in these equations are the velocity components and the water level. Therefore, additional information about the bed shear stress and the radiation stresses is needed before being able to solve this system. The radiation stress components can be evaluated on the basis of a wave propagation model, the bed shear stress is related to the velocity and a number of wave parameters (cf. Soulsby et al.,

1993).

Theoretically, there is nothing wrong with this approach, but practically there is: it is not very transparent as far as the wave-induced forces are concerned. Therefore, we will consider an alternative formulation of these forces:

$$\begin{pmatrix} F_x \\ F_y \end{pmatrix} = \frac{D}{c_w}\begin{pmatrix} \cos\vartheta \\ \sin\vartheta \end{pmatrix} + \rho h \begin{pmatrix} \frac{\partial \Phi}{\partial x} \\ \frac{\partial \Phi}{\partial y} \end{pmatrix} \tag{5.5}$$

in which D is the wave energy dissipation rate per unit area, c_w is the phase speed of the waves, ρ is the mass density of the fluid and ϑ is the angle between the direction of wave propagation and the positive x-axis.The potential Φ is given by

$$\Phi = \frac{(n - \frac{1}{2})E}{h} \tag{5.6}$$

in which E is the wave energy density, and n denotes the ratio between the group celerity and the phase celerity of the waves.

This way to compute the forces is essentially simpler and more transparent than differentiating the radiation stress components. Note that the first part in the RHS of Eq. (5) represents a rotational force field, which can drive circulation currents. This part of the force vector is proportional to the wave-energy dissipation rate and its direction coincides with the direction of wave propagation. Via these properties, wave-induced current fields are much easier to interpret than via the forces based on the radiation stress gradients.

The second part of the forces according to Eq. (5.5) is irrotational and will generally yield just a ‘landscape’of water surface elevations. Here we will ignore this part of the forcing.

Substituting the dissipation-related force components into the momentum equations (5.2) and (5.3) yields

$$\frac{\partial \bar{u}}{\partial t} + \bar{u}\frac{\partial \bar{u}}{\partial x} + \bar{v}\frac{\partial \bar{u}}{\partial y} = -g\frac{\partial z_s}{\partial x} - \frac{\tau_{bx}}{\rho h} + \frac{D}{\rho h c_w}\cos\vartheta + HDT \tag{5.7}$$

$$\frac{\partial \bar{v}}{\partial t} + \bar{u}\frac{\partial \bar{v}}{\partial x} + \bar{v}\frac{\partial \bar{v}}{\partial y} = -g\frac{\partial z_s}{\partial y} - \frac{\tau_{by}}{\rho h} + \frac{D}{\rho h c_w}\sin\vartheta + HDT \tag{5.8}$$

In the case of steady flow near a prismatic coast along the x-axis, this reduces to

$$0 = -\frac{\tau_{bx}}{\rho h} + \frac{D}{\rho h c_w}\cos\vartheta \tag{5.9}$$

$$0 = -g\frac{\partial z_s}{\partial y} + \frac{D}{\rho h c_w}\sin\vartheta \qquad (5.10)$$

So here the longshore and cross-shore momentum equations get separated, the former describing the momentum balance for a uniform longshore current and the latter the set-up balance.
In the case of a complex topography with interrupted breaking, however, the situation is much more complicated. A simple example concerns a shoal on which waves are breaking (Figure 5.14).

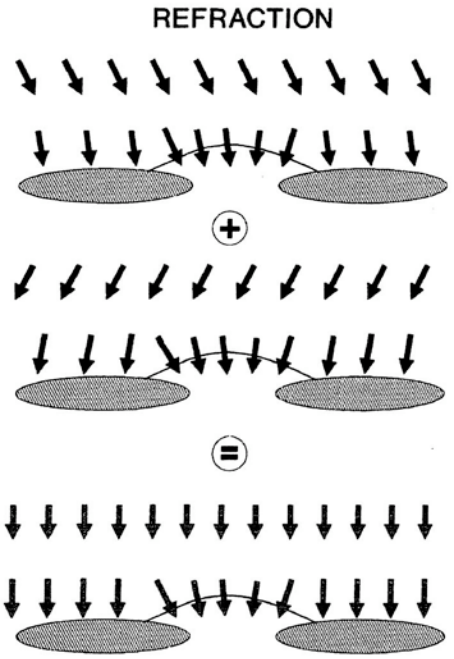

Figure 5.14. Wave-induced forces and currents around a shoal

Due to refraction, the waves will tend to converge toward the top of the shoal. As the wave break on the seaward slope of the shoal, they generate a current-driving force. At the top of the shoal, however, there is no closed boundary to stop the water. Hence the 'cross-shore' component of the force cannot build up a water level set-up. Instead, the water will flow in the direction of the force, until it reaches the channel behind the shoal, where water level gradients will deflect it and drive it to the sides of the shoal. There it has room to flow seawards again, thus closing the circulation.
Figure 5.15 gives an example of a residual transport computation for the Frisian Inlet. Apart from the longshore drift along the coast of Ameland, it clearly shows the above circulations around the shoals, always with the current at the top of the shoal in the direction of wave propagation. Apparently, the longshore drift and the transport by the wave-driven currents around the shoals on the outer delta are so strong, that they dominate the tidal residuals.
In principle, the wave-driven current in this type of situation is 3-D. The mechanisms which use to be called 'cross-shore' in the case of a prismatic coast, are actually acting in the direction of wave propragation.

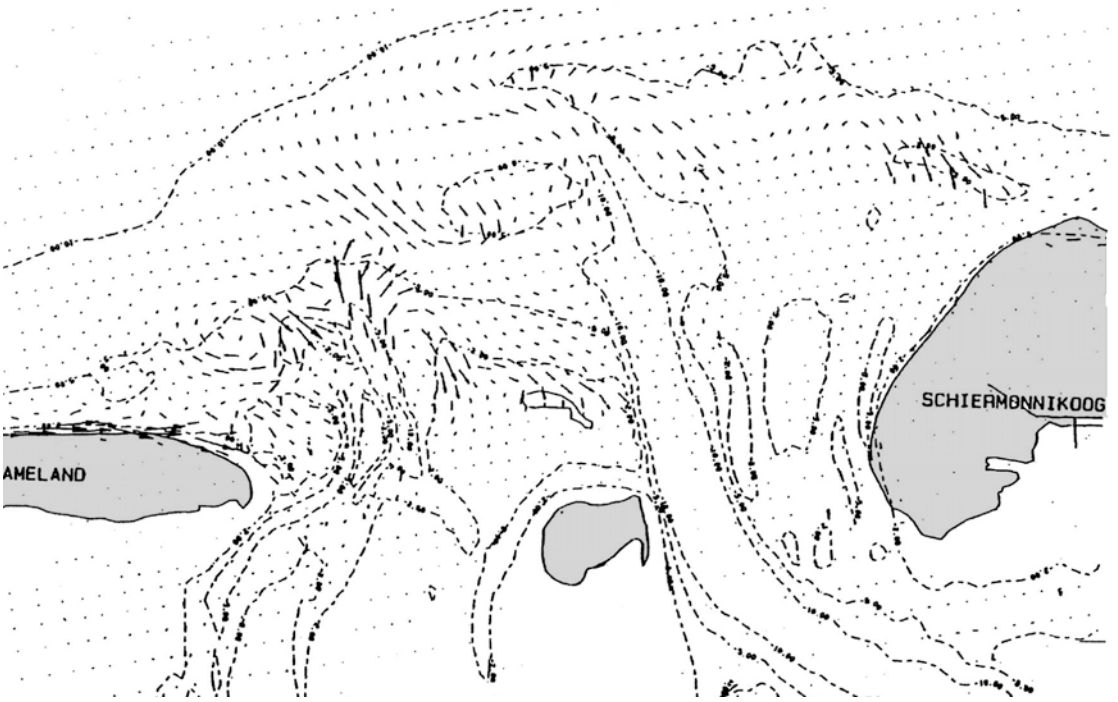

Figure 5.15. Yearly residual transport patern on the outer delta of the Frisian Inlet

The effective surface shear stress which drives the undertow is basically the same as the forcing of the whole wave-driven current. In a depth-averaged model, this force is treated as if it were distributed uniformly over the vertical, but in fact it is concentrated near the water surface. Since it acts in the direction of wave propagation and the wave-driven current or the set-up gradient does not necessarily have the same direction, the undertow-type of current which we know from prismatic coasts is probably rare here.
The cross-shore current induced by the mass flux is even more complicated here. In fact, the return current due to the Eulerian mass flux between the crest and trough levels of the waves is part of the primary flow, since the mass flux terms ought to be included in the depth-averaged flow eqautions. As long as the mass-flux contributions are small relative to the other current components, they can be included by replacing the velocity components by

$$\begin{pmatrix}\bar{u}\\ \bar{v}\end{pmatrix} \rightarrow \begin{pmatrix}U\\ V\end{pmatrix} = \begin{pmatrix}\bar{u}\\ \bar{v}\end{pmatrix} + \frac{1}{\rho h}\begin{pmatrix}M_x\\ M_y\end{pmatrix} \quad with \quad \begin{pmatrix}M_x\\ M_y\end{pmatrix} = \frac{E}{c_w}\begin{pmatrix}\cos\vartheta\\ \sin\vartheta\end{pmatrix} \tag{5.11}$$

in which M_x and M_y are the components of the wave-induced mass flux. Thus the same numerical solver can be used as for Eqs. (3) through (5), but now with U and V as dependent variables and with slightly different the boundary conditions. The computed velocities *(U,V)* have to be corrected afterwards for the mass-flux contribution.
The implication is, that the magnitude and direction of the primary flow contribution of the mass flux are difficult to assess, since the extent to wehich this effect creates a set-up or a current velocity depends entirely on the situation. In any case, mass-flux contributions exactly opposite to the direction of wave propagation, like in the case of a prismatic coast, are not likely to be abundant in outer delta flow.

5.4.6 Wind-induced currents

An often forgotten type of currents in tidal inlets are the wind-driven currents, either directly, via the wind-induced shear stress on the water surface in the inlet area, or indirectly, via the set-up of the water level against the coast. The former effect emerges directly when including the wind shear stress components τ_{wx} and τ_{wy} into the depth-averaged momentum equations:

$$\frac{\partial \bar{u}}{\partial t} + \bar{u}\frac{\partial \bar{u}}{\partial x} + \bar{v}\frac{\partial \bar{u}}{\partial y} = -g\frac{\partial z_s}{\partial x} - \frac{\tau_{bx}}{\rho h} + \frac{\tau_{wx}}{\rho h} + \frac{D}{\rho h c_w}\cos\vartheta + HDT \tag{5.12}$$

$$\frac{\partial \bar{v}}{\partial t} + \bar{u}\frac{\partial \bar{v}}{\partial x} + \bar{v}\frac{\partial \bar{v}}{\partial y} = -g\frac{\partial z_s}{\partial y} - \frac{\tau_{by}}{\rho h} + \frac{\tau_{wy}}{\rho h} + \frac{D}{\rho h c_w}\sin\vartheta + HDT \tag{5.13}$$

In these equations, the wind stress terms are divided by the water depth, which means that the wind tends to be more effective in driving a current when it acts on shallower water. Due to the large variations in water depth which are inherent to a tidal inlet, the wind-driven current field will therefore strongly vary in space. In general there will be a tendency of the flow to follow the wind in the shallower parts, and to oppose it in the deeper parts, but this picture can be complicated greatly by spatial interactions via water level gradients.

As the wind forcing acts at the water surface, there will also be an effect on the vertical structure of the flow: the primary flow profile (e.g. logarithmic) will be disturbed by a ‘secondary’flow component which follows the wind in the upper part of the water column and goes against it in the lower part. Note that this secondary flow has to be superimposed on the primary flow (the depth-averaged circulation with a primary flow profile). The result can be a complex 3-D flow pattern.
Probably even more important than the direct wind-induced forcing is the effect of the water level set-up during a severe storm. Although the peak of the wind speed usually does not last much more than a few hours, the water level set-up can last much longer. However, it takes time for the back-barrier basin to follow the water level at open sea, as setting up such a basin by a few metres takes huge amounts of water, all of which has to be squeezed in through the inlets. Hence it sometimes occurs that the ebb current is entirely suppressed and that the there is a flood current in the inlet during a day or more. Clearly, such events may offset the inlet morphology considerably. It is also clear that new inlets and channels will preferably be created under such conditions, when there is a large head differences between the sea and the basin.

5.4.7 Summary

In summary, we have seen that the current field around an inlet is essentially more complex than on a uniform straight coast, and that all consituents of this field are essentially 3-D. So when modelling currents around inlets, we have to think 3-D, even if we decide to use a 2-D depth-averaged model. The interpretation and postprocessing of

the results (e.g. bed shear stress to be put into the sediment transport model) is much less straightforward here.

5.5 Wave-current interaction

The tidal and wave-driven current pattern on the outer delta is largely concentrated in the deeper channels. Consequently, there can be strong currents which affect the wave propagation via the so-called current refraction. This may even go as far as wave blocking. When standing on the coast and overlooking a tidal inlet, one often sees a sharp distinction between areas with waves and areas with a flat water surface. This is simply because the current is strong enough to prevent the waves from entering this area. Moreover, where waves do occur, their patter is often quite irregular, again as a consequence of refraction on a strongly varying current field.

This form of wave-current interaction makes it particularly difficult to predict the wave field on the outer delta. Such a prediction should be based on a combined wave and current model, and both should be carefully calibrated in order to find the right pattern. In fact, this is an impossible task without synoptic wave data (also see Section 3).

A more straightforward form of wave-current interaction is the effect of waves on the bottom shear stress experienced by the current. The mechanisms underlying this effect are not essentially different from those in the case of a prismatic coast, though waves and near-bed currents can have arbitrary directions now. The result is a complex 3-D boundary layer with a strongly veering velocity vector and a non-trivial direction of the bed shear stress. In large-scale models like the ones we use for tidal inlets, however, this effect is usually ignored and the shear stress is assumed to be opposite to the mean current. What we do take into account, however, is the bed shear stress enhancement induced by the waves. This may have major effects on the current pattern: especially the tidal flow will tend to avoid shallow areas, where wave action and shear stress enhancement are strongest.

An anecdotic example concerns a model of one of the inlets of the Wadden Sea, which was run not only for the usual ‘representative’ – realtively low – wave conditions, but also for an extreme storm event. To our surprise, the longshore tidal current in the vicinity of the outer delta virtually vanished in the storm case! Our initial response, being unexperienced in storm modelling: this cannot be right, there must be something wrong with the model ….

5.6 Sediment transport processes

Waves and currents, separate and combined, are known to be able to transport sediment in various modes:

- bed load transport, primarily via the migration of small-scale bedforms,
- sheetflow transport, with the top layer of the bed fluidized during part of the wave cycle,
- suspended load transport, with the grains suspended in the water column.

The quantitative description of these transport modes is still largely empirical (e.g. Van

Rijn, 1989; Fredsoe and Deigaard, 1992). There is a variety of transport formulae and models, each with its own strong points and weaknesses. This is not the place to discuss them in depth, since such a discussion is not typical for tidal inlets. For an overview we refer to Horikawa (1988), Van Rijn (1989) and Fredsoe and Deigaard (1992).
For morphological computations, an important, but much neglected transport component is the one due to gravitation along a sloping bed: moving grains will rather go downhill than uphill. This gives a transport component which is directed downhill. A highly simplified transport model including this term reads

$$\begin{pmatrix} q_x \\ q_y \end{pmatrix} = q_{tot} \left[\frac{1}{u_{tot}} \begin{pmatrix} \bar{u} \\ \bar{v} \end{pmatrix} - \beta \begin{pmatrix} \frac{\partial z_b}{\partial x} \\ \frac{\partial z_b}{\partial y} \end{pmatrix} \right] \tag{5.14}$$

in which q_{tot} is the total transport rate, z_b is the bed level and the factor β is a known scalar. The factor βq_{tot} basically measures the degree of sediment motion. Note that, if this motion is oscillatory, like in the case of combined waves and currents, this degree is much larger than one would tell from the wave-averaged transport rate. In that case, the factor in front of the slope term should rather be $\beta<q_{tot}>$, in which the brackets indicate wave averaging.
If we subsitute Eq. (14) into the sediment balance equation, we find

$$(1-\varepsilon_p)\frac{\partial z_b}{\partial t} = -\frac{\partial q_{bx0}}{\partial x} - \frac{\partial q_{by0}}{\partial y} + \beta q_{tot}\left(\frac{\partial^2 z_b}{\partial x^2} + \frac{\partial^2 z_b}{\partial y^2} \right) + h.o.t. \tag{5.15}$$

in which the suffix ‘0’ refers to the situation with the same water motion on a horizontal bed and ‘*h.o.t.*’ stands for higher-order terms, i.e. terms which are of higher order (quadratic or more) in terms of the bed slope. Clearly, the downhill gravitational transport component yields a diffusion term in the sediment balance equation, and thus has a smoothing effect on the bed topography. This effect is of great importance to the morphological stability of the bed and to the equilibrium state to which the bed topography tends (but which it probably never reaches, since this state is a function of the ever changing input conditions). For further reference: see De Vriend et al., 1993.
So far, little is known about the downhill gravitational effect on the transport under sheetflow conditions. Since this type of transport is typical of highly energetic wave conditions, when large amounts of sediment are brought into motion, the effect may well be considerable.
The same goes for suspended load transport. At first sight, it may seem unlogical to assume that suspended load transport be subject to bed slope effects: the sediment grains are in suspension, and therefore not in contact with the bed, so how can the experience any effect of the bed slope? We have to realise, however, that the suspended state applies to the average sediment concentration, but not permanently to each individual grain; each grain will get into contact with the bed from time to time, and thus experience the slope effect. There are indications from river research that this influences

the bed topography, e.g .in river bends. The nature and the magnitude of this effect under coastal conditions, however, are still in the dark

Suspended load transport is a quite common condition in the coastal environment, maybe even more common than pure bed load. From a morphological modelling point of view, we must distinguish two types of suspended load: one which is determined entirely by the hydrodynamic conditions and the sediment properties at the point of consideration, and one which includes a 'memory effect' and responds to the conditions in all points it has come through in the past. The former type can be modelled with a sediment transport formula (e.g. the Bijker or the Bailard formula), or with a simple intra-wave model which describes the suspension process during a wave cycle (cf. Fredsoe and Deigaard, 1992).

The sediment concentration associated with the second type of suspended load transport is described by an advection/diffusion equation of the type (e.g.Wang and Ribberink, 1986 for tidal currents, and Katopodi and Ribberink, 1992, for nearshore applications)

$$T_A \frac{\partial \bar{c}}{\partial t} + L_A \left[\frac{\bar{u}}{\overline{u_{tot}}} \frac{\partial \bar{c}}{\partial x} + \frac{\bar{v}}{\overline{u_{tot}}} \frac{\partial \bar{c}}{\partial y} \right] = \overline{c_e} - \bar{c} \tag{5.16}$$

in which T_A is a time scale of the order of magnitude h/w_s and L_A is a length scale of the order of magnitude $u_{tot}h/w_s$. The equilibrium concentration, c_e, corresponds with the uniform situation and is usually derived from a sediment transport formula, or from a simpler model which applies to uniform situations.

Note that Eq. (16) can also be considered as a decay equation of the type

$$\frac{d\bar{c}}{dt} + \frac{\bar{c}}{T_A} = \frac{\bar{c}_e}{T_A} \tag{5.17}$$

in which the *d/dt* stand for the material derivative, i.e. moving along with the sediment flow. If the concentration at $t = 0$ is given, the general solution can be witten as

$$\bar{c}(t) = \bar{c}(0) e^{-t/T_A} + \int_0^t \overline{c_e}(\tau) e^{-(t-\tau)/T_A} \, d\tau \tag{5.18}$$

in which τ is a formal time variable which runs from 0 to the actual time *t*. Apparently, all values of the equilibrium condition encountered in the time interval between 0 and *t* contribute to the forcing term (i.e. the second term in the right-hand part of the equation), but their contribution becomes smaller as they occurred longer ago. This shows that the memory of the system is not infinite, but has a certain time scale, viz. T_A.

This memory effect of the suspended load concentration can be rather important in a tidal inlet, with its strong spatial variations of the bed topography and the hydrodynamic conditions.

The combination of suspended load transport with secondary flows has another important effect. The sediment concentration is usually not uniform ovr the vertical: most of the sediment is concentrated in the lower part of the water column. Consequently, secondary flows will have a net effect on the transport direction. The curvature-induced

secondary flow, for instance, will give a net transport component in towards the centre of curvature, and the undertow-induced secondary flow will give a net transport component against the direction of wave propagation. Another potentially important contribution of this type is associated with the deformation of the velocity profile as the flow moves up or down a steep slope (see Figure 5.16). When averaged over the tide, this gives a net upslope transport. This may explain why steep banks of tidal channels can be stable.

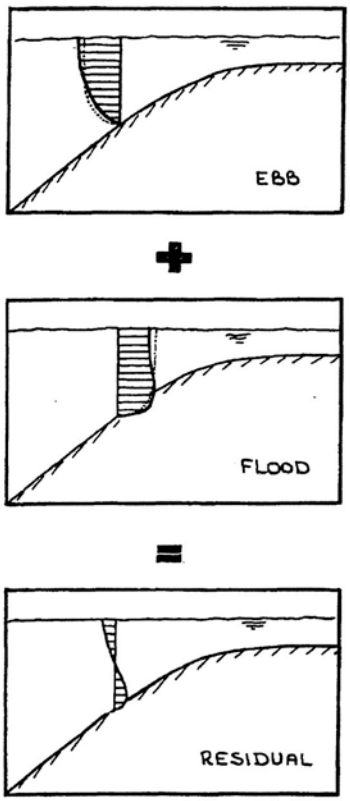

Figure 5.16. Residual uphill transport due to deformations of the velocity profile

5.6.1 Sediment transport patterns

The combination of wave, curerent and sediment transport mechanisms on the outer delta gives rise to a typical residual sediment circulation pattern. Figure 5.4 shows a highly schematised picture of it, reality is usually more irregular and diffuse (cf. Figure 5.17). In general, the flood channels carry sediment from the adjacent coasts to the inlet. Depending on the demand of the basin, this sediment is transporte into the basin, or somehow it ends up in the main ebb channel, which brings it out towards the edge of the outer delta. There part of it is picked up by wave-driven and/or tidal longshore currents (storms!) and transported along the delta edge, ultimitely towards the downdrift island, or towards the updrift one, depending on the situation. Figure 5.18 gives an example of such a residual transport pattern.

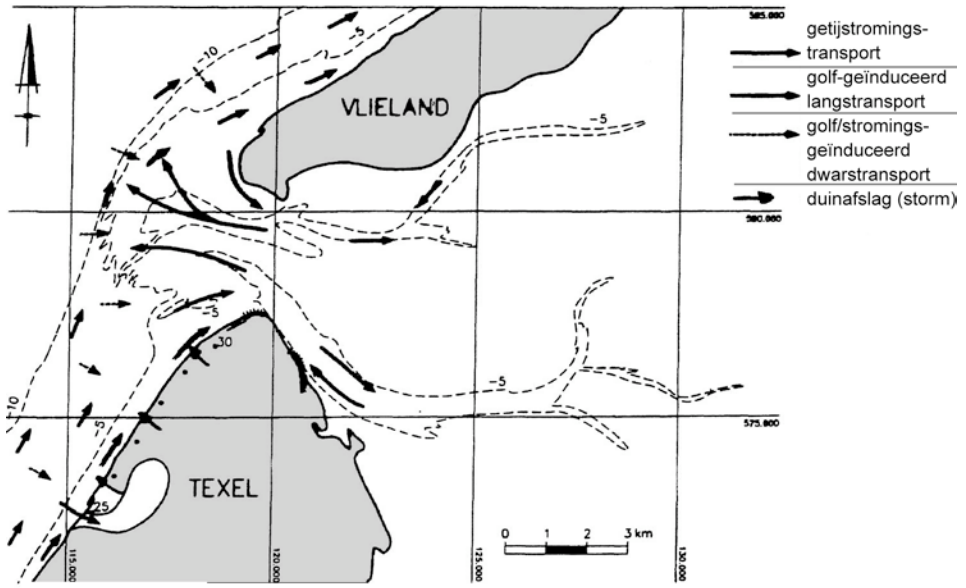

Figure 5.17. Residual transport pattern around the Eijerlandse Gat, as derived from field observations and results of various mathematical models

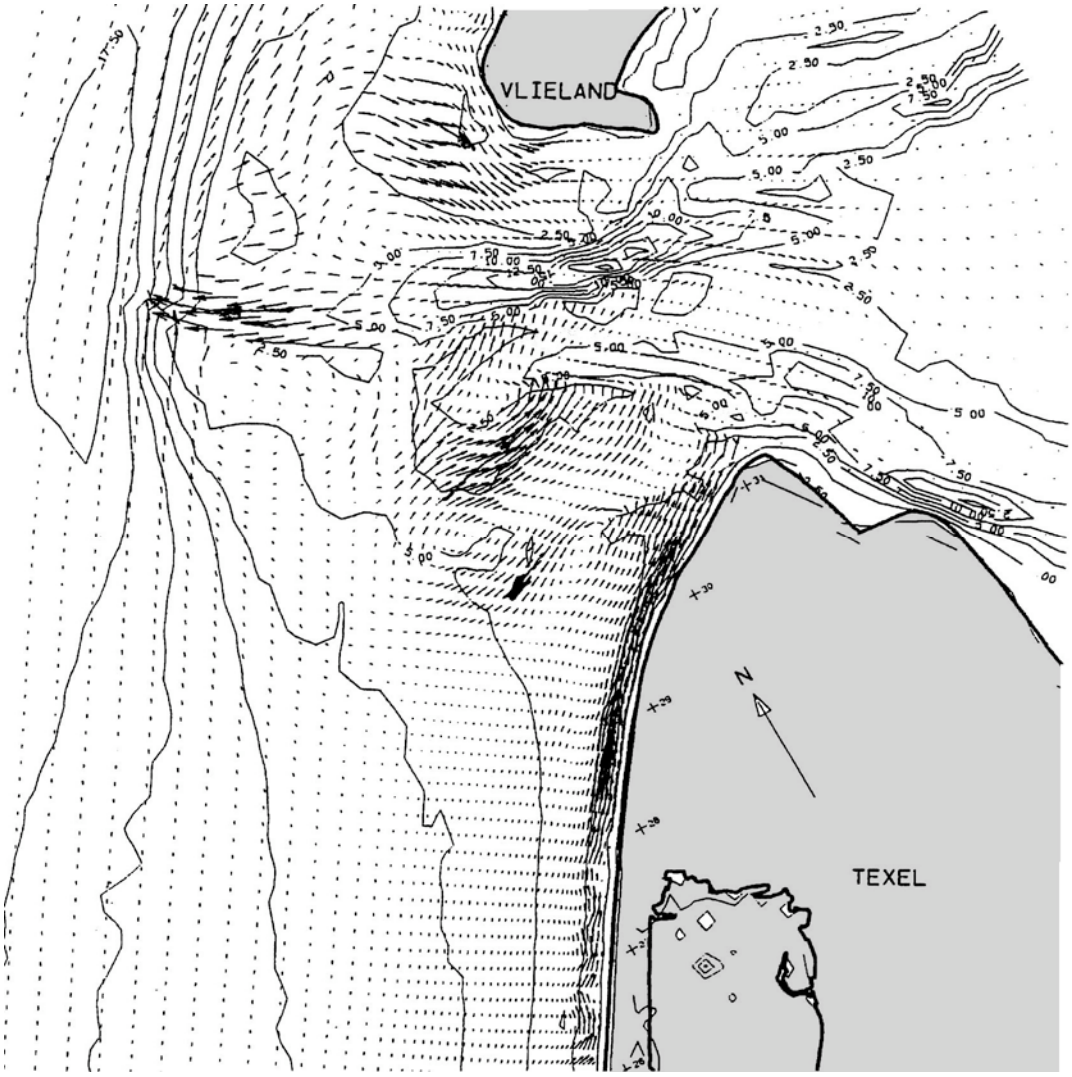

Figure 5.18. Yearly residual transport pattern on the outer delta of the Eijerlandse Gat

Another part of the sediment from the ebb channel, as well as part of what is brought into the area by the longshore drift along the updrift island, end up in the shoal system on the outer delta. Due to the various hydrodynamic and sediment transport processes around these shoals, there is a long-term residual transport and a slow migration of the shoals in the direction of the longshore drift (Figure 5.19). The time needed for a shoal to cross the inlet may be tens of years (for the Borndiep, for instance, the inlet between Terschelling and Ameland, it is typically 40 years).

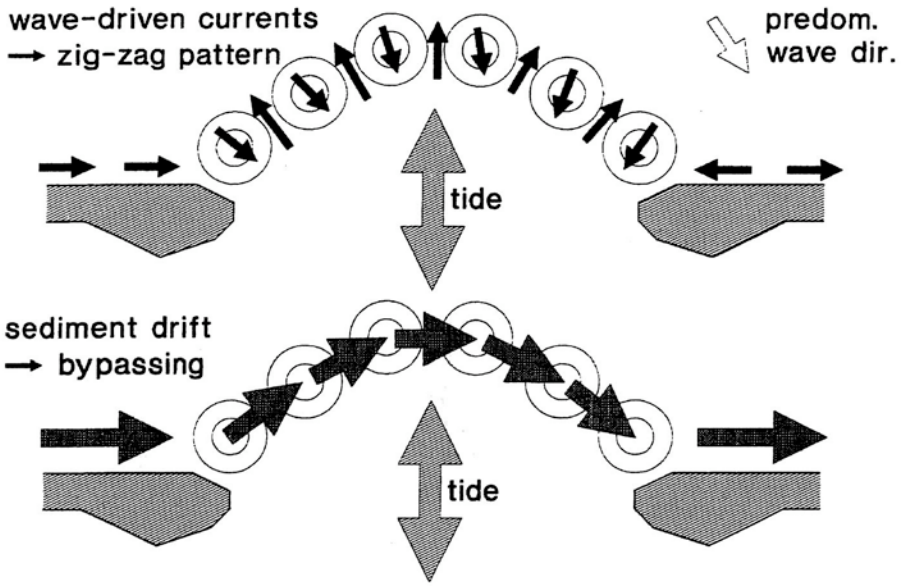

Figure 5.19. Sediment bypassing via shoal migration on the outer delta.

An example of what can go wrong when ignoring the nature of this sediment circulation refers to Nerang River, Australia, where an inlet to a tidal lagoon was made into a shipping channel by building groynes at either side of the inlet and bypassing the longshore drift via a pumping system. This scheme works well from the point of view of downdrift erosion, but it does a much worse job for the outer delta and the hydrodynamic conditions in the inlet are concerned. By artificially bypassing all the sediment which arrived at the updrift side of the inlet, the shoal bypassing system was cut off from its sand supply, the shaols rapidly degraded, and the outer delta disappeared. As a consequence, the tidal motion into and out of the lagoon was no longer hampered by the delta and increased considerably. This led to a dramatic increase of the flow velocities in the inlet, due to which its navigation function (the prime reason for carrying out the scheme) is heavily threatened.

5.7 References

De Vriend, H.J., Zyserman, J., Nicholson, J., Péchon, Ph., Roelvink, J.A. and Southgate, H.N., 1993. Medium-term 2-DH coastal area modelling. *Coastal Engineering*, 21(1-3): 193-224.

Ehlers, J., 1988. *Morphodynamics of the Wadden Sea*. Balkema, Rotterdam, 397 pp.

Fredsøe, J. and Deigaard, R., 1992. *Mechanics of Coastal Sediment Transport*. Adv. Series on Ocean Eng. - Vol. 3, World Scientific, Singapore, 369 pp.

Horikawa, K., 1988. *Nearshore dynamics and coastal processes.* University of Tokyo Press, 522 pp.

Katopodi, I. and Ribberink, J.S., 1992. Quasi-3D modelling of suspended sediment transport by currents and waves. *Coastal Engineering,* 18(1&2): 83-110.

Soulsby, R.L., Hamm, L., Klopman, G., Myrhaug, D., Simons, R.R. and Thomas, G.P., 1993. Wave-current interaction within and outside the bottom boundary layer. *Coastal Engineering,* 21(1-3): 41-69.

Steijn, R.C., Roelvink, J.A., Rakhorst, D., Ribberink, J.S. and Van Overeem, J., 1998. North-coast of Texel: a comparison between reality and prediction. In: B.L. Edge (Editor): *Coastal Engineering 1998,* ASCE, New York (in press).

Van Rijn, L.C., 1989. *Handbook Sediment Transport by Currents and Waves.* Delft Hydraulics, Rept. H461, appr. 400 pp.

Wang, Z.B. and Ribberink, J.S., 1986. The validity of a depth-integrated model for suspended sediment transport. *J. Hydr. Res.*, 24(1): 53-67.

6 Aggregated modelling of coastal inlets and tidal basins

Mathematical modelling of meso-tidal barrier island coasts

Part 1: EMPERICAL AND SEMI-EMPERICAL MODELS

6.1 Introduction

A large part of the world's coastline consists of more or less elongated barrier islands. They are separated from the mainland by a shallow tidal basin and from each other by relatively narrow inlets to that basin. For various reasons, these barrier island coasts are important issues in coastal zone management.
Barrier islands tend to be morphologically quite active, whence they are difficult to be controlled by engineering measures. Yet, many of these islands are inhabited, and the houses and properties often require protection measures. This is a continuous source of problems at the engineering level.
The outer deltas in front of the inlets store large amounts of often well-sorted sand, which is attractive to be mined for all sorts of purposes (for instance beach

nourishment). As the delta is part of a coherent morphological system, however, this sand mining may have detrimental effects on the other parts of this system (viz. the adjacent island coasts and the basin).

The sheltered borders of estuaries and lagoons are attractive places for economical and recreational activities related to the sea. This explains why many inlets are important navigation channels. As inlet channels tend to be morphologically even more active than the barrier islands, it is tempting to try and stabilize them with engineering works like jetties and revetments. The connection of such works with the mobile natural system is rather problematic and costly.

Many tidal lagoons, especially the intertidal zones, are of paramount importance to the ecosystem as feeding and breeding grounds for many species throughout the food chain. Thus these areas have a high nature-preservation status. At the same time, the system is quite vulnerable, because the intertidal area is very sensitive to changes in the physical system (e.g. accelerated mean sea-level rise).

Since tidal inlet systems respond to the mean sea level, the tide and the wave conditions, they are not only threatened by sea level rise and subsidence. Also changes in the tidal regime (amplitude, asymmetry) and the wave climate (mean wave height and direction, storm climate, chronology of events) can have a major impact.

The ability to understand and predict the morphological behaviour of barrier island coasts, including inlets and basins, is therefore an important issue in coastal zone management. Mathematical models are particularly attractive here, because of their flexibility and because the complexity of the system makes physical scale modelling very difficult, especially when it concerns long-term morphological evolution.

In recent years, tidal inlets have come within the reach of mathematical modellers. It has become possible to model many of the complex physical processes (waves, currents, sediment transport, morphological changes) which take place in the vicinity of an inlet. Such models enable researchers to develop and test hypotheses on how an inlet system works, and to identify the most important knowledge gaps. They also enable practitioners to analyse the response of a given inlet system, for instance to proposed engineering measures.

In spite of the computer power which is available at present, these process-based simulation models are as yet unable to cover time spans which are much larger than the principal inherent morphological time scales. Much of the empirical knowledge on the equilibrium state of tidal inlets, for instance, cannot yet be reproduced by these models. This has boosted the formulation of semi-empirical long-term models which are based on elementary physics, but include the empirical knowledge.

As it is hardly possible to cover the entire range of coastal inlets, this chapter focuses on what Hayes (1979) calls *mixed-energy tide-dominant* inlets. This is the type of inlets which is common along the Northwest European coast, for instance. The tidal range is typically a few metres and the yearly average significant wave height is typically 1 m. In their natural state, these inlets are rather wide, with a large dynamic outer delta and drumstick-shaped barrier islands.

After a brief outline of the practically relevant phenomena which inlet models should be

able to cover, the various model types are classified. Except for the process-based simulation models, which are treated in a companion chapter, each of the classes is described and its potentials, shortcomings and perspectives are discussed.

6.2 Phenomena to be modelled

In the present state of development it is not realistic to claim that one model type can provide the necessary morphological information for all possible practical problems. In other words: the all-purpose model for tidal inlet morphodynamics does not exist and is not likely to emerge in the near future. This means that the present models are linked to classes of phenomena.
Barrier islands, outer deltas, inlet channels and flood basins are all elements of one coherent morphodynamic system (Figure 6.1). The nature of this "tidal inlet system", however simple at first sight, is very complex. It is forced by a partly unpredictable input signal (waves, storm surges), and its behaviour involves a wide range of space and time scales. Part of this behaviour is imposed by variations of the forcing signal, part is inherent to the system. An example of forced behaviour is the 18.6-yearly variation of the inlet geometry due to the nodal cycle of the tide (Oost et al., 1993). An example of inherent behaviour is the formation and migration of channel and shoal patterns in the flood basin and on the delta fringe (for instance, see Ehlers, 1988).

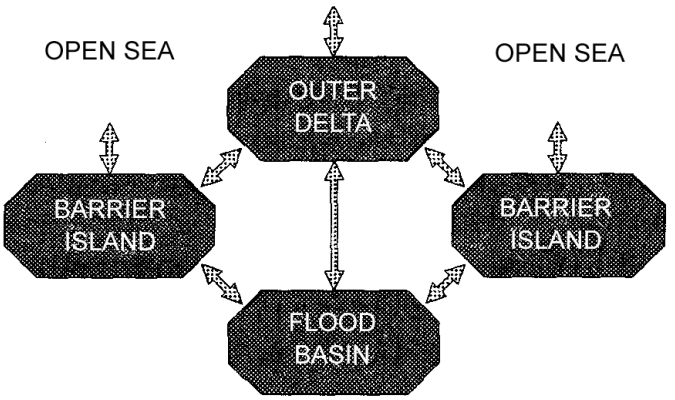

Figure 6.1: Larg-scale tidal inlet system

The complexity and the scale range of this inherent behaviour make tidal inlets particularly difficult to model. Models which perform well in describing small-scale phenomena are not necessarily suited for long-term predictions, even if there is ample computer time available. The phenomena which a model is able to describe are therefore classified relative to the inherent scale of the corresponding morphodynamic process. The latter represents both the space and the time scale, because these are assumed to be coupled: larger-scale phenomena will proceed more slowly than small-scale ones (cf. De Vriend, 1991; Fenster et al., 1993). This leads to the following classification:

1. Micro-scale (***process-scale***) phenomena take place at an essentially smaller scale than the corresponding morphodynamic behaviour. It concerns primarily the

constituent processes (waves, currents and sediment transport). Examples of practically relevant information are

- wave conditions in channels, on shoals and near structures;
- relevance: navigation, habitat, coastal defence;
- current speed in channels, on shoals and near structures;
- relevance: navigation, habitat, local scour;
- patterns of water mass exchange;
- relevance: water quality, import of nutrients, larvae, etc.;
- suspended sediment concentration and turbidity;
- relevance: habitat, mobility of channels and shoals;
- sediment transport rate;
  relevance: mobility of channels and shoals; import of adhering nutrients and pollutants.

2. Meso-scale (***dynamic scale***) phenomena concern the "primary" morphodynamic behaviour, due to the interaction of the constituent processes and the bed topography. The scales involved are of the order of magnitude of those inherent to this interaction, which is generally much larger than those of the constituent processes. Examples of practically relevant information are
   - bedform (ripples, dunes, sandwaves) dimensions, propagation and patterns;
   - relevance: influence on current and transport patterns, depth for navigation,
   - risk of denudation of pipelines.
   - shoaling and migration rates of natural channels;
   - relevance: navigation, coastal defence.
   - reside time of bottom pollutants;
   - relevance: water quality, habitat.
   - morphological changes around man-made works;
   - relevance: stability of structures, (un)burial of pipelines, shoaling of dredged navigation channels, filling-up of sand-mining pits.
   - response to human interference, such as land reclamation, persistent sand mining, repeated channel dredging, etc.; relevance: to avoid detrimental effects elsewhere in the system.

3. Macro-scale (***trend-scale***) phenomena concern slow trends at scales much larger than those of the "primary" morphodynamic behaviour. These trends can be due to secular effects in the system's inherent behaviour, or to gradual changes in the extrinsic forcing or the system parameters. The cyclic migration of channels in a wide inlet (Bakker and Joustra, 1970; Oost and De Haas, 1993; Oost, 1995) may be considered as a secular effect. Gradual changes in the extrinsic forcing may be due to mean sea-level rise, subsidence, tidal range evolution, etc. Erodibility is an example of a system-parameter which is is affected by changes in the cohesive sediment content, the intensity of mussel fishing, and the marshland vegetation (due to pollution, for instance). Examples of practically relevant phenomena are:

- evolution of channel/shoal patterns in the basin and on the delta; relevance: habitat and ecosystem, coastal defence at barrier islands, navigability, stability of pipelines;
- evolution of the intertidal zone (area, level, duration of flooding and drying);
- relevance: habitat and ecosystem, (indirectly:) coastal defence at barrier islands;
- inlet instability;
  relevance: coastal defence, ecosystem, navigation.

The above classification is relative, so the scale classes cannot be expressed in absolute terms of metres or years. Figure 6.2 illustrates that the three classes exist for a wide range of phenomena at different scales.

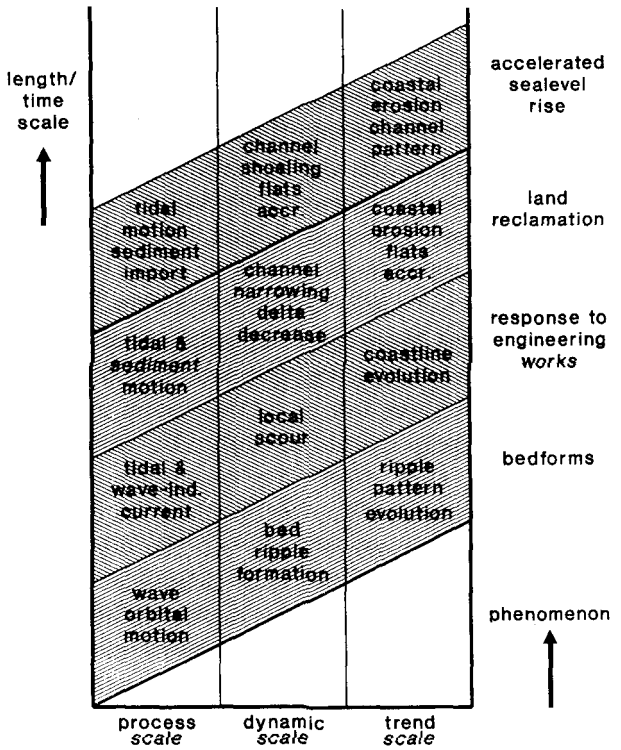

Figure 6.2: Phenomena and scales

6.3 Classification of mathematical models

The statement that the all-purpose model does not exist is substantiated by the wide variety of tidal inlet models which has been proposed. The above classification of phenomena can be used to structure this set.
Another axis of classification is the model approach. In broad outline, the following model types can be distinguished:

- ***data-based models***, making use of measured data only and aiming directly at the phenomena to be described;
- ***empirical relationships***, also observation-based, but establishing a relationship

between input and output of the system;

- ***process-based models***, which describe waves, currents, sediment transport and bed level changes via a set of mathematical equations based on first physical principles (conservation of mass, momentum, energy, etc.);
- ***formally integrated long-term models***, which are derived from a process-based model by formal integration over time (and space), with empirical or parametric closure relationships;
- ***semi-empirical long-term models***, which describe the dynamic interaction between large elements of the system, using empirical relationships to represent the effects of smaller-scale processes.

Figure 6.3 shows that these two axes of classification are not entirely orthogonal. Henceforth, the various model types will therefore be distinguished by approach only.

	process scale	dynamic scale	trend scale
process based models	x	x	
formally integrated models	x	x	x?
semi-empirical models		x	x
data-based models			x
empirical relationships			x

Figure 6.3: Mathematical models and phenomena

6.4 Data-based models

Geostatistical models belong to the class of data-based models. The simplest form of geostatistical modelling is the extrapolation in time of a certain parameter of the system's state (for instance the minimum depth of a certain channel) via a linear regression analysis of observed values. The model essentially consists of the coefficients which result from the regression analysis, together with the assumption that the parameter to be predicted will continue its past evolution. The underlying assumption is that the processes which determine the trend in this evolution will remain constant.
Fenster et al. (1993) decribe a more sophisticated version for the multi-scale nonlinear system of an uninterrupted coast. Although inlet systems are essentially more complicated, the technique should be transferable to tidal inlets. A necessary condition for validity as a prediction tool is that the processes which lead to the described behaviour will remain unaltered in the future.
Another form of data-based modelling is "translation" of observations at one site to

predictions at another. This approach may be applicable if the system is to undergo changes (due to engineering works, for instance) which have taken place before in a well-monitored similar system. The underlying assumption is that the two systems will exhibit a similar response to this interference.
Empirical Orthogonal Function (EOF) analysis (Preisendorfer and Mobley, 1988) is a form of data-based modelling which separates various modes of variation in space and time. The weighted sum of products of these modes constitutes the complete data set, and for each of these products the content of measured information can be assessed. Thus EOF-modes can be ordered according to their content of information on the observed behaviour. In the case of uninterrupted coasts, these series use to converge rapidly, which means that the behaviour can largely be mapped onto a few EOF-modes (cf. Medina al., 1992; Wijnberg and Wolf, 1994; also see De Vriend et al., 1993a). As yet, aplications to tidal inlet systems are scarce, so it is unclear whether this favourable property also applies there.
In general, EOF-analysis allows for a certain degree of physical interpretation per component. Hence extrapolation into the future can be done per component, based on physical considerations. At any future time, the state of the system can be composed of the various components.
Data-based models of tidal inlets typically concern macro-scale phenomena, such as the historical or geological evolution of the system as a whole. Their concept ("let nature tell what it is like") may seem attractive for complex systems, because it seems to evade the necessity to analyse the system's behaviour. It is exactly this complexity, however, which rules out such a "black-box" approach. In simple cases it is relatively easy to predict whether or not the relevant conditions and processes are likely to remain unaltered. The system's behaviour is transparent and it is determined by one or a few predominant mechanisms. The relevant input and process parameters are not many, which makes it easier to predict whether the system's behaviour is likely to change in the future.
In a system as complex as a tidal inlet, however, there are many input and process parameters to take into account, and the system's behaviour is difficult to analyse. Hence it is difficult to asses which mechanisms determine which aspect of the system's evolution. Utilizing data-based models in such a situation therefore requires an equally thorough insight into the mechanisms at work as any physics-based model.

6.5 Empirical models

6.5.1 Equilibrium-state relationships

O'Brien (1931, 1969) was the first to suggest a linear relationship between the cross-sectional area of an inlet and the tidal prism, defined as the total amount of water which moves in and out the inlet during one tide,

$$A_c = c_A P \tag{6.1}$$

in which

A_c = cross-sectional area of the inlet channel below MSL [m^2],

c_A = coefficient of proportionality; Eysink (1990) suggests for the Dutch Wadden Sea a value of 7.0×10^{-5} m^{-1}, to be used in combination with the mean tidal prism,

P = representative tidal prism [m^3].

Qualitatively speaking, a positive correlation between A_c and P makes sense, because channels are likely to be larger if they have to convey more water. An obvious disadvantage of the above form is that the constant of proportionality is dimensional.

Measured data from many inlets all over the world have confirmed that such a relationship exists (Figure 6.4), although Jarrett (1976) claims that the exponent of P should be 1.1 for the inlets on the U.S. coasts. The validity of Eq,. (1) has also been shown for the Dutch and German Wadden Sea inlets (cf. Eysink, 1990; Schroeder et al., 1994). Moreover, a similar relationship was shown to exist over a very wide range of scales for channels inside the flood basin (Gerritsen, 1990; Eysink et al., 1992). In that case, P stands for the total amount of water conveyed by the channel during one tide.

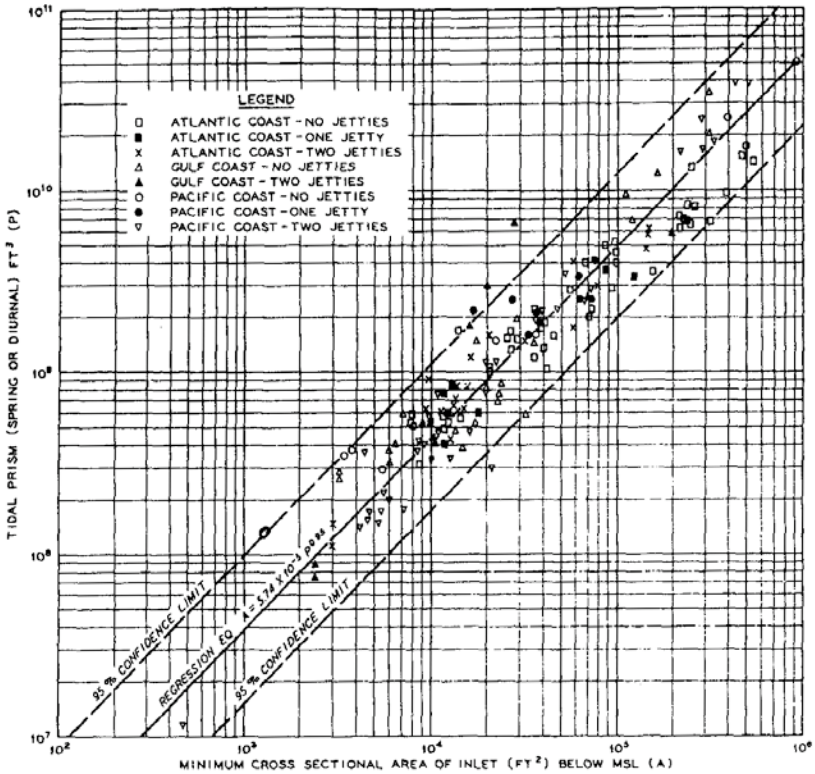

Figure 6.4: Emperical relationship between cross-sectional area and tidal prism [from: Jarrett, 1976]

An alternative version of this relationship expresses A_c in terms of the so-called "stability shear stress", which is defined as the shear stress needed to maintain a zero net transport gradient along the channel (Gerritsen, 1990; Friedrichs, 1995). This shear stress is not necessarily equal to the critical shear stress for sediment motion.

In systems terms, Eq. (1) represents a typical "black-box" input/output relationship. Unlike a geostatistical model, it describes the state of the system (represented by A_c) as a function of the forcing (represented by P). Clearly, a widely valid empirical relationship

like this must concern the equilibrium state, otherwise site-specific history-effects would have led to a much larger scatter in the A_c-P diagram.
Later work on inlet data has revealed a number of other relationships between equilibrium-state properties and the tidal prism, such as

- the flood-basin volume below MSL (Eysink, 1990), found to be proportional to $P^{1.5}$. This volume is largely equal to the sum of volumes of the flow-conveying channels. Since the cross-sectional area of these channels is proportional to P and their length probably scales with the square root of the basin area, the proportionality with $P\sqrt{P}$ seems to make sense.
- the sand volume of the outer delta (Walton and Adams, 1976; Eysink et al., 1992), which is proportional to $P^{1.23}$. As the outer delta is mainly formed by the ebb-jet out of the inlet, a relationship with P is to be expected. The weak dependency on the wave conditions, however, is rather surprising. Apparently, the system's sand budget is almost closed and the waves only deform the body of sand;
- the protrusion of the outer delta (De Vriend et al., 1994), which turns out to be proportional to $P^{0.6}$, at least for the Dutch and the East-Frisian Wadden Sea. Note that the effect of the wave conditions cannot be identified here, because the wave cllimate is largely the same throughout the area.

This may give the impression that any large-scale equilibrium-state property of tidal inlets can be expressed in terms of the tidal prism. Clearly, this is only true for the properties which are directly related to the amount of water which moves through the system during the tide.
A very important aspect of the morphological system, viz. the level of the intertidal flats, is mainly correlated to the mean high-water level (MHW) and the local wind/wave climate. In broad outline, shoals tend to be built up by the tide during calm weather and their top is eroded by waves during rough weather (cf. De Vriend et al., 1989).
Another important property which has a rather weak correlation with the prism is the flats' area. By definition, this quantity is equal to the difference between the basin area and the channel area, and the latter is equal to the channel volume divided by some characteristic channel depth. This leads to a relationship of the type

$$A_f = A_b - A_{ch} \approx A_b - \alpha \frac{P\sqrt{A_b}}{D_{ch}} \approx A_b - \beta \frac{H_m}{D_{ch}} A_b^{3/2} \tag{6.2}$$

in which
A_f = the flats' area, i.e. the area above MSL [m^2],
A_b = the gross basin area (flats and channels) [m^2],
A_{ch} = the horizontal area covered by all channels [m^2],
α = constant of proportionality [m^{-1}],
D_{ch} = characteristic channel depth [m],
β = constant of proportionality [m^{-1}],
H_m = mean tidal range [m].

Renger and Partenscky (1974) suggest, on the basis of data from the inlets in the German Bight,

$$A_f = A_b - 0.025\, A_b^{3/2} \tag{6.3}$$

which would mean that the flats' area depends exclusively on the basin area. According to Eq. (6.2), this can only be the case if D_{ch} is proportional to H_m. Eysink (1990) shows that if a channel-depth relationship exists, it contains a power of P (or H_m) which is significantly less than 1. Apparently, Eq. (6.3) is an oversimplification of reality.
These properties of the intertidal zone are not only important for the functions of the inlet system (ecosystem, mussel banks), but also for the large-scale morphodynamics. The bathymetric variation in a tidal basin gives rise to a tidal rectification which can contribute significantly to the residual transport (Van de Kreeke and Robaczewska, 1993; Bakker and De Vriend, 1995), and hence to the net import or export of sediment. Via the so-called "hypsometry effect" (Pethick, 1980; Boon and Byrne, 1981; also see Van Dongeren and De Vriend, 1994), the flats also influence the tidal asymmetry in the gorge: the smaller the flats' area relative to the basin area, the more positive the asymmetry. Thus the flats regulate the import or export of sediment and enable the system to reach an equilibrium state.

6.5.2 Example of application

The empirical relationships for the large-scale equilibrium state can be utilized to give off-hand predictions of the impact of factors which affect the tidal prism, the basin area, or the MHW-level. An example of such a case is "The Friesche Zeegat", one of the inlets of the Dutch Wadden Sea (Figure 6.5) with had following characteristics until 1969:

H_{m0} = 2 m ; A_{b0} = 2.1 10^8 m^2 ; P_0 = 3.0 10^8 m^3 ;

A_{c0} = 1.9 10^4 m^2 ; V_{b0} = 3.5 10^8 m^3 ; $V_{\Delta 0} \approx$ 1.8 10^8 m^3 ; A_{f0} = 1.6 10^8 m^2

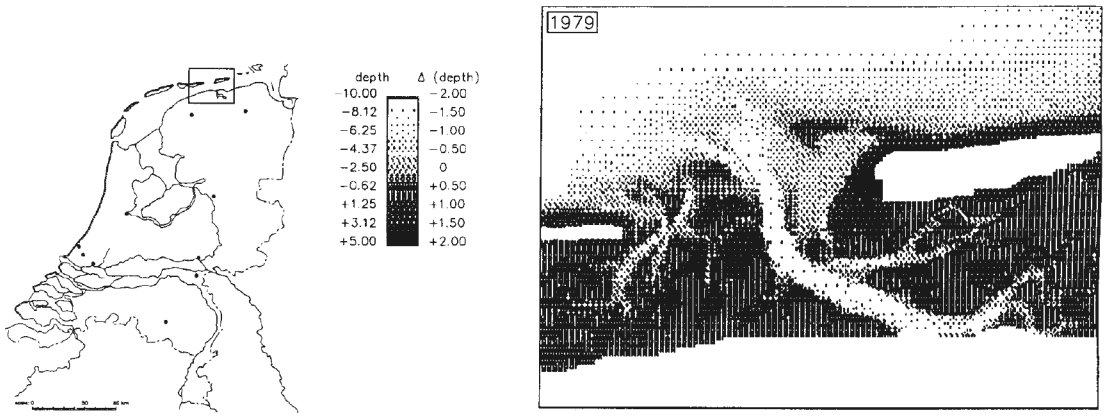

Figure 6.5: The Frisian inlet after closure of the Lauwerszee

In 1969, the Lauwerszee, with an area of 90 10^6 m^2, was separated from the basin by a dam and reclaimed. This means that in 1969 the above values changed abruptly into

$H_m = 2$ m ; $A_b = 1.2\ 10^8$ m^2 ; $P = 2.0\ 10^8$ m^3 $\approx 0.65\ P_0$;

$A_c = 1.9\ 10^4$ m^2 ; $V_b = 2.7\ 10^8$ m^3 ; $V_\Delta \approx 1.8\ 10^8$ m^3 ; $A_f \approx 0.75\ 10^8$ m^2

Obviously, the system has responded to this major interference. According to the above relationships, it should seek a new equilibrium state in which

$H_m = 2$ m ; $A_b = 1.2\ 10^8$ m^2 ; $P = 2.0\ 10^8$ m^3 ;

$A_c \approx 0.65\ A_{c0} = 1.2\ 10^4$ m^2 ; $V_b \approx (0.65)^{1.5}\ V_{b0} = 1.9\ 10^8$ m^3 ;

$V_\Delta = (0.65)^{1.23}\ V_{\Delta 0} \approx 1.1\ 10^8$ m^3 ; $A_f \approx 0.85\ 10^8$ m^2

Note that the relative flats' area is expected to increase after closure, because the value of this parameter in the remaining basin is initially too small (the Lauwerszee used to be the back part of the basin, and hence contained a relatively large portion of flats).
In reality, a rapid narrowing of the inlet gorge has taken place, by the formation of a large sandy hook at the east side of the inlet (Figure 6.6). The actual amount of sediment import into the basin was initially 7 10^6 m^3/yr, and between 1970 and 1987 it is estimated at 34 10^6 m^3 (Oost and De Haas, 1992). Clearly, the adjustment process has not yet come to an end. Although the delta evolution is rather dependent on long-term meteorological variations, its volume has decreased by 26 10^6 m^3 and its seaward protrusion has decreased roughly by 1.5 km in these 17 years (De Vriend et al., 1994). So the volume decrease is of the same order of magnitude as the sediment demand in the basin. Apparently, the delta serves a buffer for the basin. Yet, the equlibrium value of V_b is proportional to $P^{1.5}$ and that of V_Δ is proportional to $P^{1.23}$, which means that the basin ultimately demands more sediment than the delta can supply. This sediment has to be provided by the sea bed or the adjacent coasts.

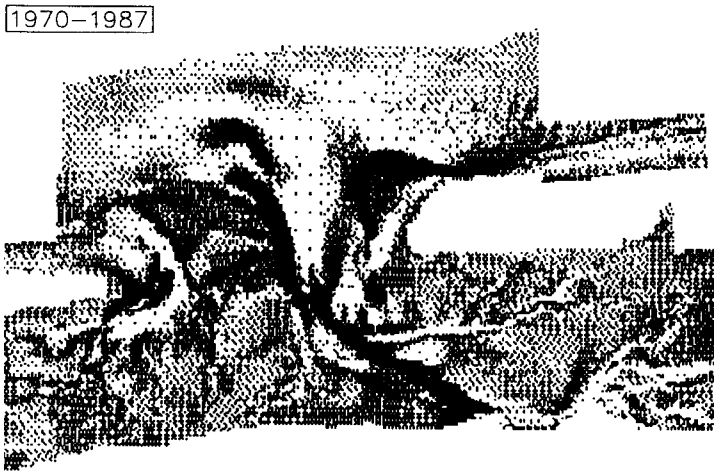

Figure 6.6: Frisian Inlet: accretion and erosion between 1970 and 1987 (the darker the shade, the stronger the accretion)

6.5.3 Transient empirical models

Transient empiricial models (O'Connor et al., 1990; Eysink, 1990; Eysink et al., 1992) are one step further along this line. Given the intital state and the equilibrium state, they describe the evolution of the discrepancy between the actual state and the equilibrium state as an exponential decay process. In mathematical terms, this is described by

$$\frac{dA}{dt} = \frac{A_e - A}{\tau} \tag{6.4}$$

in which

A = morphological state parameter (e.g. A_c, V_b, or A_f),
t = time,
A_e = equilibrium value of A,
τ = characteristic time scale of the decay process.

If A_e is a constant, the corresponding solution reads

$$A(t) = A_e - \left[A_e - A(0)\right] \exp(-\frac{t}{\tau}) \tag{6.5}$$

If A_e exhibits a slow linear variation in time, for instance in the case of the flats' level responding to mean sea-level rise, the solution reads

$$A(t) = A_e(t) - \tau \frac{dA_e}{dt} - \left[A_e(0) - \tau \frac{dA_e}{dt} - A(0)\right] \exp(-\frac{t}{\tau}) \tag{6.6}$$

The example in Figure 6.7 shows that, after the effect of the initial condition has damped out ($t \gg \tau$), the actual state keeps on lagging behind the equilibrium state. This should be borne in mind when trying to find empirical flat-level relationships in areas with a significant rate of sea-level rise.

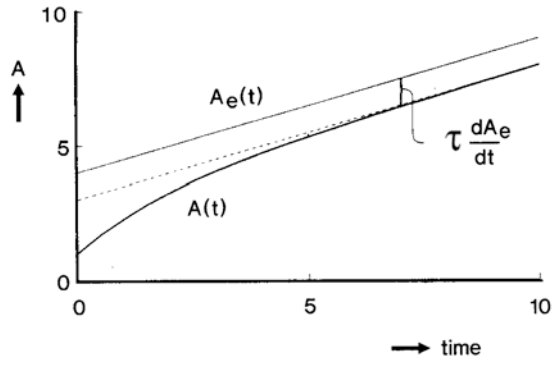

Figure 6.7: Flats 'level' evolution for rising mean high-water level

Transient models of this type concern primarily macro-scale phenomena. They rest upon the implicit assumption that each system element behaves independent of the others. In other words: the element would exibit this behaviour if sufficient sediment would be available. In a coherent system like a tidal inlet, this may be true for some elements, but presumably not for all of them. If, for instance, Eq. (4) is utilized to assess the sediment

demand of a basin under the influence of sea level rise, the interaction with the outer delta and the adjacent island coasts is ignored.

6.6 Semi-empirical long-term models

6.6.1 General approach

Although a theoretical approach based on formal integration of the constituting equations (see the companion chapter) is probably the most accurate, it is a long shot. The identification of the relevant physical processes and the understanding of their nonlinear interaction requires much further research, which is going to take its time. Therefore, it seems wise to pursue a more pragmatic line of development at the same time: semi-empirical long-term modelling. This approach tries to make use of all information available, from the field via the empirical equilibrium-state relationships, and from theory via the large-scale balance equations. Wherever needed, parameterized results of more detailed models are included.
Since the empirical information is not available at a very detailed scale, it is important to think at a high level of aggregation, for instance in terms of the principal system elements (basin, gorge, outer delta, island coasts). In the following a brief outline will be given of a number of models for various of these elements.

6.6.2 Stability of the gorge

Wide-open inlets like those in the Wadden Sea are not likely to have a strong reducing effect on the tide inside the basin. The tidal amplitude there is closely similar to that at open sea, apart from possible shallow-water effects. If the inlet is narrower, however, it will hamper the tide to enter the basin, with a reduction of the amplitude and the tidal prism as a consequence. But if the tidal prism is reduced, the cross-sectional area of the inlet will also be reduced, which leads to a further reduction of the prism, etc. This phenomenon of positive feedback, which ends up in the closure of the inlet, is usually called inlet instability.
Escoffier (1940) was the first to point out and model this instability phenomenon. He compared the maximum tidal velocity through the inlet, V_{max}, with the critical velocity for sediment transport in the inlet channel, V_{cr}. V_{max} is a function of the cross-sectional area of the channel, A_c. If A_c is small, this function will be increasing, because the growth of the tidal prism will be predominant. If A_c is large, the function will be decreasing, because the the tidal prism has become independent of A_c and the same amount of flow through a wider channel leads to smaller velocities. Figure 6.8 outlines the curves of V_{max} and V_{cr} against A_c. If $V_{max} = V_{cr}$, which is the case in Figure 6.8 for two values of A_c, the system is in equilibrium. The stability of the system in these "stationary points" can be estimated via

$$\Delta(V_{\max} - V_{cr}) = \frac{dV_{\max}}{dA_c}\,\Delta(A_c - A_{cs}) \qquad (6.7)$$

In the stationary point *SP1* the derivative of V_{max} with respect to A_c is positive, so V_{max} - V_{cr} increases if $A_c - A_{cs}$ increases. On the other hand, A_c tends to increase with V_{max}, which means that around this stationary point $V_{max} - V_{cr}$ and A_c A_{cs} are positively coupled and the system is unstable. Conversely, the system is stable around the other stationary point, *SP2*. All inlets of the Wadden Sea are within this stable domain.
Van de Kreeke (1990 a,b) uses a similar technique to analyse the stability of a multiple-inlet system and arrives at the conclusion that a two-inlet system cannot be stable. He suggests that the same conclusion holds for a multiple-inlet system.

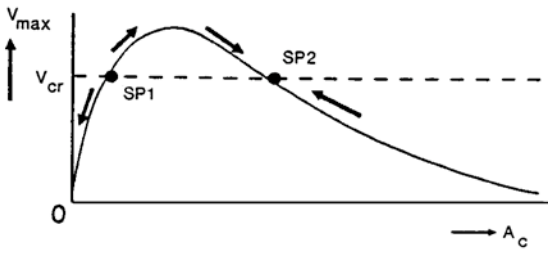

Figure 6.8: Stability diagram for tidal inlets

6.6.3 Di Silvio's basin models

Di Silvio (1989) proposes a simple box model for the basin, consisting of one deep part which represents all channels and one shallow part which represents all flats (Figure 6.9). The total cross-sectional area of the channels and the level of the flats are the dependent variables. The model works with a long-term representative sediment concentration in each part of the model (sea, channel, flat). This concentration is assumed to depend only on local parameters, such as the water depth, but not on the tide. The concentration at sea is assumed to be independent of the state of the basin, so it is a given constant.

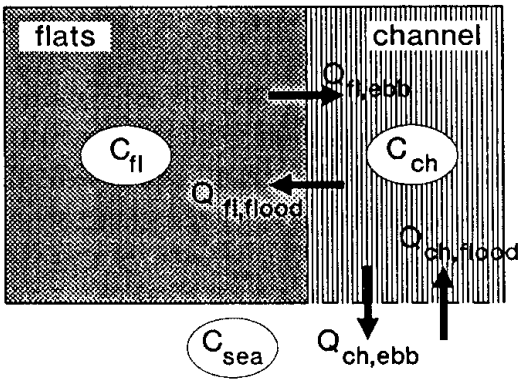

Figure 6.9: Principle of Di Silvio's (1989) box model

The sediment fluxes between the model parts are assumed to be purely advective, which means that they can be written as

$$S_1 = Q_{ch,ebb}\, C_{ch} \;;\; S_2 = Q_{ch,\,flood}\, C_{sea}$$
$$S_3 = Q_{fl,ebb}\, C_{fl} \;;\; S_4 = Q_{fl,\,flood}\, C_{ch} \qquad (6.8)$$

in which

C_{ch},C_{fl} = representative sediment concentration in the channel and the flats part, respectively,

C_{sea} = representative concentration in the sea part of the model,

$Q_{ch,ebb}$ = total water mass which flows from the channel part to the sea during ebb,

$Q_{fl,ebb}$ = total water mass flowing from the flats part to the channel part during ebb, etc.

Clearly, the conservation of water mass requires

$$Q_{ch,ebb} = Q_{ch,\,flood} \;;\; Q_{fl,ebb} = Q_{fl,\,flood} \qquad (6.9)$$

The sediment balance equations for the channel and the flat parts of the model read

$$B_{ch}\frac{dA_{ch}}{dt} = S_1 - S_2 - S_3 + S_4$$
$$= Q_{ch,ebb}\, C_{ch} - Q_{ch,\,flood}\, C_{sea} - Q_{fl,ebb}\, C_{fl} + Q_{fl,\,flood}\, C_{ch}$$

$$B_{ch}\frac{dA_{ch}}{dt} = S_1 - S_2 - S_3 + S_4$$
$$= Q_{ch,ebb}\, C_{ch} - Q_{ch,\,flood}\, C_{sea} - Q_{fl,ebb}\, C_{fl} + Q_{fl,\,flood}\, C_{ch} \qquad (6.10)$$

$$B_{fl}\frac{dz_{fl}}{dt} = S_4 - S_3 = Q_{fl,\,flood}\, C_{ch} - Q_{fl,ebb}\, C_{fl} \qquad (6.11)$$

in which $A_{ch}(t)$ denotes the total cross-sectional area of the channels and $z_{fl}(t)$ the flats' level. The constants B contain geometrical properties (channel length, flats' area) and the sediment content per unit volume of bed. Combination with Eq. (6.9) shows that the system is in equilibrium if $C_{fl} = C_{ch} = C_{sea}$.

The sediment dynamics of the system are reflected by a relationship between the concentration and the dependent variable in the relevant model part. In a linear approximation in A_{ch} and z_{fl}, Eqs. (6.10) and (6.11) can be elaborated to morphological evolution equations of the form

$$\frac{dA_{ch}}{dt} + X_{ch}\, A_{ch} = Y_{ch}\, z_{fl} + Z_{ch} \qquad (6.12)$$

$$\frac{dz_{fl}}{dt} + X_{fl}\, z_{fl} = Y_{fl}\, A_{ch} \qquad (6.13)$$

in wich X, Y and Z are constants. These coupled linear decay equations form a second-order system, as can be shown by reducing them to

$$\frac{d^2 A_{ch}}{dt^2} + (X_{ch} + X_{fl}) \frac{dA_{ch}}{dt} + (X_{fl} X_{ch} - Y_{fl} Y_{ch}) A_{ch} = 0 \qquad (6.14)$$

If X_{ch}, X_{fl} and $Y_{fl}Y_{ch}$ are positive, the solution of this equation is of the type

$$A_{ch}(t) = A_{ch,e} + P_1 \exp(-\lambda_1 t) + P_2 \exp(-\lambda_2 t) \qquad (6.15)$$

in which $A_{ch,e}$ is the equilibrium value of A_{ch}, P_1 and P_2 are constants which follow from the initial conditions, and λ_1 and λ_2 are the (real and positive) roots of the characteristic equation of Eq. (6.14).

Apparently, the dynamic interaction between the flats and the channel parts give rise to a behaviour which differs from the exponential decay which would be found if the model parts were mutually independent (cf. Section 6.5).

The above model was used with reasonable success to hindcast the morphological evolution of the Venice Lagoon over the last 180 years (Di Silvio, 1991). The same author describes a 2-D finite-difference version of the concept, in which each grid cell represents a channel or a flat element. The sediment transport in this model is described with an advection/diffusion model, still in terms of the long-term representative concentration C.

In either of these models, the constituting equations are reduced to a set of tide-integrated morphological evolution equations which can be solved at the morphological time scale. Thus the same line of thought is followed as in the formally averaged models which are described in the companion chapter.

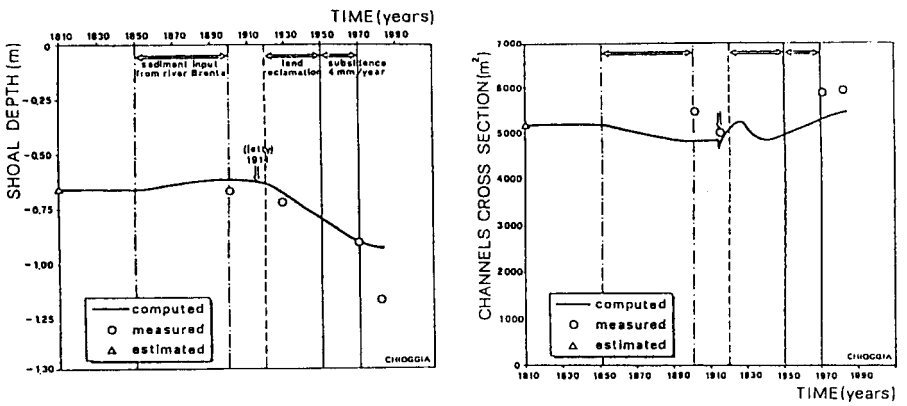

Figure 6.10: Hindcast of the morphological evolution of the Chioggia basin (Venice Lagoon) between 1810 and 1990 with Di Silvio's (1989) box model, a. flats' level, b. cross-sectional area of the channels (from Di Silvio, 1991; courtesy author)

6.6.4 Van Dongeren's basin model

Van Dongeren and De Vriend (1994) suggest to divide a channel/shoal system into a chain of consecutive boxes, aligned according to their distance from the gorge. In each box there is a channel part and a flats part (Figure 6.11). The dependent variables in each box are the channel cross-sectional area, A_{ch}, the flats' area, A_{fl}, and the flats' level, z_{fl}. Empirical relationships are used to determine the equilibrium values of these variables. The sediment balance for the channel part of each box involves the exchange with the

neighbouring channel sections and the adjacent flats. The sediment balance of the flats part involves only the exchange with the adjacent channel part (there is no sediment exchange between flats parts).

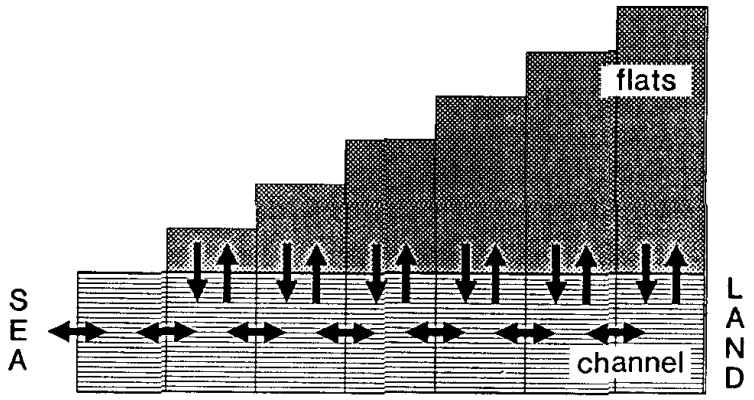

Figure 6.11: Principle of Van Dongeren's basin model

In contrast to the models in Section 6.3, the constituting equations are not reduced to one or more morphological evolution equations. In fact, this element of the model is replaced by introducing empirical decay equations for A_{ch} and A_{fl}, which apply if there is enough sediment supply to (or export from) the relevant part of the box:

$$\frac{dA_{ch}}{dt} = \frac{A_{ch,e} - A_{ch}}{\tau_{ch}} \quad \text{and} \quad \frac{dA_{fl}}{dt} = \frac{A_{fl,e} - A_{fl}}{\tau_{fl}} \tag{6.16}$$

where $A_{ch,e}$ and $A_{fl,e}$ denote equilibrium values and τ_{ch} and τ_{fl} are characteristic time scales.

The former two quantities follow from empirical relationships, the latter two are input parameters, to be estimated from measured data or otherwise. If there is not enough sediment supply or export, the available supply/export is used for morphological changes, with a fixed sequence of priority (see Figure 6.12).

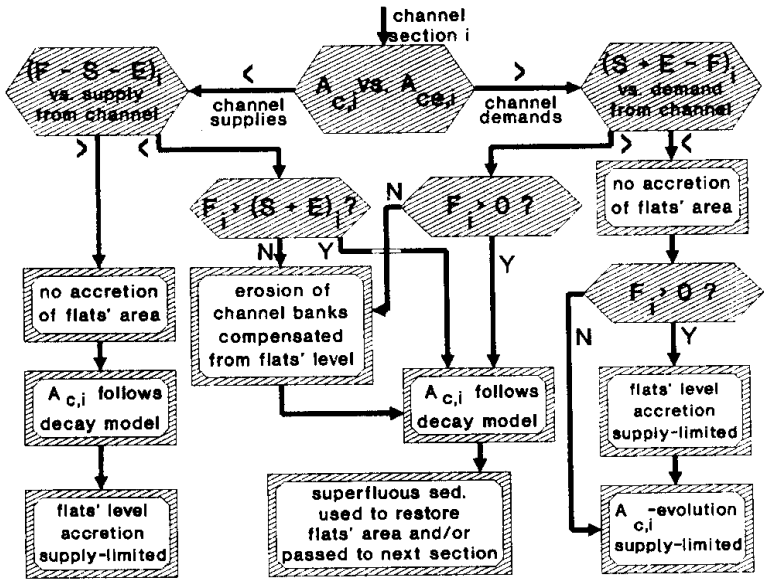

Figure 6.12: Flow chart of Van Dongeren's basin model

The boxes are handled consecutively, in a sequence which corresponds with the direction of propagation of the morphological information ("sand wave"). Sometimes this sequence is rather obvious, like in the case of the Friesche Zeegat (see Section 6.5), but in other cases this is much less clear (cf. Goldenbogen et al., 1994).
The system is essentially driven by the hypsometry effect (see Section 6.5): if the flats' area is too small, the tidal asymmetry in the gorge is positive and sediment is imported. Conversely, sediment is exported if the flats' area is too large. The dynamic response of the basin actually boils down to a tendency of the channel cross-section to adjust rapidly to the hydrodynamic conditions, if necessary at the expense of the flats. In the longer run, when the sand (or sand-deficit) wave from the gorge has reached the relevant section, part of the incoming sediment is used to restore the flats.
The spatial resolution along the channel provides the possibility to model bifurcating systems, and to reproduce something of the wave-type behaviour of the morphological changes. Yet, the concept is essentially large-scale, and the model results should be treated that way.

This model has been applied with reasonable success to the Friesche Zeegat (Van Dongeren and De Vriend, 1994), but in other cases it yields somewhat poorer results, especially for the evolution of the flats' level (Goldenbogen et al., 1994). Clearly, the interaction of flats and channels needs further investigation. Since the concept is limited to basins which are small compared with the tidal wave length (the water surface elevation has to be in phase throughout the basin), the model in its present form does not work in larger basins. Bakker and De Vriend (1995) describe an alternative network model for such basins.

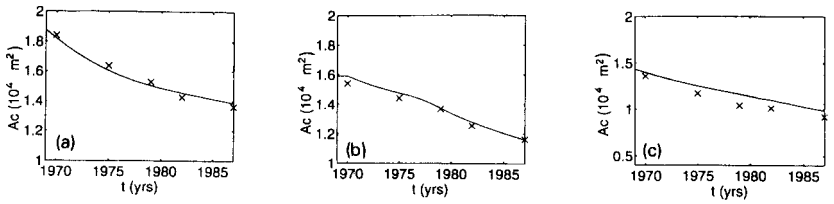

Figure 6.13: Hindcast of channel evolution in the Frisian Inlet with Van Dongeren's (1994) basin model, at (a) 3km, (b) 7 km, © 9 km from the gorge. (From: De Vriend et al., 1994; courtesy Elsevier)

6.6.5 Karssen's basin model

Karssen (1994a, 1994b) takes a somewhat similar approach as Di Silvio in a 1-D network model concept for estuaries and tidal basins. The basis is a 1-D network model for unsteady flow, in which the cross-section of each channel consists of a deep channel part, a low-lying flats part and a high flats part. The results of a tidal computation with this network model are used to determine a number of equilibrium-state parameters via empirical relationships.

The sediment is assumed to be transported primarily as suspended load, which means that a representative sediment concentration in each of the three parts of the channel cross-section can be used as a dependent variable. The transport mechanisms in the channel are advection and longitudinal diffusion. The transport on the flat sections is diffusive in the cross-channel direction, i.e. there is no longitudinal transport over the flats. Upon integration of these diffusive fluxes in the cross-channel direction, the net lateral sediment flux between the various parts of a cross-section becomes proportional to the difference in concentration:

$$F_{lc} = D_l\, h_l \frac{C_l - C_c}{L_{lc}} \quad \text{and} \quad F_{hl} = D_h \frac{h_h}{4} \frac{C_h - C_l}{L_{hl}} \tag{6.17}$$

in which

F_{lc} = net sediment flux from the low-lying flats to the channel
F_{hl} = net sediment flux from the high to the low-lying flats
D_l,D_h = lateral diffusion coefficients for the low-lying and high flats, respectively,
h_l,h_h = effective water depth above these flats,
C_l,C_h = representative sediment concentration above these flats,
C_c = representative sediment concentration in the channel,
L_{lc} = the distance over which the cross-channel integration takes place, so a typical distance from the low-lying flats to the channel, and
L_{hl} = the same from the high to the low-lying flats.

Thus the concentration evolution equations for the high and the low-lying flats become

$$\frac{\partial (A_h C_h)}{\partial \tau} = W_h\, w_s\, (C_{he} - C_h) - F_{hl} \tag{6.18}$$

$$\frac{\partial(A_l C_l)}{\partial \tau} = W_l\, w_s\, (C_{le} - C_l) - F_{lc} + F_{hl} \qquad (6.19)$$

in which
A_l,A_h = cross-sectional area on the high and the low-lying flats part, respectively,
W_l,W_h = settling coefficients on these flats,
C_{he},C_{le} = equilibrium concentration on these flats,
τ = “slow" time co-ordinate, which varies at the morphological time scale,
w_s = sediment settling velocity.

The corresponding sediment balance equation describes the evolution of the cross-sectional areas of the three channel parts in terms of the net sediment flux from the bed:

$$\frac{\partial A_i}{\partial \tau} = W_i\, w_s\, (C_{ie} - C_i) \qquad (6.20)$$

in which the suffix i (i=c,l,h) refers to each of the parts.
Unlike Di Silvio's (1989) model, these sediment balance equations are not elaborated to morphological evolution equations by expressing C_i in terms of A_j (j=c,l,h). Instead, Eqs. (6.20) are solved in a simulation loop, together with the concentration equations and the empirical equilibrium-state parameters computed from the tidal model results. After the topography has changed enough to influence the tide, another hydrodynamic model run is made. To that end, the cross-sectional areas which result from the morphological computation are translated into a 7-point cross-sectional shape per channel section.
A critical point is this model is the definition of the nodal point relationships for the transport (concentration). Depending on how these are chosen, a bifurcated channel system can persist or not (Wang et al., 1993). If the transport is distributed according to the flow rates through the channel sections connected to the node, for instance, part of the channels will fill up.
A first application of this model to the "Friesche Zeegat" case (Section 6.5) was rather succesful in hindcasting the evolution of the channels' cross-sectional area throughout the basin (Karssen, 1994b). Whether the model performs equally well for the tidal flats remains to be investigated.

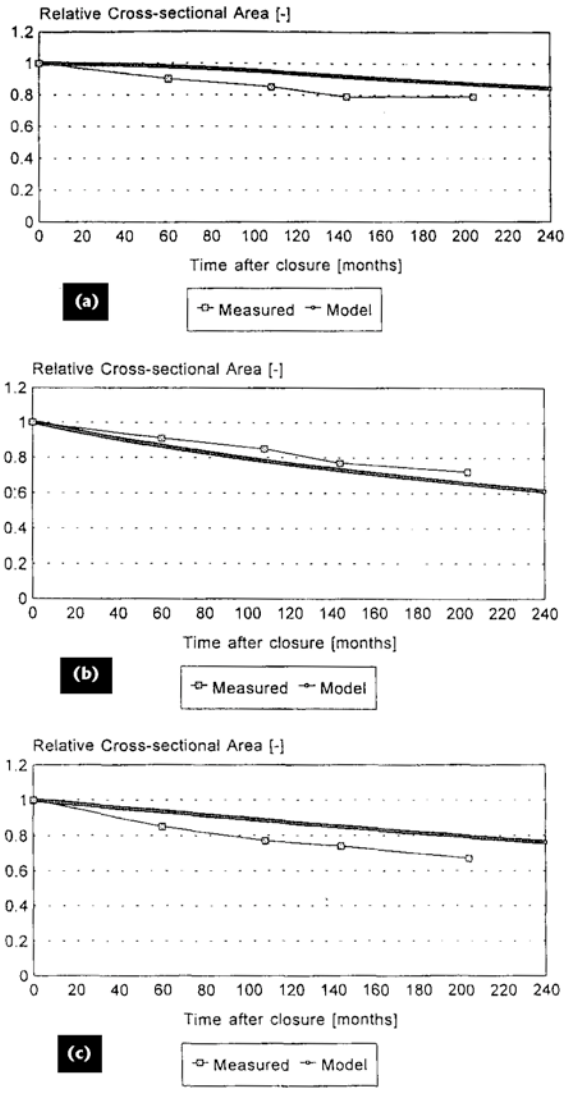

Figure 6.14: Hindcast of channel evolution in the Frisian Inlet with Karsten's (1994) basin model, at (a) 2.5 km, (b) 7 km, (c) 8 km from the gorge. (From: Karsten, 1994; courtesy DELFT hYDRAULICS)

6.6.6 De Vriend et al.'s delta model

The morphological evolution of the basin has its effects on the outer delta. In the "Friesche Zeegat" case (Section 6.5) the delta volume decreased with about the same amount as was deposited in the basin. Although there is no evidence that it was the sediment from the delta which was deposited in the basin, the amounts of sediment involved are so large (approx. 30 10^6 m^3) that this must have been the case to a large extent.

The behaviour of the outer delta is determined by tide and sea waves. The tide generally tends to build out the delta seawards, the waves tend to squeeze it shorewards (bulldozer-effect). The evolution of the outer deltas in front of the Delta-works, in the southwest of The Netherlands, is a spectacular illustration of what happens when one of these agents is eliminated. After closure of the inlets, the deltas were pushed up against the shore and formed large systems of shoals, which seem to be the onset of barrier islands (cf. Stive,

1986; De Vriend and Ribberink, 1988; Steijn et al., 1989). Also the closure of the Lauwerszee led to a spectacular morphological response of the delta of the Friesche Zeegat, viz. the formation of a major sandy hook at the tip of the isle of Schiermonnikoog (see Figure 6.6).
These observations illustrate that there are two very powerful, but largely counteracting agents at work on the outer delta. Any morphodynamic model of the outer delta should therefore take each of these agents into account. A large-scale concept which seems to contain them both is a two-line model in which there is a forced transfer of sediment from the beach line to the inshore line (Figure 6.15). This forced cross-shore transport represents the ebb-dominated tidal transport on the outer delta. The "normal" longshore and cross-shore transport components represent the wave-induced effects. The beach and inshore lines respond by taking such an orientation that the wave-induced transport is exactly big enough to feed the forced cross-shore transport at the shoreward end, and to remove the sediment which it delivers at the seaward end. If the forced cross-shore transport is cut off, the system will return to a straight coast.

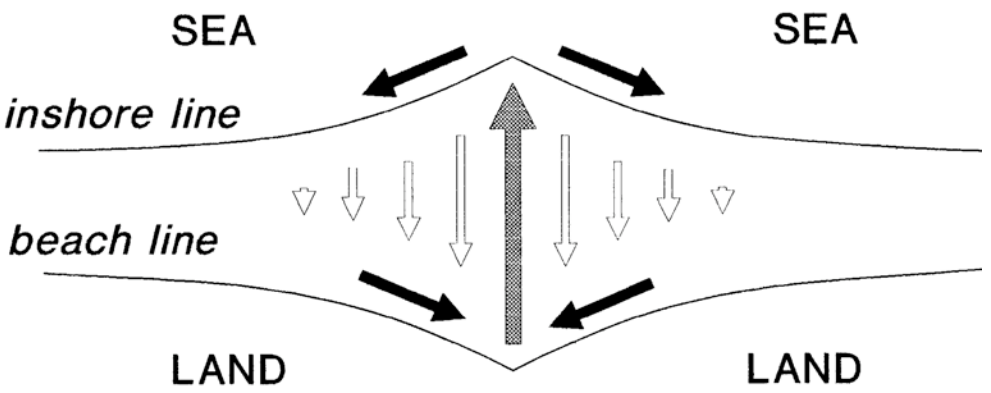

Figure 6.15: Delta formation in a two line model

De Vriend et al. (1994) describe a model of the outer delta and the adjacent coasts which is based on a refined version of this concept (Figure 6.16). It includes not only the main ebb channel, but also the flood channels near the island tips. The equilibrium state of the delta (volume, seaward protrusion) is described using empirical relationships. The sediment balance is maintained throughout the evolution, and the sediment demand or supply by the basin is taken into account as an input parameter. The model output consists of the cross-shore positions of the beach line and the inshore line as a function of time and the longshore co-ordinate, but these results should be interpreted at a higher aggregation level (for instance, in terms of the total sand volume changes in a certain coastal section).

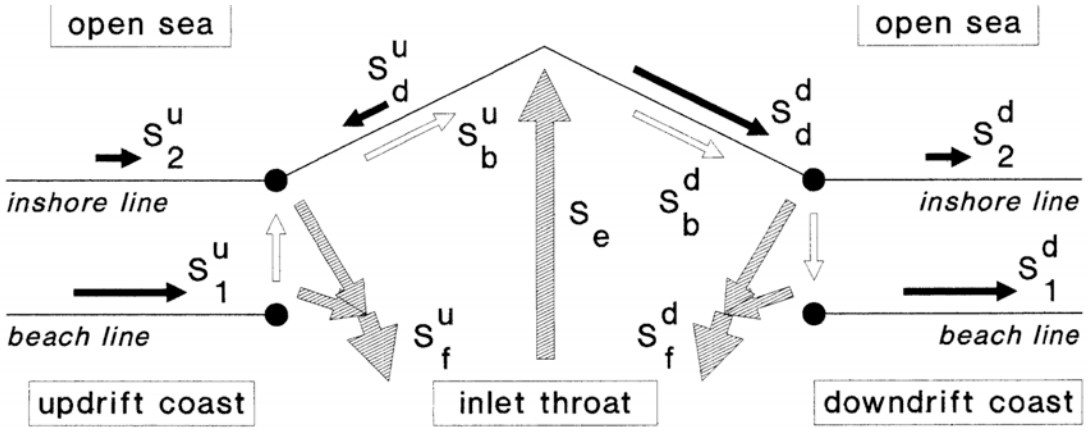

Figure 6.16: Principle of De Vriend et al. 's (1994) outer delta model

The model was validated against measured data from the Friesche Zeegat (cf. Section 6.5), of which the delta evolution after closure could be reproduced reasonably well. Further analyses of the results made clear that the delta acts as a mid-term sediment buffer for the basin, but that in the long run the sediment surplus or deficit of the delta has to be compensated by the adjacent island coasts. This indicates that sand mining from the delta can have detrimental long-term effects on the island coasts.

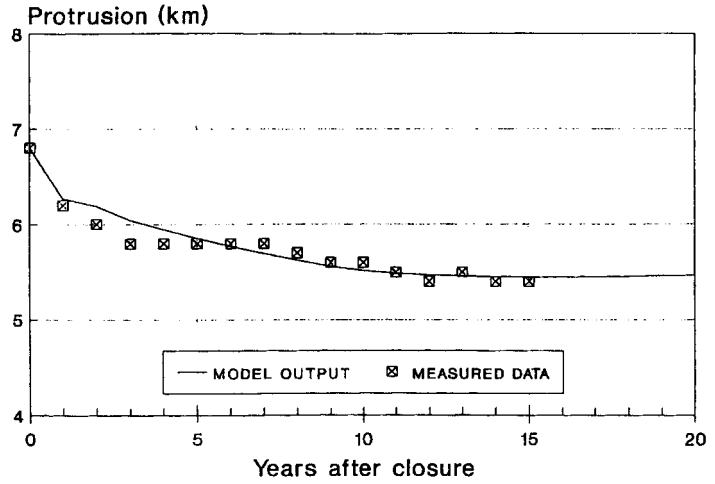

Figure 6.17: Hindcast of the outer delta protusion of the Frisian Inlet with De Vriend et al.'s (1994) model

6.6.7 Steetzel's model of the entire Wadden Sea coast

Steetzel (1994) uses a similar model to hindcast and predict the large-scale evolution of the entire 150 km long multi-inlet coast of the Dutch Wadden Sea, under the influence of accelerated sea level rise, climatic change and subsidence due to oil and gas mining. The response of the basin volume to the relative sea level rise is assumed to be described by an exponential decay model as given by Eq. (6.4). The resulting time-evolution of the sediment demand from the basin is determined for each of the inlets. With these time-functions as input conditions at the basin end, the model computes the positions of the island coastlines and the edge of the outer delta.

The basic concept of Steetzel's model is the same as described by De Vriend et al. (1994), but it is based on 5 lines instead of 2, in order to be able to deal with the variety of transport mechanisms in the various depth zones. The layers concern the dune front, the subaerial beach, the surf zone, the middle shoreface and the lower shoreface. They cover the zone between O.D. + 7 m and O.D. - 20 m.
Information from detailed process-based models of the Eierlandse Gat and the Friesche Zeegat is used to set some of the model parameters. The model is validated against 25 years of data from the JARKUS data set (yearly profiles of 800 m length, taken at alongshore distances of 250 m).

Table 6.1: Overall sediment balance for the Dutch Wadden Sea coast [from: Steetzel, 1994; courtesy DELFT HYDRAULICS]

model boundary	sediment flux into the model domain
Callantsoog (SW end of the model)	+ 1.1 10^6 m^3/yr alongshore
Schiermonnikoog (NE end of the model)	- 2.1 10^6 m^3/yr alongshore
O.D. - 20 m (seaward model boundary)	+ 0.8 10^6 m^3/yr cross-shore
O.D. + 7 m (dune top = landward model boundary)	- 0.3 10^6 m^3/yr cross-shore
inlet gorges (demand from basins)	- 12.7 10^6 m^3/yr cross-shore
nourishments (sand mined offshore)	+ 2 to 3 10^6 m^3/yr source

Table 6.1 summarizes the overall sediment balance for the model area, which extends from Callantsoog at the SW end to the easternmost tip of Schiermonnikoog at the NE end. Clearly, the demand from the basins is of predominant importance to the evolution of this coast.
A further analysis of JARKUS and other bathymetric survey data has revealed that 75% of the net sediment loss in the area goes at the expense of the outer deltas, and that 50 to 60% takes place at the middle and lower shoreface. Apparently, the erosion is concentrated at the delta edges.
These findings are confirmed by the model. Figure 6.18 shows a typical result: the predicted accretion/erosion per coastal section over the next 50 years. The spatial resolution of the presented results is much smaller than that of numerical model, which computes the cross-shore position of each line as a function of time and longshore position. This aggregation of output is in line with the strong geometrical schematization in the model.

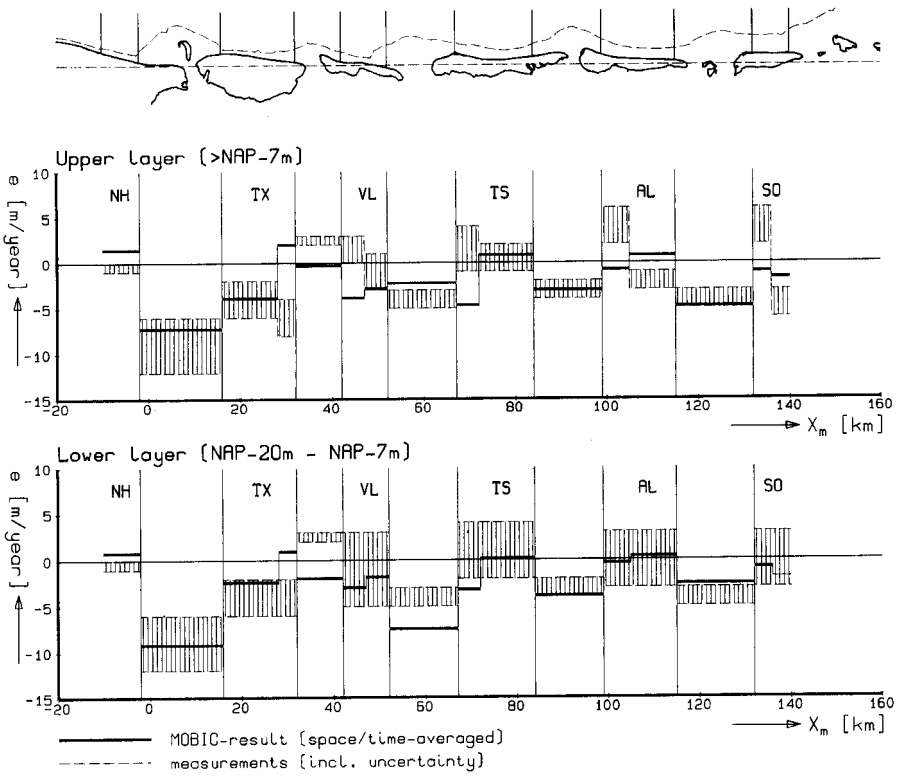

Figure 6.18: Long-term evolution of the Wadden Sea coast as predicted with Steetzel's (1995) model

6.6.8 Compound models

The semi-empirical models which were discussed so far concern either the basin or the coast (including the outer delta). In both cases, the long-term residual transport through the gorge is prescribed, either as a function of the basin state (basin model), or as a given quantity (delta model). A logical next step would be to couple basin, delta and island coasts, to yield a model for the entire inlet system.

This job is less trivial than it may seem at first sight. Since the transport through the gorge is modelled differently in either case, it is not just a matter of patching. In fact, the processes in the gorge which link the basin to the outer coast should be reanalysed, taking the influence of all elements of the system into account (for instance, the combined effect of the outer delta and the intertidal flats on the residual transport through the gorge). Process-based simulation models can be of help to such an analysis.

One possible way to couple the basin and the outer coast is to extend the basin model through the gorge and let it interact with the outer coast model. Bakker and De Vriend (1995) suggest to use a network model for the basin morphology, and to let one or more branches of this network stick through the inlet into the open sea. It must be possible to let the sediment which is transported through these braches be picked up or deposited near the delta edge, thus feeding a multi-line coastal model like the one described in the foregoing. If these channels are allowed to migrate, die out and regenerate, for example under the influence of the longshore drift, it may even be possible to achieve an essentially higher resolution than in the present models of the outer coast.

At this moment, these is little more than ideas which need to be substantiated, implemented and tested against reality. Detailed process-based simulation models and frequent (remote-sensing!) topographic surveys can be of great help here.

6.6.9 Conclusion

Empirical and semi-empirical models have been shown to be of great value to tidal inlet modelling, although (or maybe because) there is still a long way to go to their understanding in terms of elementary physical processes. The empirical knowledge of inlet systems is based on data from many inlets all over the world. This, together with the vast scientific effort stored in these models, makes that anomalies have probably been removed from most of the empirical equilibrium-state relationships. Thus these relationships provide valuable knowledge which should not be ignored, but used to bridge the present gap between process-based simulation and long-term prediction of tidal inlet behaviour.

The semi-empirical model approach tries to combine the empirical knowledge with basic physical principles, such as the conservation of sediment and water mass. Thus it can be a powerful tool to predict the long-term dynamic behaviour of tidal inlet systems, as has been shown in various instances. The further development of this approach, together with process-based simulation models, is certainly worth pursuing.

An important research issue in this area is the theoretical substantiation of the empirical equilibrium-state relationships, starting from first physical principles. Furthermore, the semi-empirical model concepts need further improvement and validation. This requires consistent bathymetric records over a sufficiently long time (relative to the morphological time scale of interest). Longlasting monitoring programmes, as well as historical and sedimentological reconstructions are therefore absolute necessities for further progress. Moreover, better use should be made of process-based simulation models and formally averaged models to improve and refine semi-empirical models.

6.7 References

Bakker, W.T. and De Vriend, H.J., 1995. Resonance and morphological stability of tidal basins. Accepted for publication in Marine Geology.

Bakker, W.T. and Joustra, D.S., 1970. The history of the Dutch coast in the last century. In: Proc. 12th Int. Conf. Coastal Eng., ASCE, New York, p. 709-728.

Boon, J.D. III and Byrne, R.J., 1981. On basin hypsometry and the morphodynamic response of coastal inlet systems. Mar. Geol., 40: 27-48.

De Vriend, H.J., 1991. Mathematical modelling of large-scale coastal behaviour. J. Hydraul. Res., 29(6): 727-753.

De Vriend, H.J. and Ribberink, J.S., 1988. A quasi-3D mathematical model of coastal morphology. In: B.L. Edge (ed.), "Coastal Engineering 1988 Proc.", ASCE, New York, p. 1689-1703.

De Vriend, H.J., Bakker, W.T. and Bilse, D.P., 1994. A morphological behaviour model for the outer delta of mixed-energy tidal inlets. Coastal Eng., 23(3/4): 305-327.

De Vriend, H.J., Capobianco, M., Chesher, T., De Swart, H.E., Latteux, B. and Stive, M.J.F., 1993. Approaches to long-term modelling of coastal morphology: a review. Coastal Eng., 23(1-3): 225-269.

De Vriend, H.J., Louters, T., Berben, F. and Steijn, R.C., 1989. Hybrid prediction of a

sandy shoal evolution in a mesotidal estuary. In: R.A. Falconer, P. Goodwin and R.G.S. Matthew (Editors), "Hydraulic and Environmental Modelling in Coastal, Estuarine and River Waters. Gower Technical, Aldershot, pp. 145-156.

Di Silvio, G, 1989. Modelling the morphological evolution of tidal lagoons and their equilibrium configurations. In: Proc. XIIIrd IAHR-Congress, Ottawa, Canada, p. C.169-C.175.

Di Silvio, G., 1991. Averaging operations in sediment transport modelling; short-step versus long-step morphological simulations. In: "The Transport of Suspended Sediment and its Mathematical Modelling", Preprints Int. IAHR/USF-Symp., Florence, Italy, p. 723-739.

Ehlers, J., 1988. The morphodynamics of the Wadden Sea. Balkema, Rotterdam, 397 pp.

Escoffier, F.F., 1940. The stability of tidal inlets. Shore & Beach, 8(4): 114-115.

Eysink, W.D., 1990. Morphologic response of tidal basins to changes. In: B.L. Edge (ed.), "Coastal Engineering 1990 Proc.", ASCE, New York, p. 1948-1961.

Eysink, W.D., Biegel, E.J. and Hoozemans, F.J.M., 1992. Impact of sea level rise on the morphology of the Wadden Sea in the scope of its ecological function; investigati ons on empirical morphological relations. Delft Hydraulic, ISOS*2 report H 1300, 73 pp.

Fenster, M.S., Dolan, R. and Elder, J.F., 1993. A new method for predicting shoreline positions from historical data. J. Coastal Res., 9(1): 147-171.

Friedrichs, C.T., 1995. Stability shear stress and equilibrium cross-sectional geometry of sheltered tidal channels. J. Coastal Res., 11(2) (in press).

Gerritsen, F., 1990. Morphological stability of inlets and channels in the Western Wadden sea. Rijkswaterstaat, Report GWAO-90.019.

Goldenbogen, R., Schroeder, E., Kunz, H. and Niemeyer, H.D., 1994. Intermediate report on the "WADE" research project. Niedersachsisches Landesamt fuer Oekolo gie, Forschungsstelle Kueste, Rept. MTK 0508, 111 pp. (in german).

Hayes, M.O., 1979. Barrier island morphology as a function of tidal and wave regime. In: S.P. Leatherman (Editor), "Barrier Islands from the Gulf of St. Lawrence to the Gulf of Mexico". Academic Press, New York, pp. 1-27.

Jarrett, J.T., 1976. Tidal prism area relationships. US Army Corps of Engineers, GITI report no. 3, 32 pp.

Karssen, B., 1994a. A dynamic/empirical model for the long-term morphological develop ment of estuaries; Part II: Development of the model, Phase I. Delft Hydraulics, DYNASTAR-rept. Z 715-I, 31 pp.

Karssen, B., 1994b. A dynamic/empirical model for the long-term morphological develop ment of estuaries; Part II: Development of the model, Phase II. Delft Hydraulics, DYNASTAR-rept. Z 715-II, 38 pp.

Medina, R., Vidal, C., Losada, M.A. and Losada, I.G., 1992. Three-mode principal component analysis of bathymetric data applied to Playa Castilla (Huelva, Spain). In: B.L. Edge (Editor), "Coastal Engineering 1992", ASCE, New York, p. 2265-2278.

O'Brien, M.P., 1931. Estuary tidal prism related to entrance areas. Civ. Eng., 1(8): 738-739.

O'Brien, M.P., 1969. Equilibrium flow areas of inlets on sandy coasts. J. Waterw. Harbors Div., ASCE, 95(WW1): 43-52.

O'Connor, B.A., Nicholson, J. and Rayner, R., 1990. Estuary geometry as a function of tidal range. In: B.L. Edge (ed.), "Coastal Engineering 1990 Proc.", ASCE, New York, p. 3050-3062.

Oost, A.P., 1995. The cyclic development of the Pinkegat Inlet system and the Engelsmanplaat/Smeriggat, Dutch Wadden Sea, over the period 1832-1991. In: "Dynamics and sedimentary developments of the Dutch Wadden Sea, with special emphasis on the Frisian Inlet", Doctoral thesis, Utrecht University (in press).

Oost, A.P. and De Haas, H., 1992. The Frisian Inlet, morphological and sedimentologi cal changes in the period 1970-1987. Utrecht Univ., Inst. Earth Sciences, Coastal Genesis

Report, 68 pp. (in dutch).
Oost, A.P. and De Haas, H., 1993. The Frisian Inlet, morphological and sedimentological changes in the period 1927-1970. Utrecht Univ., Inst. Earth Sciences, Coastal Genesis Report, 94 pp. (in dutch).
Oost, A.P., De Haas, H., IJnsen, F., Van den Boogert, J.M. and De Boer, P.L., 1993. The 18.6 yr nodal cycle and its impact on tidal sedimentation. Sediment. Geol., 87: 1-11.
Pethick, J.S., 1980. Velocity surges and asymmetry in tidal channels. Est. Coastal Mar. Sci., 11: 321-345.
Preisendorfer, R.W. and Mobley, C.D., 1988. Principal Component Analysis in meteorology and oceanography. Elsevier, New York, 425 pp.
Renger, E. and Partenscky, H.W., 1974. Stability criteria for tidal basins. In: Proc. 14th Coastal Eng. Conf., Copenhagen. ASCE, New York, p. 1605-1618.
Schroeder, E., Goldenbogen, R. and Kunz, H., 1994. Parametrization for conceptual morphodynamic models of Wadden Sea areas. In: B.L. Edge (Editor), "Coastal Engineering 1994", ASCE, New York (in press).
Steetzel, H.J., 1994. Modelling of the interrupted coast; prediction of the coastline and the outer deltas of the Wadden Sea coast over the period 1990-2040. Delft Hydraulics, Coastal Genesis Rept. H 1887 (in dutch).
Steijn, R.C., Louters, T., Van der Spek, A.J.F. and De Vriend, H.J., 1989. Numerical model hindcast of the ebb-tidal delta evolution in front of the Deltaworks. In: Falconer, R.A. et al.: "Hydraulic and Environmental Modelling of Coastal, Estuarine and River Waters", Gower Technical, Aldershot, p. 255-264.
Stive, M.J.F., 1986. A model for cross-shore sediment transport. In: B.L. Edge (ed.): Coastal Engineering 1986 Proc.", ASCE, New York, p. 1551-1564.
Van de Kreeke, J., 1990a. Stability analysis of a two-inlet bay system. Coastal Eng., 14: 481-497.
Van de Kreeke, J. 1990b. Can multiple inlets be stable? Est., Coastal Shelf Sci., 30: 261-273.
Van de Kreeke, J. and Robaczewska, K., 1993. Tide-induced transport of coarse sediment: application to the Ems estuary. Neth. J. Sea Res., 31(3): 209-220.
Van Dongeren, A.R. and De Vriend, H.J., 1994. A model of morphological behaviour of tidal basins. Coastal Eng., 22(3/4): 287-310.
Walton, T.L. and Adams, W.D., 1976. Capacity of inlet outer bars to store sand. In: Proc. 15th Coastal Eng. Conf., Honolulu, HI. ASCE, Nw York, pp. 1919-1937.
Wang, Z.B., Fokkink, R.J. and Karssen, B., 1993. Theoretical analysis on nodal point relations in one-dimensional morphodynamic models. Delft Hydraulics, Report Z 473-II, 26 pp.
Wijnberg, K. and Wolf, F.C.J., 1994. Three-dimensional behaviour of a multiple bar system. In: A.S.-Arcilla, M.J.F. Stive and N.C. Kraus (Editors): "Coastal Dynamics '94", ASCE, New York, p. 59-73.

7 Network modelling

7.1 Introduction

Mathematical modelling of morphological development is applied for evaluating impacts of natural developments e.g. sea level rise and human interference e.g. dredging / dumping, land reclamation, etc. Examples of practise problems in the Netherlands are the deepening of the navigation channels in the Western Scheldt and opening of the Haringvliet sluices.
Two types of network models will be dealt with, i.e. process based models and semi-empirical models. By process based models we mean morphodynamic models based on mathematical descriptions of the relevant processes, i.e. flow, sediment transport, and bed level change, using physical laws. Semi-empirical models are models based on combination empirical relations and description of physical relations.
This chapter consists of two parts. In the first part, section 7.2 and section 7.3 discussing the two types of models respectively, contains the obligatory material of the lecture. The second part, sections 7.4 through 7.6, contains three recently published papers containing additional information on the subjects considered in the first part.

7.2 Process based models

One-dimensional network morphodynamic models for tidal basins can be considered as an extension of 1D morphological models for rivers, which are discussed in the lectures ctwa3340 and ctwa5311. Therefore the basic theory on 1D morphological modelling will not be discussed here. Only some specific aspects for tidal regions are discussed. The lecture mainly deals with application rather than design of models (software development).

7.2.1 A comparison to river case

First a comparison with the non-tidal river case is made in order to highlight the special aspects of morphological modelling in tidal regions.

Morphological equilibrium

For the river case morphological equilibrium state is well defined. If the upstream discharge, the upstream sediment transport and the river width is given the equilibrium water depth and the equilibrium bed slope can be determined. Human interference usually implies a new morphological equilibrium at the long-term. The influence of the various model parameters on the morphological equilibrium is well known. This makes morphological modelling relatively easier. The computation starts at a known (initial) state and end at the long term to a known state if the hydrodynamic condition remains the same.

In estuaries and tidal inlets the driving forces for morphological development is much more complicated than in the case of (non-tidal) rivers. In addition to the upstream discharge the other relevant components of the driving forces are tidal motion, wind, (short) waves, density flow, etc. We restrict here to the simplest situation, i.e. only tidal motion is considered. For most tidal basins in the Netherlands tidal motion is the dominating driving force for sediment transport and morphological development. Even with this simplification the morphological equilibrium cannot be derived from the equations describing the water motion and sediment transport. The relation between the morphological equilibrium and the driving forces, i.e. the upstream discharge and the tide in the open sea cannot be made explicit. It is not even clear whether or not a morphological equilibrium theoretically exists. This makes the morphological modelling much more complicated: the computation starts at a known state but goes to an unknown end.

Inter-tidal area

Inter-tidal area, or the tidal flat, is the area, which is dry at low water and drowned at high water. It may be compared to the floodplains of rivers, which are only drowned during flood waves. However, the inter-tidal area plays a much more important role for the morphology in estuaries and tidal inlets than the floodplain for rivers. Take for example a short (relatively to the length of tidal wave) tidal inlet. The morphology of the inter-tidal area determines the amount of water flowing in and out during flood and ebb, i.e., the discharge and the tidal volume. This means that the morphology of the inter-tidal area itself influences the driving force of the morphological development. This complicated interaction is one of the reasons why morphological equilibrium in tidal regions is difficult to be determined. It has also the consequence that the impact of human interference in the inter-tidal area is usually not restricted locally. Consider e.g. land reclamation, its impact can immediately (speaking on the morphological time scale, the exact propagation velocity is that of the tidal wave) be felt at the entrance of the tidal basin.

Morphological tide

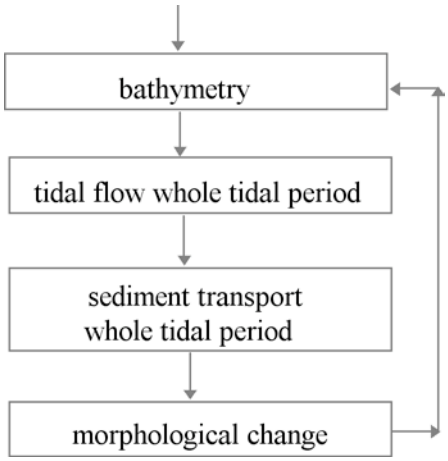

Figure 7.1: Computational procedrure

Morphological modelling for rivers makes often use of the quasi-steadiness assumption. An extension of this assumption for tidal regions is the quasi-periodicity assumption. The basic idea is that the time scale of morphological development is much larger than the tidal period. The morphological time step can be much larger than the tidal period. This makes it possible to adopt a computational procedure as shown in Figure 7.1.
At each morphological time step the tidal flow and the sediment transport during a whole tidal period are calculated. Then the net sediment transport is used to calculate the morphological change.
A simplification usually made is replacing the ever-changing tide (e.g. due to spring-neap variation) by a single periodic tide. This single periodic tide is called the morphological tide. This is often defined as the tide representing the averaged net sediment transport, which is usually between the averaged tide and the spring tide. However, if this definition is followed strictly, the morphological tide is usually different at each location of the model area. This is the reason that another definition of the morphological tide has been introduced recently. The tide, for which the relative spatial variation of the ratio between the net transport due to this tide and the net transport in reality (e.g. due to the spring-neap tidal cycle) is minimal, is chosen as the morphological tide. A constant correction coefficient is introduced to reproduce the realistic averaged transport.
At present the consequence of the application of morphological tide on the computed morphological development is not clear. A comparable concept for rivers is the dominant discharge, which is used, in the early days of morphological modelling for rivers. However, it is now known that a single discharge can never represent all the relevant morphological features of a river.

Residual sediment transport

The net transport or residual transport determines the morphological development in tidal regions. It is a small difference between the large ebb transport and flood transport. This makes the accurate calculation of the residual transport very difficult.

Tidal flow velocity can be written into the sum of a residual flow velocity and many harmonic components.

$$u(t) = u_0 + u_1 \sin(\varpi_1 t) + u_2 \sin(\varpi_2 t) + \cdots \quad (7.1)$$

Using a simple power-law as sediment transport formula one can show that the residual sediment transport is not determined by the main tidal component u_1 only, but it is mainly determined by the small residual flow u_0, and the small higher frequency component (tidal asymmetry). This put a special requirement to the flow module in the morphological model. During the set up and the calibration of the flow module this should already be kept in mind. Morphological modelling is not simply post-processing of flow modelling.

It is noted that during the calibration of flow models a calibration parameter like the Chezy coefficient is some times used as a “garbage bascket”. Be aware that this may have consequences for the sediment transport modelling. As an example, for reproducing the tidal asymmetry and the residual circulation in 1D network tidal flow model it may be necessary to use direction-dependent roughness coefficient, with a distinction between the ebb channels and flood channels. However, if the so resulted Chezy coefficient is also used in the sediment transport formula it may produce unrealistic sediment transport pattern.

7.2.2 Nodal point relations and stability of bifurcations

In a network model for a tidal area each nodal point represents a confluence as well as a bifurcation since the flow during ebb is in the opposite direction as during flood. For the case of bifurcation a user defined nodal point relation is required for the sediment transport. This nodal point relation has important influence on the stability of the bifurcation and thereby it determines to a large extent the behaviour of the morphodynamic model.

For the river case this subject is extensively discussed in the paper enclosed in Section 7.4. In the practice it has been proven that all the conclusions drawn for the river case also apply for the estuarine tidal flow case.

Here the stability problem is illustrated with a simple example of river case: a river bifurcates into two identical downstream branches with half the width of the opstream branch. Take for the upstream branch the following properties:

Width	B_0 =	100 m
Discharge	Q_0 =	400 m^3/s
Sediment transport	S_0 =	0.04 m^3/s
Chezy coefficient	C =	50 $m^{0.5}/s$

Suppose that the following sediment transport formula applies:

$$S = BMu^5 \quad (7.2)$$

Herein

B = River width

M = Constant coefficient (= 0.0004 here)

u = Flow velocity

It can then be shown that the equilibrium depth is $a_0 = 4$ m and the equilibrium slope is $i_0 = 0.0001$.

The two downstream branches have the same length and width ($B_1 = B_2 = 0.5\ B_0$). Further it is assumed that the Chezy coefficients in the two branches are the same as in the upstream branch. It is then obvious that the equilibrium state with the two branches open is

$a_1 = a_2 = a_0 =$ 4 m
$i_1 = i_2 = i_0 =$ 0.0001
$Q_1 = Q_2 = 0.5Q_0 =$ 200 m^3/s
$S_1 = S_2 = 0.5S_0 =$ 0.02 m^3/s

To examine whether this equilibrium state is stable, consider a small disturbance of 0.1 m:

$a_1 =$ 4.1 m
$a_2 =$ 3.9 m

The discharge distribution among the two branches is governed by the following equations:

$$Q_1 = B_1 C a_1^{3/2} i_1^{1/2} \tag{7.3}$$

$$Q_2 = B_2 C a_2^{3/2} i_2^{1/2} \tag{7.4}$$

$$Q_1 + Q_2 = Q_0 \tag{7.5}$$

$$i_1 = i_2 \tag{7.6}$$

Solving these equations yields:

$Q_1 =$ 207.5 m^3/s
$Q_2 =$ 192.5 m^3/s
$i_1 = i_2 =$ 0.00009955

Suppose the following nodal point relation is applied:

$$\frac{S_1}{S_2} = \frac{Q_1}{Q_2} \tag{7.7}$$

It follows then that at the initial state of the disturbed situation:

$S_1 =$ 0.02075 m^3/s
$S_2 =$ 0.01925 m^3/s

However, the flow velocities and the sediment transport capacities of the two branches are:

$u_1 =$ 1.0122 m/s $S_{1e} =$ 0.02125 m^3/s
$u_2 =$ 0.9872 m/s $S_{2e} =$ 0.01875 m^3/s

Thus, the disturbance causes overloading in branch 2 ($S_2 > S_{2e}$) and underloading in branch 1 ($S_1 < S_{1e}$). This means that branch 2, which is shallower, will become even

shallower and that the deeper branch 1 will become even deeper. This indicates that the equilibrium state ($a_1 = a_2 = 4$ m) is unstable.
One can do the same exercise, but now with the following nodal point relation instead of (5.6):

$$\frac{S_1}{S_2} = \left(\frac{Q_1}{Q_2} \right)^k \tag{7.8}$$

And try different values of *k*. By doing this one will find out that as long as $k < 5/3$ the equilibrium is unstable, and the equilibrium becomes stable when $k > 5/3$.
Mathematical analysis of the stability for the general river bifurcation case is presented in Section 7.4. It is important to notice that there is not one, but at least three physically realistic equilibrium states, representing the following situations:

- Both branches are open; each branch transports a part of the water and sediment.
- Branch 2 is closed and all the water and sediment is transported through branch 1.
- Branch 2 is closed and all the water and sediment is transported through branch 1.

It is also important to know that the nodal point relation

$$\frac{S_1}{S_2} = \left(\frac{Q_1}{Q_2} \right)^k \left(\frac{B_1}{B_2} \right)^{1-k} \tag{7.9}$$

For small values of k the equilibrium with both branches open is unstable and for large values of *k* it is stable. The critical value of *k* depends on the sediment transport formula. If the sediment transport is proportional to the nth power of the flow velocity then the critical value of *k* is *n*/3.
In the analysis described in Section 7.4 the simple mass-balance equation for sediment are used for describing the morphodynamic development of the branches:

$$\frac{da_1}{dt} = \frac{S_{1e} - S_1}{B_1 L_1} \tag{7.10}$$

$$\frac{da_2}{dt} = \frac{S_{2e} - S_2}{B_2 L_2} \tag{7.11}$$

As demonstrated in the example above, it is possible to calculate the sediment transport and the sediment transport capacities for a given combination of the water depths in the two branches. It is thus relatively easy to construct a table like the following using a simple computer program.

a_1	a_2	da_1/dt	da_2/dt
---	---	---	---
---	---	---	---
…	…	…	…
---	---	---	---

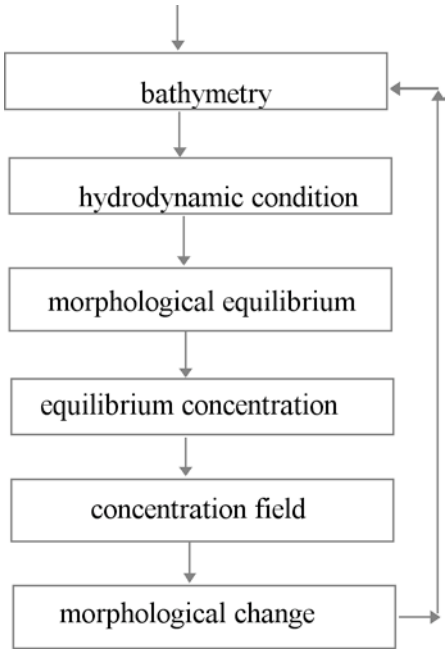

Figure 7.2.

With some graphical presentation software it is then easy to draw a picture as shown in Figure 7.2. The cross points of the iso-lines $da_1/dt = 0$ and $da_2/dt = 0$ represent the equilibrium states and the vectors (da_1/dt, da_2/dt) show then the stability of the equilibrium states. Such a figure gives the same information as the phase diagram presented in Section 7.4.

This technique can easily be used for more complicated sediment transport formulas, like that of Meyer-Peter-Müller as used in Figure 7.2 By including an extra source and/or sink term in equations (7.9) and (7.10), the technique can also be used to investigate the influence of dredging and/or dumping on an originally stable bifurcation, as shown in Figures 7.3 and 7.4

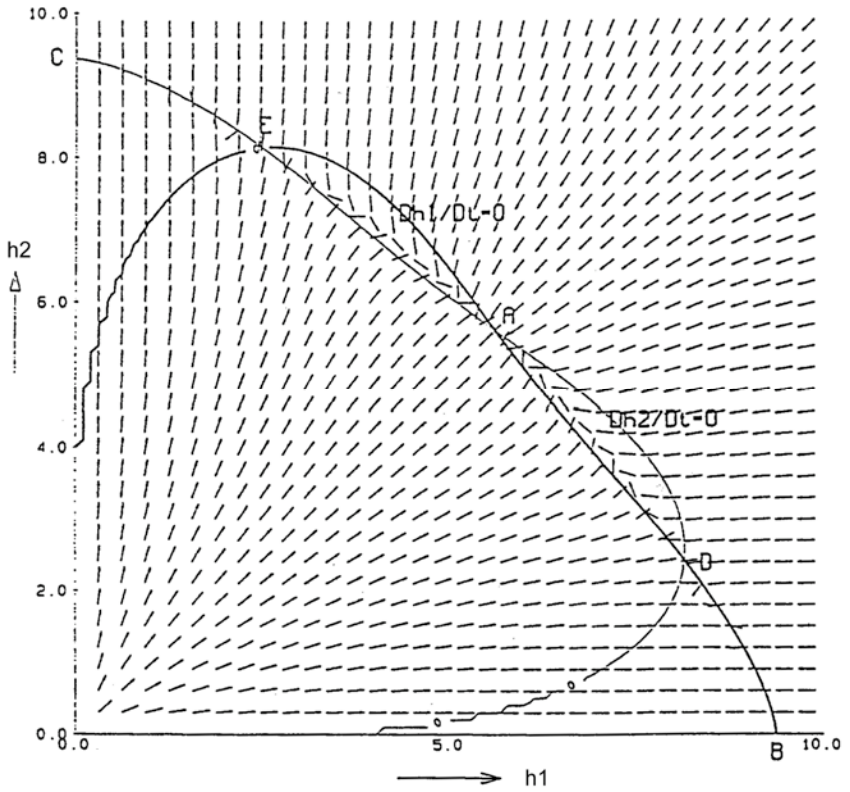

Figure 7.3: Equilibrium states and their stability, Symmetric case, no dredging

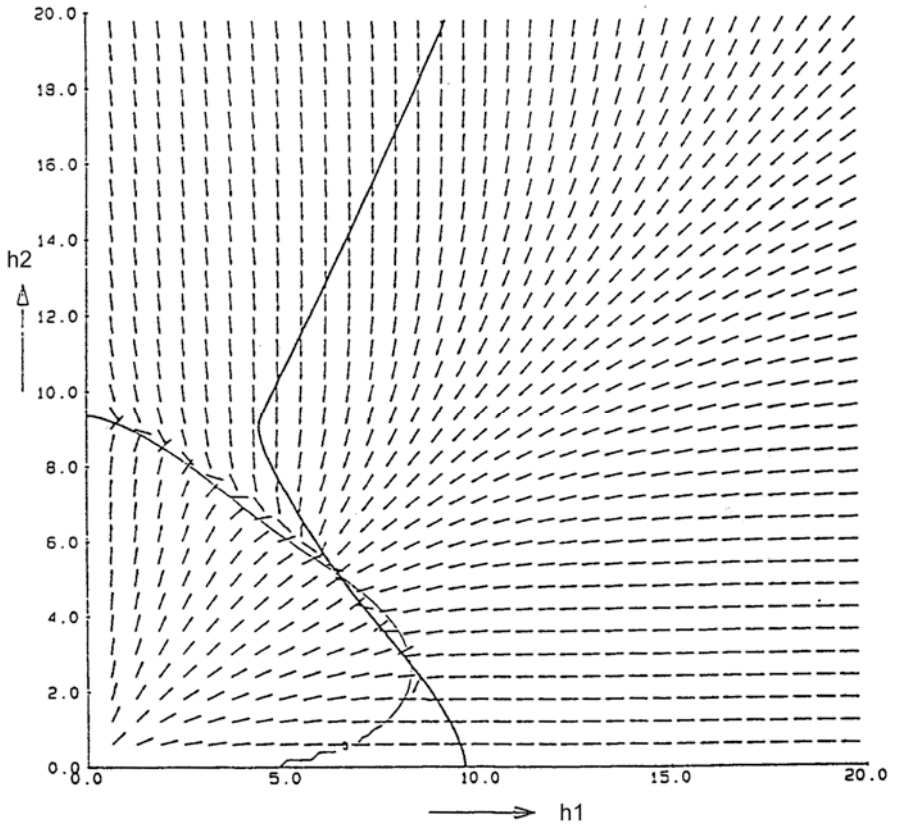

Figure 7.4: Equilibrium states and their stability, Symmetric case under influence of dredging (10%)

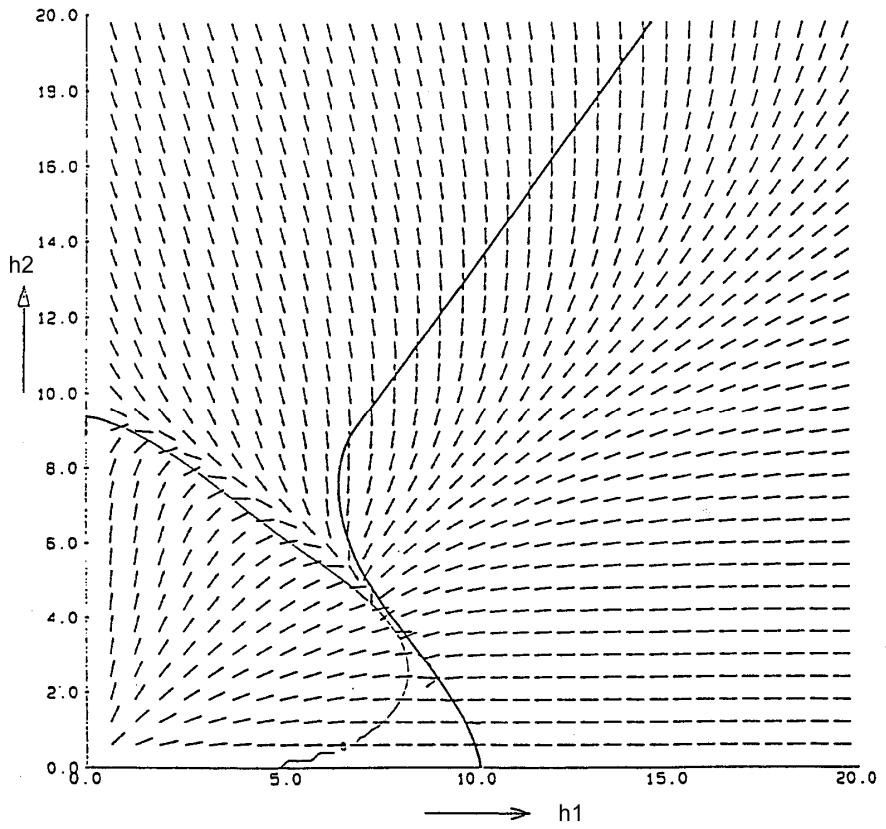

Figure 7.5: Equilibrium states and their stability, Symmetric case under influence of dredging (30%)

7.3 Semi-empirical models

7.3.1 Principles

As mentioned in the previous section, one of the difficulties in morphodynamic modelling for tidal regions is that it is usually impossible to derive a morphological equilibrium for given hydrodynamic conditions from the equations in the model. On the other hand data from the practise show that morphological equilibrium in tidal region can be defined and the equilibrium state is well related to the hydrodynamic parameters. A well-known example of such empirical relations is the linear relation between the cross-sectional area of a tidal channel and the tidal volume through the channel. The semi-empirical models combines such empirical relations describing morphological equilibrium and process descriptions. The basic principle of such models can be summarised as follows

a) At each time step, a morphological equilibrium state exists if the hydrodynamic condition is given.
b) The net sediment transport can be described by advection-dispersion equation based on residual flow field. A consequence is then that there exists an overall equilibrium sediment concentration that is present in the whole model area when the whole system is in equilibrium.

c) When an area is out of equilibrium, a tendency of sedimentation or erosion exists. This is expressed in the locally adjusted equilibrium concentration.
d) The exchange between the bottom and water, thus also the morphological change, is determined by the difference between the local concentration en de local equilibrium concentration.

In the following the theory is explained for a network system, and illustrated with simple examples. In Sections 7.5 and 7.6 more extensive description of this type of models are given.

7.3.2 Basic equations

Consider a network consisting of morphological elements connected to each other. For each element a variable describing the morphological state, e.g. the wet volume V, is defined. Further per element a sediment concentration c, and an equilibrium concentration c_e. The following equations applies per element:

Morphological equilibrium

$$V_e = f\left(\text{hydrodynamic parameters}\right) \tag{7.12}$$

Herein:
V_e = equilibrium volume.

Equilibrium concentration

$$c_e = c_E\left(\frac{V_e}{V}\right)^n \tag{7.13}$$

Herein:
c_E = overall equilibrium concentration,
n = constant.

Mass-balance in the water phase

$$\sum_i T_i = w_s A\left(c_e - c\right) \tag{7.14}$$

Herein:
T_i = outgoing transports along the boundaries of the element,
A = horizontal area of the element,
w_s = exchange velocity between water en bottom.

Morphological change

$$\frac{dV}{dt} = w_s A\left(c_e - c\right) - I + A\frac{d\zeta}{dt} \tag{7.15}$$

Herein

I = dredging and dumping (dumping = positive);
ζ = sea level.

The transport in equation (7.13) is defined per connection between two elements. This consists of a diffusive part and an advective part (due to residual flow):

$$T = \delta(c_1 - c_2) + Q(c_1 + c_2)/2 \tag{7.16}$$

Herein
T = transport from element 1 to element 2,
δ = horizontal exchanging coefficient between the two elements due to dispersion,
Q = discharge of residual flow from element 1 to element 2.

At an open boundary the transport is determined in the same way. The concentration outside the model area should be given as boundary condition and it is usually assumed to be equal to the overall equilibrium concentration. At a closed boundary the transport equals zero.

7.3.3 Computational procedure

The computational procedure in the model is as shown in Figure 7.5 At each time step the equilibrium volumes of the element are determined first from the hydrodynamic parameters (7.11). Then the equilibrium concentrations per element are determined with equation (7.12). The concentrations in the elements are determined by solving a system of equation, which is set up by substituting (7.15) into equation (7.13). Then the morphological change can be determined from equation (7.14).

7.3.4 Illustrative examples

A single element model

In order to illustrate the working of the model we consider first a simple example: a network existing of only one single element. For this single element we have then the following equations:

Morphological equilibrium

$$V_e = f(\text{hydrodynamic parameters}) \tag{7.17}$$

Equilibrium concentration

$$c_e = c_E\left(\frac{V_e}{V}\right)^n \tag{7.18}$$

Mass-balance in the water phase

$$T_o = w_s A(c_e - c) \tag{7.19}$$

There is only one transport T_o, i.e. the transport from the element to the outside world. Suppose that there is no residual flow, then

$$T_o = \delta\left(c - c_E\right) \tag{7.20}$$

Morphological change (no dredging / dumping, no sea level change)

$$\frac{dV}{dt} = w_s A\left(c_e - c\right) \tag{7.21}$$

Combination of the equations (7.17) through (7.20) yields:

$$\frac{dV}{dt} = \frac{\delta w_s A c_E}{\delta + w_s A}\left[\left(\frac{V_e}{V}\right)^n - 1\right] \tag{7.22}$$

Obviously when $V = V_e$ no morphological change takes place. Consider a small disturbance from this equilibrium state $V = V_e + \Delta V$, and linearize equation (7.20) it can be shown that the disturbance ΔV is decaying with a time scale (time in which the ΔV is decreased by a factor e)

$$T = \frac{1}{nc_E}\left(\frac{V_e}{w_s A} + \frac{V_e}{\delta}\right) \tag{7.23}$$

The part outside the brackets shows that the morphological time scale is smaller if more sediment is in motion. The time scale is also smaller if the power in the equilibrium concentration equation is larger, which is similar as in the process based models where the time scale is dependent on the power flow velocity in the sediment transport formula. The two terms between the brackets represent respectively a time scale for the vertical exchange (between water and bottom) and for the horizontal exchange.

A two elements model

Consider now a network consisting of two elements, with a connection between them, and with one of the elements connected to the outside world. Following the same procedures as given above it can be shown that the morphological development is described by a system of two equations:

$$\frac{dV_1}{dt} = f_1\left(\frac{V_{e1}}{V_1}, \frac{V_{e2}}{V_2}\right) \tag{7.24}$$

$$\frac{dV_2}{dt} = f_2\left(\frac{V_{e1}}{V_1}, \frac{V_{e2}}{V_2}\right) \tag{7.25}$$

It is now important to notice that there are now two morphological time scales. A disturbance (ΔV_1,ΔV_2) with respect to the equilibrium state (V_{e1}, V_{e2}) still decays, but the decaying rate depends on the disturbance itself. It is obvious that the decay is much faster for the case $\Delta V_1 = -\Delta V_2$ than for the case $\Delta V_1 = \Delta V_2$.

7.4 Stability of river bifurcations in 1D morphodynamic models

7.4.1 Introduction

Nowadays, 1D morphodynamic models for single-channel rivers, based on water flow and sediment transport equations, have become useful tools for engineering practise. However, 1D morphodynamic models for river networks have rarely been reported in the literature, despite of the common use of 1D network hydrodynamic models. This is possibly due to the difficulty in representing bifurcations in such models.
At a bifurcating node in a 1D model a user-defined nodal-point relation is needed, which determines the sediment distribution over the downstream branches. In contrast to other equations in the model, this relation lacks a theoretical basis. Physically, the sediment distribution into the downstream branches is determined by the geometry and the (three-dimensional) current structure at the bifurcation. Obviously, it is impossible to represent this accurately in a 1D model. Because of this uncertainty of the nodal-point relation it is very important to understand its influence on the behaviour of the model.

The influence of the nodal-point relation on 1D network morphodynamic models has been analyzed mathematically in this paper. The conclusions from the analysis are verified by numerical simulations using SOBEK, a general 1D network package for flow, sediment transport and morphological development.

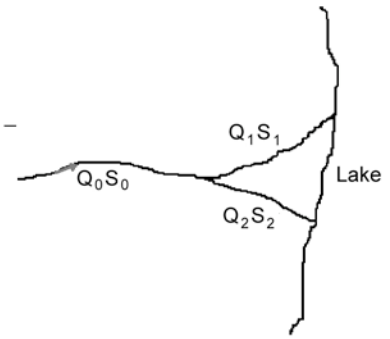

Figure 7.6

7.4.2 Nodal-point relations

Consider the simple river network as shown in Figure 7.6: a river bifurcates into two branches ending in a lake. In a 1D model, it is reasonable to assume that the nodal-point relation at the bifurcation depends on dimensionless quantities, as follows

$$\frac{S_1}{S_2} = f\left(\frac{B_1}{B_2}, \frac{Q_1}{Q_2}, \frac{C_1}{C_2}, \frac{a_1}{a_2}, \ldots\right) \tag{7.26}$$

in which:
S = sediment transport

Q = water discharge
a = water depth
B = channel width
C = Chézy coefficient

The properties of the sediment in all three branches are assumed to be the same in this paper.
Model-technically, the function f should satisfy the following requirements:

(i) It is symmetric, i.e. the computed sediment transport into a branch does not depend on the numbering of the branches, or mathematically,

$$f\left(\frac{B_1}{B_2},\frac{Q_1}{Q_2},\frac{C_1}{C_2},\frac{a_1}{a_2},\ldots\right)=\frac{1}{f\left(\frac{B_2}{B_1},\frac{Q_2}{Q_1},\frac{C_2}{C_1},\frac{a_2}{a_1},\ldots\right)} \tag{7.27}$$

(ii) It allows the model to represent all possible physically realistic situations.

A simple function satisfying the first requirement is the power function:

$$\frac{S_1}{S_2}=\left(\frac{B_1}{B_2}\right)^{k_B}\left(\frac{Q_1}{Q_2}\right)^{k_Q}\left(\frac{C_1}{C_2}\right)^{k_C}\left(\frac{a_1}{a_2}\right)^{k_a} \tag{7.28}$$

Note that a linear relation such as

$$\frac{S_1}{S_2}=\alpha\frac{Q_1}{Q_2}+\beta \tag{7.29}$$

does not fulfil requirement (i) unless $\alpha = 1$ and $\beta = 0$.
In particular, the following case is considered.

$$\frac{S_1}{S_2}=\left[\frac{Q_1}{Q_2}\right]^{k}\left[\frac{B_1}{B_2}\right]^{1-k} \quad (k>0) \tag{7.30}$$

This equation implies that the ratio between the specific sediment transport rates (transport per unit of width) is related to the ratio between the specific discharges. It will be shown in this paper that this relation satisfies requirement (ii).

Measurements in scale models and/or in nature are required to verify the physical validity of the nodal-point relation (7.30). Unfortunately, measurements of sediment distribution at bifurcations are scarce. Here data for the bifurcation at Pannerden (The Netherlands) of the River Rhine are presented. The sediment distribution over the downstream branches has been measured, in nature as well as in a scale model (Van der Zwaard, 1981). The result of these measurements is shown in Figure 7.7.

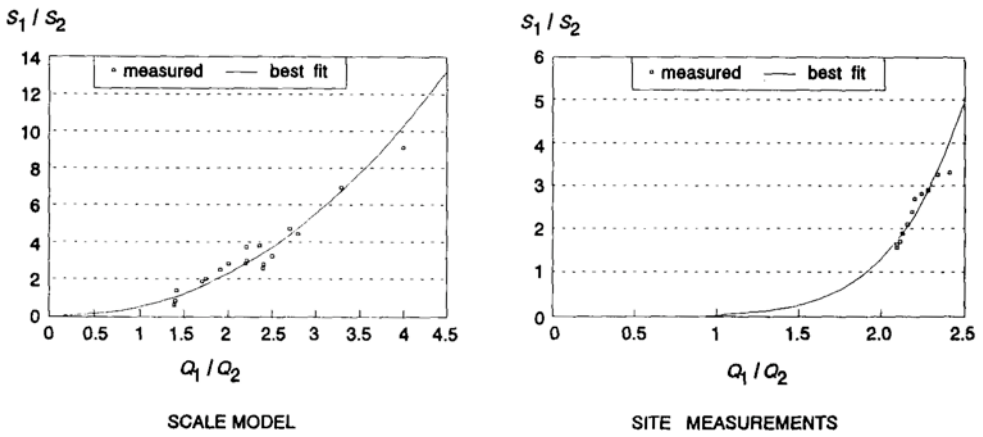

Figure 7.7 : Measurments of sediment distribution at Pannerden bifurcation

The least squares fit of a power of Q_1/Q_2 for the results of the scale-model is:

$$\frac{S_1}{S_2} = 0.51\left(\frac{Q_1}{Q_2}\right)^{2.2} \tag{7.31}$$

The least squares fit for the site measurements is:

$$\frac{S_1}{S_2} = 0.02\left(\frac{Q_1}{Q_2}\right)^{6.0} \tag{7.32}$$

The values of the exponent k in Eqs (7.31) and (7.32) are clearly different, but both equations fulfil Eq. (7.30) if B_1/B_2 is equal to 2.2, which is close to the ratio in reality. Observe that the variation of the ratio Q_1/Q_2 is relatively small for the site measurements. It is also noted that the accuracy of the site measurements is much worse than that of the scale model measurements. Further the scale model was distorted. Hence in detail the current pattern at the bifurcation may not be similar, resulting in a different k value.

7.4.3 Equilibrium states

The river network system as shown in Figure 7.6 is in equilibrium if the flow is uniform in all branches and if the sediment transport capacity of each branch is equal to the sediment supply at the upstream end of the branch. The equilibrium state of the two downstream branches is determined by the following equations.

Mass-balance for water

$$Q_1 + Q_2 = Q_0 \tag{7.33}$$

Water motion described by the Chézy formula

$$Q_j = B_j C_j a_j^{3/2} i_j^{1/2} \qquad j = 1,2 \tag{7.34}$$

Geometric relation

$$i_1 L_1 = i_2 L_2 \tag{7.35}$$

Mass-balance for sediment

$$S_1 + S_2 = S_0 \tag{7.36}$$

Sediment transport described by a power-law

$$S_j = B_j\, m \left(\frac{Q_j}{B_j a_j} \right)^n \qquad j = 1,2 \tag{7.37}$$

In these equations i denotes the slope. Together with the nodal-point relation (1) these equations can be solved to determine the eight variables Q_j, S_j, a_j, i_j (for j = 1,2) as follows. From Eqs (7.34) and (7.35) it follows

$$\frac{Q_1}{Q_2} = \frac{B_1}{B_2}\frac{C_1}{C_2}\left(\frac{a_1}{a_2}\right)^{\frac{3}{2}}\left(\frac{L_1}{L_2}\right)^{-\frac{1}{2}} \tag{7.38}$$

Together with Eq. (7.37) this gives a relation between the sediment transport ratio and the depth ratio:

$$\frac{S_1}{S_2} = \frac{B_1}{B_2}\left(\frac{C_1}{C_2}\right)^n\left(\frac{a_1}{a_2}\right)^{\frac{n}{2}}\left(\frac{L_1}{L_2}\right)^{-\frac{n}{2}} \tag{7.39}$$

Substituting Eq. (7.38) into the nodal point relation (7.26) yields another relation between these two variables:

$$\frac{S_1}{S_2} = f\left(\frac{a_1}{a_2}\right) \tag{7.40}$$

From Eqs (7.39) and (7.40) S_1/S_2 and a_1/a_2 can be solved. With the known sediment transport ratio S_1 and S_2 can be solved from Eq. (7.36). With the discharge ratio determined by Eq. (7.38) Q_1 and Q_2 can be solved from Eq. (7.33). The depth values a_1 and a_2 then follow from Eq. (7.37).

It is important to note that there are not one but three equilibrium states, representing the following situations:

- Both branches are open, each branch transports a part of the water and sediment.
- Branch 2 is closed ($Q_2 = S_2 = a_2 = 0$) and all the water and sediment is transported through branch 1.
- Branch 1 is closed ($Q_1 = S_1 = a_1 = 0$) and all the water and sediment is transported through branch 2.

All three possibilities are physically realistic. For the symmetric case ($B_1 = B_2 = B_0/2$, C_1

$= C_2$, $L_1 = L_2$) and a nodal point relation satisfying the symmetry requirement (i) the three equilibrium states are (a_0,a_0), $(2^{(n-1)/n}a_0,0)$ and $(0,2^{(n-1)/n}a_0)$, where B_0 is the width and a_0 is the equilibrium water depth of the upstream branch.

Remark: Nodal point relations leading to not uniquely determined equilibria with both branches open are not considered because they seem physically not realistic.
When a simulation of the morphodynamic development is carried out for a network system, one of these equilibrium states will be reached. Which one of the three equilibrium states will be reached depends on the stability of the equilibrium states and on the initial conditions. In the section below, the stability of all three equilibrium states is analyzed for the general nodal-point relation (7.26).

7.4.4 Stability of the equilibrium states

In order to analyze the stability of the equilibrium states the morphological development of the system out of equilibrium is considered. To ease the analytical treatment, it is assumed that the bathymetry of each branch can be represented by a single depth value, even if the system is not in equilibrium. Under this assumption the morphological development is described by a system of ordinary differential equations instead of a system of partial differential equations.
With a uniform depth, the mass-balance for sediment in each branch yields

$$\frac{da_j}{dt} = \frac{S_{je} - S_j}{B_j L_j} \quad (j = 1,2) \tag{7.41}$$

L_j = length of the branch
S_j = sediment transport as supplied by the main channel
S_{je} = sediment transport at the downstream boundary
t = time

With Eqs (7.35), (7.36) and (7.37) the discharges in the two downstream branches can be expressed as function of the water depths.

$$Q_1 = \frac{\beta_1 a_1^{3/2}}{\beta_1 a_1^{3/2} + \beta_2 a_2^{3/2}} Q_0 \tag{7.42}$$

$$Q_2 = \frac{\beta_2 a_2^{3/2}}{\beta_1 a_1^{3/2} + \beta_2 a_2^{3/2}} Q_0 \tag{7.43}$$

Herein $\beta_j = B_j C_j L_j^{-1/2}$, j = 1,2. With the general nodal-point relation (7.26), the ratio between the sediment transports at the upstream end of the two branches can be expressed as a function of the ratio between the depths.

$$S_1 = \frac{f\left(a_1 / a_2\right)}{1 + f\left(a_1 / a_2\right)} S_0 \tag{7.44}$$

$$S_2 = \frac{1}{1 + f\left(a_1 / a_2\right)} S_0 \tag{7.45}$$

The sediment transport at the end of a branch is determined by the transport capacity of the branches defined by Eq. (7.37).

$$S_{je} = \frac{B_j^m \, C_j^n a_j^{n/2} L_j^{-n/2} Q_0^n}{(B_1 C_1 a_1^{3/2} L_1^{-1/2} + B_2 C_2 a_2^{3/2} L_2^{-1/2})^n} \qquad j = 1,2 \tag{7.46}$$

Substitution of Eqs (7.44), (7.45) and (7.46) into Eq. (7.41) gives a system of ordinary differential equations for a_1 and a_2:

$$\frac{da_1}{dt} = \frac{Q_0^n}{B_1 L_1}\left[\frac{\gamma_1 a_1^{n/2}}{(\beta_1 a_1^{3/2} + \beta_2 a_2^{3/2})^n} - \frac{f(a_1/a_2)}{1 + f(a_1/a_2)} \frac{m_0}{B_0^{n-1} a_0^n}\right] \tag{7.47}$$

$$\frac{da_2}{dt} = \frac{Q_0^n}{B_2 L_2}\left[\frac{\gamma_2 a_2^{n/2}}{(\beta_1 a_1^{3/2} + \beta_2 a_2^{3/2})^n} - \frac{1}{1 + f(a_1/a_2)} \frac{m_0}{B_0^{n-1} a_0^n}\right] \tag{7.48}$$

The parameters γ_j for j = 1 or 2, are defined as $\gamma_j = mB_j C_j^n L_j^{-n/2}$.

The set of differential equations (7.47) and (7.48) is of the general form

$$\frac{da_1}{dt} = \phi_1(a_1, a_2) \tag{7.49}$$

$$\frac{da_2}{dt} = \phi_2(a_1, a_2) \tag{7.50}$$

where ϕ_1, ϕ_2 are functions in two variables. The depths at the equilibrium states satisfy $\phi_1 = \phi_2 = 0$.

The stability of an equilibrium state depends on the eigenvalues of the Jacobian. If the eigenvalues have negative real parts, perturbations of the equilibrium decay exponentially in time and the equilibrium is stable. If one of the eigenvalues has a positive real part, however, the equilibrium is unstable.

For general values of the parameters, the eigenvalues of the Jacobian cannot be determined by straightforward computation. Only in the special case with symmetric branches, it is easy to compute the eigenvalues. The Jacobian at (a_0,a_0) is

$$J(a_0, a_0) = \frac{S_0}{B_0 a_0 L_1}\begin{bmatrix} -\frac{n}{4} - \frac{2a_0}{(1+f)^2}\frac{\partial f}{\partial a_1} & -\frac{3n}{4} - \frac{2a_0}{(1+f)^2}\frac{\partial f}{\partial a_2} \\ -\frac{3n}{4} + \frac{2a_0}{(1+f)^2}\frac{\partial f}{\partial a_1} & -\frac{n}{4} + \frac{2a_0}{(1+f)^2}\frac{\partial f}{\partial a_2} \end{bmatrix} \tag{7.51}$$

The eigenvalues of the matrix are

$$-n\frac{S_0}{B_0 a_0 L_1},\quad \left(\frac{n}{2}+\frac{2a_0}{(1+f)^2}\left(\frac{\partial f}{\partial a_2}-\frac{\partial f}{\partial a_1}\right)\right)\frac{S_0}{B_0 a_0 L_1} \tag{7.52}$$

The stability of the equilibrium (a_0,a_0) depends on the sign of the second eigenvalue. If this sign is positive, the equilibrium is unstable; if this sign is negative, the equilibrium is stable. The equilibrium is stable if, and only if, the following condition is satisfied

$$\frac{\partial f}{\partial a_1}-\frac{\partial f}{\partial a_2}>\frac{n(1+f)^2}{4a_0} \tag{7.53}$$

For the proposed nodal-point relation (7.30), the equilibrium is stable if $k > n/3$ and unstable if $k < n/3$. For $k = n/3$ Eq. (7.30) is not a good nodal point relation since then the equilibrium with both branches open is not well defined. If Eq.(7.29) is used as nodal-point relation the equilibrium is unstable, independent of the parameters.
The Jacobians at the other two equilibria $(2^{(n-1)/n}a_0,0)$ and $(0,2^{(n-1)/n}a_0)$ are

$$J(2^{\frac{n-1}{n}}a_0,0)=\frac{S_0}{B_0 a_0 L_1}\begin{bmatrix}-\dfrac{n}{2^{\frac{n-1}{n}}} & 0\\ 0 & 0\end{bmatrix} \tag{7.54}$$

$$J(0,2^{\frac{n-1}{n}}a_0)=\frac{S_0}{B_0 a_0 L_1}\begin{bmatrix}0 & 0\\ 0 & -\dfrac{n}{2^{\frac{n-1}{n}}}\end{bmatrix} \tag{7.55}$$

The eigenvalues of these matrices are independent of the nodal-point relation, because these equilibria consist of one channel only. One of the eigenvalues is negative and the other one is zero. So, the equilibria can be stable or unstable. The stability depends on the stability of the equilibrium at (a_0,a_0). If (a_0,a_0) is a stable equilibrium, then $(2^{(n-1)/n}a_0,0)$ and $(0,2^{(n-1)/n}a_0)$ are unstable. If (a_0,a_0) is unstable, then $(2^{(n-1)/n}a_0,0)$ and $(0,2^{(n-1)/n}a_0)$ are stable.
For general parameters the stability of the equilibria remains the same. This follows from a continuity argument. The general case can be seen as a deformation of the symmetric case: start from the symmetric case and slowly deform the geometry of the system. The stability of an equilibrium can only change if a mathematical bifurcation occurs, i.e., if the number of equilibria changes. This happens possibly when Eqs. (7.49) and (7.50) degenerate. For our nodal-point relation, this does not happen unless $k = n/3$.

The qualitative behaviour of the system can be represented in a phase diagram, which shows the evolution of a_1 and a_2 in time (see Figure 7.8). In case $k > n/3$, the system evolves to a unique stable equilibrium, independent of the initial position of a_1 and a_2. In case $k < n/3$, one of the two branches silts up, depending on the initial conditions.

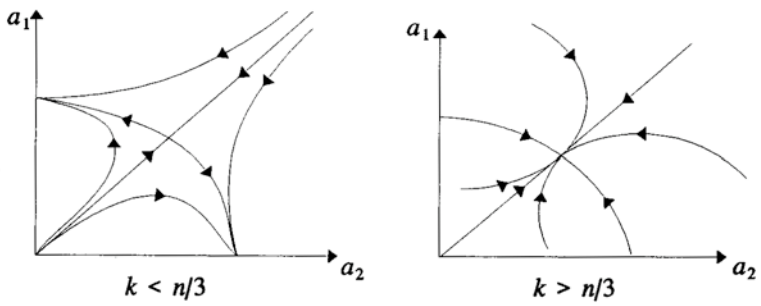

Figure 7.8: Phase diagram of the differential equations

The absolute values of the eigenvalues determine the time scales of the decay or growth of a perturbation of the equilibrium. They are the reciprocals of the time in which a perturbation grows or decays with a factor e (relaxation times). In case $0 < k < n/3$, the eigenvector (1,–1) has a positive eigenvalue, and the eigenvector (1,1) has a negative eigenvalue. It follows that a difference between a_0 and the average of a_1 and a_2 decays, but a difference between a_1 and a_2 grows. Moreover, in absolute value the positive eigenvalue is much smaller than the negative eigenvalue. It follows that a difference between a_0 and the average of a_1 and a_2 decays rapidly compared to the growth of a difference between a_1 and a_2. This is illustrated by the numerical simulations.
A more detailed description of the stability analysis with Eq. (7.30) as nodal point relation is given in Wang et al (1993).

7.4.5 Numerical Verification

The analysis above shows that the nodal-point relation has a crucial influence on the behaviour of a 1D network morphodynamic model. It shows also that relation (7.30) is able to represent both the stable and unstable case. These conclusions have been verified by numerous computations (Fokkink and Wang, 1993; Den Dekker and Van Voorthuizen, 1994), which all agree with the theoretical analysis.
The results of two simulations are presented here. The numerical simulations consider the same problem as the theoretical analysis: a channel bifurcates in two branches. The sediment transport formula of Engelund-Hansen is applied which is equivalent to Eq.(7.37) with $n = 5$.
The parameters used in both simulations are

model parameters	main channel	branch 1	branch 2
length	100 km	10 km	10 km
width	100 m	50 m	50 m
relative density of sand	$\Delta = 1.65$		
representative grain diameter	$D_{50} = 0.2$ mm.		
roughness	$C = 50$ m/s$^{1/2}$		
total discharge	$Q_0 = 1000$ m^3/s		
bed slope	0.00004		
total transport	$S_0 = 0.02345$ m^3/s		
spatial step	$\Delta x = 1000$ m		
Morphological time step	$\Delta t = 1$ day		

The water flow in the model is quasi-steady.
The first simulation is carried out with the nodal-point relation (7.30) using $k = 1$ and the second one with $k = 3$.
According to the analysis, $k = 1$ should lead to one branch silting up and $k = 3$ should keep both branches open. This is confirmed by the computations. Figure 7.9 shows the water depths of the two branches at the nodal-point as a function of time and Figure 7.10 shows the evolution on the a_1–a_2 plane which gives a kind of phase diagram.

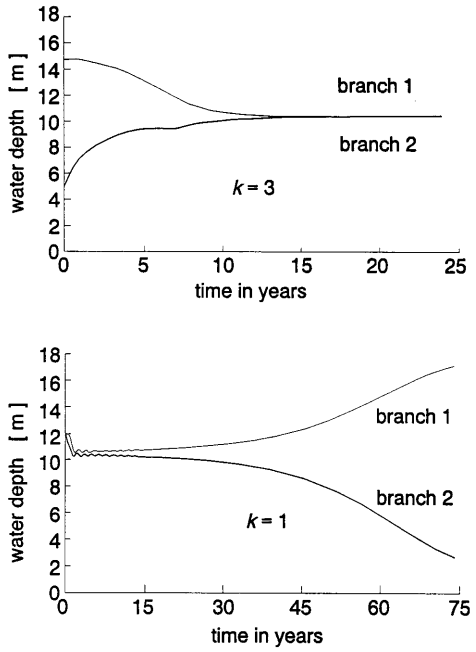

Figure 7.9: Computed water depth of the two branches diagrams

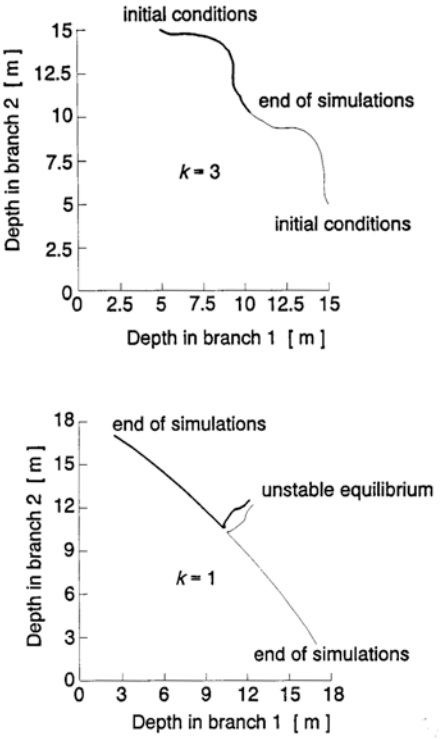

7.10 Computed phase diagrams

Clearly, for $k = 1$ the bifurcation is unstable. A very small difference between the initial depths in the two branches leads to the situation that the shallower branch silts up. Note that there is also a difference between the averaged value of the two initial depths and the equilibrium depth. In the first period of the simulation this difference decreases quickly. When both depths a_1 and a_2 are almost equal to the equilibrium value, the difference between the two depths starts to grow significantly. As remarked in the previous section, this is explained by the fact that the absolute value of the negative eigenvalue (for the development along $a_1 = a_2$) is five times as large as the positive eigenvalue (for the development along $a_1 = a_2$). If a modeller is unfamiliar with this behaviour of the system, such results can be very frustrating.
For $k = 3$, the bifurcation is stable. Even a considerable large difference between the initial depths in the two branches is damped out on the long-term.
The theoretical analysis predicts that the equilibrium with both branches open is stable for $k > 5/3$ and unstable for $k < 5/3$. In reality, this transition can occur between 1.5 and 2, depending on the geometry of the branches in the model (Fokkink and Wang, 1993;

Den Dekker and Van Voorthuyzen, 1994). This is due to the fact that the hydraulic radius of a branch is not equal to the water depth, as is assumed in the analysis.

7.4.6 Conclusions

A nodal-point relation is proposed, which relates the ratio between specific sediment transport rates to a power of the ratio between the specific discharges. The scarce data available for sediment distributions at bifurcations support this power relation. However, the exponent seems to vary from case to case.
Unlike a single-channel system more than one physically realistic morphological equilibrium state is possible in a network system. The morphological development of such a system is strongly influenced by the stability of the equilibrium states.
In a simple model of a bifurcation, the influence of the proposed nodal point relation on the behaviour of 1D network morphodynamic models is analyzed. The exponent in the relation appears to have crucial influence on the stability of the equilibrium states. For small values of the exponent the bifurcation is unstable: only one of the downstream branches tends to remain open at long-term. For large values of the exponent the bifurcation is stable: all branches tend to remain open.
The conclusions from the theoretical analysis have been verified by the results of numerical simulations using a general 1D network package.

7.4.7 References

Dekker P. den and J.M. van Voorthuizen (1994), Research on the morphological behaviour of bifurcations in rivers, M-Sc Thesis, Delft University of Technology, The Netherlands.

Fokkink R.J and Z.B. Wang (1993), Study on fundamental aspects of 1D-network morphodynamic models, report Z654, DELFT HYDRAULICS.

Wang Z.B., R.J. Fokkink and B. Karssen (1993), Theoretical analysis on nodal-point relation in 1D network morphodynamic models, Report Z473, DELFT HYDRAULICS.

Zwaard, J. van der (1981), Bifurcation Pannerden, sediment distribution at the bifurcation (in Dutch), Report M932, DELFT HYDRAULICS.

7.5 ESTMORF model
A Dynamic-Empirical Model for Estuarine Morphology

7.5.1 Introduction

Morphological development is the result of interactions between flow and alluvial bed. The relevant processes for morphological development are flow, sediment transport and bed level change. A mathematical model for morphological development can be set-up by simulating each of these processes using physical laws. Such a process-based morphological model is called a dynamic model.
At present (1996), the dynamic type of models, one-dimensional as well as two-dimensional, are already commonly used in engineering practice for rivers. For estuaries, however, the long-term morphological development under the influence of natural processes, e.g. sea level rise, and/or under the influence of human activities, e.g. land

reclamation, dredging and dumping, can still not be predicted by dynamic models. In practice, prediction of long-term morphological development in estuaries still relies to a large extent on empirical relations, in which the morphological variables, such as the cross-sectional area of channels, are related to integrated hydrodynamic parameters, e.g. the tidal volume.
Recently, ESTMORF is developed by DELFT HYDRAULICS and Rijkswaterstaat, a mathematical model for predicting the long-term (decades) morphological development of estuaries and tidal lagoons, under the influence of natural processes and human interference. The model is partly based on process descriptions and partly on empirical relations which combines the advantages of the dynamic type of models with those of the empirical ones.

7.5.2 Model description

General model concept

The most important hypothesis used in the ESTMORF model concept is that an equilibrium state can be defined for each morphological element of the system depending on the hydrodynamic conditions. An empirical relation is required for each element to define the morphological equilibrium state. This kind of empirical relations are commonly used for tidal systems.
Various morphological models for estuaries and tidal inlets are based on such relations in combination with a transient model describing the evolution of the actual state with respect to its equilibrium as an exponential decay process (O'Connor et al., 1990, Eysink, 1990, Eysink, 1992). When this model concept is applied to a system consisting of more than one element, linked with each other, extra assumptions are required to guarantee the mass-balance of sediment (Allersma, 1988, Van Dongeren and De Vriend, 1994). This can make the model results sensitive to the sequence in which the various elements are dealt with in the computation: e.g. computations starting from the sea side give different results than computations starting from the land side.
In the tidal basin model of Di Silvio (1989) this problem is overcome by introducing a characteristic sediment concentration in each element of the model. The concentration field is governed by the advection-diffusion equation based on a residual flow field, which guarantees the fulfilment of the sediment mass-balance. This concept is adopted in the ESTMORF model.
The basic philosophy is as follows. If all elements in the morphological system are in equilibrium, there is no accumulation of sediment or water anywhere in the area. If the sediment is mainly transported in suspension, the sediment flux field is therefore likely to be proportional to the flow rate. The ratio between sediment flux and flow rate can be considered as a sediment concentration and is called in this paper the overall equilibrium concentration c_E. For each element in the system a local equilibrium sediment concentration c_e is defined such that it equals c_E if the element is in morphological equilibrium, that it is larger than c_E if a tendency for erosion exist (e.g. the cross-sectional area of a channel is smaller than the equilibrium value), and smaller than c_E if a tendency for sedimentation exists. Morphological changes occur when the local

sediment concentration deviates from its local equilibrium. Erosion occurs when the sediment concentration is smaller than its equilibrium value and sedimentation occurs if it is larger than its equilibrium value.

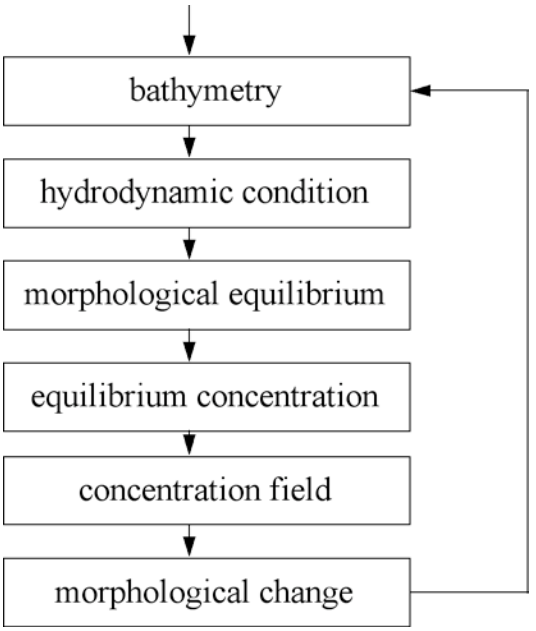

Figure 7.11. Computational procedure

The ESTMORF model described here belongs to the semi-empirical type according to the classification due to De Vriend (1996). An important difference between the present model and the process-based models is that the equilibrium concentration is not directly computed from the hydrodynamic parameters, but via the equilibrium morphological state (see Figure 7.11). This makes the model always converging to a state of which the equilibrium relations are satisfied.

Geometrical schematisation

The model uses an existing one-dimensional network flow model to simulate the flow. Therefore, the modelling area is schematised into a network consisting of branches. The cross-sections of the branches are schematised as shown in Figure 7.12 (Note that in the figure the tidal flat is shown only at one side of the channel). It is divided into three parts: the channel part (under the low water level, MLW), the low tidal flat between MLW and the mean water level (MSL), and the high tidal flat between MSL and the high water level (MHW). The channel part is assumed to have a trapezoidal cross-section. The two parts of the tidal flat are described by their widths as well as their heights. This schematisation of the cross-section is adopted from Eysink (1992). Morphological changes in the three parts are calculated separately, and can be due to sedimentation/erosion and to changes in the relative water level e.g. sea level rise/land subsidence.

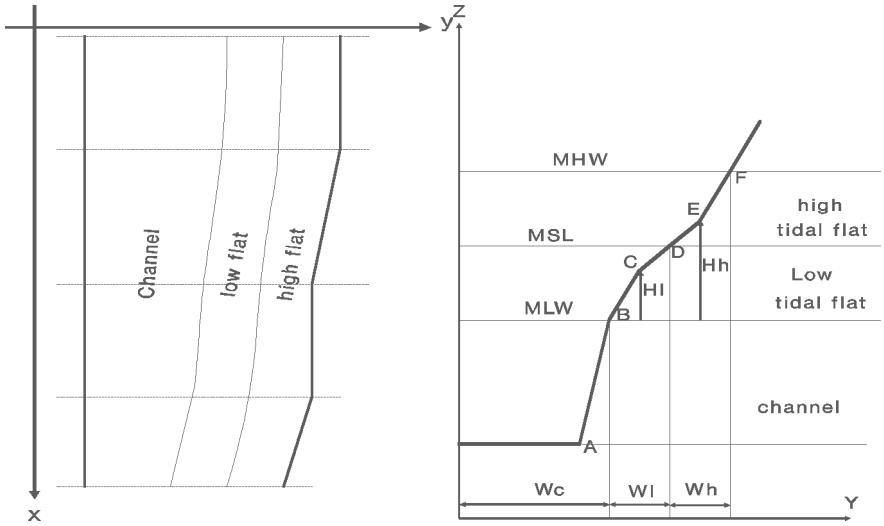

Figure 7.12: Schematisation of geometry

The equilibrium state

The model uses three variables, the cross-sectional area of the channel, the height of the low tidal flat and the height of the high tidal flat. For each of these variables an empirical relation is required defining the morphological equilibrium state of the system.
The equilibrium cross-sectional area of the channel is related to the tidal volume. For the Wadden Sea such a relation is given by e.g. Eysink (1992).

$$A_{ce} = f_1(P_v) \tag{7.56}$$

where:
A_{ce} = equilibrium cross-sectional area under MSL
P_v = tidal volume.

The equilibrium heights (measured from MLW) of the two parts of the tidal flat are related to the tidal range and the total area of the basin (see e.g. Eysink 1992).

$$H_{he} = f_2(H, A_b) \tag{7.57}$$

$$H_{le} = f_3(H, A_b) \tag{7.58}$$

In these two equations
H_{he} = equilibrium height of the high tidal flat measured from mean low water,
H_{le} = equilibrium height of the low tidal flat measured from mean low water,
H = tidal range,
A_b = total area of the basin.

In equations (7.56) through (7.58) no specific relations are given. They have to be chosen on the basis of field data when the model is applied for a specific area. This part is kept as flexible as possible to guarantee a wide applicability of the model. The coefficients in the equations may also vary spatially such that an existing equilibrium

state can be represented throughout the system.

Morphological development

When the system is not in equilibrium, morphological changes will occur. The sedimentation and/or erosion rate is assumed to be proportional to the deficit/excess of the local sediment concentration, following the formulation of Galappatti and Vreugdenhil (19985). The bed level change is then described by the following simple formulation:

$$\frac{\partial z}{\partial t} = w_s \left(c - c_e\right) - \alpha_s \tag{7.59}$$

Herein

z = bed level,
w_s = coefficient having the dimension of velocity, to be called vertical exchange velocity,
t = morphological time,
c = sediment concentration,
c_e = local and instantaneous equilibrium sediment concentration,
α_s = rate of land subsidence.

Applied to the three parts of the cross-section, the following equations are derived:

$$\frac{\partial A_c}{\partial t} = W_c\left[w_s\left(c_{ce} - c_c\right) + \alpha_s + \alpha_r\right] \tag{7.60}$$

$$\frac{\partial A_l}{\partial t} = W_l\left[w_s\left(c_{le} - c_l\right) + \alpha_s + \alpha_r\right] \tag{7.61}$$

$$\frac{\partial A_h}{\partial t} = W_h\left[w_s\left(c_{he} - c_h\right) + \alpha_s + \alpha_r\right] \tag{7.62}$$

In these three equations we define (see Figure 7.12):

A_c = cross-sectional area of the channel par (below MSL),
A_h = cross-sectional area of the high tidal flat,
A_l = cross-sectional area of the low tidal flat,
c_c = sediment concentration in the channel part,
c_h = sediment concentration in the high tidal flat part,
c_l = sediment concentration in the low tidal flat part,
c_{ce} = local equilibrium sediment concentration in the channel part,
c_{he} = local equilibrium sediment concentration in the high tidal flat part,
c_{le} = local equilibrium sediment concentration in the low tidal flat part,
W_c =width of the channel part,
W_h = width of the high part of the tidal flat,
W_l = width of the low part of the tidal flat,
α_r = rate of sea level rise.

Sediment transport

The equilibrium concentrations are determined as follows:

$$c_{ce} = C_E \left(\frac{A_{ce}}{A_c} \right)^{n_c} \tag{7.63}$$

$$c_{le} = C_E \left(\frac{H_l}{H_{le}} \right)^{n_l} \tag{7.64}$$

$$c_{he} = C_E \left(\frac{H_h}{H_{he}} \right)^{n_h} \tag{7.65}$$

In these equations:
C_E = overall equilibrium sediment concentration,
A_c = cross-sectional area of the channel,
H_h = height of the high tidal flat measured from MLW,
H_l = height of the low tidal flat measured from MLW,
n_l = constant coefficient,
n_h = constant coefficient,
n_c = constant coefficient

When the whole system is in equilibrium, the sediment concentration will be equal to its overall equilibrium value. When for example the cross-sectional area is larger than the equilibrium value it means in fact that the local flow velocity will be lower by the same factor as the ratio A_{ce}/A_c. The formulation (7.63) of the local equilibrium sediment concentration is thus similar to the sediment transport capacity formula using power law. The actual sediment concentration is governed by an advection-diffusion model. It is further assumed that the tidal flat can only exchange sediment with the channel in the same section. In other words, there is no longitudinal sediment transport over the intertidal tidal flats.
The mass balance equation for sediment in the channel may be written as:

$$\frac{\partial A_c c_c}{\partial t} + \frac{\partial A_c u c_c}{\partial x} - \frac{\partial}{\partial x}\left(A_c D_c \frac{\partial c_c}{\partial x} \right) = W_c w_s (c_{ce} - c_c) + F_{lc} \tag{7.66}$$

where:
c_c = sediment concentration by volume in the channel,
D_c = horizontal dispersion coefficient in the channel,
F_{lc} = exchange rate of sediment between the channel and the low tidal flat,
t = time,
u = residual flow velocity.

The sediment flux from the tidal flat to the channel F_{lc} is elaborated as follows:

$$F_{lc} = D_l \overline{\Delta h_l} \frac{c_l - c_c}{L_{lc}} 1 \tag{7.67}$$

Herein:
D_l = diffusion coefficient,
L_{lc} = distance between the centre of the channel and that of the low part of the tidal flat,
$\overline{\Delta h_l}$ = time-averaged water depth at MLW

The mass balance for sediment at the low part of the tidal flat is given by the following equation:

$$\frac{\partial (A_l c_l)}{\partial t} = W_l w_s \left(c_{le} - c_l\right) - F_{lc} + F_{hl} \tag{7.68}$$

And at the high part of the tidal flat the mass-balance reads

$$\frac{\partial (A_h c_h)}{\partial t} = W_h w_s \left(c_{he} - c_h\right) - F_{hl} \tag{7.69}$$

The exchange rate between the two parts of the tidal flat is formulated as

$$F_{hl} = D_h \overline{\Delta h_h} \frac{c_h - c_l}{L_{hl}} \tag{7.70}$$

Herein:
D_h = diffusion coefficient,
L_{hl} = distance between the centre of the high flat and that of the low flat,
$\overline{\Delta h_h}$ = time-averaged water depth at MSL.

7.5.3 Comparison with dynamic models

The behaviour of the model can be analysed by considering some simplified cases. Here two extreme cases are considered. It will be shown that in both cases the behaviour of the model is very similar to a process-based model.
The first case concerns the unidirectional steady flow in a river without tidal influence (hence no tidal flats exist). In this case the tidal volume is proportional to the river discharge, so the equations describing the sediment transport and the morphological development used in the model become identical to those in a process-based one-dimensional model using depth-averaged model for suspended sediment transport (see e.g. Galappatti and Vreugdenhil, 1985). The only difference is that the morphological equilibrium state in the present model is merely determined by the river discharge, whereas in a 1D process-based model it is determined by the discharge, the upstream sediment supply and the river width. It is obvious that the empirical relations used in the model should be site-specific.
The second case concerns a rectangular tidal basin, with one end closed and the other end connected with the sea. This case has been used for extensive sensitivity analysis with respect to the various model-parameters (Karssen, 1994). A typical example of the

results is shown in Figure 7.13. The simulation start with a horizontal bed and ends with a linear bottom, which is in full agreement with the commonly used empirical relation that the cross-sectional area is proportional to the tidal volume through that cross-section (note that the diffusion coefficient at the end of the basin is not set to zero). Also in this case the simulated morphological development is very similar to that simulated with a process-based model (see Wang, 1992, Schuttelaars and De Swart, 1996). From the sensitivity analyses it is further concluded that the vertical exchange velocity, the overall equilibrium concentration, the dispersion coefficient and the power in the equilibrium concentration equations are the most important parameters influencing the simulated morphological development.

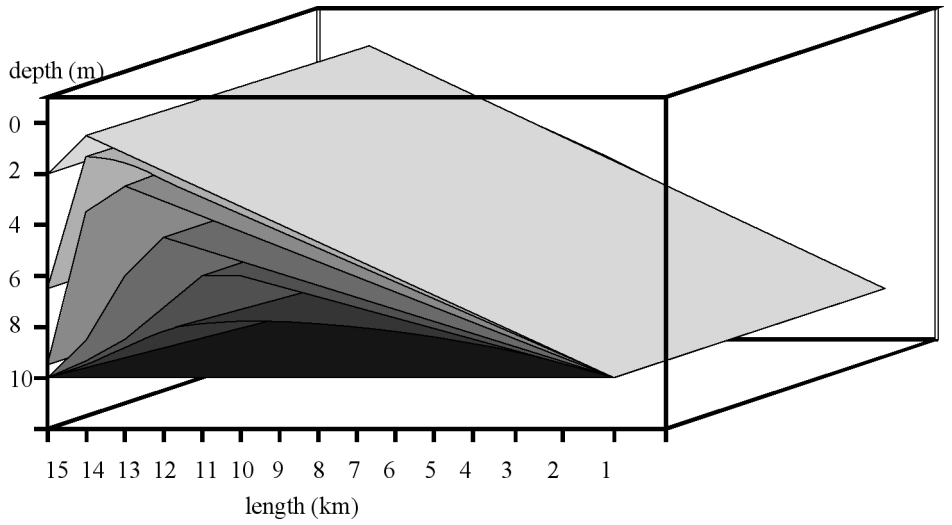

Figure 7.13: Filling of a prismatic tidal basin

7.5.4 Morphological time scale

Another way of examining the behaviour of the model is by analysing how the morphological time scale is related to the relevant length scale. Knowledge of how the morphological time scale is determined by the model parameters is very important for the calibration of the model. For this purpose a linear analysis is carried out for a small disturbance on a system in equilibrium. The time scale defined is the time in which the disturbance decreases its amplitude with a factor *e*. For the sake of simplicity only the channel is considered, and the residual flow is neglected. The time scale in this case is:

$$T = \frac{T_S + T_D}{c_E \; n_c} \tag{7.71}$$

Herein $T_S = \frac{a}{w_s}$ and $T_D = \frac{1}{k^2 D}$

and k is the wave number of the disturbance. It is clear that the time scale consists of two parts, one related to the vertical exchange of sediment and the other related to the horizontal exchange of sediment. It is also clear that the parameters D, w_s, c_E and n are

the important model parameters determining the morphological time scale. More extensive and detailed analysis of the morphological time scale related to the model parameters is given by Fokkink (1996).

7.5.5 Applications

Het Friesche Zeegat

"Het Friesche Zeegat" is a tidal inlet in the Wadden Sea (Figure 7.14). Since 1969, this tidal inlet system, with an area of about 450 km^2, has undergone significant morphological changes due to the reclamation of a large part, the Lauwerszee. As a consequence the in- and out-going tidal volume has been reduced by about 34%. The response of this tidal inlet system to the closure of the Lauwerszee is well documented. The deeper parts of the outer delta are eroding, large bars are forming, the tidal channels are shoaling and the eastern watershed is shifting eastwards.
The ESTMORF model is applied to simulate the morphological development induced by the closure of the Lauwerszee in 1969. The simulation focuses on the morphological development of the tidal basin, especially the channels.
The model is set-up based on an existing 1D network model for this inlet. The schematisation is also shown in Figure 7.15. It must be pointed out that the schematisation was originally designed for flow simulation purposes only. From the morphological modelling point of view it is not an ideal schematisation. Nevertheless the application has been rather successful in hindcasting the evolution of the channels' cross-sectional areas throughout the basin as shown in Figure 7.17, which presents the morphological evolution of some of the channel cross-sections. As can be observed in Figure 7.15, there is a channel bifurcation at the entrance of the Lauwerszee. The closure has cut off one of the branches of this bifurcation. After the closure sedimentation has occurred in the channel west of the bifurcation and erosion took place east of the bifurcation. The sedimentation in the western part (cross-sections 1 and 2) of the channel as well as the erosion in the eastern part (cross-sections 3 and 4) are well reproduced (Figure 7.17).

The Western Scheldt

The Western Scheldt is an estuary located in the South-west of The Netherlands. It is the entrance to Antwerp Harbour. Dredging operations maintaining and improving the navigation conditions can have significant impact on the morphological development, which in turn can influence the ecological conditions in the estuary. In the near future a significant deepening of the navigation channel is planned. It is very important to predict the morphological and ecological impacts of the capital dredging and of the increased maintenance dredging in the future.
An ESTMORF model is set-up for the estuary to simulate the morphological developments under influence of human activities, like dredging and dumping, and under influence of natural processes, like sea level rise. Also in this case the model is based on an existing 1D-network tidal flow model. The schematisation of the model is shown in Figure 7.15. As an example of the model results, the simulated bed level change after 25

years is shown in Figure 7.16. The results have also been used for ecological modelling. For this purpose a two-dimensional interpretation is made of the simulated morphological changes in order to evaluate the changes of relevant habitats.

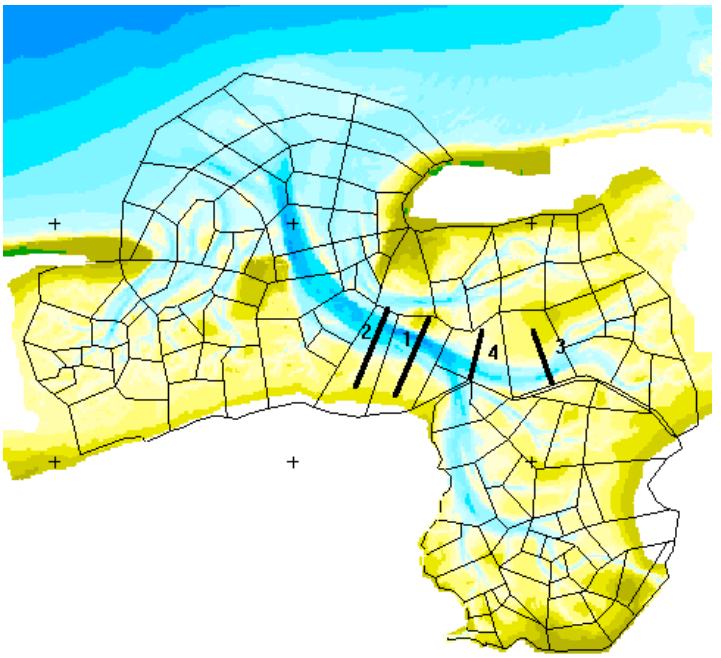

Figure 7.14: Het Friesche Zeegat

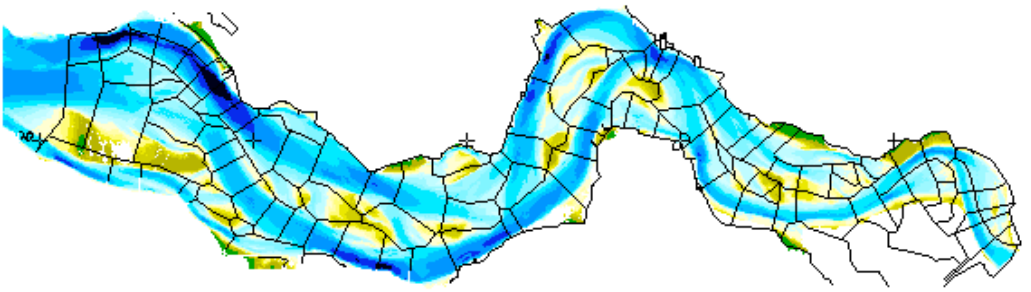

Figure 7.15: Schematisation of the Westernscheldt estuary

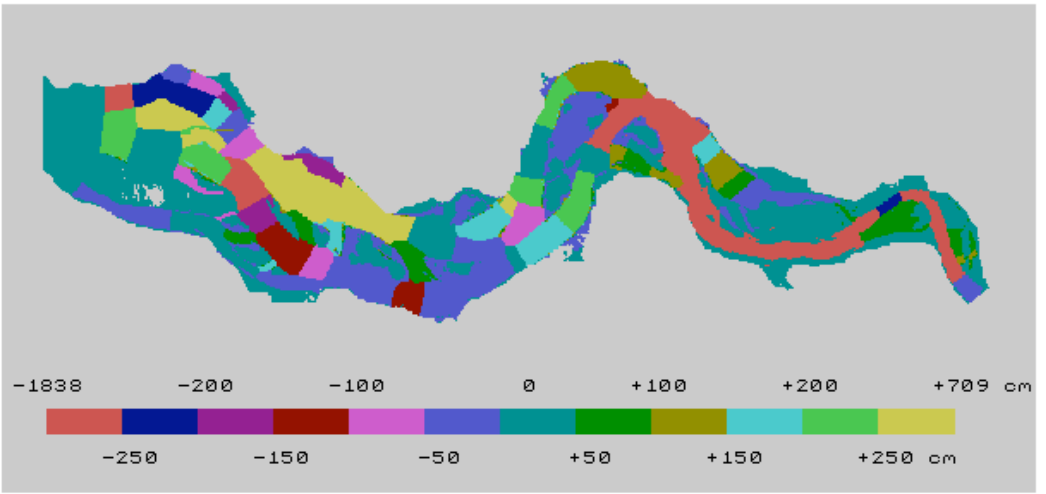

Figure 7.16: Computed bed level change after 25 year

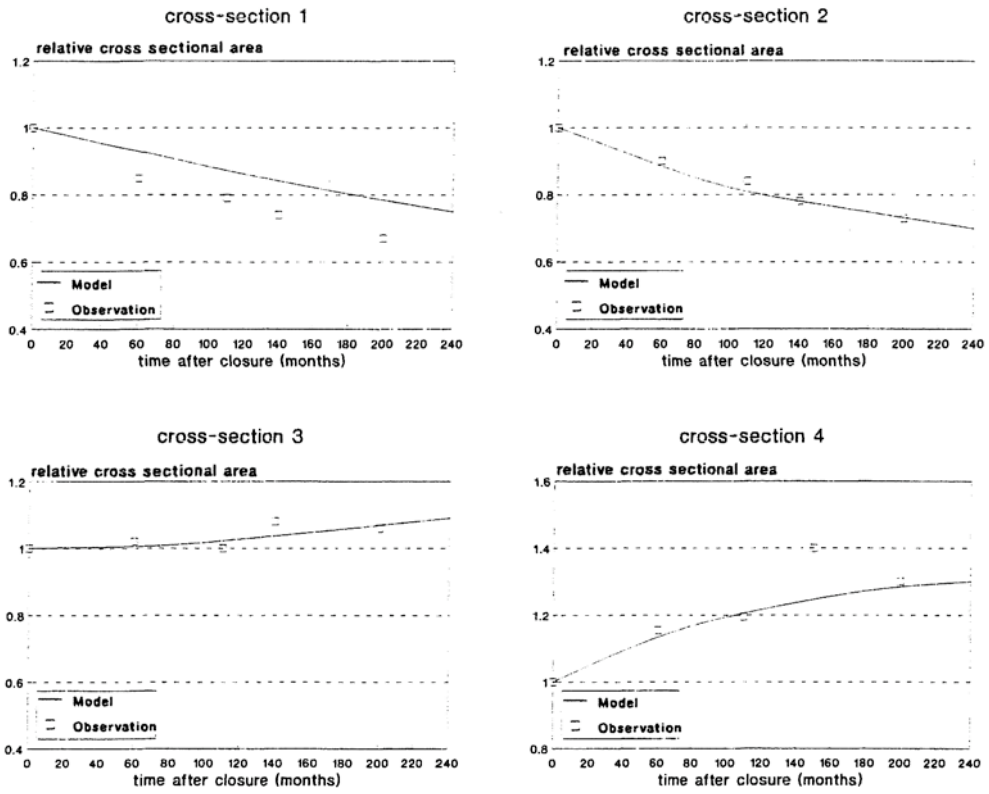

Figure 7.17: Computed and measured cross-sectional areas

At present the study is still continuing. More detailed discussion on the morphological modelling for the Western Scheldt is given by Fokkink et al. (1996).

7.5.6 Conclusions

A semi-empirical model for morphological changes in estuaries and tidal lagoons is developed on the basis of a one-dimensional network tidal flow model. The model uses well-established empirical relations between the morphological equilibrium state and integrated tidal flow parameters. The sediment is assumed to be transported primarily as suspended load.

Tidal flow is considered as the major force causing morphological changes, but the influences of other factors like sea level rise and human activities (e.g. dredging and dumping) can also be included. The model can be used for predicting morphological changes on a time scale of decades.

The model makes a distinction between the morphological changes in the channel and those on the intertidal flats. Morphological changes on these flats are important for the ecosystem, and morphological changes in the channel for navigation.

For two extreme cases, a river flow without tidal action and a prismatic tidal basin without river input, the model behaves the same as the process-based morphodynamic models. This gives the confidence that the model is widely applicable to estuaries. In addition to the empirical relations defining the morphological equilibrium, the most important parameters determining the behaviour of the model are the overall equilibrium concentration, the vertical exchange velocity of sediment, the horizontal diffusion coefficient for sediment and the power in the equilibrium concentration formula.

The model has been applied to “Het Friesche Zeegat”, a tidal inlet in the Wadden Sea, and The Western Scheldt, an estuary in the Southwest of The Netherlands. In the first case the morphological changes, especially in the channel, caused by the closure of a part of the tidal basin, have been successfully simulated by the model. Good agreement between the computed and observed changes of the cross-sectional areas of the channels has been obtained. In the second case the study is still going on but encouraging results have already been achieved in simulating the impact of dredging and dumping activities in the navigation channel.

7.5.7 References

Allersma, E., 1988: Morfologisch onderzoek Noordelijk Deltabekken, Morfologische modellering deel III: modellering van de transporten. Report Z71-03, DELFT HYDRAULICS, Delft, September 1988.

Di Silvio, G., 1989: Modelling the morphological evolution of tidal lagoons and their equilibrium configurations. XXII Congress of the IAHR, Ottawa, Canada, 21-25 August 1989.

Dongeren, A.R. van and H.J. De Vriend, 1994: A model of the morphological behaviour of tidal basins, Coastal Eng., 22(3/4): 287-310.

Eysink, W.D., 1990: Morphological response of tidal basins to changes. Proc. 22nd Coastal Engineering Conference, ASCE, Delft, p. 1948-1961.

Eysink, W.D., 1992: Impact of sea level rise on the morphology of the Wadden Sea in the scope of its ecological function, Report H1300, phase 3.

Fokkink, R.J. (1996), A new evaluation of ESTMORF, Delft Hydraulics, Report Z930.

Fokkink, R.J., Karssen B., Wang Z.B., Van Kerkhoven, J. and A. Langerak, 1996, Morphological modelling of the Western Scheldt Estuary, Submitted to this volume.

Galappatti, R. and C.B. Vreugdenhil 1985, A depth-integrated model for suspended sediment transport, J. of Hydr. Res., 23(4), 359-377.

Karssen, B. and Z.B. Wang, 1991a: Note on preliminary study of ESTMORF, DELFT HYDRAULICS, Delft.

Karssen, B. and Z.B. Wang, 1991b: Morphological modelling in estuaries and tidal inlets. Part I: A literature survey. DELFT HYDRAULICS report project Z473, Delft, December 1991.

Karssen, B. and Z.B. Wang, 1992: A dynamic/empirical model for the long-term morphological development of estuaries, Note Z473.20, DELFT HYDRAULICS, Delft, October, 1992.

Karssen, B., 1994, A dynamic/empirical model for the long-term morphological development of estuaries, Part II: Development of the model, Delft Hydraulics, Report no. Z715.

O’Connor, B.A., Nicholson, J. and R. Rayner, 1990, Estuary geometry as a function of tidal range. In: B.L. Edge (ed.), “Coastal Engineering 1990 Proc.”, ASCE, New York, P.3050-3062.

Schuttelaars, H.M. and H.E. De Swart, 1996, An idealized long-term morphodynamic model of a tidal inlet, Eur. J. Mech. B/Fluids 15, 55-80.

Vriend, H.J. de, 1996, Mathematical modelling of meso-tidal barrier island coasts, Part I: Empirical and semi-empirical models, in Liu Ph.L.F. (ed.), “Advances in coastal and ocean engineering”, World Scientific.

Wang, Z.B., 1992, Fundamental considerations on morphodynamic modelling in tidal regions (part I), Delft Hydraulics, Rep. no. Z331.

7.6 ASMITA model

7.6.1 Introduction

The motivation for the present work is derived from studies into the response of the Mediterranean deltaic plains of Ebro, Po and Rhone rivers to climate and other human-induced changes, with an emphasis on the larger time- and space-scales (see e.g. Jimenez et al., 1996; and Capobianco et al., 1996). A specific part of those studies is concerned with the land-sea interface of the deltaic plains. A common element of this interface, which we term the deltaic fringe, is that of sediment starvation due to the upstream regulation of water resources and to artificialisation of the deltaic plains. This implies that the three deltaic fringes are nowadays fairly wave-dominated in as far as it concerns their morphological evolution and they have been progressively reducing their extension because of sea forcings on the one side and human reclamation activities on the other side. Typical geophysical elements which the deltas have in common are, beside the rivers' mouth regions, lagoons and bays which interrupt the more continuous coastal stretches, which latter exhibit strong local curvatures. The lagoons and bays provide an important sediment accommodation space for a situation in which relative mean sea level has been dramatically rising in the past and is still rising in a significant way nowadays.
Obviously, morphological interactions take place between the adjacent coastal stretches, the lagoons and their submerged deltas at different spatial and temporal scales, according to intrinsic dynamics, that we would like to characterise, and to external forcing factors. The work presented here focuses on the "residual" interaction occurring on a long term scale. Based on existing field information and on generic modelling knowledge regarding tidal basins and lagoons on the one hand and wave-dominated coastal stretches on the other hand, we have formulated a modelling approach which would allow to determine the possible impact of increased, or decreased, relative sea-level rise, of changes in wave climate and human-induced regulation of the lagoons and the adjacent coastal areas . Because of the time-scales of interest we consider the geophysical elements of the coastal fringe at an aggregated scale, e.g. single-inlet lagoons are schematised into two or at most three spatial units such as channel area, and (high and low) flats area. The new element in our approach is that we study the non-linear dynamic interaction between the lagoon elements, the submerged delta and the adjacent coastal sections.

7.6.2 Model formulation

From our aggregated scale model perspective we view a tidal inlet system as consisting of three major morphological elements, viz. the lagoon or tidal basin, the ebb tidal delta and the directly adjacent coast. Each of these elements is primarily influenced by the basin related tidal prism flows and secondarily by wave related hydrodynamics. However, within these elements the relative importance of the tidal prism flow and wave related hydrodynamics for their morphological development is different. For the coast,

the additional effects of short waves and wave driven flow may be assumed strongest. Within the lagoon it is the tidal flow that is most important. For the ebb-tidal delta wave action as well as tidal action are important.
Like in many other classical situations in coastal morphodynamics, here we enter the problem of definition of possible equilibrium conditions. Particularly in situations where the relative role of the wave forcing with respect to tides is significant, it could happen that the ebb-tidal delta, as a distinct morphological unit, is nonexisting. An inlet in equilibrium is due to the balance between the wave energy which tends to close the inlet and the tidal energy which maintains the opening. For the theory of stability of the lagoon inlets, we refer to Bruun (1978). We hereby just recall some elementary concepts. Stability and equilibrium must be used in relative terms. No absolutely "stable" or "in equilibrium" inlet exists in a situation of significant longshore sediment transport; it is always subject to changes in its planform as well as in its cross-sectional area and geometry. Our approach is based on the use of morphological equilibrium relations and on equilibrium assumptions that, however, are still subject of active research investigation.

In our integrative effort, the most delicate point is represented by the ebb-tidal delta which is in fact the interfacing component by excellence. Apparently, such a sedimentary environment can undergo a self-organisation leading to a (quasi-) equilibrium morphology for each of the elements under relatively constant hydrodynamic forcing conditions. Our conceptual starting point is that we accept the existence of such a (quasi-) equilibrium state, and that we are specifically interested in the response of the system to disturbances of the equilibrium state. While earlier work has studied this for individual elements (see e.g. De Vriend, 1996), we find that the different elements cannot be isolated from each other when their morphological development is considered. The interactions between the different elements through sediment exchange play an important role for the morphological development of the whole system as well as of the individual elements.
Our approach can be considered as an aggregation on the one hand and an extension on the other hand of a model formulation for tidal basins (the so-named ESTMORF model, see Wang et al., 1996; and Fokkink et al., 1996). The aggregation concerns the fact that we characterise the system elements by only one state variable (viz. a total wet or dry volume). The extension concerns the incorporation of formulations for the ebb tidal delta and directly adjacent coast as well, without modifying the basic concepts. This applicability is based on the idea that also there tidal basin related flows are of sufficient importance to apply the ESTMORF concepts for equilibrium concentrations, sedimentation and transport. These concepts are:

- under constant (in a long term average sense) external (hydrodynamic) conditions the equilibrium situation for the morphological state variables is known as a function of those conditions or it is assumed to be known under the given scenario;
- in the equilibrium situation an overall long-term averaged equal sediment

concentration in each system element exists;
- in case of external forcing of the elements' state variables new local equilibrium concentrations are defined. This leads to net sediment exchanges between the elements which are described by a diffusion-type transport, where the diffusion is assumed to take into account all the possible transport processes.

First, the state variables describing the system need to be defined. An ESTMORF model uses a network schematisation for spatial elements covering the tidal basin. In practice, this network can be as detailed as one wishes; the more detailed the network is the more the model would resemble a bidimensional finite element schematisation of the lagoonal area. Within the network each element or branch is divided into three parts: the channel part, the low tidal flat and the high tidal flat. However, the degree of schematisation in the present case is determined by that element of our system which delivers the lower boundary to the relevant spatial scale. This concerns typically the ebb-tidal delta, for which we presently have no other option than to consider its volume as an integral state variable, implying that the ebb tidal delta is modelled as a single element. It is then not very sensible to model the tidal basin and/or the adjacent coasts in more detail, and we logically start with the same level of schematisation, i.e. using the same spatial scales, for all the elements in the system. Later the model may be extended by using more detailed schematisation for the elements. Therefore the following basic elements are included in the model (Figure 7.18).

- the ebb tidal delta as a whole;
- the total inter tidal flat area in the basin;
- the total channel volume in the basin;
- the adjacent coast at one side;
- the adjacent coast at the other side.

It is assumed that sediment exchanges only occur between the tidal flat and the channel in the basin, between the channel in the basin and the ebb tidal delta, between the adjacent coasts and the ebb tidal delta, and between the coasts and the adjacent boundaries. The sediment exchange with the surrounding zones, viz. the more offshore shoreface and the coastal stretches further away, is assumed to not play a role in the morphodynamic interactions considered. This assumption looks reasonable in the presence of undisturbed situations where we could have a "migrating inlet", but this is probably not the case in the presence of artificially disturbed situations, where a morphological modification could occur. In such a case it would certainly be important to implement a more process-based integrative formulation between the ebb-tidal delta dynamics and the adjacent coastal area longshore dynamics.

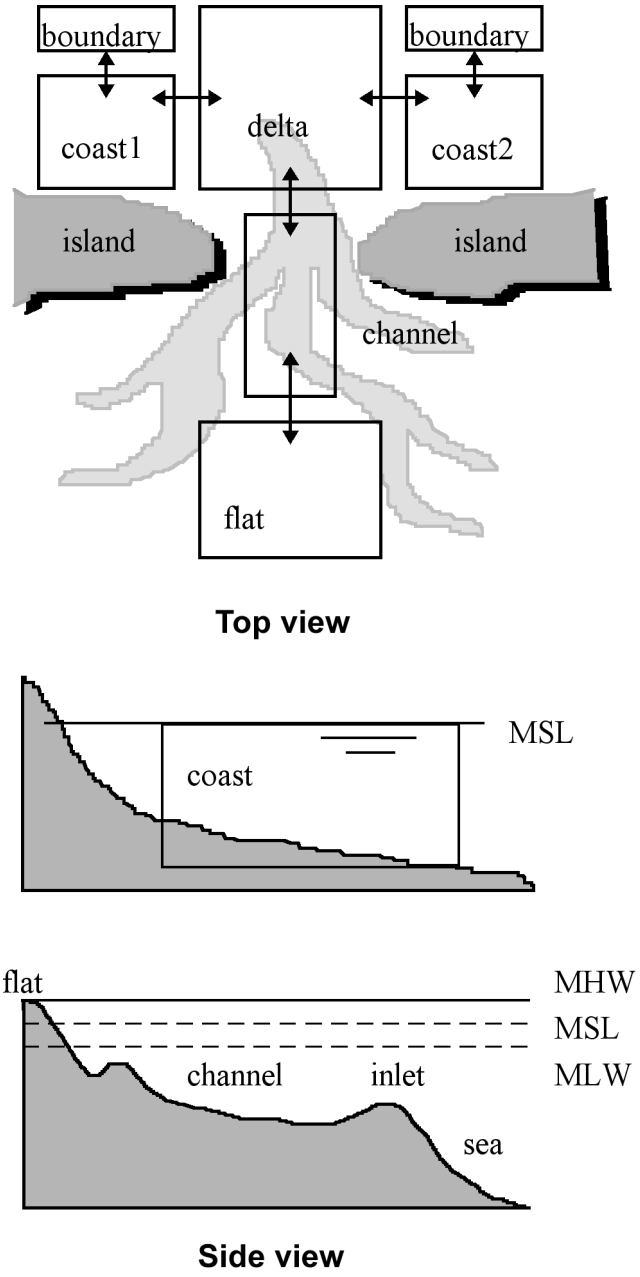

Figure 7.18: Schematisation of the present model (ASMITA)

As described above each of these elements is described by one morphologic variable representing its bathymetry:

- for the ebb tidal delta the total volume of the delta V_d above a fictive sea bottom, which would be there if there was no inlet (sand volume);
- for the tidal flat the total volume of the flat V_f between MLW and MHW (sand volume);
- for the channel the total channel volume under MLW V_C (water volume)
- for the two coast elements the volume below MSL and above a certain depth line V_{C1} and V_{c2}. (water volume)

The most important hypothesis used in the model concept is that an equilibrium state can

be defined for each element depending on the hydrodynamic condition. An empirical relation is required for each element to define the morphological equilibrium state. These relations are derived from literature (cf. Eysink, 1990) and, even if derived for situations where tide-induced sediment transport is more significant than wave-induced sediment transport, we assume to be of general enough validity under the assumption that extreme waves are limited in such a way not to open and close new inlets and the occurrence of extreme wave events is "regular enough".
In the above equilibrium conditions two hydrodynamic parameters are the tidal range (H) and the tidal prism (P):

$$V_e = f(P,H) \tag{7.72}$$

In the present study a very simple hydrodynamic model is used. The size of the tidal basin is assumed to be small compared with the tidal wave length. Spatial variation of the water level in the basin is neglected. The tidal range is assumed to be given as function of (morphological) time. The tidal prism can thus be calculated from:

$$P = H \cdot A_b - V_f \tag{7.73}$$

where A_b equals the total basin area.
A key element in the modelling concept is the equilibrium concentration. The definition thereof is based on the following arguments. When all the elements in the morphological system are in equilibrium a constant sediment concentration is present in the whole system. This constant concentration is called the overall equilibrium concentration c_E.
For each element in the system a local equilibrium sediment concentration c_e is defined such that it is equal to c_E if the element is in morphological equilibrium, larger than c_E if tendency of erosion exist (e.g. the volume of the ebb tidal delta is larger than the equilibrium value), and smaller than c_E if tendency of sedimentation exists. The local equilibrium concentration depends on the actual volume V_c. To represent this behaviour a simple power relation is used for the equilibrium concentrations, e.g. for the channel element this reads:

$$c_{ce} = c_E \cdot \left(\frac{V_{ce}}{V_c} \right)^n \tag{7.74}$$

where the power n is larger than one, must commonly taken as 2 in compliance with a third power for the sediment transport as a non-linear function of the mean flow velocity.
According to the modelling concept morphological changes occur when the local sediment concentration deviates from the local equilibrium sediment concentration. Erosion occurs when the sediment concentration is smaller than its equilibrium value and sedimentation occurs if it is larger than its equilibrium value. Again, for the channel element this reads:

$$\frac{\partial V_c}{\partial t} = w_s \cdot A_c \cdot (c_{ce} - c_c) \tag{7.75}$$

where: w_S is the vertical exchange coefficient and A_c is the horizontal area of the element.

The sediment concentration and sediment transport is governed by the advection-diffusion equation with the source/sink term representing the sediment exchange with the bottom. The general form of this equation for the channels as used in ESTMORF reads:

$$\frac{\partial A_c \cdot c_c}{\partial t} + \frac{\partial A_c \cdot u \cdot c_c}{\partial x} + \frac{\partial}{\partial x}\left(A_c \cdot D_c \cdot \frac{\partial c_c}{\partial x} \right) + \frac{\partial}{\partial y}\left(A_l \cdot D_l \cdot \frac{\partial c_c}{\partial y} \right) = W_c \cdot w_s \cdot (c_e - c_c) \tag{7.76}$$

where: u is a residual flow velocity,
D_c and D_l are the transversal and lateral diffusion coefficients,
A_c and A_l are an effective transversal and lateral cross-section respectively,
W is the width of the element.

For the present case only individual elements of constant cross-section in transversal sense are considered, which means that a discretized form of the equations is used. Furthermore, it is assumed that the morphological time scale is much larger than the time scale for the sediment concentration adjustment to its equilibrium value and to its surrounding environment, so that the first term averages out. It is also assumed that advection transport only occurs along the coast due to longshore current with a constant discharge Q, so that the second term applies along the coast only. The third term applies to the tranversal sediment exchanges between the coast elements and the delta and between the delta and the channel, while the fourth term applies to the lateral sediment exchange between the channel element and the flats. The above equations applied to all elements result in a system of five linear equations for the concentrations in the five elements in the system. Considering the neighbouring elements flat and delta, the diffusion based sediment exchange yields:

$$\delta_{cd} \cdot (c_c - c_d) + \delta_{cf} \cdot (c_c - c_f) = w_s \cdot A_c \cdot (c_{ce} - c_c) \tag{7.77}$$

Here δ represents the horizontal exchange coefficient.
Every element has a morphological time-scale, depending on the magnitude of the disturbance and the geometry of the elements. For a single element the morphological time-scale τ equals:

$$\tau = \frac{1}{c_E \cdot n} \cdot \left(\frac{V_e}{w_s \cdot A} + \frac{V_e}{\delta} \right) \tag{7.78}$$

Simplified "process-based" computation of the equilibrium concentration

The concept of equilibrium concentration was used extensively, even if still in a rather experimental way, for the evaluation of the morphological evolution of the inlets in the Lagoon of Venice (Di Silvio, 1989). The equilibrium concentration represents the fundamental link between hydrodynamics, sediment transport and morphology at the entrance of the lagoon. We can say that c_E is the average annual concentration induced

by waves and currents. In principle we could say that it is possible to obtain a formulation for c_E by integrating over a long period of time any sediment transport formula, and obtaining something like:

$$c_E = c_E \text{ (local wave climate, tidal currents, water depth, grain diameter)} \qquad (7.79)$$

Further, it should be noted that if a constant c_E is used[2], than c_E by itself does not have any influence on the final equilibrium state of the system but it is an important parameter determining the time scale of the morphological development together with the dispersion coefficients and the fall velocity. Therefore c_E could be used as one of the calibration parameters in the model.
We could for instance write a formulation for c_E by simply considering the Acker & White (1973) formula:

$$c = \frac{\alpha}{h} \cdot \left(u - U_0\right)^m \qquad (7.80)$$

where:
c is the average concentration on the depth h,
u is the current velocity,
U_o is the critical value for inducing the movement of a single particle.

The coefficient α, the exponent m and the threshold value U_o are a function of the grain size (d). Experiences from the lagoon of Venice (Di Silvio & Teatini, 1995) give values such as summarised in Table 7.1.

Table 7.1 Calibrated coefficient for various grain sizes

d (μm)	α	m	U_o (m/s)
0.06	$209\ 10^{-4}$	6.58	0.24
0.15	$6.5\ 10^{-4}$	3.64	0.28
0.50	$3.17\ 10^{-4}$	2.25	0.42

The equation could be applied not only to sediment suspended by tidal currents but also, with some approximation, to sediment suspended by waves by assuming the instantaneous velocity close to the bottom. The equilibrium concentration value is then obtained by averaging the equation over the whole year and by considering both currents and waves.
Considering tidal currents, we obtain:

$$c_{Et} = \frac{1}{T_a} \cdot \int_0^{t_0} c_t(t)\,dt \qquad (7.81)$$

where:
$c_t(t)$ is the instantaneous concentration computed from the instantaneous tidal current

[2] This is not a logical incongruence; simply, as we will further state in the following, the equilibrium concentration can be made dependent on variables that are subject to change.

$U_t(t)$,
t_0 is the time, on the period T_a, when the tidal current is higher than U_0.
In the lagoons of the northern Adriatic sea we can consider an almost linear curve for $U_t(t)$:

$$U_t(t) = U_{tm} \cdot \left(1 - \frac{t}{T_a}\right) \tag{7.82}$$

where U_{tm} is the maximum annual velocity in a certain point. Simplifying, we obtain:

$$c_{Et} = \frac{\alpha \cdot \left(U_{tm} - U_0\right)^{m+1}}{h \cdot U_{tm} \cdot \left(m+1\right)} \tag{7.83}$$

As far as the wave motion is concerned, the equilibrium concentration is still obtained by integrating the instantaneous concentration obtained from the instantaneous velocity:

$$c_{Ew} = \frac{1}{T_a} \cdot \int_0^{t_0} c_w(t)\,dt \tag{7.84}$$

In such a case, however, the bottom velocity is obtained by waves of different height coming from different directions and related to wind strength, wind direction and fetch. In a certain point of the lagoon at depth h, the maximum velocity at the bottom $U_w(\alpha)$ induced by the wave of height $H(\alpha)$,generated by the wind $W(\alpha)$ in the direction α, can be approximately computed as (shallow water approximation):

$$U_w\left(\alpha\right) = \frac{\sqrt{g}}{2 \cdot \sqrt{h}} \cdot H\left(\alpha\right) = \varphi\left(\alpha\right) \cdot W^w\left(\alpha\right) \tag{7.85}$$

where $\varphi(\alpha)$ depends on the length of the fetch and the average depth while w is a coefficient approximately equal to 3/4.
We now assume that the curve of duration of the wave height $H(t)$, once aggregated to include all the waves conditions coming from all directions, can be defined with an exponential function:

$$\frac{U_w\left(t\right)}{U_{wm}} = \frac{H\left(t\right)}{H_m} = e^{-\frac{\gamma \cdot t}{T_a}} \tag{7.86}$$

where U_{wm} is the maximum velocity at the bottom, corresponding to the maximum wave H_m that may occur in the period T_a. The ratio T_a/γ represents the “persistence” of the wave motion and is of course site dependent.
If we now consider that during an event the instantaneous velocity varies linearly from the maximum value to zero, the curve of duration of the instantaneous velocity results:

$$U_w\left(t\right) = U_{wm} \cdot e^{-\frac{2\gamma \cdot t}{T_a}} \tag{7.87}$$

or, approximately:

$$U_w(t) = U_{wm} \cdot \left(1 - \frac{2\gamma \cdot t}{T_a}\right) \tag{7.88}$$

Simplifying:

$$c_{Ew} = \frac{1}{2 \cdot \gamma} \cdot \frac{\alpha}{h} \cdot \frac{\left(U_{wm} - U_0\right)^{m+1}}{U_{wm} \cdot (m+1)} \tag{7.89}$$

The equilibrium concentration is given by the annual average for both waves and tidal currents, i.e. the sum of the contributions given by waves and by tidal currents:

$$c_E = c_{Et} + c_{Ew} \tag{7.90}$$

It should be noted that, given the fact that U_{tm} tends to be very small in the shallow areas while W_{tm} tends to be very small in the channels, c_{Et} and c_{Ew} may be respectively neglected when the equilibrium concentration in the two areas is computed. The value of c_{Et} may be computed in the channels for various sets of values ($U_{tm} = q_m/h$, h) i.e. for those sets (q_m, h) for which q_m represents the maximum annual value of tidal flux per unit of channel width and h is the depth. Similarly, the value of c_{Ew} could be computed in the shallow water areas for various combinations ($U_{tm} = H \cdot \sqrt{g}/(2\sqrt{h})$, h, γ) i.e. for various combinations H_m, h, γ, where H_m is the maximum annual wave height and $1/2\gamma$ the persistence of wave motion in that area.
The interesting aspect is that the values of q_m, γ, h can be computed through an hydrodynamic tidal model and with a wave generation model (see Ruol and Sclavo, 1996). It is in addition interesting to consider that (differently from U_m and U_{wm} such values are not much dependent on local variations of depth determined by erosion or accretion and by sea level rise or subsidence, being much more related to the large scale characteristics of the lagoon, i.e.: dimension of tidal basins, width of channel subject to tidal motion (as far as q_m is concerned); wind speed, extension and depth of the fetch area (as far as H_m, γ, are concerned). The computation of H_m, γ, q_m should not be undertaken very often, unless we want to consider such drastic human induced modification of the lagoon extension.
The computation of c_E through formulas may be subject to various simplifications. Such formulas, on the other hand may be calibrated by using morphological and granulometric information about the lagoon.

7.6.3 Applications

Simple normalised case

To illustrate the working of the model a simple normalised case is considered: all the system variables have the equilibrium value unity, all the relevant coefficients have the value unity. The ASMITA model consists of the five elements which are described in the above. The system is disturbed from the equilibrium by giving one or more of the variables an initial value different from the equilibrium value unity. Also the case considered is symmetric, i.e. the two coast elements are identical. The results of a

number of simulations are discussed below. The following observations have been made:
If only one of the elements in the system is disturbed from equilibrium, the system reacts quickest if the disturbed element is the coast (Figure 7.19) and slowest if the disturbed element is the tidal flat (Figure 7.20). The disturbance for the coast equals a decrease of 10% and for the flat a decrease of 20%. A simple explanation for this is that the coast is the nearest to the outside world and the tidal flat is furthest from the outside world.

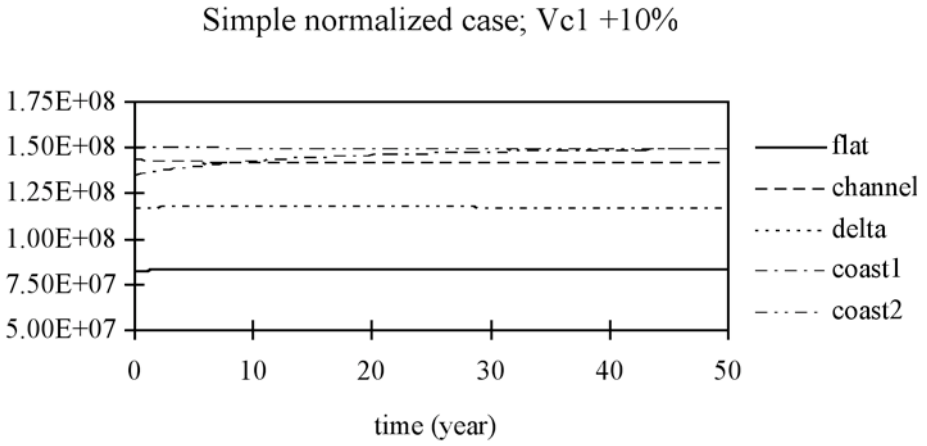

Figure 7.19 Initial volume of coast1 is decreased with 10%

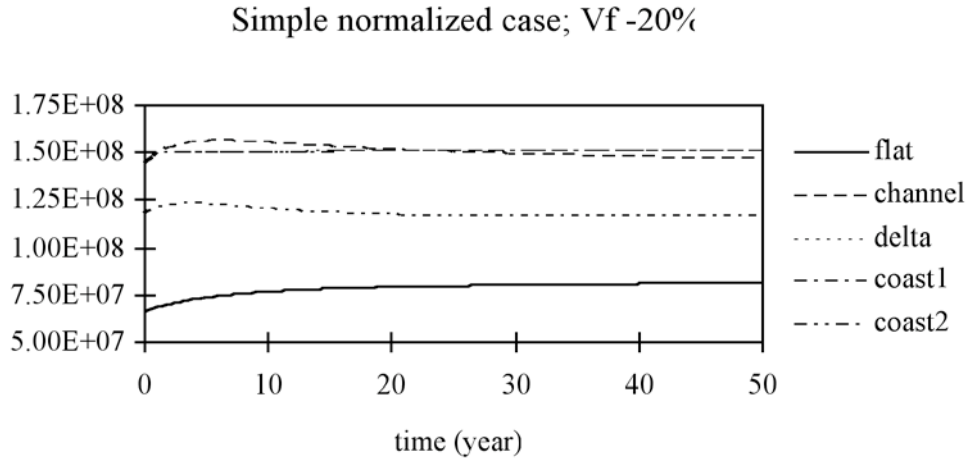

Figure 7.20 Initial volume of tidal flat is decreased with 20%

More than one time scale can be identified in the response of the system to the disturbance. The first reaction of the system with the smallest time scale is related to the diffusion of the disturbance to the other elements. This causes disturbances in all other elements in the system. Later all the disturbances are damped out with a much larger time scale. In fact it can be shown mathematically that the number of time scales in the system is at least equal to the number of elements in the system. For the present case

there are thus at least four different time scales[3]. This behaviour does not agree with the assumption in many empirical models that the disturbance in an individual element is damping out exponentially.
The system reacts quickest when two neighbouring elements have the opposite disturbance. For instance the case where the channel and the ebb tidal delta have been disturbed in the opposite direction (Figure 7.21). Both the volumes of the ebb-tidal delta and the channel are enlarged with 10 million cubic metres. The dominating reaction of the system in this case is the compensation of the disturbances in the two elements between each other. The two undisturbed elements, the tidal flat and the coast, almost do not feel the disturbances. It is also noticed here that the reaction of the ebb tidal delta is faster than that of the channel in the basin although the magnitude of both disturbances are similar. It should be noted that such a case occurs when the tidal basin is made smaller by e.g. reclamation or closure. The decreased basin area causes a decrease in the tidal volume which means that the equilibrium values of the channel volume and the ebb tidal volume decrease. In other words the channel will tend to be deposited and the ebb tidal delta tends to be eroded.

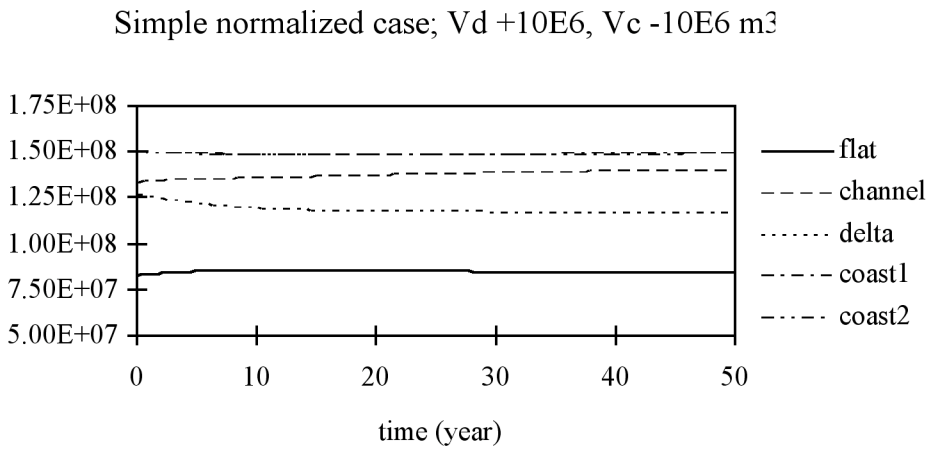

Figure 7.21 Initial volume of both delta and channel enlarged with 10 million cubic metres

Friesche Zeegat

A first realistic application of the model is the application of the model for the Friesche Zeegat along the Dutch Wadden coast. The five-element model ASMITA is calibrated for the development of the Zoutkamperlaag Inlet (Figure 7.22) since the closure of the Lauwerszee in 1969. As a result of the closure both the channel and the delta are too large.

[3] In the linear approximation, i.e. for small disturbances around the equilibrium, there are exactly four time scales; under non linear regime, i.e. for large disturbances around the equilibrium, "additional" time scales appear.

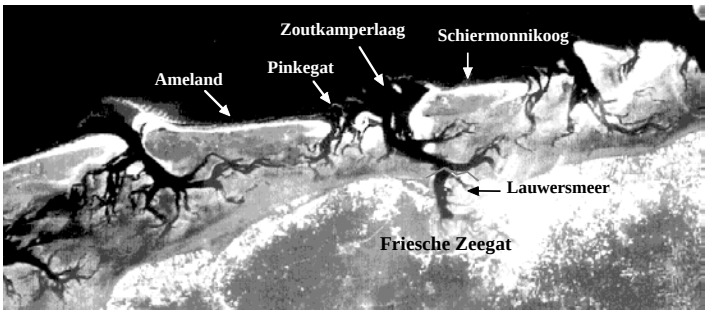

Figure 7.22: The Friesche Zeegat consists of the Zoutkamperlaag and the Pinkegat Inlet

For the calibration we used the data set of Biegel (1993) for flat and channel and the data set of Oost (1995) for the ebb-tidal delta. Table 7.2 shows some characteristics of the Zoutkamperlaag Inlet before and directly after the closure and in the calculated equilibrium state.

Table 7.2: Characteristic values for the Zoutkamperlaag Inlet of the Friesche Zeegat

	before closure	equilibrium
basin data		
lagoon area at MHW A_b (10^6 m^2)	230	123
exchanged volume V per tidal cycle (tidal prism or flood volume) (10^6 m^3)	320	193
tidal range H (m)	2.25	2.25
channel data:		
channel area A_{ch} (10^6 m^2)	57	41.2
channel volume V_{ch} (10^6 m^3)	230	143
flat data:		
tidal flat area (10^6 m^2)	150	81.6
tidal flat volume (above MLW) (10^6 m^3)	170	83
delta data:		
delta area (10^6 m^2)	78	78
delta volume V_d (10^6 m^3)	145	117
coast1 or coast2:		
coast area (10^6 m^2)	25	25
coast volume (10^6 m^3)	150	150

The equilibrium volumes are calculated with the equilibrium relations for the flat between MLW and MHW (Eysink, 1990):

$$V_{fe} = \alpha_f \cdot A_b \cdot H \tag{7.91}$$

for the channel below MLW (Biegel, 1993):

$$V_{ce} = \alpha_c \cdot P^{1.55} \tag{7.92}$$

and for the delta (Biegel, 1993):

$$V_{de} = \alpha_d \cdot P^{1.23} \tag{7.93}$$

The coefficient α_f depends on the tidal basin area at MHW. The original values and the used values of these relations are mentioned in Table 7.3.

Table 7.3: Coefficients of the equilibrium relations

Coefficients	original	used
α_f (-)	-	0.3
α_c ($m^{-1.65}$)	16 10^{-6}	20.5 10^{-6}
α_d ($m^{-0.69}$)	63.6 10^{-4}	75 10^{-4}

It is assumed that the coefficients of the used relations fall within the ranges of uncertainty. For the calibration the basic five-element model is used. We assumed a net discharge of 100 m^3/s along the coast in eastern direction. The developments in time of the five elements after the Lauwerszee closure are presented in Figures 7.23 to 7.26. The model was calibrated to reproduce the observed changes in the volumes of the channels, the flats and the delta.

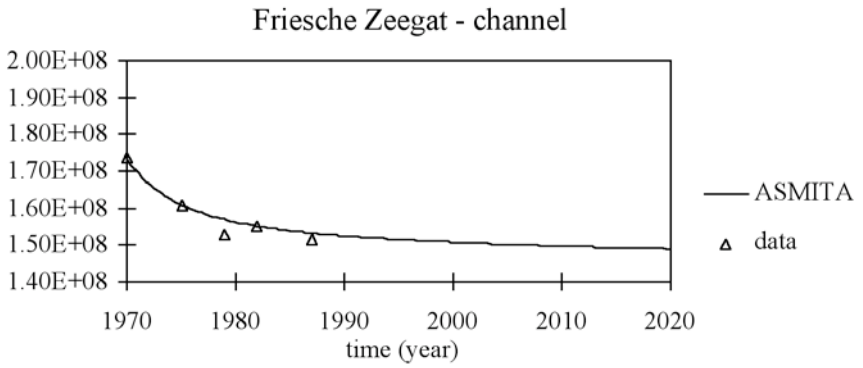

Figure 7.23: Development of the channel below MLW

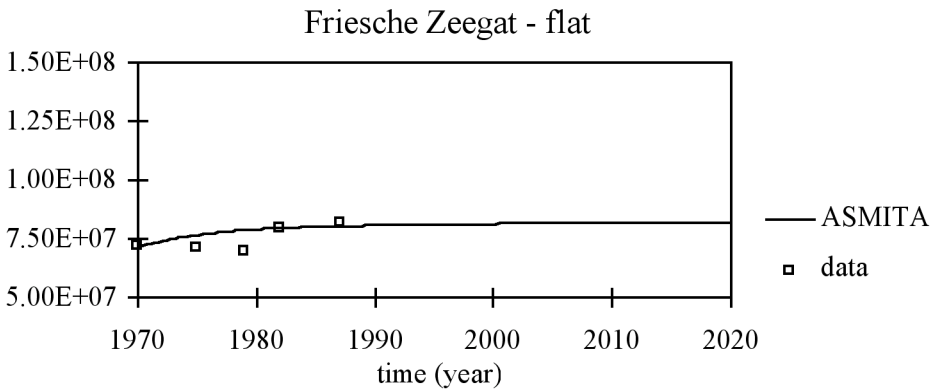

Figure 7.24: Development of the flat between MLW and MHW

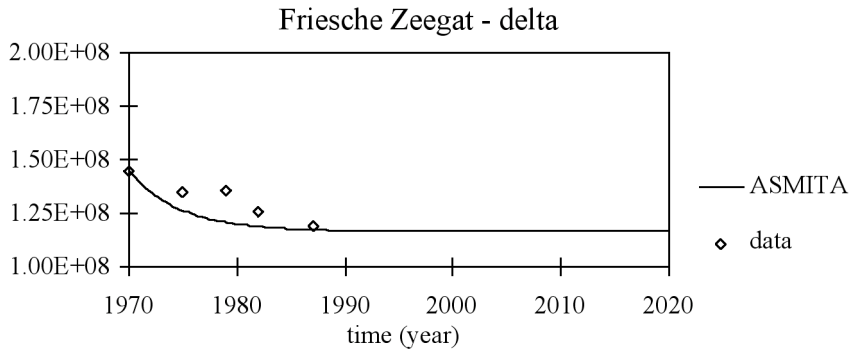

Figure 7.25: Development of the ebb tidal delta

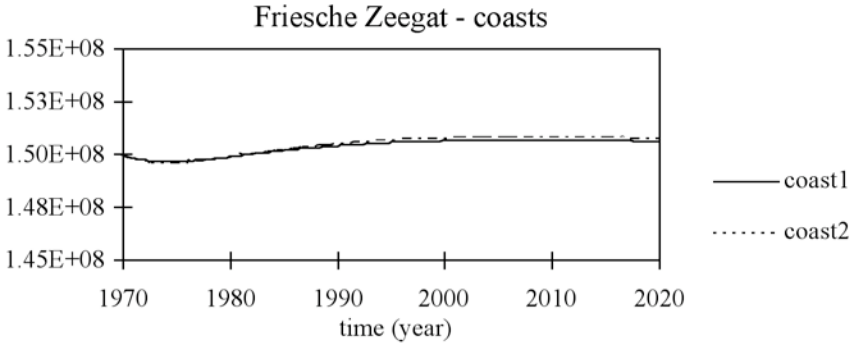

Figure 7.26: Development of coast1 and coast2

Our interpretation of the results is as follows. The ebb-tidal delta is too large, and much sediment is transported to the channel, which accretes. The larger ebb-tidal delta causes the coasts to accrete. The difference between the two graphs in Figure 7.26 is the result of the longshore net discharge.
Some remarkable observations of the results may be made, which are in good accordance with observations:
The time scale of the first reaction of the system is less then 10 year, corresponding with a rapid erosion of the ebb tidal delta and a rapid sedimentation in the channel.
After 20 years, the system is still not in equilibrium although the disturbances in the ebb tidal delta and the channel have almost been damped out.
The slow extension of the tidal flat in the basin has the largest time scale.
The first reaction of the adjacent coast is sedimentation and later followed by a much slower erosion.

Scardovari lagoon

In the framework of the earlier mentioned climate change project (see the Acknowledgements) a model application was defined for one of the lagoons in the southern part of the Po Delta, viz. Scardovari Lagoon (Table 7-4). Available data for Scardovari Lagoon in the Po Delta were rather scarce. The inner channel network and the recent morphological evolution of the inlet was derived from bathymetric information, see Table 7-4. In Figure 7.27 a plan view of the Scardovari Lagooon is shown. The equilibrium state was calculated with the Wadden Sea relations, with $\alpha_c = 65$

10^6 $m^{-1.5}$ and α_d = 6.57 10^6 $m^{-0.69}$ (Eysink, 1990).

Table 7.4: Characteristics of the Scardovari lagoon

Scardovari	initial	equilibrium
basin data		
lagoon area at MSL A_b (10^6 m^2)	29.0	29.0
exchanged volume V per tidal cycle (tidal prism or flood volume) (10^6 m^3)	15.7	15.7
tidal range H (m)	1.28	1.28
channel data:		
total length (10^6 m)	18.0	18.0
average depth (m)	1.75	1.75
mean width (m)	150	150
channel area A_{ch} (10^6 m^2)	2.7	2.7
channel volume V_{ch} (10^6 m^3)	4.7	4.0
flat data:		
lagoon area at MHW (10^6 m^2)	30.0	30.0
lagoon area at MLW (10^6 m^2)	28.0	28.0
tidal flat area (10^6 m^2)	27.3	27.3
tidal flat volume (above MLW) (10^6 m^3)	22.7	22.7
delta data:		
active base over a slope of 1:100 (m)	7.0	7.0
longshore extension (km)	2.0	2.0
delta volume V_d (10^6 m^3)	4.9	4.7
coast:		
active base over 500 m cross-shore (m)	5.0	5.0
longshore extension (km)	2.0	2.0
coast volume (10^6 m^3)	7.5	7.5

From comparing the Wadden Sea equilibrium results with those of our crude estimates, we thus conclude that the equilibrium data are applicable to our case and are therefore adopted. Lacking validated information about the equilibrium flat volume we assume that the flats are in equilibrium in the case of the Scardovari lagoon.

The basic ASMITA model was applied to the Scardovari lagoon (Figure 7.28, Figure 7.29 and Figure 7.30). In this case the effects of longshore transport are neglected. In Figure 7.28 it is shown that the channel and delta volumes in the initial states are a little larger than in their equilibrium states.

It is management practice to dredge the channels for navigation and flushing purposes. To maintain its initial volume we adapt a scenario in which the channel is dredged with an interval of about 4.1 years. In Figure 7.28 it can be seen that the flat suffers mostly from the dredging. Much sand is transported directly from the flat to the channel. Because of the import of sand across the boundaries the small ebb-tidal delta starts to grow. As can be seen all elements develop to a new equilibrium.

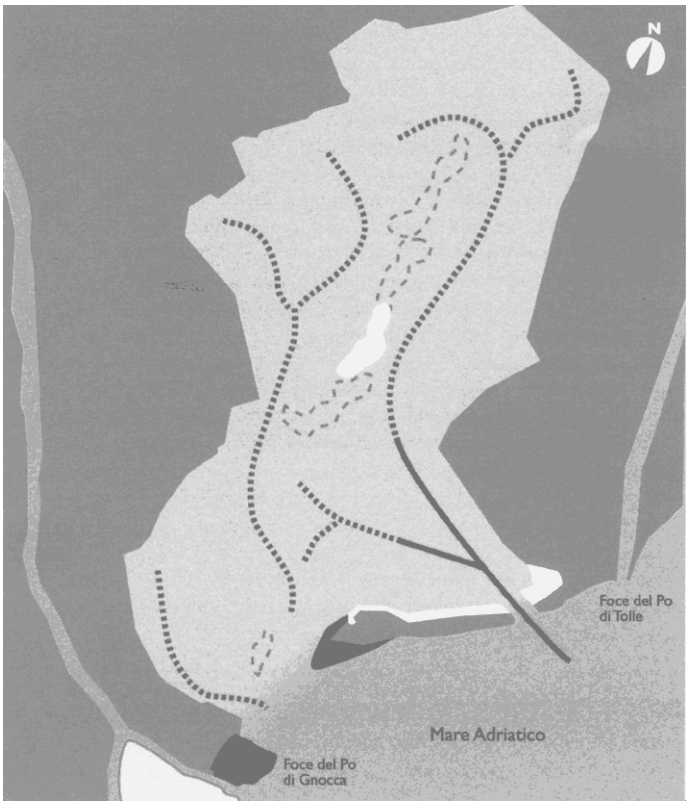

Figure 7.27: Plan view of the Scardovari Lagoon

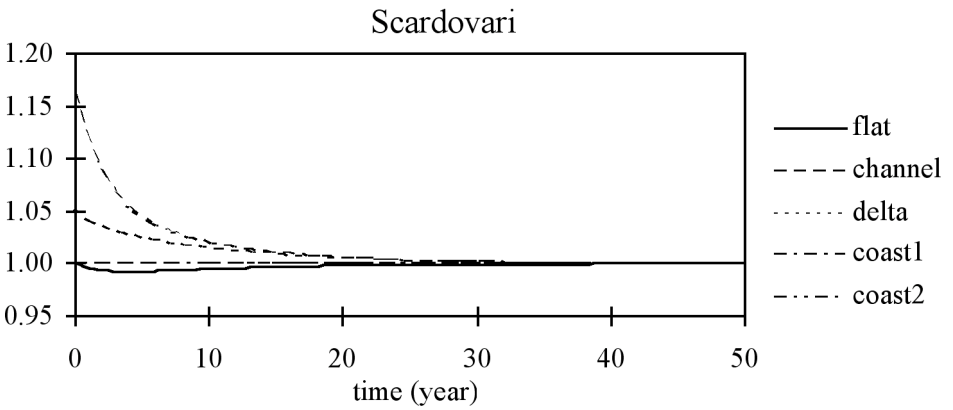

Figure 7.28: Applying the Wadden Sea relations to the Scardovari lagoon

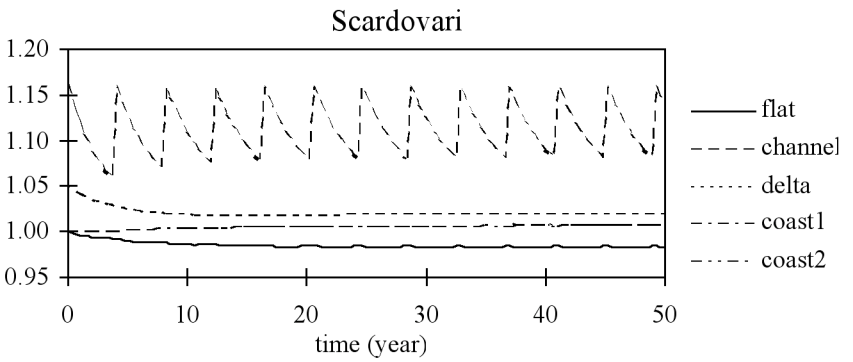

Figure 7.29: Dredging the channel of the lagoon Scardovari with an interval of 4.1 years

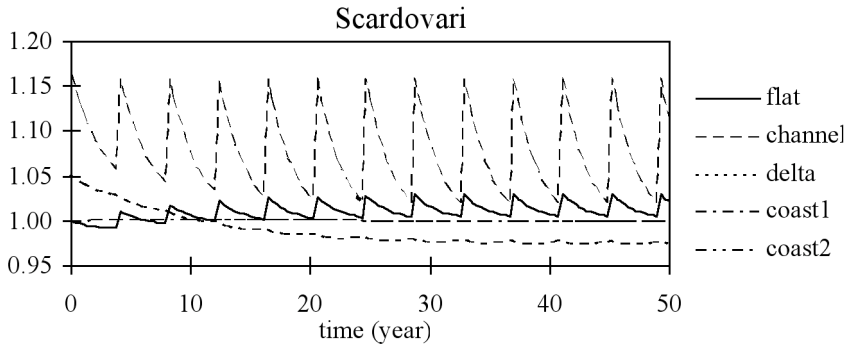

Figure 7.30: Dredging and dumping of sediment in the Scardovari lagoon

Another possible management practice is to dump the dredged sediment onto the tidal flats (Figure 7.30). As we can see in Figure 7.30 the delta is negatively affected by the dumping of sediment onto the flats. Because the import of sediment across the boundary is zero, the demand of sand of the channel affects also the delta. The volume of the flat increases as a result of sand-storage.
As regards the model-results we can conclude the following:
The smaller the lagoon the quicker the response time of the system to disturbances.
The time-scales of the system of the Scardovari lagoon are less then 10 year.
In the case of dredging only the time-scales are larger then in the case of dredging and dumping.
The attempt to enlarge the flat volume in small lagoons is cancelled out by the quick response of the small lagoon.

7.6.4 Discussion and conclusion

Since the Netherlands' Coastal Defence Policy Study published in 1990, the morphological interaction between tidal basins and their ebb-tidal deltas and directly adjacent coasts (e.g. as encountered along the Wadden barrier island systems) has been identified as a basically unknown physical phenomenon. The most accepted working hypothesis has been that the tidal channel and flat elements obey equilibrium or empirical transient relations (of a relaxation character) strongly depending on the tidal prism strength and independent of the ebb-tidal delta and adjacent coast morphological behaviour. The idea behind the latter assumption is that the morphological adjustment process of the basin overrules that of the other system elements, thereby demanding a time-varying net influx (in case of sea-level rise driven creation of sediment accommodation space), which is finally delivered by the adjacent coastal elements. The morphological behaviour of the ebb-tidal delta is assumed to be subordinate to that of the other two systems, such that in the case that the adjacent coast delivery capacity is temporally constrained the ebb-tidal delta acts as a sediment buffer. These hypotheses are based on sediment budget observations and interpretations over decadal time scales. On a relatively smaller spatial scale and in a relatively more wave-dominated environment like the Po Delta fringe, under the above mentioned working hypothesis, the observation of the conditions of the ebb-tidal deltas would allow us to assess the balance of on-going processes for long term protection and management strategies. As a necessary

prerequisite we should probably define the ebb-tidal delta more accurate as a distinctive morphological feature in wave-dominated environments.
Here we have presented an initial formulation of an aggregated-scale behaviour model for the interaction between tidal basin and its adjacent coastal environment, without adopting the a-priori assumptions described above. Necessarily so, the model combines observations and findings resulting from analogous model applications. It is based on existing field information and on generic modelling knowledge regarding tidal lagoons and basins on the one hand and wave-dominated coastal stretches on the other hand. Because of the time-scales of interest we consider the geophysical elements of the coastal fringe at an aggregated scale, e.g. single-inlet lagoons are schematised into two or at most three spatial units such as channel area, and (high and low) flats area. This leads to a box-type or lumped-parameter model, which is not new in tidal inlet processes modelling (Mayor-Mora, 1974). The new element in our approach is that we study the non-linear dynamic interaction between the lagoon elements, the submerged delta and the adjacent coastal sections.
This modelling approach should allow to determine the morphological response of the system to any imposed modification within the lagoon or along the coasts: for example new channel dredging or marshes creation within the lagoon as well as shore protection intervention along the outer region can be simulated and analysed. By means of the model application it is also possible to determine the impact of increased (or decreased) relative sea-level rise, of changes in wave climate and human-induced regulation of the tidal basin, the tidal inlet and the adjacent coast. The important aspect to consider is that the approach allows us to produce reasonable results with relatively poor initial information. A more complex modelling framework would not have produced better or more precise results. What remains to be done is to quantify, to the maximum possible extent, the uncertainty that, in our opinion, is a very time-scale related concept for such applications.

7.6.5 References

Ackers, P.; White, W.R., 1973. Sediment Transport: new approach and analysis. Proc. ASCE, J. Hydr. Div., v. 99, HY11, pp. 2041-2060.

Biegel E. J.; 1993. Morphological changes due to sea level rise in tidal basins in the Dutch Wadden Sea versus concepts morphological response model MORRES. Report IMAU-93.14. Institute for Marine and Atmospheric Research Utrecht, Utrecht University.

Bruun, P. (editor); 1978. Stability of tidal inlets. Elsevier Sc Publ Cy, Amsterdam.

Capobianco, M.; Stive, M.J.F.; Ruol, P.; 1996. Impact of Climatic Change on Po Delta. Deltaic Fringe Modelling, MEDDELT Final Workshop, Venezia, Italy, Oct. 2-6.

De Vriend H.J.; 1996. Mathematical modelling of meso-tidal barrier island coasts. Part I: Empirical and semi-empirical models. In press.

Di Silvio, G.; Teatini P.; 1995. Evoluzione morfologica a lungo termine delle lagune a marea con granulometria non uniforme. Istituto Veneto di Scienze, Lettere ed Arti, Rapporti e Studi, v. XII, pp. 35-51.

Di Silvio, G.; 1989. Modelling the Morphological Evolution of Tidal Lagoons and their Equilibrium Configuration. In Proc XXIIIrd IAHR Congress, Ottawa, Canada, pp 169-175.

Eysink, W.D.; 1990. Morphologic response of tidal basins to changes. Proc. Int Conf Coastal Eng., ASCE, New York, pp. 1948-1961.

Fokkink, R.J.; Karssen, B.; Wang, Z.B.; Van Kerckhoven, J. and Langerak, A.; 1996. Morphological modelling of the Western Scheldt estuary, this conference.

Jiménez, J.A.; Sánchez-Arcilla, A.; Gracia, V.; Valdemoro, H.I.; Nieto, F.; 1996. A conceptual model for the Ebro delta coastal behaviour, MEDDELT Final Workshop, Venezia, Italy, Oct. 2-6.

Mayor-Mora, R., 1974. Hydraulics of Tidal Inlets on Sandy Coasts. Proc. XIV Coastal Engineering Conference, ASCE, New York, pp. 1524-1545.

Oost, A. P.; 1995. Dynamics and Sedimentary Development of the Dutch Wadden Sea with Emphasis on the Frisian Inlet: a study of the barrier islands, ebb-tidal deltas, inlets and drainage basins. No.126. Universiteit Utrecht, Faculteit Aardwetenschappen.

Ruol P.; and Sclavo M., 1996. Wave and tidal current effects on a lagoon inlet. In: Partnership in Coastal Zone Management. Taussik & Mitchell Ed. 1996. Samara Publishing Limited, Cardigan, UK.

Wang, Z.B.; Karssen, B.; Fokkink, R.J. and Langerak, A.; 1996. A dynamic/empirical model for estuarine morphology, this conference.

8 Process-based simulation models of coastal inlets

8.1 Introduction

Mathematical modelling of tidal inlets can be based on either of the following strategies (cf. Terwindt and Battjes, 1990):

- down-scaling, which starts from large-scale field information on the system's behaviour and tries to unravel the underlying physical processes only as far as needed for good predictions. This approach is followed in most of the empirical and semi-empirical models which are discussed in the companion chapter.
- up-scaling, which starts from the observation that tidal inlet behaviour, however large-scale, is the effect of water and sediment motion. Hence it must be possible to simulate this behaviour with a model based on descriptions of the elementary hydrodynamic and sediment transport processes. The constituting equations of such a model are derived from conservation laws for wave energy, wave number, water mass, mean flow momentum and sediment mass. This process-oriented approach is the key element of the models which will be discussed hereafter.

Present-day computer capacity and the development of powerful software systems for the mathematical modelling of waves, currents and sediment transport have brought process-based mathematical simulation models of morphological evolutions within the reach of tidal inlet research. Yet, the literature on applications of this type of models to tidal inlets is far from abundant.
A possible explanation is that tidal inlets are extremely complex dynamic systems with a variety of processes and mechanisms. At this moment, they are insufficiently understood to be sure that the elementary physics incorporated in a simulation model are sufficient

to reproduce the phenomena of interest. Any simulation model, at one scale level or another, has to call upon "black-box" empirical or parametric submodels (cf. turbulence modelling, or wave-driven current modelling). This implies simplifications and approximations of which the long-term effects on the morphodynamic behaviour can hardly be overseen.
Process-based simulation modelling has not yet reached the stage in which one can claim that "everything" is in the model, and that it takes only a big computer to simulate large-scale behaviour.

8.2 ISE-models vs. morphodynamic models

Process-based simulation models consist of a number of modules which describe waves, current and sediment transport, respectively. Depending on whether the dynamic interaction of these processes with the bed-topography changes is taken into account, these modules are used in series or in a time-loop (see Figs. 1a and b, respectively). Models of this type essentially work at the hydrodynamic time scale (typically one tidal period). Larger time scales are reached by continuing the computations over a longer time-span.
Models which take the interaction with the topographic changes into account are called *Medium-Term Morphodynamic* (MTM) models. In principle, they are able to describe the meso-scale dynamic behaviour of a morphological system, such as the formation and migration of morphological features (channel shoaling or deepening, bar formation and migration, sandwaves, etc.). Models which don't take this interaction into account only describe micro-scale phenomena such as the sedimentation/erosion rate on a given bed topography. In the time-evolution of the system's state, this represents the initial changes. Therefore, this type of models is called *Initial Sedimentation/Erosion* models (ISE-models).
The above terminology is relative to the inherent morphodynamic time scale of the phenomena of interest. The term "initial" therefore does not imply that the results of such a model only provide a snapshot at the hydrodynamic time scale. In the case of large-scale evolution of an inlet system, for instance, the morphological time scale can be of the order of decades or centuries. Morphological changes over a few years at this large spatial scale may therefore be considered as "initial". The essence of ISE-models that the feedback of morphological changes on the water and sediment motion is negligible.
This may explain why, in spite of the inherent limitations of ISE-models, there is a demand for their practical application, especially to 3-D cases. Most of the practical tidal inlet problems belong to this category. The model is utilized to investigate wave, current and sediment transport fields in the area, and their response to projected interferences (engineering works, sand mining concessions, land reclamation projects, etc.). An example of such a case will be discussed in a later section.

Both the ISE- and the MTM-modelling process consists of a number of steps, such as

problem definition, formulation of objectives, analysis of physical processes, model set-up, model composition, input schematization and definition of runs, processing and visualization of results, verification, interpretation and reliability assessment of results, etc. In the following sections, some of these steps will be discussed in further depth, with the emphasis on specific aspects of tidal inlet modelling.

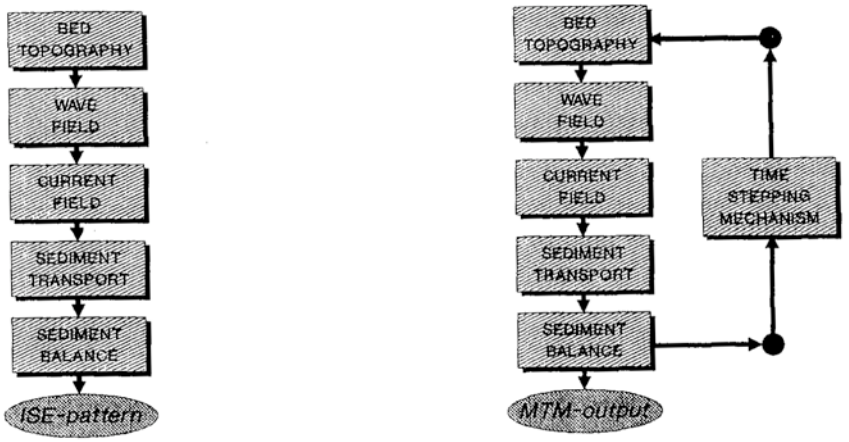

Figure 8.1: Aggregated flow charts of proces-base simulation models for tidal inlets, (a) Initial Sedimentation/Erosion models, (b) Medium-Term Morphodynamic models

8.3 Model composition

8.3.1 General

Both ISE- and MTM-models require a careful selection of the constituent models. Clearly, each of the relevant constituent processes has to be modelled adequately. This adequacy, however, is not only a matter of the process description per se, but also of the combination of modules which form the model as a whole. If, for instance, the wave model gives reasonable predictions of the wave height distribution, and the tidal model has been shown to reproduce water levels and current velocities within acceptable bounds, their combination does not necessarily give good results for the near-bed velocity which is put into the sediment transport model.

Especially in complex situations such as tidal inlets, the model composition ought to be the result of an analysis which starts from the objective of the study and its translation into phenomena to be modelled. This analysis should identify the relevant underlying processes and mechanisms, and assess the type of constituent models which is needed to describe them. The combination of constituent models which is ultimately chosen should be balanced from an efficiency and accuracy point of view, and it should not lead to spurious interactions or a blow-up of inaccuracies (cf. De Vriend, 1987).

Tidal inlets involve a number of specific aspects which need due consideration when modelling the constituent processes. In the following sections, the most important of these aspects will be discussed.

8.3.2 Aspects of wave modelling

The complex topography of the outer delta, with one or more deep ebb-channels and often a well-developed channel/shoal system on the fringe, leads to a much more complex wave field than an uninterrupted piece of exposed coast. The channels tend to convey the wave energy, and the shoals give rise to complex refraction patterns. Wave breaking and the associated current-driving force (radiation-stress gradient) are quite variable in space
and drive complex circulation patterns (Figure 8.2). In order to describe these phenomena, a spectral or semi-spectral (single-frequency) refraction model with directional spreading (the HISWA-model, for instance; see Holthuysen et al., 1989) will usually do for wide natural inlets. The computation of the wave-induced forces via the radiation stresses requires caution, in order to avoid large numerical errors (cf. Dingemans et al., 1987).
Inlets which are fixed by engineering works such as jetties and revetments are usually narrower (see many inlets at the east coast of the U.S.A.) and more reflective. This can lead to very complex wave patterns which can only be described if reflection and diffraction are included (cf. Kirby et al., 1994).

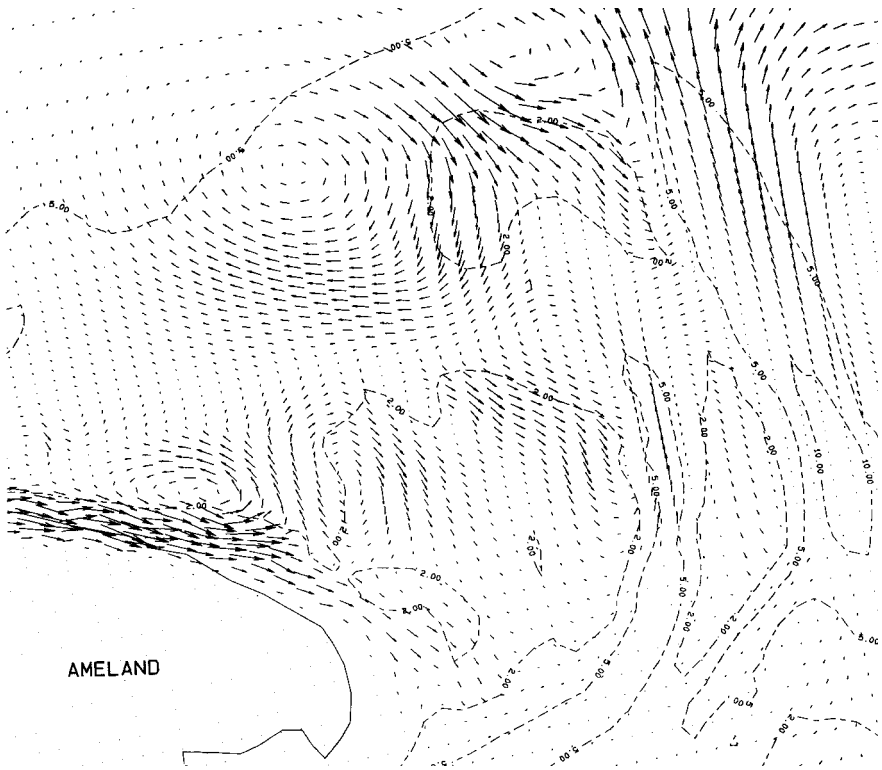

Figure 8.2: Residual circulation pattrens on the outer delta of the Frisian Inlet. (From: Steijn and Hartsuiker, 1992; courtesy DELFT HYDRAULICS)

Wave penetration into the basin mainly occurs via the deeper channels (Figure 8.3), where the waves experience less bottom friction and where they tend to be trapped by refraction. For the wide inlets considered herein, these phenomena are described reasonably well with the aforementioned type of (semi-)spectral refraction model.
The top level of the tidal flats inside the basin is the result of two opposing agents, viz.

tide (accretive) and wave action (erosive; see De Vriend et al., 1989). Since this level, as well as the wave conditions on the flats, are important factors to the ecosystem, the ability to adequately predict the waves in the intertidal zone will be a requirement in many applications. This means that the model has to include wave generation. Depending on the situation (exposure to sea waves, fetch inside the basin), it may also be necessary for the wave model to describe sea waves and locally generated waves together, i.e. to allow for a double-peaked spectrum.

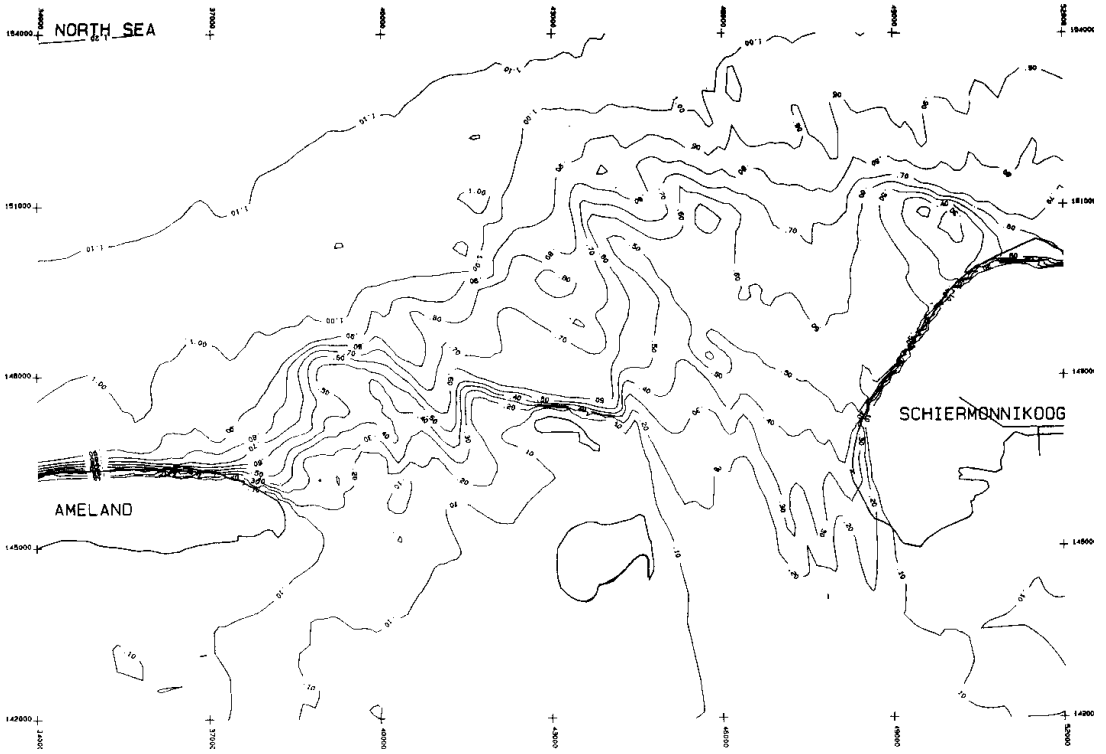

Figure 8.3: Wave penetration in the Frisian Inlet (From: Steijn and Hartsuiker, 1992; courtesy DELFT HYDRAULICS)

8.3.3 Aspects of current modelling

As sediment transport responds nonlinearly to the current velocity, the net transport through an inlet is quite sensitive to asymmetries in the tidal velocity and stage curves (Figure 8.4). One type of asymmetry concerns higher harmonics (overtides), which can be due to shallow-water effects, or to asymmetric flooding and drying of the intertidal zone (hypsometry-effect; cf. Pethick, 1980; Speer and Aubrey, 1985; Friedrichs and Aubrey, 1994). Another type concerns tidal rectification (subharmonics, residual currents), for instance due to inertial effects (ebb-jet), coriolis effects (ebb- and flood-branches of a channel), and topography-induced rectification (Bakker and De Vriend, 1995).

The latter phenomenon is related to the phase coupling between velocity and water level, due to which the residual current above low water tends to be flood-dominated and that below low water ebb-dominated. As the transport of sand through the channels is determined mainly by the near-bed velocity, this mechanism tends to export sand

through the channels.
Also storm surges can give rise to important asymmetries of either type. Although current measurements under storm-surge conditions are scarce, observations by fishermen suggest that surge-induced currents through the inlet can be so strong, that the tide does not even turn. Bathymetric surveys before and after such an event show large morphological changes, but if the inlet is sufficiently stable, these effects tend to be annihilated within a few months (Niemeyer, 1994, private communication). If the inlet is less stable, a major event can bring it into an essentially different state from which it does not return.

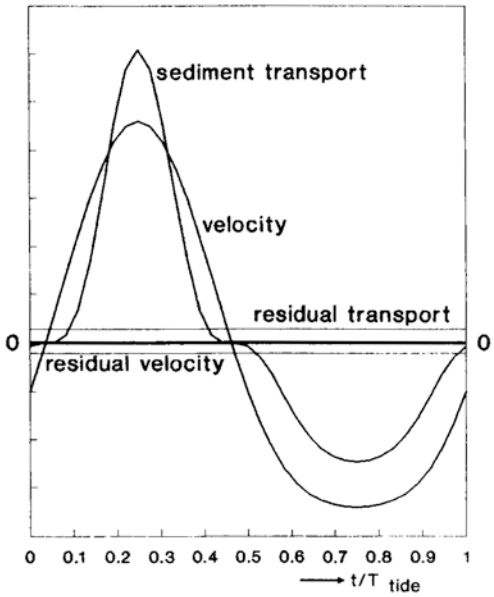

Figure 8.4: Tidal asymmetry, residual current and residual transport

The relative importance of these various sources of asymmetry depends on the situation and the time-scale which is considered. Van de Kreeke and Robaczewska (1993) show for the tide-dominated Ems-Dollard estuary that the contribution of the residual current to the long-term residual transport is even larger than that of the overtides.
A carefully calibrated 2-D depth-integrated model for combined tidal and wave-driven currents generally suffices to describe these phenomena, provided that it contains a flooding and drying procedure which takes due account of the hydrodynamics involved (i.e. not only based on mass conservation). In formulae, such a model reads

$$\frac{DU}{Dt} - f_c Vh = -gh\frac{\partial \zeta}{\partial x} + \frac{\tau_{wx}}{\rho} + \frac{F_x}{\rho} - \frac{\tau_{bx}}{\rho} + HDT \tag{8.1}$$

$$\frac{DV}{Dt} + f_c U = gh\frac{\partial \zeta}{\partial y} + \frac{\tau_{wy}}{\rho} + \frac{F_y}{\rho} - \frac{\tau_{by}}{\rho} + HDT \tag{8.2}$$

$$\frac{\partial \zeta}{\partial t} + \frac{\partial}{\partial x}\left(Uh + \frac{M_x}{\rho}\right) + \frac{\partial}{\partial y}\left(Vh + \frac{M_y}{\rho}\right) = 0 \tag{8.3}$$

in which

t	=	time,
x,y	=	horizontal cartesian co-ordinates,
U,V	=	x- and y-component of the depth-averaged velocity,
h	=	water depth below MSL,
ζ	=	water surface elevation above MSL,
D/Dt	=	material derivative, moving along with the depth-averaged flow,
f_c	=	coriolis parameter,
g	=	acceleration due to gravity,
ρ	=	mass density of the fluid,
τ_{wx},τ_{wy}	=	x- and y-component of the wind shear stress,
F_x,F_y	=	x- and y-component of the wave-induced effective stress,
τ_{bx},τ_{by}	=	x- and y-component of the bottom shear stress,
M_x,M_y	=	x- and y-component of the wave-induced mass flux.

Note that the wave effects are included via the wave-induced effective stress, the bottom shear stress and the wave-induced mass flux. The latter usually has a rather small contribution to the total velocity. It has to be included, however, if the wave-induced undertow is taken into account, e.g. via a $2\frac{1}{2}$-D approach (further see below).

Various types of 3-D currents are common in tidal inlets. Channel curvature and coriolis effects give rise to secondary circulations in the vertical, and also wave-induced mass flux and undertow play a part. These secondary flow components usually have a relatively weak contribution to the instantaneous sediment transport, but some of them are not changing sign during the tide, whence their relative contribution to the residual transport can be significant. Moreover, if these residual transport components have to be compensated by the downslope gravitational transport, their morphological impact can be large. An example of such a case is the formation of a point bar near the inner bank of a curved channel, to compensate for the net centripetal transport component due to the curvature-induced secondary flow.

Wang et al. (1991) investigate the role of secondary flow effects in a medium-term morphodynamic model (tide only) of the inlet "Het Friesche Zeegat" (Frisian Inlet) in the Dutch Wadden Sea (see Figure 8.5). They find that secondary flows, curvature-induced as well as coriolis-induced, cannot be disregarded in such a situation. The morphological evolution near the tip of the updrift barrier island (Ameland), for instance, is predicted essentially wrong if the curvature-induced secondary flow is disregarded. Also channel migration is likely to be influenced by secondary flow effects.

A rather efficient way to include these effects is a "$2\frac{1}{2}$-D" approach, in which the results of a 2-D depth-averaged flow computation are used in 1-D vertical profile models for the main velocity and the secondary flow (Kalkwijk and Booij, 1986). Depending on the input needed for the sediment transport module, this yields the total bottom shear stress or the total near-bed velocity as a function of space and time. This approach only works if the secondary flow velocity is much weaker than the main velocity. A more elegant and robust version is the "quasi-3D" approach, in which the 1-D profile models and the 2-D

depth-averaged model are intrinsically coupled (see Zitman, 1992, for tidal currents; also see De Vriend and Stive, 1987, for wave-induced currents).). Examples of $2\frac{1}{2}$-D and quasi-3D model applications to tidal inlets are described by Wang et al. (1991, 1995), for the basin and the gorge, and De Vriend and Ribberink (1988), for the outer delta.

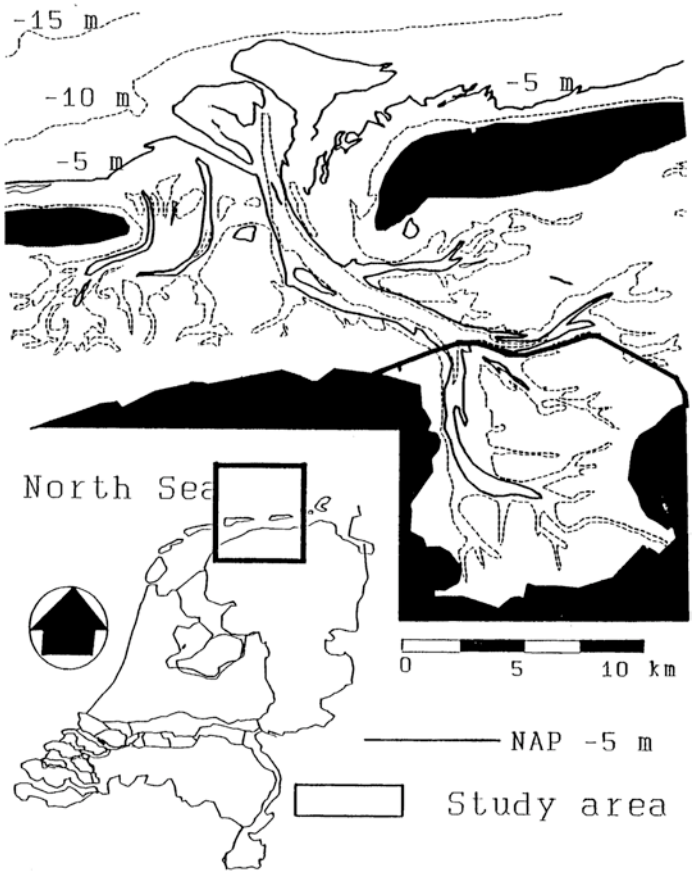

Figure 8.5: MTM-model of the Frisian inlet

8.3.4 Aspects of sediment transport modelling

Sediment transport can occur in various modes, roughly divided into bed load and suspended load. Sediment grains which are transported in the bed-load mode are in more or less continuous contact with the bed (sliding, rolling, jumping, fluidized), and they often move intermittently, between periods of being trapped in bed forms. In the suspended-load mode, the grains are held in suspension by turbulent diffusion. Modellers usually make a slightly different distinction, viz. between transport formulae and advection/diffusion models. Each of the largely empirical transport formulae relates the transport rate (bed load and some forms of suspended load) in a point to local parameters such as near-bed velocity, bed shear stress, critical shear stress, grain size, etc. Horikawa (1988) and Van Rijn (1989) give reviews of transport formulae for fluvial, estuarine and coastal applications.

In the case of a horizontal bed, the transport direction is assumed to coincide with the direction of the bed shear stress. If the bed is sloping, a downslope gravitational transport component deflects the transport direction. This component usually forms only

a small part of the total transport. Nevertheless it can have strong morphological effects, as stated before. Even if this is not the case, it is worthwhile to take this component into account in morphodynamic models, since it represents a natural smoothing effect on bottom perturbations (cf. De Vriend et al., 1993b).
The current-induced transport rate according to a transport formula is an odd nonlinear function of the near-bed current velocity. Thus a periodic velocity can give rise to a residual transport if there are higher harmonics. This residual transport has very little to do with the residual current velocity, it may even be in the opposite direction (Figure 8.4). If in a point all tidal constituents are given, and the M_2-component is predominant, it can be shown that only M-constituents contribute significantly to the long-term residual transport (Van de Kreeke and Robaczewska, 1993). All other constituents have a frequency which differs from an exact multiple of the M_2-frequency, whence their interaction with the M_2-constituent leads to time-modulations and a zero mean contribution in the long run.
Yet, it is not sufficient in a tidal inlet model to impose the net current, the predominant tidal constituent and its overtides at the open boundaries. Due to the complex flooding and drying topography, each constituent generates residual currents which do contribute to the residual transport.
Advection/diffusion models for suspended load transport usually concern the sediment concentration. Their basic form reads

$$\frac{\partial c}{\partial t} + u \cdot (\nabla c) - w_s \cdot (\nabla c) = \nabla \cdot (D \nabla c) \tag{8.4}$$

in which

c = sediment concentration, by weight or by volume,
∇ = gradient vector,
u = current velocity vector,
w_s = settling velocity vector,
D = turbulent diffusion coefficient.

These models reflect that in the horizontally uniform equilibrium state (zero gradients in time and horizontal space) the upward diffusive flux is balanced by the downward settling flux. Away from the equilibrium state, an observer who moves along with the current sees a tendency of the concentration to adjust to the equilibrium state. This means that the transport has a non-local character in space and time: the concentration in a given point depends on its history further upstream. The characteristic length and time scales involved in these lag effects can be estimated by (cf. Wang, 1992; Katopodi and Ribberink, 1992)

$$L_c = O\left(\frac{|u|h}{w_s}\right) \quad and \quad T_c = O\left(\frac{h}{w_s}\right) \tag{8.5}$$

in which

L_c = characteristic decay-length,

T_c = characteristic decay-time,
h = water depth,
$|\upsilon|$ = a representative measure of the current velocity,
w_s = magnitude of the settling velocity.

The characteristic time scale for sand with a settling velocity in the order of 10^{-2} m/s is usually less than 15 min., so much smaller than the the tidal period. The corresponding length scale is of the order of a kilometre, which is not small relative to the dimensions of channels and shoals. Spatial lag-effects should therefore be taken into account a suspended-sediment model for such a case.
This spatial lag-effect may explain how the tide can build up a shoal (Figure 8.6). When the flats are flooded, sediment-laden water from the channels moves up the shoals, where the velocity drops and the sediment tends to settle. Due to the lag-effect, the sediment is brought further up the flats. When the tide turns and the flats are drying, the water which comes from the flats contains little sediment when it reaches the channels. There the concentration tends to grow, but due to the lag-effect less sediment is brought back into the channels during ebb then has been carried up the flats during flood. This picture reverses in the presence of waves, which are much more effective in stirring sediment on the flooded flats than in the deep channels. In that case, the ebb flow from the flats contains more sediment than the flood flow towards them and the flats are eroded. Since accretion and erosion occur at different times, flats can only be in dynamic equilibrium.

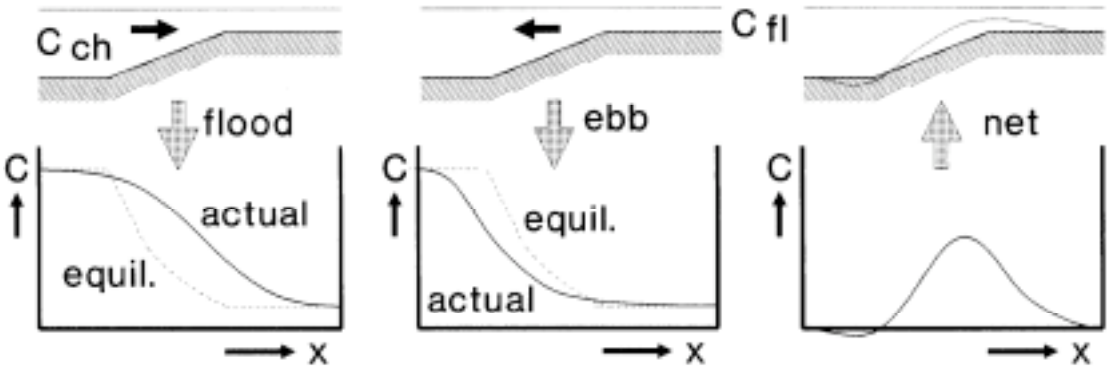

Figure 8.6: Shoal formation by tidal transport

The settling velocity of fine cohesive sediment is much smaller than that of sand. Hence the characteristic time scale of the adjustment process is of the order of magnitude of the tidal period or larger, and the length scale is of the order of the basin size or larger. An advection/diffusion model is therefore essential to describe the transport of this type of sediment. As a consequence of these large characteristic scales, the residual transport is determined by other properties of the tidal motion than in the case of sand (cf. Dronkers, 1986).
Apart from this, cohesive sediment behaves quite different from sand (for instance, see Berlamont et al., 1993, and Teisson et al., 1993). One specific complication of cohesive sediment is consolidation, which makes erodibility a function of the time elapsed since deposition. In a tidal environment, this introduces a time-hysteresis which can lead to

residual deposition (cf. Fritsch et al., 1989). In order to take this into account, a model should include an administration of the time since deposition of different bottom layers.

Lag-effects in suspended sand transport are sometimes taken into acccount via the depth-averaged equation

$$\frac{\partial(h\bar{c})}{\partial t} + \gamma \frac{\partial(\bar{u}h\bar{c})}{\partial x} + \gamma \frac{\partial(\bar{v}h\bar{c})}{\partial y} = -\alpha(\bar{c} - \bar{c}_e) \tag{8.6}$$

in which the overbars denote depth-averaging and

x,y = horizontal cartesian co-ordinates,

u,v = velocity components in x- and y-direction, respectively,

γ = ratio between the depth-avaraged sediment flux and the product of the depth-averaged velocity and the depth-averaged concentration,

α = decay coefficient,

c_e = equilibrium concentration, given as a function of flow and sediment parameters.

This is a very crude approximation which does not do much justice to the physical processes involved. A quasi-3D approach yields a physically much better founded equation of the type (Wang, 1992; Katopodi and Ribberink, 1992)

$$T_c \frac{\partial \bar{c}}{\partial t} + \frac{L_c}{|\bar{u}|}\left[\bar{u}\frac{\partial \bar{c}}{\partial x} + \bar{v}\frac{\partial \bar{c}}{\partial y}\right] = \frac{\alpha}{h}(\bar{c} - \bar{c}_e) \tag{8.7}$$

in which the decay parameters T_c, L_c and α folllow from a 1D-vertical model of the sediment concentration profile. An alternative to this quasi-3D approach is to solve the complete 3-D concentration equation (4). Van Rijn et al. (1991) describe such a model for current-borne suspended sediment.

The above models concern the wave-averaged current-borne transport. They may include the net stirring effect of waves, but they ignore typical wave-related mechanisms such as the residual wave-borne transport due to the asymmetry of the wave orbital motion, and the transport due to the wave-induced boundary layer streaming. These mechanisms play a part in wave-dominated environments like to outer delta and the adjacent island coasts. Too often, they are lumped under the heading "cross-shore transport mechanisms" and ignored as being too difficult to model.

In recent years, coastal morphological modellers have started to open this "black box", trying to simulate coastal profile evolution (cf. Roelvink and Broker, 1993). A fairly crude way to take these effects into account is to apply an intra-wave transport formula (e.g. Bailard, 1981). A more sophisticated approach is to model the suspended sediment concentration at the intra-wave level (Deigaard et al., 1986; also see Fredsoe and Deigaard, 1992). Obviously, it is not efficient to simulate tidal inlet morphodynamics at an intra-wave time scale. This problem can be overcome by running the intra-wave transport model for the full range of possible inputs and tabulating the resulting residual transport rates and directions as functions of input parameters such as wave height, wave

direction, wave period, current velocity, etc. This table replaces the transport module in the inlet simulation model (cf. Broker Hedegaard et al., 1993).

8.4 Input schematization and definition of model runs

The natural variability of input conditions such as waves, wind stress and storm surges poses a special problem to the practical operation of process-based simulation models. Firstly, running the model with real-time input is seldomly feasible, or even impossible if it concerns the future. In the case of ISE-models, running input time-series other than the tide does not make much sense. In the cae of MTM-models, which can have long intervals between two consecutive hydrodynamic updates with the complete wave and current models, the "pace" of the computation process seldomly coincides with the frequency of variation of the input conditions.
Therefore, the randomly varying input conditions have to be replaced by representative steady conditions (waves, wind), or a representative storm surge. This input schematization leads to a manageable number of input sets, each with its own probability of occurrence. The model is run for each set, and the results are weighted according to the probability of occurrence of the input, p_i. In the case of sediment transport, the nonlineariy of the system leads to weight factors which differ from p_i (cf. De Vriend, 1994). Criteria to determine these factors are, for example, the correct representation of the longshore drift on a given part of the coast, or the correct representation of the tidal transport capacity in another point of the model domain (cf. De Vriend et al., 1993a).
Note that the method of input schematization, the model runs to be made and the weighted composition of the results of the runs to predictions are mutually coupled. If the schematization principle changes, the weights will also change.

8.5 Validation

Validation is a continuous process during the entire course of a modelling project. It involves not only the verification of model results against measured data, but also other activities which contribute to the user's control of the model results, such as analyses of the system's behaviour in reality and according to the model, analyses of the effects of model simplifications, execution of test-runs on simple and verifiable cases, sensitivity analyses, etc.
In the case of long-term predictions, the empirical verification (i.e. against measured data after realization of the situation for which the predictions were made) is often impossible within a reasonable time. Hindcasts may help, but they are not always appropriate, since the model usually concerns future situations which are different from the past (otherwise, the model could just as well be replaced by a geostatistical extrapolation technique). Validation therefore depends to a large extent on other activities than empirical verification.
The possibility of empirical verification via hindcasts depends to a large extent on the quality of the available data. This goes for the wave, current and sediment transport fields and for the morphological evolutions. Process data should provide information of the

wave, current or sediment transport *patterns* on the complex inlet topography. Due to the strong spatial variability, isolated point values are of little use. Remote sensing techniques can possible offer new perspectives here, also for measurements under rough conditions, when it is impossible to send out vessels. Depending on the time scale of interest, it may be more useful to have a quick RS-scan of the bed topography every month than vary accurate depth soundings every five years.

8.6 Example of an ISE-model application

8.6.1 Problem definition

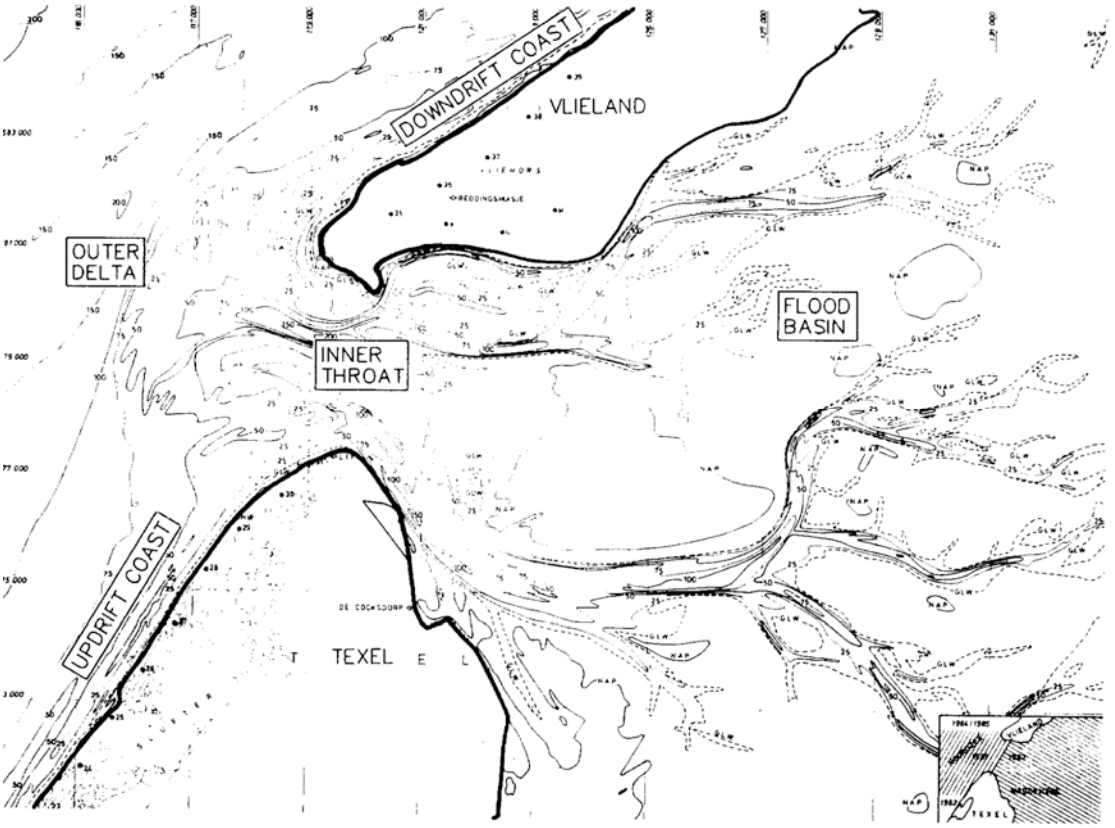

Figure 8.7: Texel case: situation

The northern tip of the isle of Texel, in the Dutch Wadden Sea (Figure 8.7), is subject to an erosion of some 5 10^5 m^3/yr. So far, the sand deficit has been replenished via beach nourishments, which releaves the symptoms of the problem, but does remove its causes. A historical reconstruction of the inlet evolution (Ribberink and De Vroeg, 1991) revealed that the sediment budget of the island tip is determined to a large extent by the course of the main ebb-channel, which used to changed more or less continually between NE-SW and SE-NW. When the main ebb-channel had a NE-SW orientation, large amounts of sediment were deposited in front of the Texel coast, whereas this coasts tended to be sediment-starved when the channel had a SE-NW orientation. Since in the last 50 years various engineering works have been made to protect the tip of the island,

the main ebb channel has stopped changing direction and has kept a SE-NW orientation. As a consequence, the isle of Texel keeps on eroding, and large amounts of sediment keep on being deposited on the vast beach plane which forms the tip of the next island, Vlieland.
As an alternative to an everlasting beach nourishment scheme, a long groyne near the tip of Texel was proposed (Figure 8.8). This groyne would trap the north-going longshore drift and thus cause accretion of the coast at its south side. The corresponding erosion at the north side could be dealt with by connecting the groyne with the exisiting revetment around the northernmost tip of the island. DELFT HYDRAULICS has carried out an extensive mathematical model study (Ribberink and De Vroeg, 1992) to investigate the effectiveness of various forms and locations of the groyne, the pattern and depth of scour around the tip, and the nature and extent of the effects on the inlet system.

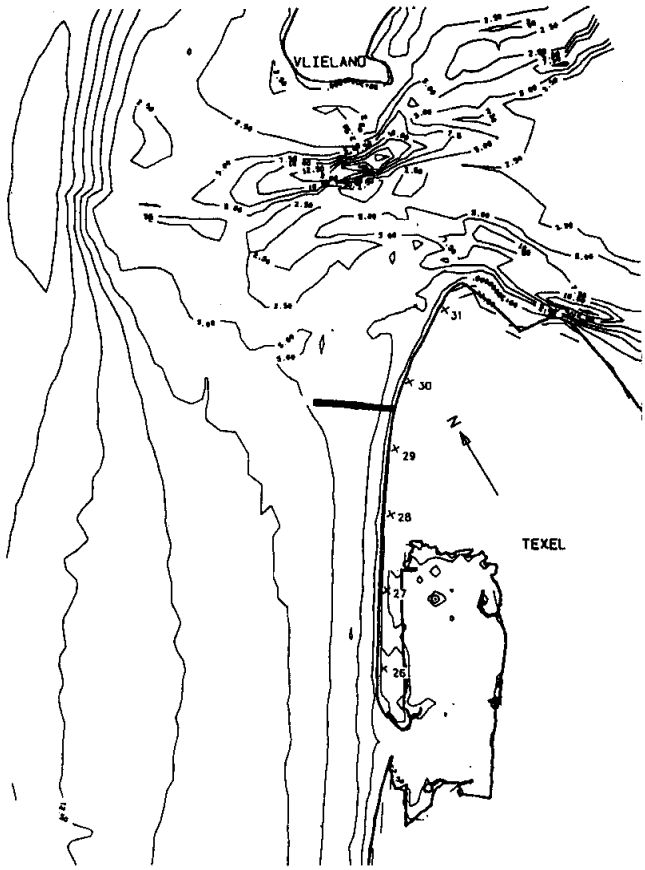

Figure 8.8: Texel case: one of the proposed groyne alternatives

8.6.2 Model composition

In order to predict the response of the inlet system to the cut-off of a sediment input of 5 10^5 m^3/yr, horizontally two-dimensional models are needed which describe the wave and current fields on a complex topography, including flooding and drying areas.
The wave field is assumed to be in equilibrium with the topography at any moment during the tide. The wave model has to include depth-refraction, shoaling and breaking. Since the spatial variations in wave height are strong, but not abrupt, diffraction is

probably less important. Because of the strong spatial variations of the current velocity, current refraction has to be included. Wind-induced growth and friction-induced decay are included in view of the large model area. In order to include some natural smoothing of wave-height variations, directional spreading is taken into account. The wave model which was used in this study is based on the HISWA-package (Holthuysen et al., 1989) and meets these requirements.
This wave model is run at 20 tidal stages, which are chosen such that they provide a maximum of information on the time-distribution of the wave properties. The water level and the tidal current velocity at each stage are derived from a larger-scale tidal model which covers the entire Dutch Wadden Sea and part of the North Sea and which is run without taking wave effects into account.
The current field is computed with a 2-D depth-integrated current model based on TRISULA-package (Stelling and Leendertse, 1992). It is basically a shallow-water tidal model, extended with (see Eqs. (8.1) through (8.3)).

- the wave-induced effective stresses, computed from the rate of wave-energy dissipation (Dingemans et al., 1987) via

$$F = D\frac{k}{\omega} \tag{8.8}$$

in which

F = wave-induced effective stress vector [N/m^2],
D = wave-energy dissipation rate [N/ms],
k = wave number vector [m^{-1}],
ω = peak frequency of the wave field [s^{-1}],

- wave-induced enhancement of the bed shear stress, according to a parameterized version of Bijker's (1966) bed shear stress model with $\xi = 1$ (cf. Soulsby et al., 1993).

The vertical structure of the wave-induced current (mass-flux compensation, undertow, boundary layer streaming), as well as the mass flux in the depth-averaged equation of continuity, is ignored because cross-shore transport mechanisms are also ignored. A first estimate of the importance of curvature-induced secondary flows led to the conclusion that these can be left out of consideration.
Estimates of the relevant sediment transport properties revealed that it must be possible to use a transport formula here. This formula should apply to situations with combined waves and currents. For reasons of feasibility, "cross-shore" transport mechanisms due to wave asymmetry, undertow, streaming, etc. are left out of consideration. The remaining current-borne transport (the waves and the current stir the sediment, the current transports it) is modelled with Bijker's (1971) formula. This formula has to be applied in each run at each of the 20 tidal stages and in each point of the computational grid. Clearly, this requires an efficient algorithm, which is achieved by parameterizing the formula.

8.6.3 Model domain

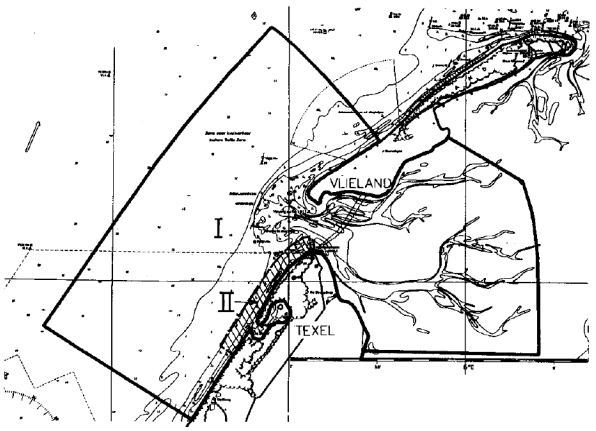

Figure 8.9a: Texel case: model domain. current and sediment transport models

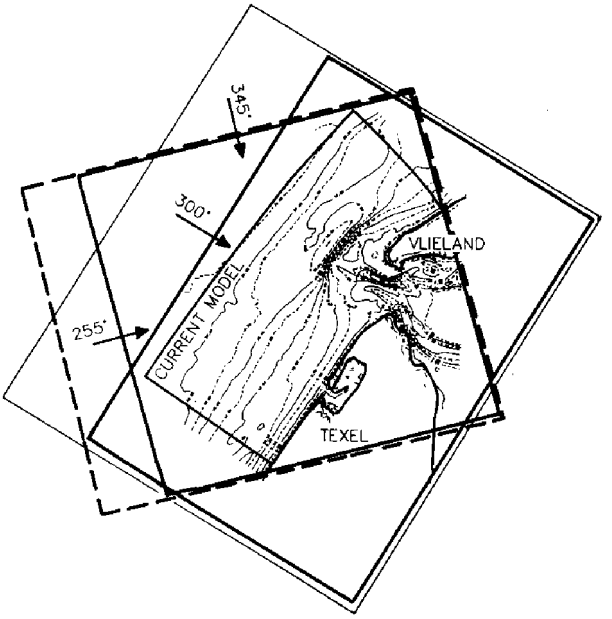

Figure 8.9b: Texel case: model domain wave models

The model domain is outlined in Figure 8.9a. Inside the basin, the boundary follows the watershed, which encloses an area of nearly 200 km^2. The island coasts form closed boundaries, which extend alongshore until "far away" from the inlet.
This longshore extent is generally chosen such, that the expected changes in the inlet are not felt at the open boundaries. This means that the boundary conditions can be the same before and after construction of the groyne. As a consequence, the seaward part of the model covers an area of some 240 km^2.
The version of the HISWA-model which is utilized here works on a rectangular grid of which the orientation of the grid lines in one direction coincides more or less with the direction of wave incidence. Since various angles of wave incidence are investigated in this study, there are various wave model grids, each of which encompasses the current-model domain (Figure 8.9b). In principle, the model works with three grids for each run, viz. an input-grid on which the bed topography is given, a computational grid, and an output-grid on which the output parameters are provided. Although the interpolations are fully automized, the variety of model domains requires extra administration, and thus it is a source of errors. Later applications of this model therefore work on the same domain as the current model.

Geometrical schematization

The wave computations are made on a rectangular grid, but the output can be given on any arbitrary set of points. Therefore, the sediment transport computations are made on the boundary-fitted curvilinear grid of the current model (Figure 8.10). This grid contains 117 · 121 = 14157 points, out of which some 4200 are permanently inactive because they are located on land. The grid size varies in space, with a minimum of 40 ·

125 m in the area of interest. Criteria for the grid generation are orthogonality (required by the current model), smoothness and spatial resolution.
Resolution-demanding parts of the model are the main tidal channels and the surf zones. Via the CFL-criterion, the small grid size in the surf zones leads to small time steps (30 s, which corresponds with a CFL-number of maximally 15).
The bed topography as represented by the bathymetric maps available was translated to the curvilinear grid using a discretizer. Another possibility would be a digital terrain model, provided that the criteria for grid and topography optimization be adjusted to the demands of a tidal model.

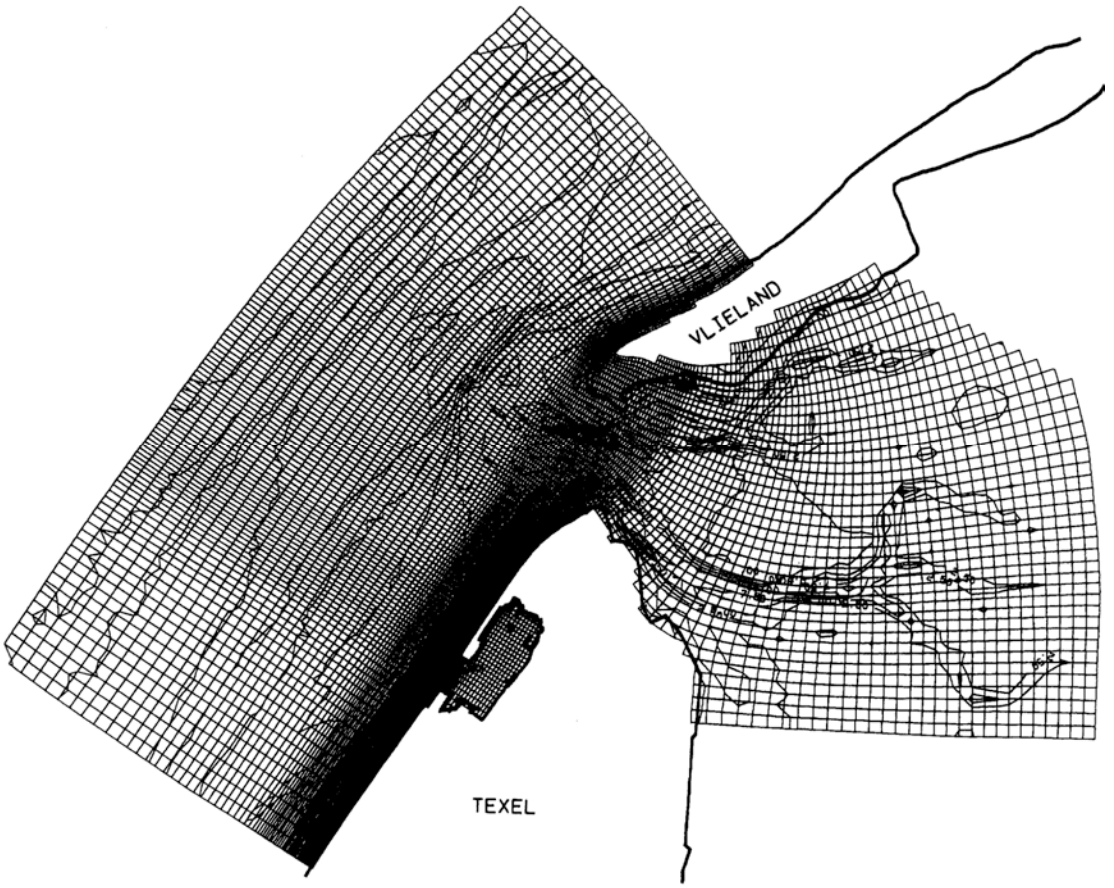

Figure 8.10: Texel case: computated grid of the current model

Boundary conditions

The boundary conditions for the wave model concern the wave height and direction at the upwind boundary. The wave energy is spread over the spectral directions according to a *cos*_-function. No boundary conditions are imposed at the lateral boundaries, which are assumed to be more or less parallel to the direction of wave propagation. Thus they are treated as wave rays, across which there is no net energy flux. All energy is supposed to be dissipated before the waves reach the landward boundaries, so there is no reflection and there is no need to impose boundary conditions there. This is consistent with the refraction approximation which underlies the model.
Tidal current models of this size are driven by the conditions imposed at the open

boundaries. The present model contains basically two open boundaries, one at the basin side and in the open sea. At the basin boundary and the NE part of the seaward boundary the waterlevel variation is prescribed, and at the SW and NW parts of the seaward boundary the tidal current velocity is imposed.
The wave-induced current is not driven at the boundaries, but by the effective wave-induced stress, $\boldsymbol{F}$, inside the domain. This means that this part of the current should be disturbed as little as possible by the boundary conditions. In practice, this means that a cross-shore boundary which intersects an area with a strong wave-induced current or set-up is usually treated as an axis of symmetry, with zero normal derivatives. The wave-induced contribution to the velocity or the water level distribution along such a boundary can be computed from a longshore uniform current or set-up model.

Representation of natural conditions

The model input has to be chosen such, that a reasonable estimate is obtained of the long-term residual transport field. Unfortunately, the relative importance of the transport-generating mechanisms varies through the model area, so an input schematization which is adequate in one point of the model domain is not necessarily adequate in all other points.
In order to tackle this unresolved problem, the pragmatic "multiple representative wave" approach (cf. De Vriend et al., 1993a) is used. This leads to the set of representative wave conditions which in Table 8.1.

Table 8.1. Representative wave conditions

name	compass angle	H_s	T_p	% occurrence
westerly	255°	1.48 m	6.7 s	39.2
northerly	345°	1.33 m	6.6 s	21.4
storm	300°	4.60 m	10.0 s	1.0
tide only	--	--	--	38.4

The method also yields a representative tide, with an amplitude some 10% above the mean. A tide of this amplitude which had already been simulated with the ambient tidal model for the entire Wadden Sea is the astronomical tide of 21 March 1976. Therefore, this tide was chosen as the morphologically representative one.
For each situation, viz. without groyne, or with one out of various alternative forms of groyne, the number of wave-model runs is 60 (3 sectors · 20 tidal stages), and the number of current-model runs is 4 (tide only and 3 wave conditions).

Parameter setting and validation

Some of the modelparameters are chosen on the basis of professional judgement, others are calibrated against known properties of the system. Examples of the former kind are the coefficients in the wave-energy dissipation model, the bottom friction factor in the wave model, and Manning's n (0.027) and the eddy viscosity (2 m^2/s) in the current model. Note that the latter value has little to do with the physical eddy viscosity: it mainly accounts for effects of the horizontal discretization.
Important elements of validation are the long-term residual total transport of sediment

through the inlet gorge, and the gap of 5 10^5 m^3/yr in the nearshore sediment balance near the tip of the island. Other validation material is provided by a coastline model which is run with a very detailed representation of the wave climate, and by additional experiments with the present model with a detailed representation of the wave climate (Negen, 1994). These experiments made clear that the wave schematization technique yields reasonably good estimates of the residual transport throughout the model domain. In order to have the long-term residual transport through the gorge right, the tidal asymmetry effect had to be enhanced by amplifying the flood transport and reducing the ebb transport, both by 20%. The computed longshore drift is somewhat smaller than that computed with the coastline model. This difference is attributed to the wavle-climate schematization, and it is compensated by enhancing the weight of the transport due to westerly winds by a factor 1.7 and that due to northerly winds by a factor 2.6 [4].

Large-scale processes without groyne

The first model application concerns the analysis of the hydrodynamic and sediment transport processes at work around the inlet. Figure 8.11 shows a typical result, based upon the weighted sum of results from the various model runs. These results are interpreted in terms of sediment drift patterns, so at an essentially higher aggregation level than the individual transport vectors.

Figure 8.11 shows a pronounced ebb-dominated transport in the main ebb channel. The sediment is deposited at the edge of the outer delta, from where it is removed understorm conditions. Furthermore, there are distinct flood-dominated transports near the island tips, in the case of Texel somewhat offshore. Between this flood "channel" and the coast there is a weakly developed ebb channel and a pronounced longshore drift into the inlet. One reason why this longshore drift is so pronounced is the orientation of the coastline, which is by no means perpendicular to the predominant incoming wave direction. Another reason is the presence of the outer delta, which shelters the island tip from high northerly waves. Thus the westerly waves and the associated NE-bound longshore drift are predominant there. Once the drift enters the inlet, the tidal current takes over and brings the sediment via the ebb-dominated main channel towards the edge of the delta and from there mainly to the tip of the other island.

The storm-induced transport pattern is quite different from the weighted average one The representative wave heights in each sector are meant to yield a good approximation of the longshore drift at a straight exposed coast. The result is a rather moderate wave height (see Table 1), and waves which only break on the beaches and on the shoals of the outer delta. Storm waves, however, break on the delta edge and drive a strong onshore and longshore transport there (Figure 8.12). Clearly, these storm waves contribute significantly to the onshore "bulldozer effect", which counteracts the tendency of the tide to extend the delta further seawards.

---

[4] These factors are not alarming, since the original weights are proportional to the percentage of occurrence of the wave height. In view of the the nonlinearity of the transport formula, this proportionality is not quite realistic.

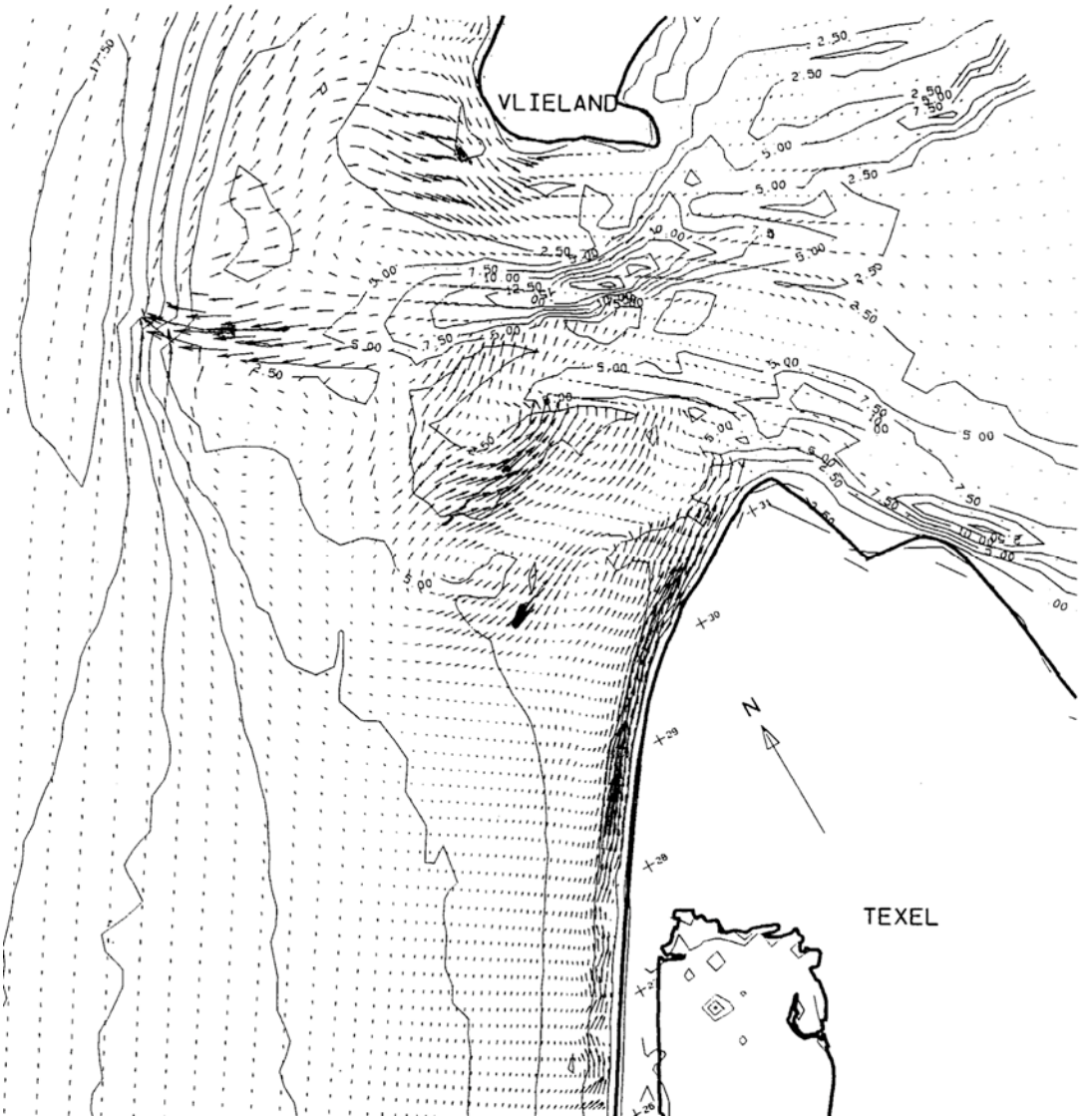

Figure 8.11: Texel case: yearly residual transport field

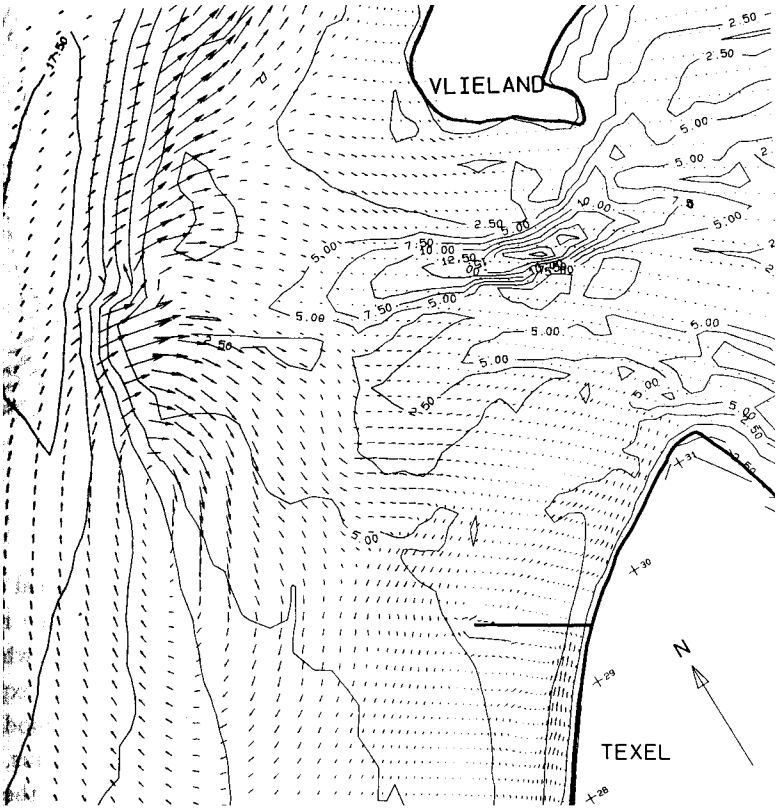

Figure 8.12: Texel case: storm induces transport field

Large-scale groyne effects

A long groyne perpendicular to the shore will interrupt the longshore drift. As a consequence, sediment will pile up at the updrift side, and erosion will occur at the downdrift side. At a fully exposed coast without a tide, this process would continue until the coastline has built out so far that the amount of sediment which bypasses the groyne is equal to the undisturbed longshore drift. In the present situation, also the tidal current moves around the tip of the breakwater and forms another bypass mechanism. As a consequence, the coastline is likely to build out less far. An ISE-model is unable to predict how much less, but it gives an indication of the bypass-potential of the tidal current. Figure 8.13 shows that this potential is significantly less than the longshore drift. This means that a substantial build-out of the coastline can be expected.

This is corroborated by the accretion/erosion patterns in Figure 8.14. Figures 8.13 and 8.14 also show that at the downdrift side the longshore transport picks up again, which leads to severe erosion. This effects is stronger the further the groyne lies from the island tip.

At the scale of the inlet as a whole, Figure 8.14 shows that the effects of the groyne are not restricted to its immediate vicinity, but that they extend all over the inlet. The nature of the effects does not become very clear, because the picture shows a sequence of erosion and deposition areas.

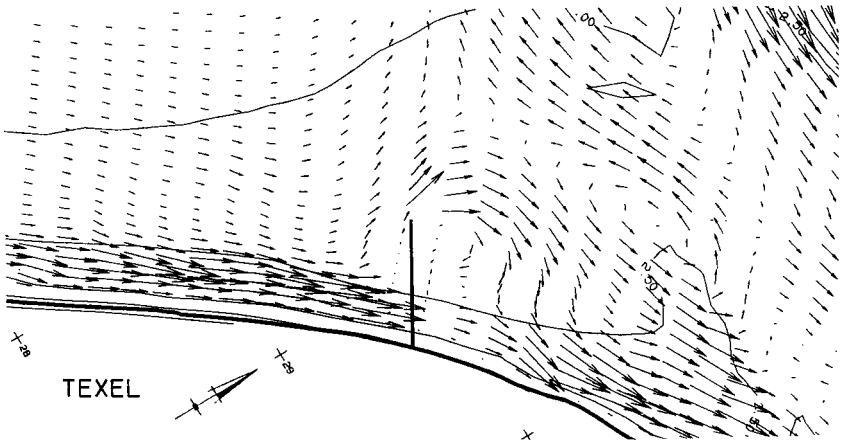

Figure 8.13: Texel case: transport around the groyne

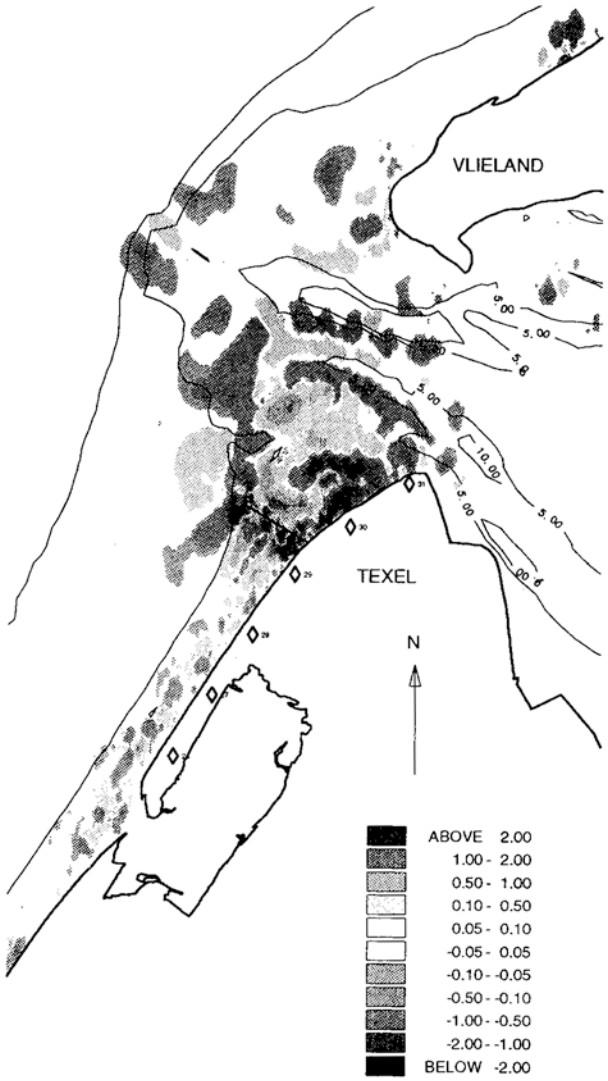

Figure 8.14: Texel case large-scale ISE-pattern

The latter phenomenon is typical for ISE-models. Morphological features have a strong tendency to migrate, but since ISE-models lack the morphodynamic interaction, they only show the onset of this migration, which is a coupled pair of erosion and deposition

areas (Figure 8.15). Moreover, experience with morphodynamic model applications shows that initially the model tends to remove irregularities from the given initial bed topography. Thus the topography is moulded into a generally smoother form which suits the model. From then on, a much slower and physically more realistic dynamic process takes place (cf. De Vriend et al., 1993b). Clearly, ISE-models represent the initial moulding process.

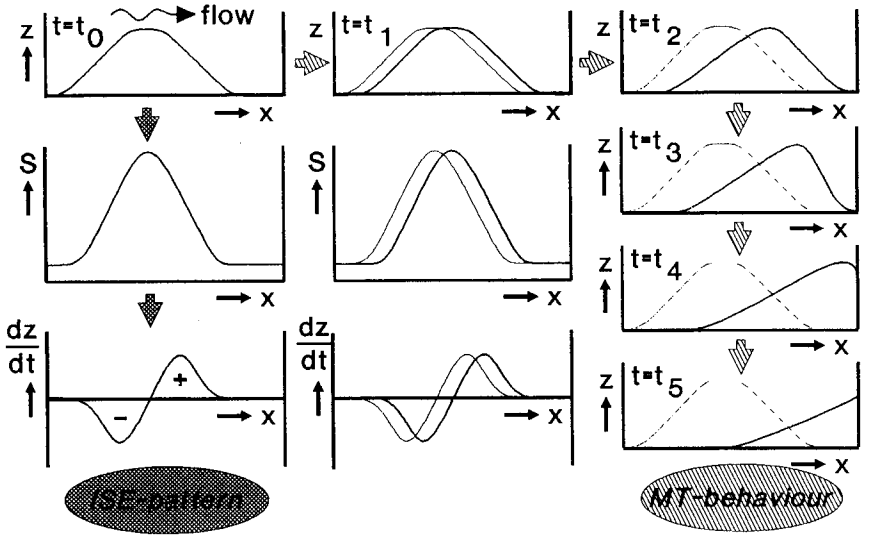

Figure 8.15: Migration of morphological features in ISE-models and MTM models

Local groyne effects

The principle near-field effect of the groyne is the formation of a scour hole near its tip. Again, the ISE-model results ought to be interpreted with care here. Instead of a single scour hole, Figure 8.14 shows a pair of erosion and deposition areas, with the transition exactly in front of the groyne. This might lead to the erroneous conclusion that the most severe erosion occurs at some distance from the tip, and thus to an underestimation of its threat to the structural stability.

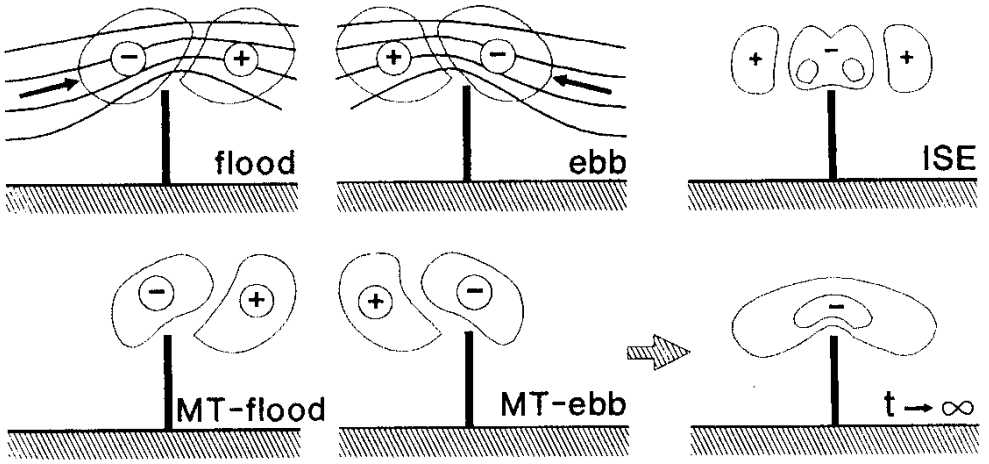

Figure 8.16: Morphological evolution around a groyne

Figure 8.16 explains what actually happens. Initial erosion occurs where the flow accelerates, deposition where it decelerates. In the longer run, however, the topography tends towards a state where the sediment flux through a streamlane is constant. In this situation the scour hole coincides more or less with the area of maximum velocity.

8.7 ISE-modelling practice

The concept of ISE-models is rather simple, at least if adequate wave, current and sediment transport solvers are available. Yet, the above example shows that their practical operation involves points of attention, such as

- software infrastructure (steering programme, data transfer system, pre- and postprocessing facilities, etc.). Efficiency and structure are important issues here, because many runs have to be made in order to cope with the natural variability of conditions.
- model composition, i.e. which combination of process modules should be applied in order to be able to achieve the objectives of the model study. ISE models pose specific problems here, because a limited number of "snapshot" runs has to provide sufficient information on the morphological evolution to be expected. On the other hand, unnecessary refinements lead to inefficiency and sometimes even to interpretation problems.
- geometrical schematization (model boundaries, grid definition, topographical schematization, etc.). Many choices and trade-offs have to be made here. One example is grid resolution vs. computer costs.
- input schematization, in order to have a manageable number of runs representing the whole spectrum of possible combinations of relevant input conditions (mean water level, deep-water wave height/period/direction, tidal constituents, etc.). This schematization is closely linked to the number of model runs to be made and to the derivation of quantitative predictions from the results of these runs.
- data transformation, if the various modules operate on different grids and in different domains (cf. the wave models in the above example). Unless special techniques are applied, data transformation gives rise to a loss of accuracy.
- interpretation of results. This is a particularly challenging part of ISE-modelling,as may have become clear from the above example (also see Section 9).

In practice, the main use of ISE-models lies in the analysis of residual tansport patterns under various conditions, and in the prediction of their reponse to large disturbances such as engineering works, land reclamation, sand mining, subsidence due to oil/gas-mining, etc. ISE-models are not suited to analyse the subtle balance of processes in an inlet system in (near-)equilibrium.

8.8 Specific aspects of MTM-modelling

MTM-models of tidal inlets will often be used to predict the effects of accelerated mean

sea-level rise, enhanced subsidence due to oil and gas mining, land reclamation, sand mining, coastal nourishments, engineering structures, etc. Many of these disturbances boil down to source or sink terms in the sediment balance equation:

$$(1-\varepsilon_p)\frac{\partial z}{\partial t}+\frac{\partial S_x}{\partial x}+\frac{\partial S_y}{\partial y}=-\frac{dMSL}{dt}-\frac{dz_{ref}}{dt}+\Phi_{dep}-\Phi_{er} \tag{8.9}$$

in which

MSL = mean sea level [m/yr],
z_{ref} = reference bed level (subsiding) [m],
Φ_{er} = deposition flux (e.g. nourishment) [$m^3/m^2/yr$],
Φ_{dep} = ersoion flux (e.g. mining) [$m^3/m^2/yr$].

These terms give rise to a forced response of the system, on top of the inherent behaviour which is present, anyway.

The numerical integration of the sediment balance equation may seem to be simple and straightforward, and so it is if the transport field is known. In an MTM-model, however, the equation is included in a time-loop, due to which there is a feedback of z on $\boldsymbol{S}$. As a consequence, the numerical problem becomes much more complicated and instability-prone. One-step explicit schemes are the most convenient in this case, and schemes of the Lax-Wendroff type turn out to be the most robust (cf. De Vriend et al., 1993b; also see Peltier et al., 1991). Like other explicit schemes, they involve a CFL-type stability criterion.

As the tidal computation is usually the most time-consuming, minimization of the number of its calls is an effective way to reduce computer costs. One rather robust technique to achieve this is the "continuity-update" (see Figure 8.18 for its incorporation in the flow chart), which reads in its simplest form

$$(\overline{uh})_{t+\Delta t}=(\overline{uh})_t \tag{8.10}$$

More sophisticated versions make use of the full equation of continuity. Tests with horizontally 2-D morphological models have shown that very significant savings of computer time can be achieved with this technique (Latteux and Peltier, 1991; De Vriend et al., 1993b).

The above technique does not include the momentum equations, so it does not take the dynamic interaction between the current and the bed topography into account. Thus the propagation character of morphological changes is ignored. This introduces systematic errors in the solution, which increase with the number of consecutive updates with this technique. However, analyses have shown that these errors tend to disappear as soon as the full hydrodynamic model is applied again. Thus the intermittent application of the full model and a number of continuity-updates yields acceptable results, also in the long run.

8.9 Examples of MTM-model applications

8.9.1 Texel case

The model system described in the foregoing has recently been extended to a morphodynamic simulation system. In essence, this boils down to feeding the bed level changes from the sediment balance equation back into the hydrodynamic and sediment modules (Figure 8.1b). This creates a time-loop which simulates the meso-scale morphodynamic behaviour of the inlet system.

Negen (1994) describes the application of this simulation technique to the Texel-case, be it with the groyne at a slightly different location. Figure 8.17 shows a typical result, after 1 year's simulation, all the time with the westerly waves (Table 8.1). The results generally confirm the effect of the groyne on the coastline position. Striking differences from the ISE-model results are:

- the formation of a channel along the downdrift side of the groyne,
- the deepening of the weakly developed NE-SW ebb channel near the tip of the groyne, and shoaling of the main ebb channel where this crosses the course of the NE-SW channel,
- the onshore migration of the shoals on the outer delta.

The first point indicates that further study is needed to design a stable groyne. The second finding may indicate that the groyne tends to promote the reorientation of the main ebb channel, back to the NE-SW position which is favourable for the sediment budget of Texel. The third observation shows that the present simulation is probably not represent full reality, because the mechanisms which tend to move the shoals offshore are underestimated.

In summary, this application shows the potentials of fully dynamic simulations of tidal inlet morphodynamics. On the other hand, the present case definitely requires further attention before definitive conclusions can be drawn from the simulation.

8.9.2 Frisian Inlet case

Another, less complicated application of a morphodynamic simulation model concerns the Frisian Inlet (Wang et al., 1991, 1995; see Section 8.5 of the companion chapter for a description of the situation). The objectives of this study were

- to hindcast the system's response to the closure of the Lauwerszee,
- to assess residual transport patterns, and
- to investigate channel migration mechanisms,

especially in the basin and the inner part of the gorge. This explains why this study could be undertaken with a model which did not include waves.

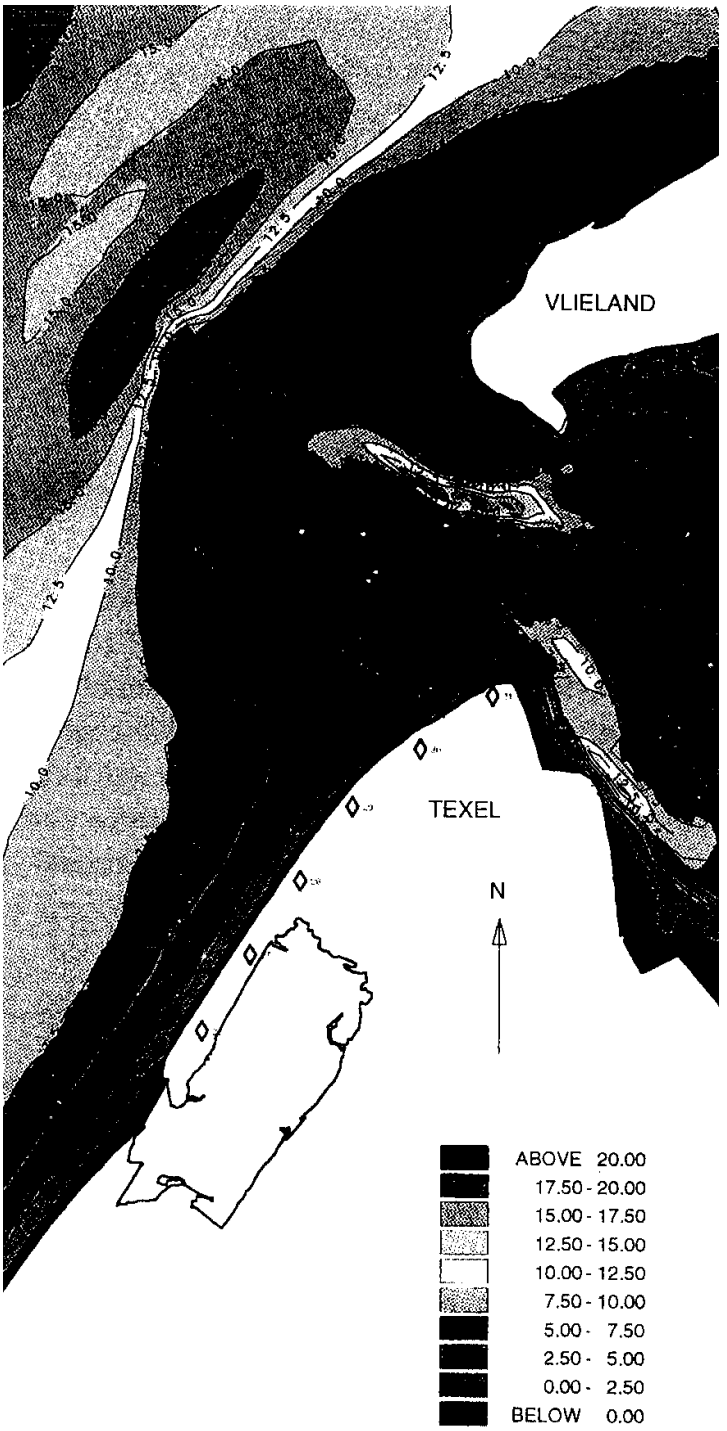

Figure 8.17: Texel case: morphological evolution after one year, according to an MTM-simulation with westerly waves (from: Negen, 1994: courtesy DELFT HYDRAULICS)

Figure 8.18 outlines the flow chart of this model, including a "continuity-update" technique to save computer time (see Section 8.8). The tidal module is essentially the same as in the Texel case, but extended to $2\frac{1}{2}$-D in order to take curvature- and coriolis-induced secondary flows into account. The sediment transport module is based on a $2\frac{1}{2}$-D advection/diffusion model for the concentration, with the equilibrium concentration derived from Van Rijn's (1984) transport formula (although other options are open). The choice of these modules was made on the basis of a number of orientating computations.

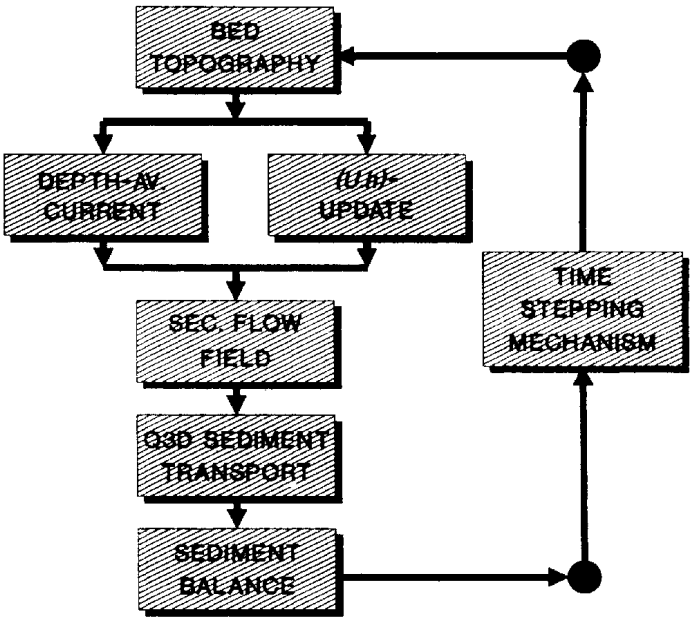

Figure 8.18: Frisian Inlet morphodynamic simulation model: flow chart

The model domain covers not only the area of interest, but also the outer delta and part of the open sea, in order to have the seaward boundary far enough away from the dynamic area to allow for the same tidal boundary conditions throughout the simulation. The schematization of the inlet geometry turned out to be critical for the system's morphodynamic stability. If the emerging shoal in the centre of the inlet, the Engelsmanplaat, is omitted, the system becomes unstable. One might claim that the model should be able to reproduce the formation of this feature if that is absent from the initial state. Closer investigation of the geological structure of the Engelsmanplaat (Oost and De Haas, 1993), however, revealed that it consists mainly of highly resistant pleistocene clay, i.e. it is not the result of a recent morphodynamic process. This feature therefore has to be included in the model as a permanent element.

As a consequence, the Frisian Inlet becomes a double inlet, with the Pinkegat subsystem in the west and the Zoutkamperlaag subsystem in the east. The large difference in size between these subsystems is reflected in a large difference in morphodynamic time scale. The model's morphological time step has to be based on the fastest evolving subsystem, the Pinkegat. Thus it is much smaller than necessary for the Zoutkamperlaag. Within the amount of computer time allotted to this model, the response of the Zoutkamperlaag could therefore only be simulated if the topography of the Pinkegat area was fixed. Clearly, such a drastic measure is bound to cause problems at the transition to the mobile-bed part of the model.

The seaward boundary conditions (tide, sediment transport) form another critical element. Disturbances due to errors or inconsistencies in these conditions are translated into bed level perturbations which tend to migrate into the model domain and sometimes even blow up. In general, a morphodynamic simulation requires one boundary condition, either to the transport or to the bed level, at every inflow boundary. This poses a special problem to tidal models, in which the open boundaries keep swapping between the inflow and the outflow type. This problem is largely unresolved, as yet, and definitely

requires further attention.
The model results obtained so far concern mainly the shorter-term phenomenon of channel formation and migration, especially in the Pinkegat area. The model, as well as field observations (Oost and De Haas, 1993; Oost, 1995) show a cyclic behaviour of the channel pattern (Figure 8.19), though at different time scales. This discrepancy is probably due to the absence of waves from the model. This leads to far too small transport rates, and hence to an overprediction of the morphological time scale. Yet, the character of the migration pattern is reproduced, which indicates that the model contains the right channel migration mechanism. Further analysis should reveal the details of this mechanism.
Another indication of the model's potential concerning channel formation follows from an experiment in which the initial bed topography was a strongly smoothed version of the measured topography. It turns out that the model tends to restore a channel/shoal system of a similar nature as before.

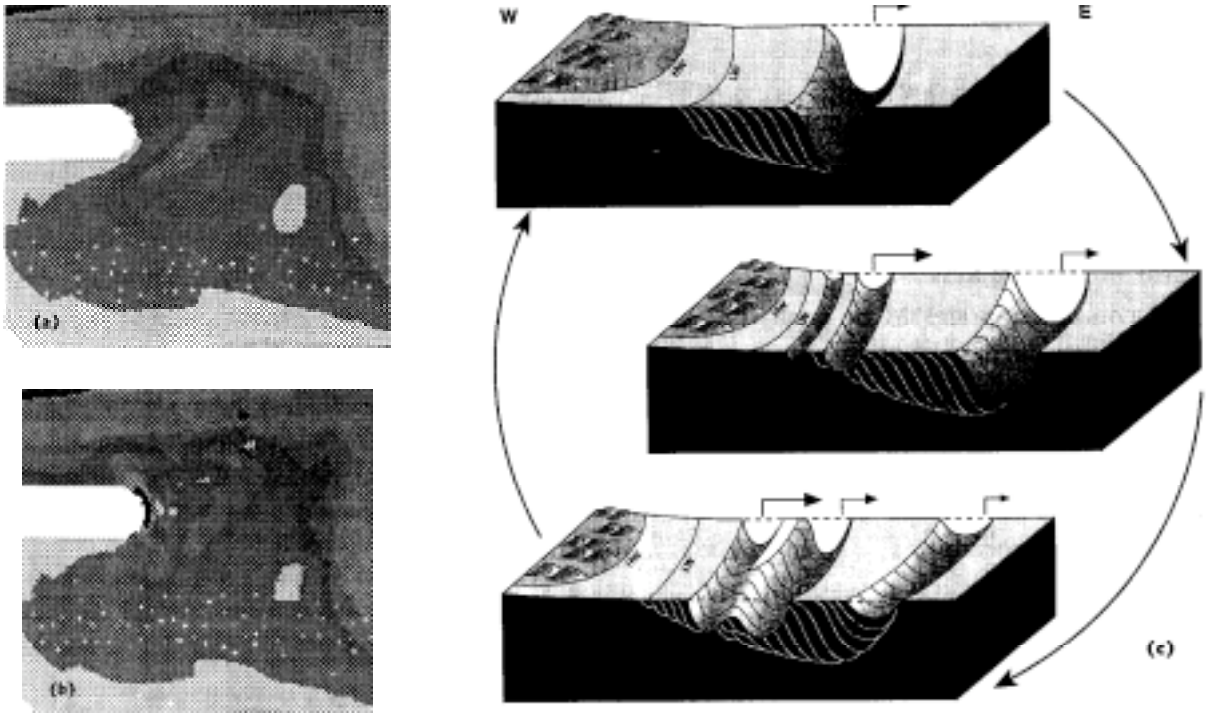

Figure 8.19: Frisian Inlet: channel pattern evolution, (a) initial conditions in the model, (b) predicted evolution, (C) observed cyclic evolution. (courtesy Z.B. Wang (a and b), A.P. Oost (c))

8.10 MTM-modelling practice

The above examples have shown to some extent that MTM-modelling involves a number of specific complications, on top of those encountered in ISE-modelling. In brief summary:

- The software infrastructure becomes even more critical now, because the coupling of the modules has to be completely automized.

- The model domain has to be the same for the process-modules and the sediment balance module, in order to avoid discontinuities in the bed topography. In the case of nested models for waves or tide, this concerns only the smallest model domains.
- The model composition should be such, that errors cannot build up to an unacceptable level during the simulation.
- The boundary conditions need to be defined with care. In general, errors in the boundary conditions tend to be reflected in an amplified form in the bed topography, and thus propagate into the model domain (Wang et al., 1991; also see De Vriend et al., 1993b).
- The time-stepping procedure in the morphodynamic loop deserves special attention, not only because it is instability-prone, but also because there is a large amount ofcomputer time involved, whence clever time-stepping may lead to significant savings.
- In spite of these time-saving techniques, there can be situations where the morphological time scales vary strongly through the model area (cf. Wang et al., 1991, 1995). In that case, the shortest time scale determines the maximum allowable morphological time step, which may imply that large amounts of computer time are needed to cover the largest time scale of interest
- Since the simulation covers a certain period of time, it is possible to mimic the natural variation of conditions via input-scenarios for waves, water levels, tides and surges. Such a scenario is only one realization of a stochastic process, so the simulation should be repeated a number of times in order to get a feel for the variability of the output.
- The same goes for verification against field observations, which are the result of only one realization of the input conditions. Therefore, such a verification cannot validate the variation of the output due to different input scenarios.

In general, it is very important to clearly identify the objectives of the model study. All-purpose simulation models are not yet available, so the model composition and set-up have to be derived from the objectives of the study, via an analysis of the relevant phenomena.
MTM-models, especially those including waves, are still in an early stage of development. Now that the numerical and software problems have largely been overcome, the focus of attention should return to the physical processes and their interactions, including the equilibrium state to which the system tends. Key issues of research are the tenability of the 2-D depth-integrated model concept and its $2\frac{1}{2}$-D or quasi-3D alternatives, and ways to deal with the natural variability of the input conditions.

8.11 Process-based long-term models

One way to achieve a long-term morphological model concept for tidal inlets is to formally avarage the constituting mathematical-physical equations over the space and

time scales which are smaller than those of the phenomena of interest. Since these constituting equations are nonlinear, this involves closure terms which have to be modelled in terms of the large-scale dependent variables (cf. the Reynolds-stress terms in turbulent flow models, and the radiation-stress terms in wave-driven current models). This can be done empirically, or based upon a theoretical analysis of the relevant interaction processes.

Krol (1990) describes a method of formal averaging for a simple 1-D morphodynamic model of a tidal estuary. This work has been followed up by various other investigators, (Fokkink, 1992; Schuttelaars and De Swart, 1994), lately also in two dimensions (Schuttelaars, 1994, private communication).

A simple example of formal averaging concerns a narrow basin of length L and width B (cf. Van Dongeren and De Vriend, 1994). L is much smaller than the tidal wave length, and B is constant, whence it can be taken equal to 1 without loss of generality. The constituting equations are:

(1) the equation of continuity of the tidal motion

$$\frac{\partial \zeta}{\partial t} + \frac{\partial \left[(\zeta - h) U \right]}{\partial x} = 0 \tag{8.11}$$

in which

ζ = water surface elevation above MSL,
h = bed level with respect to MSL (so usually $h < 0$),
U = cross-sectional average velocity,
x = spatial co-ordinate along the basin.

(2) the dynamic equation for the tide, which reduces to

$$\frac{\partial \zeta}{\partial x} = 0 \tag{8.12}$$

(3) the sediment transport formula

$$S(x,t) = a\, U^b \tag{8.13}$$

in which a and b are constants.

(4) the sediment balance equation

$$\frac{\partial h}{\partial t} + \frac{\partial S}{\partial x} = 0 \tag{8.14}$$

Integration of Eq. (8.11) over the length of the basin yields for $\zeta \ll h$ [5]

$$U(x,t) \approx \frac{L - x}{-h(x,\tau)} \frac{d\zeta}{dt} \tag{8.15}$$

[5] This assumption is made for explanatory reasons. Clearly, it does not hold in the shallow parts of the basin. Yet the resulting linear distribution of $h_e(x)$ turns out to be a reasonable approximation (Schuttelaars and De Swart, 1994).

in which ζ denotes a time co-ordinate at the slow time scale of the morphological changes. Substitution into Eq. (8.13) and averaging over the tidal cycle yields

$$\bar{S}(x,\tau) = a\left[\frac{L-x}{-h(x,\tau)}\right]^b Z_T \quad \text{with} \quad Z_T = \frac{1}{T}\int_0^T \left(\frac{d\zeta}{dt}\right)^b dt \tag{8.16}$$

Formal averaging of the sediment balance equation (8.14) over the tidal cycle yields

$$\frac{\partial h}{\partial \tau} + \frac{\partial \bar{S}}{\partial t} = 0 \tag{8.17}$$

or, with Eq. (16),

$$\frac{\partial h}{\partial \tau} + \frac{b\,\bar{S}}{-h(x,\tau)}\frac{\partial h}{\partial x} = \frac{b\,\bar{S}}{L-x} \tag{8.18}$$

This equation describes the evolution of $h(x,\tau)$ at the morphological time scale. Apparently, this equation is of the forced nonlinear advection type, with the advection speed bS/h which is found in many other morphological systems with a transport formula of the same type as in Eq. (8.13). Note that for $b > 1$ the source term vanishes towards the back end of the basin. This means that the evolution process proceeds ever slower as x approaches L.
The equilibrium state which follows from Eq. (8.18) is given by

$$\frac{\partial h_e}{\partial x} = -\frac{h_e}{L-x} \quad \text{whence} \quad h_e \text{????} \; L-x \tag{8.19}$$

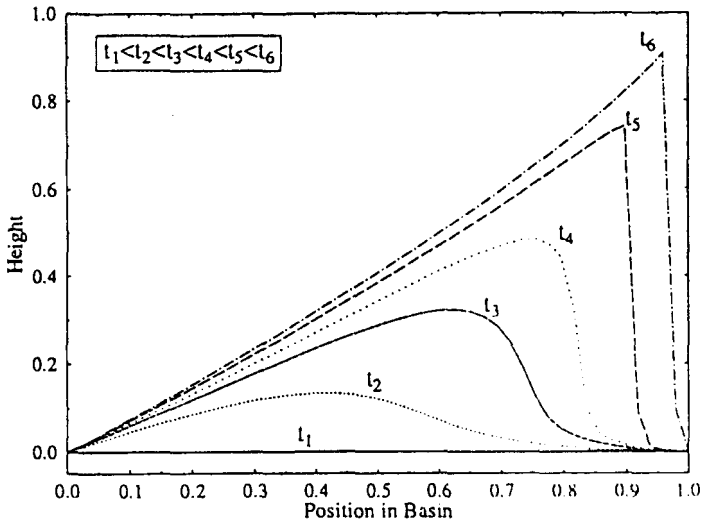

Figure 8.20: Morphological evolution of a dead-end tidal channel

As long as no part of the basin falls dry at low water, the tidal prism at any point x is also proportional to $L–x$. Hence the equilibrium cross-sectional area in this case is proportional to the tidal prism. This corresponds with O'Brien's (1931, 1969) empirical findings.

Figure 8.20 shows the result of a fully non-linear analytical model of the morphological evolution in a dead-end tidal channel without flats (Schuttelaars and De Swart, 1994). It shows that the above simplified linear model is a reasonable approximation. Note that the evolution process becomes infinitely slow towards the end of the channel, because the current velocity and the transport rate go to zero there (also see Van Dongeren and De Vriend, 1994).

The derivation of the above linearized model shows the essence of many long-term morphological model concepts, viz. to express the residual transport, and hence the time-derivative of the bed level, in terms of the bed elevation. The result is an evolution equation in *h*. The same approach is taken by Bakker (1995) to derive a bed evolution equation for a tidal channel in a network, i.e. with two open ends. Bakker and De Vriend (1995) use the result in a network model of a near-resonant basin. One of the research questions which they address is to what extent a small interference at one place in the basin can have large effects elsewhere.

This theoretical approach of tidal inlet morphodynamics is quite complex on the one hand, and quite powerful on the other. Analyses of the mathematical system, once it has been formulated, are able reveal the inherent morphodynamic behaviour, such as channel pattern formation and stability of channel/shoal systems. This information can not only be

of use for the validation of numerical models, it may even indicate to what extent numerical models will ever be able to handle these nonlinear phenomena.

8.12 Conclusion

Computer-intensive multi-dimensional model types are now available for application to tidal inlets. ISE-model systems have reached a more or less operational stage (Latteux and Peltier, 1992; Broker Hedegaard et al., 1993; Roelvink et al., 1994; Chesher et al., 1993) and have proven their use to describe physical processes, such as residual transport patterns, under a variety of input conditions. This information can be used to analyse how waves, tide, currents and sediment transport influence each other in an area as complex as a tidal inlet, and to estimate the impact of human interference in the system (engineering structures, land reclamation, sand mining, etc.).

Process-based morphodynamic simulation models are still in an earlier stage of development. It is technically possible to run such models and pilot applications are being made, but the stage of routine practical application has not yet been reached. This requires further investments into a more thorough understanding of the processes and mechanisms at work, and a further build-up of know-how, experience and confidence in these models.

One objective of further research should be a better insight into the relevance of phenomena at the process level to larger-scale morphological behaviour in a given situation. Thus it must become clearer what physics should be included in the constituent models in order to simulate these evolutions.

Another research issue is how to deal with the natural variability of the conditions which

drive a tidal inlet model, and how to interpret predictions which result from an assumed future input scenario. Conversely, it should become clear which aspects of the input time series are important to the morphological evolution of the system.
Finally, the formal averaging approach and the correponding theoretical analyses should be pursued further, if it were only for the large amount of insight which they provide.
At the development level, knowledge and tools for the adequate selection of model components would be welcome. Also, the insight into accuracy and reliability of these compound dynamic models should be improved, in conjunction with practical methods to deal with the limited predictability of inputs.

8.13 References

Bailard, J.A., 1981. An energetics total load sediment transport model for a plane sloping beach. J. Geoph. Res., 86(C11): 10938-10954.

Bakker, W.T., 1995. Effect of tidal resonance on the morphology of Wadden and estuaries. Publication in preparation.

Bakker, W.T. and De Vriend, H.J., 1995. Resonance and morphological stability of tidal basins. Accepted for publication in Marine Geology.

Bakker, W.T. and Joustra, D.S., 1970. The history of the Dutch coast in the last century. In: Proc. 12th Int. Conf. Coastal Eng., ASCE, New York, p. 709-728.

Berlamont, J., Ockenden, M., Toorman, E. and Winterwerp, J., 1993. The characteristics of cohesive sediment properties. Coastal Eng., 21(1-3): 105-128.

Bijker, E.W., 1966. The increase of bed shear in a current due to wave action. In: Proc. 10th ICCE, Tokyo, Japan, p. 746-765.

Bijker, E.W., 1971. Longshore transport computations. J. Waterways, Harbours and Coastal Eng. Div., 97(WW4): 687-701.

Broker Hedegaard, I., Mangor, K. and Lintrup, M.J., 1993. Modelling of sediment transport in connection with tidal inlets. In: Proc. Comp. Appl. Coastal and Offshore Eng. (ICE-CACOE '93), Kuala Lumpur, Malaysia.

Chesher, T.J., Wallace, H.M., Meadowcroft, I.C. and Southgate, H.N., 1993. PISCES, a morphodynamic coastal area model; first annual report. HR Wallingford, Rept. SR 337.

De Vriend, H.J., 1987. 2DH mathematical modelling of morphological evolutions in shallow water. Coastal Eng., 11(1): 1-27.

De Vriend, H.J., 1994. Two-dimensional horizontal and weakly three-dimensional models of sediment transport due to waves and currents. In: M.B. Abbott and W.A.Price (Editors), "Coastal, Estuarial and Harbour Engineers' Reference Book". E & FN Spon, London, p. 215-238.

De Vriend, H.J. and Ribberink, J.S., 1988. A quasi-3D mathematical model of coastal morphology. In: B.L. Edge (ed.), "Coastal Engineering 1988 Proc.", ASCE, New York, p. 1689-1703.

De Vriend, H.J. and Stive, M.J.F., 1987. Quasi-3D modelling of nearshore currents. Coastal Engineering, 11(5&6): 565-601.

De Vriend, H.J., Bakker, W.T. and Bilse, D.P., 1994. A morphological behaviour model for the outer delta of mixed-energy tidal inlets. Coastal Eng., 23(3/4): 305-327.

De Vriend, H.J., Capobianco, M., Chesher, T., De Swart, H.E., Latteux, B. and Stive, M.J.F., 1993a. Approaches to long-term modelling of coastal morphology: a review. Coastal Eng., 23(1-3): 225-269.

De Vriend, H.J., Louters, T., Berben, F. and Steijn, R.C., 1989. Hybrid prediction of a sandy shoal evolution in a mesotidal estuary. In: R.A. Falconer, P. Goodwin and R.G.S. Matthew (Editors), "Hydraulic and Environmental Modelling in Coastal, Estuarine and

River Waters. Gower Technical, Aldershot, pp. 145-156.
De Vriend, H.J., Zyserman, J., Nicholson, J., Péchon, Ph., Roelvink, J.A. and Southgate, H.N., 1993b. Medium-term 2-DH coastal area modelling. Coastal Engineering, 21(1-3): 193-224.
Deigaard, R., Fredsoe, J. and Broker Hedegaard, I., 1986. Suspended sediment in the surf zone. J. Waterway, Port, Coastal and Ocean Eng. Div., ASCE, 112(1): 115-128.
Dingemans, M.W., Radder, A.C. and De Vriend, H.J., 1987. Computation of the driving forces of wave-induced currents. Coastal Engineering, 11(5&6), p.539-563.
Dronkers, J., 1986. Tidal asymmetry and estuarine morphology. Neth. J. Sea Res., 20: 117-131.
Fokkink, R.J., 1992. Fundamental considerations on morphodynamic modelling in tidal regions; Part II: A semi-analytical method for tidal basins. Delft Hydraulics, Res. Rept. Z 331-II, 36 pp.
Fredsoe, J. and Deigaard, R., 1992. Mechanics of coastal sediment transport. Adv. Series on Ocean Engineering - Vol. 3, World Scientific, Singapore, 369 pp.
Friedrichs, C.T. and Aubrey, D.G., 1994. Tidal propagation in strongly convergent channels. J. Geoph. Res., 99(C2): 3321-3336.
Fritsch, D., Teisson, C. and Manoha, B., 1989. Long-term simulation of suspended sediment transport, application to the Loire estuary. In: Proc. XXIIIrd IAHR Congress, Ottawa, Canada, p. C276-284.
Holthuysen, L.H., Booij, N. and Herbers, T.H.C., 1989. A prediction model for stationary short-crested waves in shallow water with ambient currents. Coastal Engineering, 13: 23-54.
Horikawa, K., 1988. Nearshore dynamics and coastal processes. University of Tokyo Press, 522 pp.
Kalkwijk, J.P.Th. and Booij, R., 1986. Adaptation of secondary flow in nearly-horizontal flow. J. Hydr. Res., 24(1), p. 19-37.
Katopodi, I. and Ribberink, J.S., 1992. Quasi-3D modelling of suspended sediment transport by currents and waves. Coastal Eng., 18: 83-110 (err. 19: 339).
Kirby, J.T., Dalrymple, R.A. and Kaku, H., 1994. Parabolic approximations for water waves in conformal coordinate systems. Coastal Eng., 23: 185-213.
Krol, M.S., 1990. The method of averaging in partial differential equations. Doctoral thesis, Utrecht Univ., 81 pp.
Latteux, B. and Peltier, E., 1992. A two dimensional finite element system of sediment transport and morphological evolution. Int. Conf. on Comp. Mod. of Seas and Coastal Regions, Southampton, U.K.
Negen, E.H., 1994. Morphological study with 2DH numerical models near Eierland (Texel). Delft Hydraulics/Delft Univ. Techn., Report H 1887/H460, 68 pp.
O'Brien, M.P., 1931. Estuary tidal prism related to entrance areas. Civ. Eng., 1(8): 738-739.
O'Brien, M.P., 1969. Equilibrium flow areas of inlets on sandy coasts. J. Waterw. Harbors Div., ASCE, 95(WW1): 43-52.
Oost, A.P., 1995. The cyclic development of the Pinkegat Inlet system and the Engelsmanplaat/Smeriggat, Dutch Wadden Sea, over the period 1832-1991. In: "Dynamics and sedimentary developments of the Dutch Wadden Sea, with special emphasis on the Frisian Inlet", Doctoral thesis, Utrecht University (in press).
Oost, A.P. and De Haas, H., 1993. The Frisian Inlet, morphological and sedimentological changes in the period 1927-1970. Utrecht Univ., Inst. Earth Sciences, Coastal Genesis Report, 94 pp. (in dutch).
Peltier, E., Duplex, J, Latteux, B., Pechon, P. and Chausson, P., 1991. Finite element model for bed-load transport and morphological evolution. In: A. S.-Arcilla, M. Pastor, O.C. Zienkiewicz and B.A. Schrefler (eds.), "Computer Modelling in Ocean Engineering 91", Balkema, Rotterdam, p. 227-233.

Pethick, J.S., 1980. Velocity surges and asymmetry in tidal channels. Est. Coastal Mar. Sci., 11: 321-345.

Ribberink, J.S. and De Vroeg, J.H., 1991. Coastal defence Texel (Eierland), hydraulic and morphological effect study; phase 1: morphological analysis. Delft Hydraulics, Report H 1241, part I (in dutch).

Ribberink, J.S. and De Vroeg, J.H., 1992. Coastal Defence Texel (Eierland), hydraulic and morphological effect study; phase 2/3: morphological compotations. Delft Hydraulics, Report H 1241, parts III/IV (in dutch).

Roelvink, J.A. and Broker, I., 1993. Cross-shore profile models. Coastal Eng., 21(1-3): 163-191.

Roelvink et al., 1994. Design and development of DELFT-3D and application to coastal morphodynamics. In: A. Verwey, A.W. Minns, V. Babovi_ and M. Maksimovi_, _. (Editors), "Hydroinformatics '94", Balkema, Rotterdam, p. 451-456.

Schuttelaars, H.M. and De Swart, H.E., 1994. A simple long-term morphodynamic model of a tidal inlet. Utrecht Univ., Dept. of Mathematics, Preprint 864, 46 pp.

Soulsby, R.L., Hamm, L., Klopman, G., Myrhaug, D., Simons, R.R. and Thomas, G.P., 1993. Wave-current interaction within and outside the bottom boundary layer. Coastal Eng., 21(1-3), p. 41-69.

Speer, P.E. and Aubrey, D.G., 1985. A study of non-linear tidal propagation in shallow inlet/estuarine systems. Part II: theory. Est. Coastal Shelf Sci., 21: 207-224.

Steijn, R.C. and Hartsuiker, G., 1992. Morphodynamic reponse of a tidal inlet after a reduction in basin area. DELFT HYDRAULICS, Coastal Genesis report H 840.40, 75 pp.

Steijn, R.C., Louters, T., Van der Spek, A.J.F. and De Vriend, H.J., 1989. Numerical model hindcast of the ebb-tidal delta evolution in front of the Deltaworks. In: Falconer, R.A. et al.: "Hydraulic and Environmental Modelling of Coastal, Estuarine and River Waters", Gower Technical, Aldershot, p. 255-264.

Stelling, G.S. and Leendertse, J.J., 1992. Approximation of convection processes by cyclic ADI-methods. Proc. Conf. Estuarine and Coastal Modelling, Tampa, Florida, p. 771-182.

Stive, M.J.F., 1986. A model for cross-shore sediment transport. In: B.L. Edge (ed.): Coastal Engineering 1986 Proc.", ASCE, New York, p. 1551-1564.

Teisson, C., Ockenden, M., Le Hir, P., Kranenburg, C. and Hamm, L., 1993. Cohesive sediment transport processes. Coastal Eng., 21(1-3): 129-162.

Terwindt, J.H.J. and Battjes, J.A., 1990. Research on large-scale coastal behaviour. In: B.L. Edge (ed.), "Coastal Engineering 1990 Proc.", ASCE, New York, p. 1975-1983.

Van de Kreeke, J. and Robaczewska, K., 1993. Tide-induced transport of coarse sediment: application to the Ems estuary. Neth. J. Sea Res., 31(3): 209-220.

Van Dongeren, A.R. and De Vriend, H.J., 1994. A model of morphological behaviour of tidal basins. Coastal Eng., 22(3/4): 287-310.

Van Rijn, L.C., 1984. Sediment transport; Part I: bed load transport. J. Hydr. Eng., ASCE, 110(HY1): 1431-1456.

Van Rijn, L.C., 1989. Handbook Sediment Transport by Currents and Waves. Delft Hydraulics, Rept. H461, appr. 400 pp.

Van Rijn, L.C. and Meijer, K., 1991. Three-dimensional modeling of sand and mud transport in currents and waves. In: "The Transport of Suspended Sediment and its Mathematical Modelling", Preprints Int. IAHR/USF-Symp., Florence, Italy, p. 683-708.

Wang, Z.B., 1992. Theoretical analysis on depth-integrated modelling of suspended sediment transport. J. Hydr. Res., 30: 403-421.

Wang, Z.B., De Vriend, H.J. and Louters, T., 1991. A morphodynamic model for a tidal inlet. In: A. S.-Arcilla, M. Pastor, O.C. Zienkiewicz and B.A. Schrefler (Editors), "Computer Modelling in Ocean Engineering 91", Balkema, Rotterdam, p. 235-245.

Wang, Z.B., Louters, T. and De Vriend, H.J., 1995. Morphodynamic modelling for a tidal

inlet in the Wadden Sea. Accepted for publication in Marine Geology.
Zitman, T.J., 1992. Quasi three dimensional current modelling based on a modified version of Davies' shapefunction approach. Cont. Shelf Res., 12(1), p. 143-158.

Index